Aus der Klinik und Poliklinik für Radioonkologie und Strahlentherapie
der Universitätsmedizin der Johannes Gutenberg-Universität Mainz

Dosisbelastungen und Nebenwirkungen der Radiotherapie: Biodosimetrische und zellbiologische Untersuchungen von DNA-Schadensmarkern

Habilitationsschrift
zur Erlangung der venia legendi
für das Fach
Experimentelle Strahlentherapie

Universitätsmedizin der Johannes Gutenberg-Universität Mainz

vorgelegt von

Dr. rer. nat. Dipl. Ing. (FH) Sebastian Zahnreich
aus Wiesbaden

Mainz, 2022

Wissenschaftliche Originalpublikationen der kumulativen Habilitationsschrift

I. **Zahnreich, S.**; Ebersberger, A.; Kaina, B.; Schmidberger, H. Biodosimetry Based on gamma-H2AX Quantification and Cytogenetics after Partial- and Total-Body Irradiation during Fractionated Radiotherapy. Radiat Res 2015, 183, 432-446.

II. **Zahnreich, S.**; Ebersberger, A.; Karle, H.; Kaina, B.; Schmidberger, H. Quantification of Radiation Biomarkers in Leukocytes of Breast Cancer Patients Treated with Different Modalities of 3D-CRT or IMRT. Radiat Res 2016, 186, 508-519.

III. **Zahnreich, S.**; Rösler, H.P.; Schwanbeck, C.; Karle, H.; Schmidberger, H. Radiation-induced DNA double-strand breaks in peripheral leukocytes and therapeutic response of heel spur patients treated by orthovoltage X-rays or a linear accelerator. Strahlenther Onkol 2020, 196, 1116-1127.

IV. **Zahnreich, S.**; Poplawski, A.; Hartel, C.; Eckhard, L.S.; Galetzka, D.; Hankeln, T.; Löbrich, M.; Marron, M.; Mirsch, J.; Ritter, S.; Scholz-Kreisel, P.; Spix, C.; Schmidberger, H. Spontaneous and Radiation-Induced Chromosome Aberrations in Primary Fibroblasts of Patients with Pediatric First and Second Neoplasms. Front Oncol 2020, 10, 1338.

V. **Zahnreich, S.**; Weber, B.; Rösch, G.; Schindler, D.; Schmidberger, H. Compromised repair of radiation-induced DNA double-strand breaks in Fanconi anemia fibroblasts in G2. DNA Repair (Amst) 2020, 96, 102992.

Inhalt

1 Problemstellung und Motivation

Ionisierende Strahlung findet eine breite klinische Anwendung in den Bereichen der radiologischen Diagnostik, der Strahlentherapie und der Nuklearmedizin. In der Strahlentherapie hat der stetige technische Fortschritt zu einer Optimierung der konformalen Hochdosisbestrahlung des Tumorvolumens bei gleichzeitiger Aussparung des Normalgewebes und von Risikoorganen geführt. Dennoch kommt es bei der Radiotherapie unweigerlich zu Niedrigdosisbelastungen des Normalgewebes, wodurch die kurative Strahlentherapie mit einem geringen aber akzeptierten Risiko für Nebenwirkungen verbunden ist. Zwischen den unterschiedlichen Bestrahlungstechniken der Radiotherapie können die integralen Dosisbelastungen der Patienten und damit die Risiken für radiogene Spätfolgen jedoch deutlich variieren. Aufgrund der stetig steigenden Zahl langzeitüberlebender Tumorpatienten durch die verbesserte Diagnostik sowie optimierte und neue onkologische Therapiekonzepte, gewinnen vor allem dosislimitierende Späteffekte der Radiotherapie immer mehr an klinischer Relevanz. Die höchsten Strahlenrisiken, einschließlich der Entwicklung therapieassoziierter Sekundärmalignome, bestehen dabei für langzeitüberlebende Patienten mit pädiatrischen Tumoren oder mit genetisch prädisponierten Einschränkungen in der Reparatur strahleninduzierter DNA-Schäden im Normalgewebe.

In diesem Feld hat die biologische Dosimetrie durch den hochsensitiven Nachweis von strahleninduzierten DNA-Schäden auf Einzelzellebene in peripheren Lymphozyten ein noch nicht vollständig geklärtes Potential für eine Abschätzung und den Vergleich der integralen Dosisbelastung der Patienten, um den bestmöglichen Strahlenschutz und die Minimierung radiogener Risiken zu gewährleisten. Zusätzlich können Biomarker strahleninduzierter DNA-Schäden und deren Reparatur in Surrogatgeweben möglicherweise als prädiktive Indikatoren für eine erhöhte Suszeptibilität gegenüber strahlenassoziierten Normalgewebstoxizitäten oder der Entwicklung von Sekundärmalignomen dienen, denen Veränderungen der intrinsischen DNA-Reparaturkapazität und damit der individuellen Radiosensitivität zugrunde liegen. Die Identifizierung und Etablierung solcher Biomarker wäre ein wichtiger Beitrag zur klinischen Überwachung und Identifizierung von Hochrisikopatienten für eine Adaption der genotoxischen Radiotherapie sowie eine intensivierte Nachsorge zur bestmöglichen Früherkennung von radiogenen Spätfolgen und die unmittelbare Einleitung von medizinischen Gegenmaßnahmen.

2 Aufbau und Zielsetzung

Diese kumulative Habilitation beruht auf 5 Publikationen die im *Peer-Review*-Verfahren durch unabhängige Gutachter desselben Fachgebiets begutachtet und in wissenschaftlichen Fachzeitschriften veröffentlicht wurden. Diese sind in der gesamten Arbeit als **Publikation I-V** [1-5] referenziert und im Kapitel 9 der Arbeit dargestellt. Die **Publikationen I-III** beschäftigen sich mit dem Vergleich der Dosisbelastung durch die Radiotherapie verschiedener maligner oder benigner Erkrankungen mit unterschiedlichen Bestrahlungstechniken anhand biologischer DNA-Schadensmarker in peripheren Lymphozyten. Dabei wurden folgende Fragestellungen adressiert:

- Eignet sich die Quantifizierung von DNA-Reparaturfoci der phosphorylierten Histonvariante H2AX (γH2AX) als ein Surrogatmarker für DNA-Doppelstrangbrüche in peripheren Lymphozyten für die Rekonstruktion der absorbierten Teil- und Ganzkörperdosis nach radiotherapeutischen Teil- oder Ganzkörperexpositionen im Vergleich zum etablierten Nachweis instabiler Chromosomenaberrationen?
- Welchen Einfluss haben dabei physiologische und physikalisch-technische Parameter wie die exponierte anatomische Region, das Zielvolumen, die Energiedosis, die Ganzkörper-Äquivalentdosis und die absolute Bestrahlungsdauer auf die Anzahl und Dispersion der DNA-Schadensmarker in peripheren Lymphozyten?
- Eignet sich diese Methodik unter Berücksichtigung von Einfluss- und Störfaktoren für einen direkten Vergleich der integralen Dosisbelastung des Patienten durch verschiedene Bestrahlungstechniken zur Optimierung des Strahlenschutzes in der Radiotherapie?

Die zwei darauffolgenden **Publikationen IV und V** untersuchen in diesem Zusammenhang die Vulnerabilität gegenüber den mit einer Radiotherapie assoziierten akuten Nebenwirkungen oder karzinogenen Spätfolgen im Normalgewebe und intrinsischen Defekten in der DNA-Reparatur. Dabei wurden folgende Fragestellungen bearbeitet:

- Zeigen Normalgewebszellen langzeitüberlebender Kinderkrebspatienten Unterschiede in der zellulären oder chromosomalen Radiosensitivität im Vergleich zu langzeitüberlebenden Kinderkrebspatienten ohne ein Sekundärmailgnom oder tumorfreien Spendern?
- Bestehen bei Fanconi-Anämie Patienten bisher nicht eindeutig nachgewiesene Einschränkungen in der Reparatur strahleninduzierter DNA-Doppelstrangbrüche, die im Zusammenhang mit einer klinischen Strahlenüberempfindlichkeit und dem Risiko für akute Normalgewebstoxizitäten und Spätfolgen der Radiotherapie stehen?

3 Einleitung

3.1 Strahlenbiologische Grundlagen

3.1.1 Die biologische Wirkung ionisierender Strahlung

Die Schädigung biologischer Systeme durch ionisierende Strahlung erfolgt entweder durch direkte Ionisationsereignisse oder indirekt durch reaktive Radikale, die bei der Radiolyse von Wasser entstehen [6, 7]. Die biologische Wirkung von locker ionisierenden Photonen (Röntgen- und γ-Strahlung) geht zu 70 % auf indirekt induzierte Schäden zurück, während dicht ionisierende Partikelstrahlung (α-Partikel und schwere Ionen) zu über 50 % direkt auf das biologische Ziel wirkt [8]. Das kritischste Ziel bei einer Bestrahlung von Zellen ist die DNA [9], deren Integrität die Proteinexpression und damit die Funktionalität der Zelle sowie deren Reproduktionsfähigkeit gewährleistet. Ionisierende Strahlung induziert eine Vielzahl verschiedener DNA-Schäden, darunter Einzelstrangbrüche, Doppelstrangbrüche (DSB), Basenmodifikationen und -schäden, DNA-DNA und -Proteinvernetzungen oder Schäden an Zuckermolekülen [7]. Ionisierende Strahlung ist ein besonders potenter Induktor von DSBs, die den schwerwiegendsten und häufig letalen Strahlenschaden im Genom darstellen [10]. Die Induktion von DSBs folgt einer linearen Dosiswirkungsbeziehung und pro Gray (Strahlendosis – Gy = J/kg) werden dabei etwa 40-50 DSBs pro Zelle erzeugt [11]. DNA-Schäden aktivieren komplexe zelluläre Signalkaskaden, die deren Reparatur sowie einen transienten Zellzyklusarrest auslösen [12]. Nach der Reparatur strahleninduzierter DNA-Schäden kann die Zelle wieder in den Zellzyklus eintreten. Sind die induzierten Strahlenschäden jedoch zu hoch und irreparabel, wird in Abhängigkeit des betroffenen Zelltyps ein permanenter Zellzyklusarrest (frühzeitige Seneszenz) oder der programmierte Zelltod (Apoptose) ausgelöst.

3.1.2 Die Reparatur strahleninduzierter DNA-Doppelstrangbrüche

DSBs werden durch den MRN-Komplex, bestehend aus NBS1, Rad50 und Mre11 erkannt, der am Bruchende bindet und die zentrale Serin/Threonin-Kinase *Ataxia-telangiectasia mutated* (ATM) rekrutiert und aktiviert [10]. Diese zählt zur Proteinfamilie der *phosphatidylinositol 3-kinase-related kinases* (PIKK) und übernimmt neben den weiteren strahlenbiologisch relevanten Kinasen *Ataxia-telangiectasia and Rad3-related* (ATR) und *DNA-dependent protein kinase catalytic subunit* (DNA-PKcs) eine zentrale Rolle in der DNA-Schadensantwort. Zu den Substraten des aktivierten ATM gehören unter anderem die zellzyklusregulierenden Kinasen Chk1 und Chk2, die Histonvariante H2AX und der Tumorsuppressor p53 [13].

DSBs werden durch zwei Hauptwege in Abhängigkeit der Zellzyklusphase repariert: durch den Mechanismus des *canonical non-homologous end joining* (c-NHEJ), der im gesamten Zellzyklus aktiv ist, und durch die homologe Rekombination (HR), die während der S-Phase und in der langsamen Reparaturkomponente der G2-Phase genutzt wird [14]. Die DSB-Reparatur erfolgt in der G1- und G2-Phase des Zellzyklus mit einer biphasischen Kinetik. In beiden Phasen stellt das c-NHEJ die schnelle Komponente dar und repariert mehr als 80 % der DSBs innerhalb der ersten Stunden nach der Induktion. Darauf folgt eine langsame Komponente, bei der die verbleibenden DSBs in G1 durch einen resektionsabhängigen Subtyp des NHEJ und in G2 durch die HR repariert werden [14-16]. Im Gegensatz zur weitestgehend fehlerfreien HR stellt das c-NHEJ durch die Erzeugung von Indels und die willkürliche Verknüpfung von DSB-Bruchenden ohne Sequenzhomologien einen fehlerbehafteten Reparaturmechanismus dar, der zur Bildung chromosomaler Aberrationen führen kann [17]. Bei einer Beeinträchtigung des c-NHEJ oder der HR können Zellen auf den DSB-Reparaturmechanismus des alternativen NHEJ (alt-NHEJ) zurückgreifen [18]. Das von Poly (ADP-Ribose)-Polymerasen (PARP) abhängige alt-NHEJ benötigt eine minimale DSB-Endresektion und verursacht Sequenzveränderungen und Translokationen in großem Umfang [19]. Bei der Bildung chromosomaler Aberrationen muss zwischen instabilen Aberrationen wie dizentrischen Chromosomen, azentrischen Fragmenten und zentrischen Ringen oder transmissiblen Aberrationen wie Translokationen und Insertionen unterschieden werden [20]. Instabile Aberrationen verursachen aufgrund asymmetrischer Umstrukturierungen Probleme bei der mitotischen Segregation der Chromosomen und führen letztlich zum reproduktiven Zelltod durch mitotische Katastrophen mit einer Letalitätsrate von etwa 50 % pro Mitose [21]. Im Gegensatz dazu können transmissible Aberrationen und damit die strahleninduzierten genetischen Veränderungen stabil an die Tochterzellen weitergegeben werden. Dies wird mit einem gesteigerten Risiko für die strahleninduzierte Karzinogenese diskutiert [22, 23]. Die Induktion von DNA-Schäden und die damit assoziierten zellulären Konsequenzen wie Zelltod, frühzeige Seneszenz und Differenzierung oder genetische Veränderungen und Mutationen bilden die Basis für die gesundheitlichen Folgen einer Strahlenexposition. Genetisch bedingte Einschränkungen in den verschiedenen Komponenten der DNA-Reparatur führen zu Reparaturdefizienzsyndromen, die durch chromosomale Instabilität, erhöhte Inzidenzen von spontanen primären und therapieassoziierten sekundären Tumoren sowie Überempfindlichkeiten für Normalgewebstoxizitäten gegenüber ionisierender Strahlung und anderen Genotoxinen gekennzeichnet sind [24, 25]. Zu diesen Syndromen zählen unter anderem Ataxia telangiectasia (AT, Louis-Bar-Syndrom), das Nijmegen-breakage-

Syndrom (NBS), das Bloom-Syndrom (BLM), das Werner-Syndrom (WRN), das Li Fraumeni-Syndrom oder die Fanconi-Anämie [26-28].

3.2 Die Radiotherapie

3.2.1 Anwendung, Techniken und Dosisbelastungen der Radiotherapie

Krebserkrankungen stellen mit einer Inzidenz von mehr als 18 Millionen neuen Fällen und 9,6 Millionen krebsbedingten Todesfällen im Jahr 2018 die weltweit zweithäufigste Todesursache dar [29]. Die perkutane Radiotherapie repräsentiert neben der Operation und der Chemotherapie einen Grundpfeiler der Tumortherapie, die im Verlauf der Behandlung bei etwa 60 % aller Krebspatienten eingesetzt wird [30]. Dabei wird ionisierende Strahlung überwiegend als hochenergetische Photonen mit großen Eindringtiefen in das Gewebe für die Behandlung von tief liegenden Tumoren mit medizinischen Linearbeschleunigern (*linear accelerator* – LINAC) appliziert. Seltener kommen Elektronenstrahlen oder niederenergetische Röntgenstrahlen als Orthovolttherapie mit geringen Eindringtiefen zur Behandlung oberflächlicher Tumore zum Einsatz. Die Orthovolttherapie findet zudem Anwendung bei der Niedrigdosis-Therapie zur Schmerzreduktion und Verbesserung eingeschränkter Funktionen bei benignen, entzündlich-degenerativen Erkrankungen des Skelettsystems wie schmerzhaften Arthrosen, Periarthritis oder Kalkaneussporn [31]. Die Radiotherapie maligner Erkrankungen mit hohen lokalen Dosen beruht hingegen auf der Induktion von DNA-Schäden, um maligne Zellpopulationen abzutöten oder zumindest ihre Proliferation und klonogene Expansion zu unterbinden. Das Reaktionsmuster von Tumorzellen wird durch die 5 R's der Radiotherapie charakterisiert: das Reparaturvermögen, die Redistribution, die Repopulation, die Reoxygenation und die intrinsische Radiosensitivität [32]. Diese Parameter definieren den Tumor und sein Ansprechen auf die Radiotherapie als ein sehr heterogenes und komplexes System [33].

Das Ziel einer Radiotherapie ist es daher, den Tumor homogen mit hohen Strahlendosen zu exponieren und dabei das Normalgewebe und Risikoorgane bestmöglich auszusparen, um radiogene Nebenwirkungen zu vermeiden. Hier war die Einführung der dreidimensional geplanten konformalen Strahlentherapie (*3-dimensional conformal radiotherapy* – 3D-CRT) in den 1980er Jahren ein großer Fortschritt. Im Vergleich zur zweidimensionalen Radiotherapie, die auf einfachen Röntgenbildern basiert, wurde durch die Nutzung der Computertomographie (CT) und damit einer bildgebungsgestützten komplexen Bestrahlungsplanung eine Anpassung und Formung des Primärstrahls an das Tumorvolumen erreicht. In den 1990er Jahren folgten fortschrittlichere Modalitäten mit aktiven Strahlmodifikationen als die sogenannte

intensitätsmodulierte Radiotherapie (IMRT) und darauf aufbauende Techniken wie die volumetrisch modulierte Rotationsbestrahlung (*volumetric intensity modulated arc therapy* – VMAT), die Tomotherapie, die bildgebungsgesteuerte Radiotherapie (*image-guided radiotherapy* – IGRT) oder die vierdimensionale Radiotherapie unter Berücksichtigung der Patientenbewegung [34, 35]. Bei IMRT-Techniken erfolgt die Anpassung des Nutzstrahls an das Tumorvolumen und die Risikoorgane durch die Modulation der Photonenfluenz während der Bestrahlung und die Nutzung mehrerer Einstrahlwinkel. Dadurch werden eine verbesserte lokale Tumorkontrolle und eine Reduktion der Strahlentoxizität durch eine komplexere und günstige Verteilung hoher Strahlendosen bei gleichzeitiger Minimierung für Risikoorgane erzielt. Bei IMRT-Techniken wird jedoch durch eine höhere Anzahl von Einstrahlwinkeln und längere Bestrahlungszeiten für die Modulation der Photonenfluenz ein größerer Anteil des Normalgewebes niedrigen Strahlendosen ausgesetzt, was einen Risikofaktor für radiogene Spätfolgen darstellt [36, 37]. Weitere periphere Niedrigdosisbelastungen des Patienten fernab des Primärstrahls entstehen durch Leckagen aus dem Strahlerkopf des LINAC und durch Streuung des Kollimatorsystems und, in geringerem Maße, durch Streuung im Körper des Patienten sowie Rückstreuungen aus dem Bestrahlungsraum [38]. Eine bestmögliche Schonung des Normalgewebes bei optimaler Tumorkontrolle wird mit einer Partikeltherapie mit Protonen oder Kohlenstoffionen durch deren spezifische Tiefen-Dosis-Profile und biologischen Eigenschaften erreicht [39]. Aufgrund der begrenzten Verfügbarkeit, der hohen Kosten und fehlenden Evidenzen für eine deutlich überlegene Wirksamkeit im Vergleich zur konventionellen Photonentherapie wird die Partikeltherapie jedoch nur bei etwa 1 % aller Tumorpatienten angewendet [40].

3.2.2 Akute Nebenwirkungen und Spätfolgen der Radiotherapie

Die Radiotherapie ist unweigerlich mit einer Exposition des Normalgewebes mit hohen Strahlendosen an den Tumorgrenzen und peripheren Niedrigdosen fernab des Primärstahls verbunden. Diese verursachen bei etwa 5-10 % der Patienten starke und klinisch diverse Nebenwirkungen, die mit einer erheblichen Beeinträchtigung der Lebensqualität einhergehen. Eine dadurch notwendige Dosisreduktion kann jedoch zu einer suboptimalen Tumorkontrolle, erhöhten Risiken für Rezidive und damit geringeren Überlebenswahrscheinlichkeiten führen [41]. Bei den gesundheitlichen Folgen einer Strahlenexposition wird allgemein zwischen deterministischen und stochastischen Effekten unterschieden [7, 42]. Deterministische Strahlenschäden werden durch übermäßigen Zelltod und degenerative Prozesse in den betroffenen Geweben und Organen ausgelöst. Sie treten nach dem Überschreiten einer Schwellendosis auf und ihr Schweregrad nimmt mit steigender Dosis zu, bis ein Plateau erreicht

wird. Die Latenzzeiten zwischen der Bestrahlung und dem Wirkungseintritt hängen dabei vom exponierten Gewebe und der Strahlendosis ab. Akute radiogene Effekte werden während oder kurz nach Abschluss der Radiotherapie beobachtet, sind in der Regel reversibel und gelten im Allgemeinen nicht als dosislimitierend. Sie treten in Geweben mit hohen Proliferationsraten wie der Haut, dem Magen-Darm-Trakt und dem hämatopoetischen System auf und sind häufig mit inflammatorischen Prozessen verbunden [43]. Zu den akuten Strahleneffekten zählen u.a. die Dermatitis, die Mukositis, die Perikarditis, Pneumopathien, die Ösophagitis oder gastrointestinale Komplikationen [43]. Die Spätfolgen einer Radiotherapie treten etwa 6 Monate bis mehrere Jahre nach der Strahlentherapie auf, sind häufig irreversibel und somit dosislimitierend. Radiogene Späteffekte betreffen typischerweise langsam proliferierende Gewebe und Organe wie die Niere, das Herz und das Zentralnervensystem [43]. Die Pathogenese strahlenassoziierter Spätfolgen umfasst die (Lungen)Fibrose, Gefäßschäden, kognitive Einschränkungen, Hormonmangel oder Unfruchtbarkeit.

Stochastischen Strahleneffekten liegen Zufallsereignisse wie die Induktion und Reparatur subletaler DNA-Schäden zugrunde, die zu der Entstehung transmissibler genetischer und epigenetischer Mutationen oder zu chromosomalen Translokationen im Genom der Zelle führen können. Zu den stochastischen Strahlenschäden zählen vererbbare Defekte in der Keimbahn oder Tumorerkrankungen. Das Risiko für stochastische Strahleneffekte folgt einer linearen Dosiswirkungsbeziehung ohne Schwellenwert und das resultierende Krankheitsbild ist dabei unabhängig von der Dosis. Für radiogene solide Tumore steigt die Inzidenz allmählich über Jahre bis Jahrzehnte nach der Exposition, während hämatologische Malignome bereits nach 2 Jahren auftreten und das Risiko nach 5-10 Jahren wieder abnimmt [44, 45].

In den vergangenen Dekaden ist die Zahl langzeitüberlebender Krebspatienten aufgrund früherer Diagnosen sowie optimierter und neuer onkologischer Therapien mit erhöhter Wirksamkeit bei der lokalen und systemischen Tumorkontrolle stetig gestiegen und damit auch das Risiko für die Entwicklung von Spätfolgen einer Radiotherapie [46, 47]. Diese Problematik gewinnt zunehmend an klinischer Relevanz und eine besondere Besorgnis gilt dabei der Entstehung therapieassoziierter Sekundärmalignome, die mit erheblichen Belastungen des Patienten und einer Verkürzung der Gesamtüberlebenszeit nach der Behandlung von primären Krebserkrankungen einhergeht. Dies gilt insbesondere für langzeitüberlebende Kinderkrebspatienten, deren durchschnittliche 5-Jahres-Überlebensrate von weniger als 30 % vor 1960 auf aktuell 80 % gesteigert werden konnte [44, 48-53]. Pädiatrische Tumorpatienten sind aufgrund der Exposition im Entwicklungsstadium sowie der langen Lebenserwartung und damit Latenzzeit nach einer erfolgreichen Tumortherapie besonders vulnerabel für

strahleninduzierte Späteffekte. So erhöht eine Radiotherapie das Risiko für der Entstehung eines Sekundärmalignoms bei Erwachsenen um das 1,2- bis 3-fache und bei Kindern um das 6- bis 10-fache [53-56].

Die mit einer Radiotherapie assoziierten Sekundärmalignome sind charakterisiert durch die Entstehung in einer strahlenexponierten Region im Normalgewebe, einer Latenzzeit von mehr als 4 Jahren und einer anderen Histologie als der Primärtumor [57, 58]. Die Exposition des Normalgewebes an den Tumorgrenzen mit hohen Strahlendosen stellt einen etablierten Risikofaktor für die Entwicklung von sekundären Sarkomen dar [59-61]. Daneben wird auch die Exposition des Normalgewebes mit peripheren Niedrigdosen, die über große Bereiche des Körpers verteilt sind, als Risikofaktor für strahlenassoziierte Spätfolgen wie kardiovaskuläre Effekte oder Sekundärmalignome angesehen [62-64]. Zum Beispiel wurden für langzeitüberlebende Prostatakarzinompatienten mit einer Radiotherapie im Vergleich zur alleinigen Operation neben Sarkomen im Hochdosisbereich auch signifikant höhere Risiken für Sekundärmalignome außerhalb des Bestrahlungsfeldes nachgewiesen, darunter ebenfalls Sarkome sowie Lungen-, Kolon-, Blasen- und Rektumkarzinome [61, 65, 66].

Daher besteht auch die Annahme, dass verschiedene Bestrahlungstechniken der Radiotherapie, die zu unterschiedlichen Niedrigdosisbelastungen des Normalgewebes führen, mit variierenden karzinogenen Risiken verbunden sind. Insbesondere für die IMRT wird durch die deutlich erhöhte Niedrigdosisbelastung des Normalgewebes im Vergleich zur 3D-CRT eine Steigerung des Risikos für Sekundärmalignome von etwa 1 % auf 1,75 % für Tumorpatienten, die mindestens 10 Jahre nach der Radiotherapie überleben, vermutet [36, 67, 68]. Aufgrund der Anwendungsdauer der IMRT und den Latenzzeiten für radiogene Tumore liegen hierfür bisher jedoch noch keine belastbaren klinische Daten und Evidenzen aus großen Studienpopulationen mit entsprechend langen Nachbeobachtungszeiten vor [69-71].

Die Risiken für das Auftreten und den Schweregrad der Nebenwirkungen einer Radiotherapie sind multifaktoriell und werden durch Parameter wie die Strahlendosis, das exponierte Normalgewebsvolumen, den Gewebetyp, andere onkologische Behandlungen, den Lebensstil sowie genetische Faktoren beeinflusst [63]. Etwa 80 % der beobachteten Unterschiede in den Reaktionen des Normalgewebes zwischen den Patienten werden auf bisher nicht bekannte genetische Variablen zurückgeführt, die an der DNA-Schadensantwort und -reparatur, Zelltodmechanismen sowie der Proliferation oder an inflammatorischen Prozessen beteiligt sind und somit intrinsische Determinanten der individuellen Radiosensitivität darstellen [63]. Nur in einer sehr kleinen Untergruppe von etwa 1 % der Patienten können schwere und fatale radiogene Normalgewebtoxizitäten oder gesteigerte Risiken für Sekundärmalignome auf bekannte

Strahlenüberempfindlichkeitssyndrome wie AT, NBS oder die Fanconi-Anämie zurückgeführt werden [26-28]. Eine wichtige Aufgabe der klinischen Strahlenbiologie ist daher die Beurteilung einer genetisch prädisponierten Radiosensitivität und Anfälligkeit für Sekundärmalignome durch genomweite Assoziationsstudien oder die Anwendung funktioneller biologischer Testsysteme zur Untersuchung der intrinsischen DNA-Reparaturkapazität in Surrogatgeweben [72, 73]. Bisher sind die Determinanten eines immanenten Strahlenrisikos in der Allgemeinbevölkerung allerdings nicht aufgeklärt und in der klinischen Routine stehen keine prädiktiven Biomarker zur Verfügung, die eine Stratifizierung von Hochrisikopatienten für die Anpassung der Strahlentherapie und eine intensivierte Nachsorge zur Reduktion der Nebenwirkungen und Verbesserung der Lebensqualität ermöglichen.

3.3 Biomarker der Strahlenexposition und biologische Dosimetrie

Die Abschätzung gesundheitlicher Risiken einer Strahlenexposition basiert meist auf der physikalischen Messung oder Approximationen der absorbierten Strahlendosis durch analytische Berechnungen oder Monte-Carlo-Simulationen und der theoretischen Modellierung des strahlenassoziierten Krebsrisikos [74, 75]. Daneben stellt aber auch die biologische Dosimetrie eine wichtige Methode für den Nachweis und die Quantifizierung der Strahlenbelastung und -risiken exponierter Personen durch die Detektion biologischer Indikatoren einer Strahlenexposition in peripheren Lymphozyten dar [76]. Den Gold-Standard repräsentiert dabei die Quantifizierung von strahleninduzierten Chromosomenaberrationen als dizentrische Chromosomen [77]. Diese Methode weist jedoch nur eine geringe Sensitivität für einen Dosisbereich von 0.1-5 Gy auf [77]. Klinisch relevante Niedrigdosisbelastungen durch die radiologische Diagnostik oder periphere Dosen in der Radiotherapie bewegen sich aber meist in einem Bereich weit unter 0.1 Gy. Hier hat sich die indirekte Detektion strahleninduzierter DSBs über den immunbasierten Nachweis von DNA-Reparaturproteinen als sogenannte Foci auf Einzelzellebene mittels Fluoreszenzmikroskopie als eine hochsensitive Methode erwiesen [78, 79]. Zu den am häufigsten verwendeten indirekten Indikatoren von DSBs zählen die durch die PIKK am C-terminalen Ser-139 phosphorylierte Variante des Histons H2AX (γH2AX) oder das Tumorsuppressor-p53-bindende Protein 1 (53BP1) [80]. Die Nachweisgrenze dieser DSB-Reparaturfoci bei maximaler Induktion 15-30 Minuten nach der Bestrahlung liegt bei etwa 1 mGy oder 3 mGy nach einer Strahlenexposition *in vitro* oder *in vivo* [15]. Die Anzahl der DSB-Reparaturfoci ist dabei proportional zur Anzahl strahleninduzierter DSBs und folgt einer linearen Dosis-Wirkungs-Beziehung [15]. Die Quantifizierung strahleninduzierter γH2AX oder 53BP1 Foci in peripheren Lymphozyten unmittelbar nach einer *in vivo* Strahlenexposition durch

radiologische oder radiotherapeutische Maßnahmen wurde bereits zur Bestimmung und den Vergleich der inhärenten Strahlenbelastung durch verschiedene Techniken und Protokolle medizinischer Strahlenexpositionen angewendet [81]. Zum Zeitpunkt der Durchführung der Arbeiten für die vorliegende Habilitationsschrift lagen jedoch keine Studien vor, die unter Anwendung dieser Methodik variierende Strahlenbelastungen der Patienten durch unterschiedliche Techniken der Radiotherapie eindeutig nachweisen konnten. Neben dem Vergleich der Strahlenbelastung zwischen verschiedenen Bestrahlungstechniken erlaubt diese Methodik auch die Abschätzung der absorbierten Strahlendosis basierend auf *ex vivo* generierten Referenzdaten. Die anhand biologischer Indikatoren ermittelten Dosiswerte können im Rahmen einer hochpräzisen geplanten Bestrahlung durch die Radiotherapie mit den durch moderne Bestrahlungsplanungssysteme vorausgesagten Dosisbelastungen des Patienten verglichen werden. Neben dem klinischen Nutzen der biologischen Dosimetrie bei beabsichtigten medizinischen Expositionen kann so die Tauglichkeit dieser Methode für die Anwendung nach Strahlenunfällen und die Ermittlung unbekannter Strahlendosen sowie Expositionsszenarien anhand dieser sehr genau geplanten *in vivo* Bestrahlungen überprüft werden. Zusätzlich bietet die Analyse dieser strahleninduzierten Biomarker in Normalgewebszellen die Möglichkeit einer Untersuchung der intrinsischen DNA-Reparaturkapazität, deren Beeinflussung unter anderem auf eine erhöhte Radiosensitivität und Anfälligkeit gegenüber radiogenen Normalgewebstoxizitäten oder Spätfolgen einer Strahlenexpositionen hinweist [78, 82, 83].

4 Ergebnisse

4.1 Biologische Dosimetrie nach der Radiotherapie

In den **Publikationen I-III** beschäftigte sich der Autor mit biodosimetrischen Dosisrekonstruktionen und dem Vergleich der Strahlenbelastung nach der Radiotherapie verschiedener maligner (**Publikation I und II**) oder benigner (**Publikation III**) Erkrankungen durch unterschiedliche Bestrahlungstechniken.

4.1.1 Publikation I

Biodosimetrie auf der Grundlage der γH2AX-Quantifizierung und Zytogenetik nach fraktionierter Teil- oder Ganzkörperbestrahlung

Für die **Publikation I** wurden 62 Brustkrebspatientinnen und 31 Prostatakarzinompatienten für Teilkörperexpositionen sowie 8 Patienten mit hämatologischen Malignomen für Ganzkörperbestrahlungen rekrutiert. Die Teilkörperexpositionen erfolgten mit 5 täglichen Fraktionen pro Woche und einer durchschnittlichen Tumordosis von 2 Gy pro Fraktion. Untergruppen von Brust- und Prostatakrebspatienten erhielten eine zusätzliche Bestrahlung der Lymphknoten. Die Prostatakarzinompatienten wurden mit der VMAT und Brustkrebspatientinnen mit der tangentialen 3D-CRT behandelt. Ganzkörperbestrahlungen wurden mittels anterior-posteriorer 3D-CRT mit zwei täglichen Fraktionen zu jeweils 2 Gy durchgeführt, die durch eine Erholungsphase von mindestens 6 Stunden getrennt waren. Für Teilkörperexpositionen wurden venöse Blutproben unmittelbar vor der ersten Fraktion der Radiotherapie, 30 Minuten und 24 Stunden nach der ersten Fraktion und 30 Minuten nach der letzten Fraktion gewonnen. Für Ganzkörperexpositionen wurden venöse Blutproben unmittelbar vor der ersten Fraktion der Radiotherapie, 60 Minuten nach der ersten Fraktion und nach 6-8 Stunden unmittelbar vor der zweiten Fraktion gewonnen. Aus allen Blutproben wurden periphere Lymphozyten isoliert und der DSB-Surrogatmarker γH2AX nach Immunmarkierung mittels Fluoreszenzmikroskopie auf Einzelzellebene quantifiziert. Zusätzlich wurden für eine ausgewählte Anzahl an gesunden Spendern (n=5) und Tumorpatienten (n=16) instabile Chromosomenaberrationen in ersten Mitosen der Lymphozyten nach der Exposition bestimmt. Die vor der Radiotherapie erhaltenen Blutproben wurden zur Analyse des individuellen basalen Niveaus von DNA-Schäden in den Lymphozyten sowie der individuellen Radiosensitivität nach einer *ex vivo* Exposition mit festgelegten Testdosen an Röntgenstrahlung genutzt. Zusätzlich wurden venöse Blutproben von 14 gesunden Spendern entnommen und für die Etablierung von Referenzdaten als Dosis-Wirkungs-Beziehungen und Reparaturkinetiken nach einer *ex vivo* Exposition mit Röntgenstrahlung eingesetzt. Die so etablierten Standardkurven wurden für

Dosisrekonstruktionen basierend auf den DNA-Schäden in Lymphozyten nach radiotherapeutischen Expositionen herangezogen, die anschließend mit den applizierten Teilkörperdosen (Tumordosen) und den kalkulierten Ganzkörper-Äquivalentdosen für jeden Patienten verglichen wurden.

Nach homogener *ex vivo* Bestrahlung der Blutproben von gesunden Spender wurden über einen Dosisbereich von 0,25-2 Gy und einen Analysenzeitraum von 45 Minuten bis 48 Stunden nach der Exposition lineare Dosis-Wirkungs-Beziehungen für die mittlere Anzahl strahleninduzierter γH2AX Foci pro Lymphozyt beobachtet. Basierend auf den linearen Regressionskoeffizienten der Dosis-Wirkungs-Beziehungen wurde eine Kinetik der Abnahme strahleninduzierter γH2AX Foci pro Lymphozyt pro Gy etabliert. Die Abnahme der γH2AX Foci pro Lymphozyt wurde durch die bi-exponentielle Funktion $Y = 8{,}2 \pm 1 * \exp(-0{,}33 \pm 0{,}071 * X) + 1{,}7 \pm 1 * \exp(-0{,}023 \pm 0{,}022 * X)$ beschrieben. Dabei repräsentiert Y die mittlere Anzahl strahleninduzierter γH2AX Foci pro Lymphozyt pro Gy und X die Zeit in Stunden nach der Exposition. Mit dieser Funktion konnte die absorbierte Strahlendosis basierend auf der mittleren Anzahl strahleninduzierter γH2AX Foci pro Lymphozyt für einen bekanntem Zeitpunkt bis 48 Stunden nach einer Exposition rekonstruiert werden. Für die Quantifizierung instabiler Chromosomenaberrationen wurden Dosiswirkungsbeziehungen von 0.25-4 Gy für die Induktion dizentrischer Chromosomen und zentrischer Ringe mit der linear-quadratischen Funktion $Y = 0{,}037 \pm 0{,}006 * X + 0{,}048 \pm 0{,}003 * X^2$ sowie überzählige azentrische Fragmente mit der linear-quadratischen Funktion $Y = 0{,}056 \pm 0{,}006 * X + 0{,}031 \pm 0{,}003 * X^2$ etabliert. Dabei repräsentiert Y die mittlere Anzahl chromosomaler Aberrationen pro Lymphozyt und X die Strahlendosis.

Die Quantifizierung basaler oder *ex vivo* strahleninduzierter γH2AX Foci und instabiler Chromosomenaberrationen in Tumorpatienten sowie gesunden Spendern zeigte einen Einfluss einer vorherigen Radiotherapie oder einer Chemotherapie auf das basale Niveau zytogenetischer Schäden. Unter Berücksichtigung dieser Zunahme basaler Chromosomenaberrationen durch vorangegangene genotoxische Behandlungen wurden nach einer *ex vivo* Strahlenexposition jedoch keine Unterschiede in der Radiosensitivität von gesunden Spender oder von Tumorpatienten für beide DNA-Schadenmarker festgestellt.

Die Analyse strahleninduzierter γH2AX Foci 30 Minuten nach der ersten Fraktion der Teilkörperbestrahlung ergab signifikante lineare Korrelation zwischen der mittleren Anzahl strahleninduzierter γH2AX Foci pro Lymphozyt und der Ganzkörper-Äquivalentdosis für die Brust- sowie Prostatakrebspatienten. Der lineare Anstieg war für die Brustkrebspatientinnen

(10,6 ± 2,6 γH2AX Foci pro Lymphozyt pro Gy) signifikant steiler als für die Prostatakrebspatienten (8,4 ± 0,7 γH2AX Foci pro Lymphozyt pro Gy). 24 Stunden nach der ersten Teilkörperbestrahlung wurden für beide Tumorentitäten signifikante Abnahmen der mittleren Werte von strahleninduzierten γH2AX Foci pro Lymphozyt festgestellt, die nur noch für die Prostatakarzinompatienten mit der Ganzkörper-Äquivalentdosis korrelierten.
60 Minuten nach Beginn der ersten Ganzkörperbestrahlung mit 2 Gy wurden strahleninduzierte γH2AX Foci in nahezu allen (93 ± 9%) analysierten Lymphozyten von 8 Patienten mit im Mittel 16 ± 1,7 γH2AX Foci pro Lymphozyt detektiert. Nach einer Erholungsphase von 6-8 Stunden und unmittelbar vor der zweiten Ganzkörperbestrahlung waren strahleninduzierte γH2AX Foci noch in 72 ± 16 % der analysierten Lymphozyten von 7 verfügbaren Patientenproben mit im Mittel 4.5 ± 1 γH2AX Foci pro Lymphozyt nachweisbar.

Die Rate strahleninduzierter Chromosomenaberrationen wurde nach der ersten Teilkörperexposition in peripheren Lymphozyten von 8 Brust- und 5 Prostatakrebspatienten bestimmt. 30 Minuten nach der ersten Fraktion war die Rate dizentrischer Chromosomen und zentrischer Ringe in peripheren Lymphozyten von 6 Brustkrebspatientinnen und allen untersuchten Prostatakarzinompatienten im Vergleich zum basalen Niveau erhöht, jedoch ohne eine Abhängigkeit von der Ganzkörper-Äquivalentdosis. 24 Stunden nach der ersten Fraktion wurde in der Mehrzahl der untersuchten Patientenproben eine weitere Zunahme von instabilen Aberrationen beobachtet, die bei den Prostatakrebspatienten mit Lymphknotenbestrahlung am stärksten ausgeprägt war und linear mit der Ganzkörper-Äquivalentdosis korrelierte. Nach der Ganzkörperexposition mit 2 Gy waren die Häufigkeiten von strahleninduzierten dizentrischen Chromosomen und zentrischen Ringen in Lymphozyten von drei Patienten nach 60 Minuten und nach 6-8 Stunden mit durchschnittlichen Raten von 0,36 ± 0,05 und 0,41 ± 0,04 pro Lymphozyt vergleichbar erhöht.

Die Dosisabschätzungen basierend auf den Raten strahleninduzierter DNA-Schäden in Lymphozyten wurden nur nach den genau definierten Bedingungen der ersten Fraktion durchgeführt, um Verzerrungen durch Fraktionierungseffekte zu vermeiden. Für Dosiskalkulationen basierend auf den Raten chromosomaler Aberrationen wurden nur die Daten für die höheren Werte 24 Stunden nach der ersten Teilkörperexposition berücksichtigt. Die Ganzkörper-Äquivalentdosen konnten anhand der 30 Minuten nach der ersten Teilkörperbestrahlung gewonnenen mittleren Raten strahleninduzierter γH2AX Foci pro Lymphozyt und der Verwendung der *ex vivo* generierten Referenzdaten gesunder Spender erfolgreich rekonstruiert werden. 24 Stunden nach der ersten Teilkörperbestrahlung führten die

Daten strahleninduzierter Chromosomenaberrationen sowie der γH2AX Foci pro Lymphozyt jedoch zu einer deutlichen Überschätzung der Ganzkörper-Äquivalentdosen. Nach Ganzkörperexpositionen konnten 60 Minuten und 6-8 Stunden nach der ersten Fraktion Anhand der mittleren Rate an Chromosomenaberrationen oder strahleninduzierten γH2AX Foci pro Lymphozyt sehr gute Übereinstimmungen mit der applizierten Ganzkörperdosis von 2 Gy festgestellt werden.

Ein weiteres Ziel der **Publikation I** war die Abschätzung der applizierten Tumordosen nach Teilkörperbestrahlungen. Die biodosimetrische Abschätzung von Teilkörperdosen beruht auf den Analysen chromosomaler Aberrationen nach Dolphin [84] oder durch die Q_{dr} Methode nach Sasaki und Myata [85]. In der **Publikation I** wurde die Q_{dr} Methode angewendet, die als die sogenannte $Q_{\gamma H2AX}$ Methode bereits von Redon *et al.* [86] für die biodosimetrische Quantifizierung von γH2AX Foci in Lymphozyten adaptiert wurde. Die Q_{dr} Methode berücksichtigt die Ausbeute an dizentrischen Chromosomen und zentrischen Ringen ausschließlich in Lymphozyten mit instabilen Aberrationen und geht davon aus, dass diese Lymphozyten zum Zeitpunkt der Teilkörperexposition einer Strahlenbelastung ausgesetzt waren. Die Methode umgeht daher das Problem der Verdünnung durch nicht strahlenexponierte Zellen bei heterogenen Bestrahlungen. Q_{dr} repräsentiert dabei die erwartete Ausbeute an dizentrischen Chromosomen und zentrischen Ringen unter den strahlengeschädigten Lymphozyten, stellt damit eine alleinige Funktion der absorbierten Dosis dar und erlaubt die Dosisabschätzung für die exponierte Teilkörperfraktion. Die $Q_{\gamma H2AX}$ Methode folgt einem ähnlichen Ansatz, der auf der Anzahl der γH2AX Foci pro strahlengeschädigtem Lymphozyt mit mindestens einem γH2AX Focus basiert. Zur Berechnung der Teilkörperdosen nach der $Q_{\gamma H2AX}$ Methode wurde eine weitere Standardkurve basierend auf den *ex vivo* Referenzdaten gesunder Spender erstellt, bei der Lymphozyten ohne γH2AX Foci ignoriert wurden. Die Funktion dieser dosisnormalisierten bi-exponentiellen Zerfallskurve war $Y = 7{,}9 \pm 0{,}33 * \exp(0{,}33 \pm 0{,}064 * X) + 2{,}1 \pm 0{,}7 * \exp(0{,}0024 \pm 0{,}0096 * X)$, wobei Y die mittlere Anzahl strahleninduzierter γH2AX-Foci pro strahlengeschädigtem Lymphozyt pro Gy und X die Zeit in Stunden nach der Exposition repräsentiert. Die Teilkörperdosisabschätzungen auf der Grundlage der $Q_{\gamma H2AX}$ Methode führten 30 Minuten nach der ersten Fraktion der Teilkörperbestrahlung zu einer deutlichen Unterschätzung der mittleren Tumordosis von 2 Gy. 24 Stunden nach der ersten Teilkörperbestrahlung wurden basierend auf der mittleren Anzahl residualer strahleninduzierter γH2AX Foci pro Lymphozyt und strahleninduzierten dizentrischen Chromosomen und

zentrischen Ringen pro Lymphozyt bessere Dosisabschätzungen der lokalen Tumordosis erzielt, die jedoch mit deutlichen Unsicherheiten behaftet waren.

4.1.2 Publikation II

Quantifizierung von DNA-Schadensmarkern in Lymphozyten von Brustkrebspatientinnen nach der Radiotherapie mit verschiedenen Techniken der 3D-CRT oder IMRT

Die **Publikation II** baute auf der **Publikation I** auf und zielte auf den biodosimetrischen Vergleich der Strahlenbelastung von Brustkrebspatientinnen, die mit unterschiedlichen Techniken der 3D-CRT oder der IMRT behandelt wurden. Zu diesem Zweck wurde das Kollektiv der Brustkrebspatientinnen aus der **Publikation I** (n=62) um weitere 49 Patientinnen erweitert (n=111). Die Radiotherapie des Mammakarzinoms ohne Lymphknotenbestrahlung wurde mit der 3D-CRT durchgeführt, wobei zur Strahlformung entweder ein mechanischer Keilfilter (n=32) oder ein virtueller Keilfilter (n=49) mit Dosisraten von 3 oder 6 Gy pro Minute angewendet wurden. Verglichen mit einem virtuellen Keilfilter erfordert die Strahlformung durch einen mechanischen Keilfilter eine höhere Anzahl von Monitoreinheiten (*monitor units* – MU), um Absorptionen im Keilfilter zu kompensieren und die gewünschte Dosis im Isozentrum zu erreichen. MU sind ein direktes Maß für die abgegebene Dosis in Abhängigkeit von der Strahlleistung des LINAC und korrelieren daher mit der Bestrahlungsdauer. Die Verwendung eines mechanischen Keilfilters führt zu einer verlängerten Bestrahlungsdauer, wodurch die Strahlenbelastung des Patienten durch Streu- und Leckstrahlung als periphere Niedrigdosen außerhalb des Primärstrahls im Vergleich zu einem virtuellen Keilfilter steigt [87-89]. Brustkrebspatientinnen mit einer zusätzlichen Bestrahlung der Lymphknoten wurden entweder mit der 3D-CRT (n=21) oder mit der IMRT (n=9) behandelt.

Nach der ersten Fraktion der Radiotherapie wurde die mittlere Rate der quantifizierten DNA-Schadensmarker in peripheren Lymphozyten mit verschiedenen Parametern der Radiotherapie wie dem Planungszielvolumen (*planning target volume* – PTV), der Energiedosis in MU, der Ganzkörper-Äquivalentdosis und der Bestrahlungszeit (*beam-on time* – BOT) in Beziehung gesetzt. Für die mittlere Anzahl strahleninduzierter γH2AX Foci pro Lymphozyt aller untersuchten Brustkrebspatientinnen (n=111) wurden signifikante Korrelationen mit allen 4 Parametern der Radiotherapie festgestellt. Im Vergleich zur 3D-CRT war dabei die mittlere Anzahl strahleninduzierter γH2AX Foci pro Lymphozyt bei den mit der IMRT behandelten Patientinnen mit ähnlichem PTV und Ganzkörper-Äquivalentdosen durch die höhere Anzahl applizierter MU und der dadurch längeren BOT deutlich erhöht. Im Gegensatz zur Quantifizierung von strahleninduzierten γH2AX Foci wurde für die mittlere Rate der strahleninduzierten Chromosomenaberrationen in Lymphozyten aller untersuchten

Brustkrebspatientinnen (n=15) 24 Stunden nach der ersten Fraktion aufgrund der geringeren Sensitivität der Methode keine Korrelation mit dem PTV oder der Ganzkörper-Äquivalentdosis festgestellt. Es wurde jedoch eine deutliche Zunahme strahleninduzierter Chromosomenaberrationen in den Lymphozyten der mit der IMRT behandelten Patientinnen bei vergleichbarem PTV und Ganzkörper-Äquivalentdosen beobachtet. Dies führte zu signifikanten Korrelationen der Rate von strahleninduzierten Chromosomenaberrationen in Lymphozyten mit den applizierten MU und der BOT.

Anschließend wurde in der **Publikation II** untersucht, ob sich die analysierten DNA-Schadensmarker in Lymphozyten für den Nachweis variierender Belastungen mit niedrigen peripheren Strahlendosen durch unterschiedliche Techniken der Radiotherapie eignen. Die Kalkulation der Ganzkörper-Äquivalentdosen in den **Publikationen I** und **II** beruhte auf den Daten kommerzieller Behandlungsplanungssysteme. Da deren Algorithmen in erster Linie auf die präzise Berechnung hoher Dosen im PTV ausgelegt sind, werden periphere Niedrigdosen meist erheblich unterschätzt [90-92]. Um daher Diskrepanzen zwischen einer Abhängigkeit der mittleren Rate der strahleninduzierten DNA-Schadenmarker nach der Radiotherapie von der kalkulierten Ganzkörper-Äquivalentdosis besser herauszuarbeiten und analysieren zu können, wurde die Ausbeute strahleninduzierter DNA-Schäden pro Lymphozyt für jede Patientin auf deren Ganzkörper-Äquivalentdosis normiert. Um dabei den vorher bereits erwähnten Einfluss der BOT auf das Niveau strahleninduzierter DNA-Schäden pro Lymphozyt näher zu untersuchen, wurden die Patientinnen in die folgenden 6 Behandlungsgruppen unterteilt, die neben der Verwendung eines mechanischen oder virtuellen Keilfilters die unterschiedliche Dosisrate von 3 oder 6 Gy pro Minute berücksichtigten:

1.) 3D-CRT mit virtuellem Keilfilter bei 6 Gy pro Minute (γH2AX Foci n=34, Chromosomenaberrationen n=5)
2.) 3D-CRT mit virtuellem Keilfilter bei 3 Gy pro Minute (γH2AX Foci n=15)
3.) 3D-CRT mit mechanischem Keilfilter bei 6 Gy pro Minute (γH2AX Foci n=19)
4.) 3D-CRT mit mechanischem Keilfilter bei 3 Gy pro Minute (γH2AX Foci n=13)
5.) 3D-CRT mit Lymphknotenbestrahlung (γH2AX Foci n=21, Chromosomenaberrationen n=5)
6.) IMRT mit Lymphknotenbestrahlung (γH2AX Foci n=9, Chromosomenaberrationen n=5)

Die auf die Ganzkörper-Äquivalentdosis normierten Daten beider DNA-Schadensmarker in Lymphozyten zeigten sehr gute Korrelationen mit der BOT. Die detaillierte Analyse der γH2AX Foci in den 6 Behandlungsgruppen zeigte jedoch auch, dass bei der gleichen Anzahl applizierter

MU eine Halbierung der Dosisrate von 6 auf 3 Gy pro Minute zu einer signifikanten Steigerung um im Mittel das 1,3-fache für die Anwendung des mechanischen Keilfilters und um das 1,2-fache für die Verwendung des virtuellen Keilfilters führte. Für die IMRT mit der höchsten Anzahl an MU und damit der längsten BOT wurde ein im Mittel etwa doppelt so hohes DNA-Schadensniveau in peripheren Lymphozyten im Vergleich zur 3D-CRT beobachtet.

Frühere Studien von Zwicker *et al.* [93, 94] wiesen darauf hin, dass nach einer Radiotherapie die Verteilung strahleninduzierter γH2AX Foci in Lymphozyten mit der physikalischen Dosisverteilung im Ganzkörpervolumen entsprechend dem kumulativen Dosis-Volumen-Histogramm (DVH) der Bestrahlungsplanungssoftware korreliert und somit ebenfalls für einen Vergleich der integralen Dosisbelastung durch unterschiedliche Bestrahlungstechniken herangezogen werden kann. Daher wurde für die 6 unterschiedlichen Bestrahlungsgruppen integrale Histogramme der Verteilung strahleninduzierter γH2AX Foci in Lymphozyten erstellt und mit der physikalischen Dosisverteilung im Ganzkörpervolumen aus der Bestrahlungsplanungssoftware verglichen. Dabei entsprachen die Unterschiede in der dosisabhängigen Verteilung strahleninduzierter γH2AX Foci in Lymphozyten sehr gut dem Muster der vorhergesagten Unterschiede in der physikalischen Niedrigdosisverteilung im Ganzkörpervolumen der Patientinnen durch die unterschiedlichen Bestrahlungstechniken. Es wurden signifikante Abweichungen zwischen den 4 unterschiedlichen Modalitäten der 3D-CRT ohne Lymphknotenbestrahlung in den Anteilen von Lymphozyten mit weniger als 6 strahleninduzierten γH2AX Foci pro Lymphozyt sowie dem Ganzkörpervolumen, das mit weniger als 0,2 Gy exponiert wurde, festgestellt. Die deutlichsten Unterschiede in der Niedrigdosisbelastung bestanden dabei zwischen der Anwendung eines mechanischen Keilfilters bei einer Dosisrate von 3 Gy pro Minute oder eines virtuellen Keilfilters bei einer Dosisrate von 6 Gy pro Minute mit der größten Diskrepanz in der BOT. Ein noch deutlicherer Unterschied wurde für den Vergleich der Radiotherapie mit Lymphknotenbestrahlung durch die 3D-CRT oder IMRT festgestellt. Im Vergleich zur 3D-CRT führte die IMRT zu einem signifikant höheren Anteil von Lymphozyten mit weniger als 10 strahleninduzierten γH2AX Foci und einem Ganzkörpervolumen, das mit weniger als 0,7 Gy exponiert wurde.

Damit wurde in der **Publikation II** gezeigt, dass die Induktion von DNA-Schadensmarkern in Lymphozyten durch die Anwendung verschiedener Bestrahlungstechniken bei der Radiotherapie einer Tumorentität maßgeblich von verschiedenen physikalisch-technischen Variablen dominiert wird. Einen besonderen Einfluss hatte die Bestrahlungsdauer, deren Verlängerung zu einer vom PTV, der Ganzkörper-Äquivalentdosis sowie den MU unabhängigen Zunahme der mittleren Anzahl der DNA-Schadensmarker pro Lymphozyt führte. Für die

Variationen in der peripheren Niedrigdosisbelastung durch unterschiedliche Bestrahlungstechniken, die am besten durch Dispersionsanalysen von γH2AX Foci in peripheren Lymphozyten angezeigt wurden, besteht ebenfalls ein potentieller Einfluss der BOT und die Aussagekraft solcher Ergebnisse muss mit entsprechender Vorsicht interpretiert werden.

4.1.3 Publikation III

Strahleninduzierte DNA-Doppelstrangbrüche in peripheren Lymphozyten und das therapeutische Ansprechen von Fersensporn-Patienten nach der Radiotherapie mit einem Orthovoltgerät oder Linearbeschleuniger

In der **Publikation III** wurden für den biodosimetrischen Vergleich der Strahlenbelastung durch unterschiedliche Bestrahlungstechniken strahleninduzierte γH2AX Foci in peripheren Lymphozyten von Patienten mit schmerzhaftem Fersensporn nach der Radiotherapie mit einem niederenergetischen Orthovoltgerät (140 kV) oder einem hochenergetischen LINAC (6 MV) untersucht. Im Vergleich zur Orthovolt-Therapie erzielt die Radiotherapie mit einem LINAC eine homogenere Dosisverteilung im Zielvolumen, der eine bessere therapeutische Wirksamkeit zugeschrieben wird [95]. Die Eindringtiefe der hochenergetischen Photonen eines LINAC übersteigt allerdings den Querschnitt des Patienten und führt zu Reflektionen im Bestrahlungsraum, die zu einer Niedrigdosisbelastung des Gewebes außerhalb des Zielvolumens beitragen können. Zusätzlich können unter Anwendung eines LINAC weitere Niedrigdosisbelastungen des Patienten durch Streuungen und Leckagen im Strahlerkopf und den Kollimatoren auftreten [38]. Die Radiotherapie mit einem niederenergetischen Orthovoltgerät weist zwar eine schlechtere Dosisverteilung im Zielvolumen auf, ermöglicht aber die Anwendung von Bleiabschirmungen, die bei einem hochenergetischen LINAC aufgrund der Erzeugung von Streustrahlung innerhalb der Bleiabschirmung nicht eingesetzt werden können. Bei einem LINAC kann jedoch eine Behandlungsplanung einschließlich einer Feldkollimation durchgeführt werden, um das Gewebe des Patienten außerhalb des Zielvolumens bestmöglich auszusparen. Als sekundärer Endpunkt wurde das therapeutische Ansprechen auf die unterschiedlichen Bestrahlungstechniken erfasst. 22 Patienten mit schmerzhaftem Fersensporn wurden entweder mit einem Orthovoltgerät (n=11) oder mit einem LINAC (n=11) mit 2 wöchentlichen Fraktionen von 0,5 Gy über 3 Wochen behandelt. Die strahleninduzierten DSBs wurden entsprechend den **Publikationen I** und **II** als γH2AX Foci in peripheren Lymphozyten 30 Minuten nach der ersten Fraktion quantifiziert. Zusätzlich wurde das individuelle basale Niveau und die Radiosensitivität nach einer *ex vivo* Bestrahlung in einer unmittelbar vor der ersten Fraktion gewonnenen Blutprobe bestimmt. Die Fersenschmerzen und die analgetische

Wirksamkeit der Behandlung wurden vor und 3 Monate nach der Radiotherapie anhand eines fünfstufigen *Calcaneodynie-Scores* (CS) bewertet [96, 97].

Nach der ersten Fraktion wurde in Lymphozyten von 78 % aller Patienten ein Anstieg von γH2AX Foci im Vergleich zum basalen Niveau vor der Bestrahlung festgestellt. Dabei kam es zu einer Zunahme bei 90 % der Patienten nach der Orthovolt-Therapie und bei 63 % der Patienten nach der Radiotherapie mit einem LINAC, wobei kein signifikanter Unterschied zwischen den Bestrahlungstechniken festgestellt werden konnte. Dabei stieg die mittlere Anzahl an γH2AX Foci pro Lymphozyt für alle Patienten signifikant von einer durchschnittlichen basalen Rate von 0,18 ± 0,21 auf 0,33 ± 0,34 an. Für die Patienten, die mit der Orthovolt-Therapie oder einem LINAC behandelt wurden, erreichte die durchschnittliche Rate strahleninduzierter γH2AX Foci pro Lymphozyt nach der ersten Fraktion dabei ein vergleichbares Niveau von 0,15 ± 0,22 und 0,15 ± 0,23.

Zur Abschätzung und den Vergleich einer Ganzkörper-Äquivalentdosis zwischen den Bestrahlungstechniken wurde diese für jeden Patienten nach Johns [98] berechnet. Im Gegensatz zu den mittleren Raten strahleninduzierter γH2AX Foci pro Lymphozyt war die durchschnittliche Ganzkörper-Äquivalentdosis nach der Behandlung mit einem LINAC (11,81 ± 1,95 mSV) signifikant höher als bei der Orthovolt-Therapie (2,73 ± 0,42 mSV). Es wurde jedoch keine Korrelation zwischen den berechneten Ganzkörper-Äquivalentdosen und den mittleren Raten der γH2AX Foci pro Lymphozyt festgestellt.

Zur Beurteilung der therapeutischen Wirksamkeit der beiden Behandlungsarme wurden für jeden Patienten die CS-Einzelwertkriterien und der CS-Summenwert vor und 3 Monate nach der Radiotherapie erfasst. Der durchschnittliche CS-Summenwert für alle Patienten vor der Radiotherapie lag bei 49,5 ± 14,1 und war vergleichbar zwischen den Patienten, die mit einem Orthovoltgerät (49,6 ± 12,2) oder einem LINAC (49.3 ± 16.4) behandelt wurden. Bei der Nachsorge nach 3 Monaten beobachteten wir einen signifikanten 1,6-fachen Anstieg des CS-Summenwertes auf 78,4 ± 14,1 für alle Patienten und auf 83,3 ± 20,3 oder 72,9 ± 22,2 in dem Orthovolt- oder LINAC-Arm ohne einen signifikanten Unterschied zwischen den Bestrahlungstechniken. 89 % aller Patienten hatten einen verbesserten CS-Summenwert und nur 5,5 % der Patienten berichteten über unveränderte oder verschlechterte Bedingungen. Nach der Orthovolt-Therapie zeigten alle Patienten eine Zunahme des CS-Summenwertes, während nach der Radiotherapie mit einem LINAC der CS-Summenwert nur bei 78 % der Patienten anstieg und bei jeweils 11 % der Patienten unverändert blieb oder sich sogar verschlechterte. Der statistische Vergleich des Anteils der Patienten mit einem verbesserten CS-Summenwert zeigte keinen signifikanten Unterschied zwischen den beiden Behandlungsgruppen. Die Patienten

wurden zusätzlich in die 4 Leistungskategorien ‚ausgezeichnet' (CS-Summenwert 90-100), ‚gut' (CS-Summenwert 70-85), ‚mäßig' (CS-Summenwert 45-65), oder ‚schlecht' (CS-Summenwert 0-40) eingestuft. Vor der Radiotherapie wurde kein Patient als ‚ausgezeichnet' und nur 10 % als ‚gut' bewertet. Die Mehrheit der Patienten wurde zu diesem Analysenzeitpunkt mit 53 % in die Kategorie ‚mäßig' und 37 % als ‚schlecht' eingestuft. Vor der Radiotherapie war die Verteilung der Patienten in die 4 Kategorien in den beiden Studienarmen vergleichbar. Bei der Nachuntersuchung nach 3 Monaten wurden 47 % aller Patienten als ‚ausgezeichnet' eingestuft, jeweils 21 % als ‚gut' oder ‚mäßig' und die restlichen 11 % als ‚schlecht'. Nach der Orthovolt-Therapie wurden 56 % der Patienten in die Kategorie ‚ausgezeichnet', 22 % in die Kategorie ‚gut' und jeweils 11 % in die Kategorie ‚mäßig' oder ‚schlecht' eingestuft. Nach der Behandlung mit einem LINAC wurden 40 % der Patienten in die Kategorie ‚ausgezeichnet', 20 % in die Kategorie ‚gut', 30 % in die Kategorie ‚mäßig' und 10 % in die Kategorie ‚schlecht' eingestuft.

Zusammenfassend wurde in der **Publikation III** gezeigt, dass die Niedrigdosis-Radiotherapie des schmerzhaften Fersensporns mit einem Orthovoltgerät oder LINAC zu einer biodosimetrisch Nachweisbaren aber sehr geringen und ähnlichen Strahlenbelastung des Patienten bei einer gleichzeitig sehr guten und vergleichbaren therapeutischen Wirksamkeit führt.

4.2 Biomarker der intrinsischen Radiosensitivität und Suszeptibilität für akute Nebenwirkungen und Späteffekte der Radiotherapie

Die **Publikationen IV und V** widmeten sich der Untersuchung der Radiosensitivität und Vulnerabilität gegenüber den mit einer Radiotherapie assoziierten adversen Effekten im Zusammenhang mit der DNA-Reparatureffizienz im Normalgewebe, insbesondere den Risiken für die Entwicklung therapieassoziierter Sekundärmalignome.

4.2.1 Publikation IV

Spontane und strahleninduzierte Chromosomenaberrationen in primären Fibroblasten von Patienten mit pädiatrischen Primärtumoren und therapieassoziierten Sekundärmalignomen

In der **Publikation IV** wurde untersucht, ob sich primäre Hautfibroblasten von langzeitüberlebenden Kinderkrebspatienten, die ein Sekundärmalignom entwickelten (n=22) oder nicht (n=23), sowie von tumorfreien Spendern (n=22) in ihrer basalen chromosomalen Stabilität oder zellulären und chromosomalen Strahlensensitivität unterscheiden.

Die zelluläre Strahlenempfindlichkeit der primären Fibroblasten wurde mit dem klonogenen Überlebensassay nach Puck und Marcus [99] bestimmt. Die durchschnittliche

Plattierungseffizienz der Fibroblasten war zwischen den tumorfreien Spendern, ehemaligen Kinderkrebspatienten mit einem Primärmalignom und ehemaligen Kinderkrebspatienten mit einem Primärmalignom gefolgt von einem Sekundärmalignom vergleichbar. Nach der Strahlenexposition mit aufsteigenden Dosen bis 6 Gy in der G1-Phase des Zellzyklus war ebenfalls kein signifikanter Unterschied in den Fraktionen überlebender Zellen zwischen den Spendergruppen feststellbar.

Bei der im Rahmen der Analyse der chromosomalen Radiosensitivität nach einer Bestrahlung in der G1-Phase durchgeführten Bestimmung des durchschnittlichen basalen Niveaus chromosomaler Aberrationen in Metaphasen wurden keine signifikanten Unterschiede zwischen den drei Spendergruppen festgestellt. Die Untersuchung der Metaphasen nicht bestrahlter Fibroblasten zeigte jedoch eine auffällige spontane chromosomale Instabilität in zwei Spendern mit einem Sekundärmalignom. Einer der Spender wies eine außergewöhnlich hohe Anzahl numerischer und instabiler struktureller Aberrationen in 4 von 100 analysierten Metaphasen auf. Bei dem zweiten Spender wurden unter Anwendung der Methode der 24-Farben Fluoreszenz *in situ* Hybridisierung 6 verschiedene Translokationen und deren klonale Expansion in Zellpopulationen unterschiedlicher Kultivierungen der Zellen detektiert.

Nach der Bestrahlung in der G1-Phase des Zellzyklus mit 3 Gy Röntgenstrahlung wurden vergleichbare Raten strahleninduzierter Chromosomenaberrationen in ersten Mitosen nach der Exposition zwischen den Spendergruppen beobachtet. Die Ergebnisse der Analyse spontaner Chromatidaberrationen nach frühzeitiger Chromosomenkondensation in der G2-Phase waren ebenfalls zwischen den 3 Spendergruppen vergleichbar. Die Quantifizierung strahleninduzierter Chromatidaberrationen nach frühzeitiger Chromosomenkondensation in der G2-Phase 3 Stunden nach der Exposition mit 1 Gy Röntgenstrahlung ergab ebenfalls keine signifikanten Unterschiede zwischen den drei Spendergruppen.

Zusammenfassend konnte in der **Publikation IV** kein allgemeiner Unterschied in der chromosomalen Stabilität und Radiosensitivität des Normalgewebes zwischen Spendern, die eine hohe Anfälligkeit für sporadische Primärtumore im frühen Kindesalter oder Suszeptibilitäten für therapieassoziierte Sekundärmalignome sowie zu tumorfreien Spendern nachgewiesen werden. Auffällige sporadische zytogenetische Anomalien, die auf ein erhöhtes Tumorrisiko hindeuten, wurden nur bei zwei Spendern mit Sekundärmalignomen festgestellt.

4.2.2 Publikation V

Beeinträchtigte Reparatur von strahleninduzierten DNA-Doppelstrangbrüchen in Fanconi-Anämie Fibroblasten in G2

In der **Publikation V** wurde die Reparatur strahleninduzierter DSBs in primären Fibroblasten von Spendern mit dem DNA-Reparaturdefizienzsyndrom der Fanconi-Anämie untersucht. Bei der Fanconi-Anämie handelt es sich um ein sehr seltenes chromosomales Instabilitätssyndrom mit verschiedenen klinischen Merkmalen und sehr hohen Inzidenzen frühkindlicher Tumore. Obwohl der Fanconi-Anämie DNA-Reparaturstörungen zugrunde liegen und die Patienten häufig klinische Hypersensitivitäten gegenüber ionisierender Strahlung zeigen, ist die experimentelle Datenlage für die Reparatureffizienz strahleninduzierter DSBs immer noch sehr kontrovers. Es wurde daher eine grundlegende Analyse der Reparatur strahleninduzierter DSBs in der G1- und G2-Phase in Fibroblasten der Fanconi-Anämie Komplementationsgruppen A, C, D1 (*breast cancer associated 2* – BRCA2), D2, E, F, G und P (SLX4) im Vergleich zu normalen humanen Fibroblasten durchgeführt. DNA-Schäden wurden als γH2AX, 53BP1 oder RPA Foci in Kombination mit Zellzyklusmarkern nach der Bestrahlung mit Röntgenstrahlung in der G1- und G2-Phase des Zellzyklus quantifiziert. Zytogenetische Analysen wurden an ersten Mitosen nach der Bestrahlung in der G1-Phase des Zellzyklus und durch die vorzeitige Chromosomenkondensation nach der Exposition in der G2-Phase durchgeführt. Darüber hinaus wurde die Rolle des c-NHEJ und des alt-NHEJ für die Reparatur strahleninduzierter DSBs untersucht.

Die zellzyklusspezifische Quantifizierung von γH2AX und 53BP1 Foci bis 24 Stunden nach der Bestrahlung mit 2 Gy Röntgenstrahlung in der G1-Phase des Zellzyklus zeigte eine vergleichbare Reparatur strahleninduzierter DSBs zwischen gesunden Spendern und Fanconi-Anämie Patienten. Im Gegensatz dazu wurde in den Fibroblasten der Fanconi-Anämie Patienten 6 Stunden nach der Bestrahlung mit 2 Gy in der G2-Phase des Zellzyklus eine höhere Anzahl residualer strahleninduzierter γH2AX und 53BP1 Foci beobachtet. Die Retention von 53BP1 an strahleninduzierten DSBs war dabei wesentlich deutlicher und für alle Fanconi-Anämie Komplementationsgruppen außer P (SLX4) signifikant gegenüber gesunden Spendern erhöht. Da die HR den relevanten Mechanismus für die Reparatur strahleninduzierter DSBs in der langsamen Reparaturkomponente der G2-Phase darstellt [100], wurde die Abnahme strahleninduzierter RPA Foci 6 Stunden nach der Exposition als Indikator für eine erfolgreiche HR-abhängige Reparatur strahleninduzierter DSBs in der G2-Phase analysiert. Das Niveau strahleninduzierter RPA Foci pro G2-Zelle war jedoch nur in Fanconi-Anämie Fibroblasten der

Komplementationsgruppe D1 (BRCA2) mit einem bekannten Defekt in der HR [100] signifikant im Vergleich zu gesunden Spendern erhöht.

Die Rate strahleninduzierter Chromosomenaberrationen in ersten Mitosen 48 Stunden nach der Exposition mit 3 Gy Röntgenstrahlung in der G1-Phase zeigte im Einklang mit den Daten der DSB-Reparaturfoci keinen signifikanten Unterschied zwischen gesunden Spendern und Fanconi-Anämie Patienten. Um die Reparatur strahleninduzierter DSBs in der langsamen Reparaturkomponente der G2-Phase im chromosomalen Kontext zu untersuchen, wurden Chromatidaberrationen durch die frühzeitige Chromosomenkondensation in der G2-Phase 8 Stunden nach der Exposition mit 3 Gy Röntgenstrahlung analysiert. Dabei wurde eine signifikant erhöhte Rate von strahleninduzierten Chromatidbrüchen pro G2-Zelle nur für die Fanconi-Anämie Komplementationsgruppe D1 (BRCA2) im Vergleich zu gesunden Spendern beobachtet. Die Rate der strahleninduzierten Chromatidaustausche in G2-Zellen unterlag insgesamt großen Varianzen, zeigte aber in den Fanconi-Anämie Komplementationsgruppen A, D1 (BRCA2), D2, E, F und G signifikante Zunahmen im Vergleich zu gesunden Spendern.

Im Hinblick auf die erhöhten Raten strahleninduzierter Chromatidaustausche als Resultat einer fehlerbehafteten DSB-Reparatur in der G2-Phase, wurde die Rolle des DNA-PK-abhängigen c-NHEJ und des PARP-abhängigen alt-NHEJ bei der Reparatur strahleninduzierter DSBs und der Bildung von Chromatidaustauschen in Fibroblasten von gesunden Spendern und ausgewählten FA-Komplementationsgruppen untersucht. Die zytogenetische Analyse wurde 4 Stunden nach der Exposition mit 3 Gy Röntgenstrahlung bei gleichzeitiger Inhibierung der DNA-PK oder von PARP in der G2-Phase des Zellzyklus durchgeführt, in der alle relevanten DSB-Reparaturmechanismen für die Zelle verfügbar sind. Nur die Hemmung des DNA-PK-abhängigen c-NHEJ hatte eine Auswirkung auf die DSB-Reparatur, die sich in einer signifikanten Zunahme von Chromatidbrüchen und einem starken Rückgang von Chromatidaustauschen zeigte. Die Hemmung des PARP-abhängigen alt-NHEJ hatte keinen Einfluss auf die Reparatur von strahleninduzierten DSBs. Diese Ergebnisse wurden durch die Quantifizierung von strahleninduzierten γH2AX Foci in der G1- und G2-Phase 6 Stunden nach der Bestrahlung mit 2 Gy Röntgenstrahlung und der Inhibierung der DNA-PK oder von PARP bestätigt.

Zusammenfassend zeigen die Ergebnisse der **Publikation V** eine beeinträchtigte Reparatur strahleninduzierter DSBs in verschiedenen Komplementationsgruppen der Fanconi-Anämie, die auf die langsame Reparaturkomponente der G2-Phase beschränkt war und mit einem erhöhten Aufkommen von Chromatidaustauschen durch die Nutzung des fehlerbehafteten c-NHEJ einherging.

5 Diskussion

5.1 Biologische Dosimetrie nach der Radiotherapie

Zunächst wurde in der **Publikation I** überprüft, ob sich die Methode der sensitiven Quantifizierung von DSB-Reparaturfoci der phoshporylierten Histonvariante H2AX in peripheren Lymphozyten für die biologische Dosimetrie in der Radiotherapie sowie nach Strahlenunfällen eignet. Die Detektion von γH2AX Foci in peripheren Lymphozyten wurde bereits in Arbeiten anderer Autoren nach medizinischen Strahlenexpositionen angewendet (Übersicht in [81]). Die Datenlage für präzise geplante Strahlenexpositionen im Rahmen einer Radiotherapie war zum Zeitpunkt der Durchführung der vorliegenden Arbeiten noch unzureichend. In der **Publikation I** wurde nach bestem Wissen des Autors zudem erstmalig ein direkter Vergleich zwischen der Quantifizierung von DNA-Reparaturfoci und instabilen Chromosomenaberrationen in peripheren Lymphozyten nach radiotherapeutischen Teil- und Ganzkörperexpositionen durchgeführt.

Die wesentlich höhere Sensitivität der γH2AX Foci Quantifizierung im Vergleich zur Detektion von Chromosomenaberrationen bestätigte sich insbesondere durch den Nachweis von linearen Dosis-Wirkungs-Beziehungen zwischen den mittleren Raten an γH2AX Foci pro Lymphozyt und der berechneten Ganzkörper-Äquivalentdosis unmittelbar nach der Radiotherapie. Dieses Ergebnis steht im Einklang mit Publikationen, die ebenfalls Korrelationen von DNA-Reparaturfoci mit der Ganzkörper-Äquivalentdosis nach einer Radiotherapie [101, 102] oder mit dem Dosis-Längen-Produkt nach CT-Scans [78, 103-106] demonstrierten. Die Steigung des linearen Zusammenhangs strahleninduzierter γH2AX Foci pro Lymphozyt in Abhängigkeit der Ganzkörper-Äquivalentdosis unterschied sich in der **Publikation I** jedoch signifikant zwischen den Brustkrebs- und Prostatakrebspatienten. Sak *et al.* [101] zeigten bereits, dass die Steigung linearer Dosis-Wirkungs-Beziehungen für γH2AX Foci pro Lymphozyt nach der Radiotherapie verschiedener Tumorentitäten deutlich von der exponierten anatomischen Region beeinflusst wird, was mit Unterschieden in den regionalen und organabhängigen Blutvolumina begründet wurde. Zusätzlich zu diesem Einflussfaktor wurden in der **Publikation I** für die verschiedenen Tumorentitäten unterschiedliche Bestrahlungstechniken angewendet. Trotz dieser Unterschiede konnten für beide Tumorentitäten gute Abschätzungen der Ganzkörper-Äquivalentdosen erzielt werden, die basierend auf dem *ex vivo* generierten Referenzdatensatz kalkuliert wurden. Im Gegensatz dazu wurde die applizierte mittlere Tumordosis von 2 Gy bei Teilkörperexpositionen zu diesem Zeitpunkt nach der Radiotherapie sehr deutlich unterschätzt. Diese Beobachtung zeigte, dass unmittelbar nach einer

Teilkörperexposition eine venöse Blutprobe periphere Lymphozyten enthält, die im Durchschnitt nur mit 15-20 % der lokalen Tumordosis während der schnellen Zirkulation durch große Blutgefäße, wie die Aorta, Arterien oder Venen in der Peripherie des PTV exponiert wurden und daher die Dosisverteilung im Ganzkörpervolumen repräsentieren.

Die Persistenz strahleninduzierter γH2AX Foci in peripheren Lymphozyten wurde in der **Publikation I** erstmalig nach Teilkörperexpositionen im Rahmen einer Radiotherapie untersucht und zeigte nach 24 Stunden eine starke Abnahme im Einklang mit der ablaufenden DNA-Reparatur. Für Prostatakarzinompatienten bestand im Gegensatz zu Brustkrebspatientinnen aufgrund des größeren PTV, insbesondere bei einer Bestrahlung der Lymphabflusswege, auch 24 Stunden nach der Teilkörperbestrahlung noch eine Korrelation der durchschnittlichen Rate residualer γH2AX Foci pro Lymphozyt mit der Ganzkörper-Äquivalentdosis. Eine dosisproportionale Persistenz strahleninduzierter DNA-Reparaturfoci *in vivo* wurde zuvor nur in einer Arbeit von Redon *et al.* [107] in Lymphozyten von ganzkörperbestrahlten nicht-menschlichen Primaten bis 4 Tage nach der Exposition gezeigt. Die Dosisrekonstruktionen basierend auf der mittleren Rate von γH2AX Foci pro Lymphozyt 24 Stunden nach der Teilkörperbestrahlung führten zu einer Überschätzung der Ganzkörper-Äquivalentdosis, aber guten Annäherungen an die applizierte Teilkörperdosis.

Diese Ergebnisse stimmen mit den Analysen der strahleninduzierten Chromosomenaberrationen und den darauf basierenden Rekonstruktionen der Teilkörperdosen und der Ganzkörper-Äquivalentdosen überein. Während die durchschnittliche Rate strahleninduzierter γH2AX Foci pro Lymphozyt 24 Stunden nach der Teilkörperbestrahlung abnahm, stieg die Rate der Chromosomenaberrationen an. Somit wurden erst zu diesem späteren Zeitpunkt nach der heterogenen *in vivo* Bestrahlung die stärker strahlengeschädigten Lymphozyten im peripheren Blutstrom detektiert, die bei langsamer Mikrozirkulation in den engen Kapillargefäßen im PTV der vollen Tumordosis ausgesetzt waren. Diese Feststellung deckt sich mit der Kenntnis, dass eine vollständige Rezirkulation und Durchmischung von Lymphozyten im Durchschnitt 12 Stunden benötigt [77]. Die Zirkulationskinetik von Lymphozyten hat somit einen signifikanten Einfluss auf die Quantifizierung von DNA-Schadensmarkern in peripheren Lymphozyten nach Teilkörperexpositionen, insbesondere für die Detektion von stark strahlengeschädigten Zellen aus dem Tumorvolumen.

Durch die Präsenz und Detektion von Lymphozyten, die höheren Strahlendosen im Bereich der lokalen Tumordosen ausgesetzt waren, wurden 24 Stunden nach der ersten Fraktion für beide DNA-Schadensmarker bessere Approximationen der applizierten Teilkörperdosis erzielt, die Ganzkörper-Äquivalentdosis wurde allerdings überschätzt. Dies Widerspricht der Annahme,

dass bei einer global homogenen Lymphozytenverteilung nach einer Teilkörperexposition die physikalische Ganzkörper-Äquivalentdosis durch die Ausbeute an Chromosomenaberrationen in lokal exponierten Lymphozyten gut approximiert werden sollte. Roch-Lefèvre *et al.* [108] beschrieben zuvor jedoch ebenfalls eine Überschätzung der Ganzkörper-Äquivalentdosis für die Quantifizierung instabiler Chromosomenaberrationen nach der ersten Fraktion der Radiotherapie von Patienten mit Kopf-Hals-Tumoren. Diese Diskrepanz könnte möglicherweise auf eine hohe Konzentration von Lymphknoten und Blutgefäßen in der exponierten Teilkörperregion zurückzuführen sein, wie es in der **Publikation I** teilweise auch der Fall war. Vergleichbare Studien zeigten, dass selbst nach einer Normierung auf die unterschiedlichen Zielvolumina der Radiotherapie variierende Raten strahleninduzierter Chromosomenaberrationen in Abhängigkeit von der exponierten anatomischen Region detektiert wurden [109-111]. Bei homogenen Ganzkörperexpositionen spielen solche physiologischen Effekte jedoch keine ausschlaggebende Rolle mehr, da in der **Publikation I** für beide Methoden und Analysenzeitpunkte nach der Radiotherapie sehr gute Übereinstimmungen mit der applizierten Ganzkörperdosis festgestellt wurden. Zusammenfassend belegen unsere Daten, dass die Quantifizierung von γH2AX Foci in peripheren Lymphozyten zuverlässige Schätzungen von klinisch relevanten Ganzkörper-Äquivalentdosen nach einer einzelnen akuten Teilkörperbestrahlung oder sogar bis zu mehreren Stunden nach einer akuten Ganzkörperbestrahlung auf der Grundlage von *ex vivo* generierten Referenzdaten ermöglicht. Bei Teilkörperexpositionen unterliegen diese jedoch physiologischen sowie physikalisch-technischen Einflussfaktoren, die Berücksichtigung finden müssen.

In der **Publikation II** wurde die in der **Publikation I** etablierte Methodik und Expertise für einen biodosimetrischen Vergleich der Strahlenbelastung von Brustkrebspatientinnen, die mit unterschiedlichen Modalitäten der 3D-CRT oder der IMRT behandelt wurden, angewendet. Die verfügbare Literatur zur physikalischen Dosimetrie und entsprechende Modellierungsdaten zeigt bereits abweichende Verteilungen von niedrigen Strahlendosen außerhalb des Primärstrahls und PTV im Normalgewebe für verschiedene Techniken der Radiotherapie, die mit unterschiedlichen Risiken für radiogene Spätfolgen diskutiert werden [36, 67, 68, 74, 75, 112]. In Phantomstudien zur tangentialen Radiotherapie des Mammakarzinoms führte die Verwendung eines mechanischen Keilfilters für die Strahlformung zu 2,4- bis 3,3-fach höheren Niedrigdosisbelastungen außerhalb des PTV im Vergleich zu virtuellen Keilfiltern [87-89]. Für die Anwendung der IMRT ermittelten Ruben *et al.* [36] eine über 80 % höhere integrale Dosis außerhalb des PTV durch 3,7-fach gesteigerte MU im Vergleich zur 3D-CRT bei vergleichbaren Feldzahlen und -größen. Solche Messungen, wie auch die Abschätzungen peripherer Dosen

durch die Bestrahlungsplanungssoftware, sind jedoch häufig mit großen Unsicherheiten von bis zu 50 % behaftet [90-92]. Hier bietet die hochsensitive Quantifizierung strahleninduzierter DNA-Reparaturfoci in peripheren Lymphozyten eine vielversprechende Möglichkeit zur Abschätzung und den Vergleich der Niedrigdosisbelastung durch radiologische oder radiotherapeutische Strahlenexpositionen.

In einer Studie von Zwicker *et al.* [93] wurde ein biodosimetrischer Vergleich zwischen der 3D-CRT und der IMRT des Prostatakarzinoms durchgeführt. Dabei konnte jedoch keine signifikante Abweichung der mittleren Anzahl von γH2AX Foci pro Lymphozyt zwischen den Bestrahlungstechniken festgestellt werden. Unterschiede zeigten sich nur in Dosis-Lymphozyten-Histogrammen, die gut mit den variierenden Mustern der DVH der 3D-CRT und IMRT übereinstimmten und eine Reduktion der mittleren Dosisbelastung im Normalgewebe durch die IMRT bestätigten. Diese Ergebnisse bekräftigen die Feststellung aus der **Publikation I**, dass unmittelbar nach einer Teilkörperbestrahlung die Verteilung der strahleninduzierten DSBs in peripheren Lymphozyten die Dosisverteilung im Ganzkörpervolumen des Patienten repräsentiert. In einer darauffolgenden Studie verglichen Zwicker *et al.* [94] mit derselben Methodik die Anwendung der helikalen Tomotherapie und der *step-and-shoot* IMRT zur Behandlung des Prostatakarzinoms. Dabei war die mittlere Anzahl von γH2AX Foci pro Lymphozyt nach der Tomotherapie signifikant niedriger als nach der *step-and-shoot* IMRT. In den Dosis-Lymphozyten-Histogrammen zeigten nach der Tomotherapie im Vergleich zur *step-and-shoot* IMRT signifikant weniger Lymphozyten eine geringe Anzahl an γH2AX Foci und damit eine niedrige Dosisbelastung (<40 % der applizierten Dosis). Die Autoren diskutierten diese Abweichungen mit Unterschieden im konstruktiven Aufbau der verschiedenen Bestrahlungssysteme und variierenden physikalischen Parametern, z.B. einer 4,4-fach höheren Dosisrate für die Tomotherapie im Vergleich zur *step-and-shoot* IMRT.

Der Einfluss physikalisch-technischer Faktoren, die unabhängig vom PTV oder der Ganzkörper-Äquivalentdosis die Frequenz von DNA-Schadensindikatoren in peripheren Lymphozyten nach der Radiotherapie beeinflussen, wurde bis dahin jedoch nicht betrachtet und in der **Publikation II** eingehend untersucht. Um die Bedeutung der Dosisrate und damit der BOT der Radiotherapie auf die Ausbeute an strahleninduzierten DSBs in peripheren Lymphozyten zu analysieren und bestenfalls auszuschließen, wurden für die 3D-CRT des Mammakarzinoms mit einem mechanischen oder virtuellen Keilfilter jeweils Dosisraten von 3 und 6 Gy pro Minute angewendet und verglichen. Da sich die Leck- und Streustrahlung proportional zur Gesamtdosis des Primärstrahls verhält, sollte die integrale Dosis außerhalb des PTV nicht von einer variierenden Dosisleistung beeinflusst werden. Entgegen dieser Erwartung wurde jedoch ein

signifikanter Einfluss der BOT auf die zuvor auf die Ganzköper-Äquivalentdosis normierten mittleren Raten von γH2AX Foci pro Lymphozyt mit einer linearen Abhängigkeit festgestellt, auch wenn die gleiche Anzahl an MU appliziert wurde. Die IMRT mit der höchsten Anzahl an MU und damit der längsten BOT induzierte die höchste Rate an DNA-Schäden in peripheren Lymphozyten. Der in der **Publikation II** gefundene Einfluss der BOT auf das mittlere Niveau strahleninduzierter γH2AX Foci pro Lymphozyt könnte somit auch den ausschlaggebenden Faktor für die von Zwicker *et al.* [94] beschriebene niedrigere Rate von strahleninduzierten γH2AX Foci nach der Tomotherapie mit einer 4,4-fach höheren Dosisrate im Vergleich zur *step-and-shoot* IMRT bei der Behandlung des Prostatakarzinoms darstellen.

Im Einklang mit den früheren Beobachtungen von Zwicker *et al.* [93, 94] wurde in der **Publikation II** eine sehr gute Übereinstimmung der Verteilung strahleninduzierter γH2AX Foci in Lymphozyten mit der physikalischen Dosisverteilung im Ganzkörpervolumen entsprechend den DVH der Bestrahlungsplanungssoftware nachgewiesen. Der festgestellte Einfluss der BOT auf die Verteilung strahleninduzierter γH2AX Foci in Lymphozyten kann hierbei aber nicht ausgeschlossen werden und ist bei der Interpretation dieser Daten zu berücksichtigen.

Auch wenn aufgrund der in der **Publikation II** identifizierten physikalisch-technischen Störfaktoren der Radiotherapie auf die DNA-Schadensfrequenzen in peripheren Lymphozyten keine eindeutigen Unterschiede in der integralen Dosisbelastung des soliden Normalgewebes der Patienten durch periphere Niedrigdosen nachgewiesen werden konnten, zeigte diese Studie durch längere BOT eine Zunahme der Strahlenbelastung des Blutsystems, das ebenfalls einen klinisch sehr relevanten Normalgewebstyp darstellt. Eine strahleninduzierte Lymphopenie und Immunsuppression repräsentiert eine sehr kritische Nebenwirkung der Radiotherapie, die das Infektionsrisiko steigert und bei verschiedenen Tumorentitäten mit einem geringeren Gesamtüberleben korreliert [113-118]. Dieser Effekt kann sich insbesondere bei der Kombination von immunonkologischen Strategien und der immunstimulierenden Wirkung der Radiotherapie, die das antitumorale Potential des patienteneigenen Immunsystems nutzt, nachteilig auf den Therapieerfolg auswirken. Daher sollten hier möglichst Lymphozyten-aussparende Techniken der Radiotherapie zur Anwendung kommen [118, 119] und der in der **Publikation II** demonstrierte Effekt der BOT berücksichtigt werden.

Die in der **Publikation II** identifizierten Einflussfaktoren der Radiotherapie auf die DNA-Schadensmarker in peripheren Lymphozyten wurden in der darauffolgenden biodosimetrischen Studie zum Vergleich der integralen Dosisbelastung durch die Behandlung des schmerzhaften Fersensporns mit der Orthovoltherapie oder einem LINAC in der **Publikation III** durch eine bestmögliche Anpassung der Bestrahlungsparameter beider Techniken, wie der Feldgröße und

der Dosisrate, berücksichtigt. Für diese Form der Niedrigdosistherapie mit einer antiinflammatorischen und dadurch analgetischen Wirksamkeit [120] ist dies die bisher einzig bekannte biodosimetrische Studie zur Dosisbelastung der Patienten. Die Wahl eines Orthovoltgerätes oder LINAC für die Radiotherapie dieses Krankheitsbildes ist meist willkürlich und abhängig von der institutionellen Ausstattung in den etwa 340 Einrichtungen in Deutschland, die diese Therapieform durchführen. Für die Behandlung der etwa 10.000 Patienten jährlich besteht aber eine Prävalenz für die Radiotherapie mit einem LINAC, die mit einer besseren therapeutischen Wirksamkeit im Vergleich zur Orthovolttherapie diskutiert wird [95, 121]. Die Radiotherapie des Fersensporns und anderen benignen inflammatorischen Erkrankungen des Skelettsystems wird aufgrund des potentiellen Risikos für radiogene Späteffekte, die allerdings als sehr gering einzuschätzen und nahezu vernachlässigbar sind [122-126], fast ausschließlich im deutschsprachigen Raum bei Patienten über 40 Jahren angewendet.

Die Daten der **Publikation III** zeigen, dass die Radiotherapie des Fersensporns nur zu einem sehr geringen aber dennoch signifikanten Anstieg strahleninduzierter DSBs in peripheren Lymphozyten führte, der zwischen den beiden Bestrahlungstechniken vergleichbar war. Es wurde jedoch keine Korrelation der Raten strahleninduzierter γH2AX Foci pro Lymphozyt mit der Ganzkörper-Äquivalentdosis festgestellt, die sich im Bereich von 2.34-14.67 mSV bewegte und sich signifikant zwischen den Bestrahlungstechniken unterschied. Studien zur Niedrigdosisbelastung durch CT-Koronarangiographien zeigten, dass auch für sehr geringe effektive Strahlendosen zwischen 2.1-23.8 mSv lineare Dosis-Wirkungs-Beziehungen für strahleninduzierte γH2AX Foci in Lymphozyten sowie signifikante Unterschiede zwischen Protokollen mit variierenden Dosisbelastungen nachgewiesen werden können [78, 105, 127]. In der **Publikation III** wurde im Vergleich dazu jedoch ein wesentlicher kleinerer Dosisbereich für eine geringere Anzahl an Patienten abgedeckt.

Beide Therapiearme zeigten eine sehr gute und gleichwertige analgetische Wirksamkeit. Bisher wurde nur von Muecke *et al.* [95] eine retrospektive Studie über den langfristigen Behandlungserfolg der niedrig dosierten Radiotherapie von 502 Patienten mit schmerzhaftem Fersensporn, die entweder zweimal pro Woche mit einem LINAC oder dreimal pro Woche mit einem Orthovoltgerät behandelt wurden, durchgeführt. Die Patienten wurden dabei entweder mit 10 Fraktionen zu je 0,5 Gy oder 5-6 Fraktionen zu je 1 Gy mit einem LINAC oder mit 6 Fraktionen zu je 1 Gy mit einem Orthovoltgerät behandelt. Eine multivariate Analyse ergab dabei eine signifikant schlechtere Prognose für die Orthovolttherapie ohne einen Einfluss der Strahlendosis.

5.2 Biomarker der intrinsischen Radiosensitivität und Suszeptibilität für akute Nebenwirkungen und Späteffekte der Radiotherapie

In der **Publikation IV** wurde untersucht, ob ein Zusammenhang zwischen der Anfälligkeit für pädiatrische Primärmalignome oder therapieassoziierte Sekundärmalignome und einer Beeinträchtigung der DNA-Reparatur und folglich der Aufrechterhaltung der Genomstabilität nach genotoxischen Ereignissen in Form einer Strahlenexposition besteht.

Die Ätiologie für die große Mehrheit der sporadischen Krebserkrankungen im Kindesalter oder eine inhärente Suszeptibilität für therapieassoziierte Sekundärmalignome ist bisher nicht geklärt. Nur weniger als 10 % der pädiatrischen Krebserkrankungen können auf erbliche oder familiäre *de novo* Mutationen in prädisponierenden Genen mit hoher Penetranz zurückgeführt werden [26, 128-131]. Im Allgemeinen besteht die Annahme, dass genetische Veränderungen in der DNA-Schadensantwort mit niedriger oder mittlerer Penetranz und deren Interaktion die Risiken für die Entwicklung sporadischer Tumore im Kindesalter sowie für adverse Effekte genotoxischer Krebstherapien steigern [132-136]. Allerdings sind die Kausalitäten für die große Mehrheit der sporadischen Krebserkrankungen im Kindesalter oder eine inhärente Anfälligkeit für therapieassoziierte Sekundärmalignome bisher noch nicht geklärt und Biomarker für zellbasierte funktionale Testsysteme stehen in der klinischen Routine nicht zur Verfügung.

In den primären Fibroblasten unserer Fall-Kontroll-Studie, bestehend aus gematchten Langzeitüberlebenden eines päditarischen Primärmalignoms, Langzeitüberlebenden desselben pädiatrischen Primärmalignoms gefolgt von einem Sekundärmalignom und tumorfreien Spendern, konnten keine signifikanten Unterschiede im klonogenen Zellüberleben nach Bestrahlung sowie in den Raten spontaner oder strahleninduzierter instabiler Chromosomenaberrationen festgestellt werden. Auffällig waren lediglich spontane Chromosomenanomalien bei zwei Spendern mit einem Sekundärmalignom, die auf ein erhöhtes Tumorrisiko hinweisen.

Studien mit großen epidemiologischen Kohorten zeigten bereits einen Zusammenhang zwischen hohen Werten von spontanen Chromosomenaberrationen in Lymphozyten und dem Risiko für sporadische Tumore, das unabhängig von früheren Expositionen gegenüber Karzinogenen war [137, 138]. Zudem wurden in den vergangenen zwei Dekaden in einer Vielzahl von Studien Korrelationen zwischen erhöhten Raten strahleninduzierter Chromosomenaberrationen in Lymphozyten und dem sporadischen und familiären Auftreten verschiedener primärer Tumorentitäten etabliert, die auf eine höhere chromosomale Radiosensitivität unter Kindern und jungen Erwachsenen mit Krebserkrankungen hindeuten [139-152]. Auch weisen zytogenetische Auswertungen in somatischen Zellen von pädiatrischen

Krebspatienten darauf hin, dass eine konstitutionelle oder behandlungsbedingte genomische Instabilität die Entwicklung eines Sekundärmalignoms fördern kann [153-155]. Bislang wurde aber lediglich in einer Fall-Kontroll-Studie von Haddy *et al.* [156] die Reparaturkapazität für strahleninduzierte DSBs in lymphoblastoiden Zelllinien von langzeitüberlebenden Patienten mit pädiatrischen Tumoren, die ein Sekundärmailgnom entwickelten oder nicht, untersucht. In diese Studie wurden jedoch keine tumorfreien Kontrollen eingeschlossen. Dabei zeigten die Autoren höhere Raten basaler sowie residualer strahleninduzierter DSBs in langzeitüberlebenden Kinderkrebspatienten mit einem Sekundärmalignom, was mit einer beeinträchtigten DSB-Reparaturkapazität und einer dadurch erhöhten Suszeptibilität für therapieassoziierte primäre Folgeneoplasien diskutiert wurde. Diese Zusammenhänge konnten in der **Publikation IV** jedoch nicht bestätigt werden, was auf Unterschiede in der statistischen Aussagekraft, den untersuchten Zelltypen sowie Sensitivitäten der verwendeten biologischen Testsysteme zurückzuführen sein kann.

Um den Zusammenhang zwischen einer eingeschränkten DNA-Reparatur und dem Auftreten pädiatrischer Tumoren sowie klinischer Radiosensitivität eingehender zu untersuchen, wurde in der **Publikation V** eine detaillierte Analyse der Reparatur strahleninduzierter DSBs in primären Fibroblasten von Spendern des DNA-Reparaturdefizienzsyndroms der Fanconi-Anämie durchgeführt. Patienten mit Fanconi-Anämie zeigen aufgrund chromosomaler Instabilität hohe Inzidenzen sporadischer Tumore im frühen Kindesalter, bei deren Radiotherapie eine starke bis fatale Hypersensitivität gegenüber ionisierender Strahlung auftreten kann [157-162]. Die Daten zur Reparatur von *ex vivo* strahleninduzierten DSBs in Patienten mit einem dysfunktionalen Fanconi-Reparaturweg, der hauptsächlich für die replikationsassoziierte Reparatur von DNA-Quervernetzungen verantwortlich ist [163], sind jedoch sehr kontrovers. In den verfügbaren Studien mit verschiedenen Komplementationsgruppen der Fanconi-Anämie wurde nur in 65 % der Untersuchungen (n=26) eine eingeschränkte Reparatur strahleninduzierter DSBs beobachtet [82, 83, 164-182]. Bei einer selektiven Exposition von Zellpopulationen in der G1-Phase war diese in etwa der Hälfte der Untersuchungen (54 %, n=13), nach der Exposition asynchroner Zellpopulationen in 73 % der Untersuchungen (n=11) und nach der Exposition in der G2-Phase in allen Untersuchungen (n=2) beeinträchtigt. Zur Klärung dieser widersprüchlichen Datenlage wurde in der **Publikation V** eine detaillierte Analyse der Reparatur von strahleninduzierten DSBs in primären Hautfibroblasten der Fanconi-Anämie-Komplementationsgruppen A, C, D1 (BRCA2), D2, E, F, G und P (SLX4) im Vergleich zu gesunden Spendern nach selektiver Strahlenexposition und Analyse in der G1- oder G2-Phase durchgeführt. Dabei konnte für die Fanconi-Anämie-Patienten nur in der langsamen Reparaturkomponente der G2-Phase eine

beeinträchtigte und fehleranfälligere Reparatur strahleninduzierter DSBs nachgewiesen werden, insbesondere durch erhöhte Niveaus strahleninduzierter 53BP1 Foci und von Chromatidaustauschen. Eine fehlende Korrelation zwischen den erhöhten Raten an γH2AX oder 53BP1 Foci und Chromatidbrüchen in der G2-Phase in Fanconi-Anämie Fibroblasten könnte auf die wesentlich höhere Sensitivität der Detektion von DSB-Reparaturfoci im Vergleich zu zytogenetischen Methoden zurückzuführen sein. Allgemein wird dabei von einem Verhältnis von 1 zu 3-6 zwischen strahleninduzierten Chromatidbrüchen in G2-PCCs und γH2AX-Foci ausgegangen [183]. Die Beobachtung der Zunahme von 53BP1 Foci und von Chromatidaustauschen bei Fanconi-Anämie Patienten steht im Einklang mit der Rolle von 53BP1 als Antagonist von BRCA1 und damit als Suppressor der HR zugunsten der Nutzung des fehleranfälligeren c-NHEJ [184]. Die dominante Rolle des DNA-PK-abhängigen c-NHEJ für die Bildung von Chromatidaustauschen in der G2-Phase konnte durch den Einsatz von Inhibitoren gegen die DNA-PK oder PARP bestätigt werden. Chromosomale Rearrangements wie Chromatidaustausche sind in ihrer instabilen Form verantwortlich für die Entstehung von mitotischen Katastrophen und folglich den reproduktiven Zelltod oder bergen in transmissibler Form ein onkogenes Potential. Zudem ist der Fanconi-Anämie Reparaturweg einer der wichtigsten Mechanismen zur Behebung replikationsassoziierter DNA-Schäden, was die Radiosensitivität von aktiv proliferierenden Zellen und Geweben erheblich steigern kann. Daher ist es naheliegend, dass die in der **Publikation V** beschriebenen Veränderungen in der Reparatur strahleninduzierter DSBs und die Stimulierung von fehleranfälligerer Reparaturmechanismen in der langsamen Reparaturkomponente der G2-Phase zur Ausprägung der klinischen Strahlenüberempfindlichkeit und gesteigerte Risiken für therapieassoziierte Folgeneoplasien bei Fanconi-Anämie Patienten beiträgt.

6 Zusammenfassung

Die vorgestellten Arbeiten des Autors zeigen, dass biologische Marker strahleninduzierter DNA-Schäden in peripheren Lymphozyten nicht uneingeschränkt für biodosimetrische Dosisrekonstruktionen oder Vergleiche der integralen Strahlenbelastung des Patienten durch unterschiedliche klinische Expositionsszenarien genutzt werden können. Zu berücksichtigen sind dabei physiologische Einflussgrößen wie variierende Blutvolumina zwischen unterschiedlichen exponierten anatomischen Regionen sowie die Zirkulationskinetiken von Lymphozyten. Daneben spielen physikalisch-technische Variablen der Bestrahlung eine entscheidende Rolle, was insbesondere für die Bestrahlungsdauer erstmalig demonstriert wurde. Für zukünftige Studien mit dem Ziel eines biodosimetrischen Vergleichs zwischen Bestrahlungstechniken mit variierenden Dosisbelastungen der Patienten durch medizinische Expositionen muss daher eine bestmögliche Anpassung und Normierung dieser physiologischen und physikalisch-technischen Paramater erfolgen, um geringe Variationen in der integralen Belastung durch periphere Niedrigdosen detektieren zu können.

Im Hinblick auf die radiogenen Risiken einer Strahlentherapie lieferte die Untersuchung der Strahlenantwort im Surrogatgewebe einer sehr vulnerablen Population von langzeitüberleben Kindekrebspatienten mit Sekundärmalignomen keine Indikatoren für intrinsische oder strahlenassoziierte karzinogene Risiken und somit auch keine direkten Hinweise auf die beteiligten molekularen Mechanismen oder prädiktive Biomarker. Dahingegen wurde in Fanconi-Anämie Patienten mit einer hohen Anfälligkeit für radiogene Normalgewebstoxizitäten, aber einer noch nicht eindeutig geklärten Reparaturkapazität für strahleninduzierte DSBs, ein auf die langsame Reparaturkomponente der G2-Phase beschränkter Defekt nachgewiesen. Diese Ergebnisse unterstreichen die Notwendigkeit einer zellzyklusspezifischen Analyse der DSB-Reparatur, um die unterschiedlichen Beiträge verschiedener Reparaturmechanismen zu berücksichtigen und dadurch auch nur sehr gering ausgeprägte Veränderungen mit klinischer Relevanz für die intrinsische Radiosensitivität erfolgreich nachweisen zu können. Insgesamt liefern diese Daten wichtige Hinweise, dass DNA-Reparaturdefekte und die damit assoziierten Biomarker Indikatoren einer Vulnerabilität für schwere strahlenassoziierte akute Normalgewebstoxizitäten darstellen, wahrscheinlich aber nicht oder nur sehr eingeschränkt für radiogene Tumorrisiken als stochastische Spätfolgen einer Strahlenexposition in der Normalbevölkerung.

7 Abkürzungsverzeichnis

3D-CRT	*3-dimensional conformal radiotherapy*
53BP1	Tumorsuppressor-p53-bindendes Protein 1
AT	Ataxia telangiectasia
ATM	*Ataxia-telangiectasia mutated*
ATR	*Ataxia-telangiectasia and Rad3-related*
BLM	Bloom-Syndrom
BOT	*Beam-on time*
BRCA2	*Breast cancer associated 2*
alt-NHEJ	*Alternative non-homologous end joining*
c-NHEJ	*Canonical non-homologous end joining*
CS	*Calcaneodynie-score*
CT	Computertomographie
DNA	*Deoxyribonucleic acid*
DNA-PKcs	*DNA-dependent protein kinase catalytic subunit*
DSB	DNA-Doppelstrangbruch
DVH	Dosis-Volumen-Histogramm
HR	Homologe Rekombination
IGRT	*Image-guided radiotherapy*
IMRT	Intensitätsmodulierte Radiotherapie
LINAC	*Linear accelerator*
MU	*Monitor units*
NBS	Nijmegen-breakage-Syndrom
PARP	Poly (ADP-Ribose) Polymerase
PIKK	*Phosphatidylinositol 3-kinase-related kinases*
PTV	*Planning target volume*
RPA	Replikationsprotein A
VMAT	*Volumetric intensity modulated arc therapy*
WRN	Werner-Syndrom

8 Literaturverzeichnis

1. Zahnreich, S., et al., *Biodosimetry Based on gamma-H2AX Quantification and Cytogenetics after Partial- and Total-Body Irradiation during Fractionated Radiotherapy.* Radiat Res, 2015. 183(4): p. 432-46.

2. Zahnreich, S., et al., *Quantification of Radiation Biomarkers in Leukocytes of Breast Cancer Patients Treated with Different Modalities of 3D-CRT or IMRT.* Radiat Res, 2016. 186(5): p. 508-519.

3. Zahnreich, S., et al., *Spontaneous and Radiation-Induced Chromosome Aberrations in Primary Fibroblasts of Patients With Pediatric First and Second Neoplasms.* Front Oncol, 2020. 10: p. 1338.

4. Zahnreich, S., et al., *Radiation-induced DNA double-strand breaks in peripheral leukocytes and therapeutic response of heel spur patients treated by orthovoltage X-rays or a linear accelerator.* Strahlenther Onkol, 2020. 196(12): p. 1116-1127.

5. Zahnreich, S., et al., *Compromised repair of radiation-induced DNA double-strand breaks in Fanconi anemia fibroblasts in G2.* DNA Repair (Amst), 2020. 96: p. 102992.

6. Nikjoo, H., et al., *Computational modelling of low-energy electron-induced DNA damage by early physical and chemical events.* Int J Radiat Biol, 1997. 71(5): p. 467-83.

7. Hall, E.J. and A.J. Giaccia, *Radiobiology for the Radiologist.* Lipponcott, Williams & Wilkins, Philadelphia, 2012.

8. Rajewsky, B., *The limits of the target theory of the biological action of radiation.* Br J Radiol, 1952. 25(298): p. 550-2.

9. Munro, T.R., *The relative radiosensitivity of the nucleus and cytoplasm of Chinese hamster fibroblasts.* Radiat Res, 1970. 42(3): p. 451-70.

10. Vignard, J., G. Mirey, and B. Salles, *Ionizing-radiation induced DNA double-strand breaks: a direct and indirect lighting up.* Radiother Oncol, 2013. 108(3): p. 362-9.

11. Roots, R., G. Kraft, and E. Gosschalk, *The formation of radiation-induced DNA breaks: the ratio of double-strand breaks to single-strand breaks.* Int J Radiat Oncol Biol Phys, 1985. 11(2): p. 259-65.

12. Khanna, K.K. and S.P. Jackson, *DNA double-strand breaks: signaling, repair and the cancer connection.* Nat Genet, 2001. 27(3): p. 247-54.

13. Kieffer, S.R. and N.F. Lowndes, *Immediate-Early, Early, and Late Responses to DNA Double Stranded Breaks.* Front Genet, 2022. 13: p. 793884.

14. Ensminger, M. and M. Löbrich, *One end to rule them all: Non-homologous end-joining and homologous recombination at DNA double-strand breaks.* Br J Radiol, 2020. 93(1115): p. 20191054.

15. Lobrich, M., et al., *gammaH2AX foci analysis for monitoring DNA double-strand break repair: strengths, limitations and optimization.* Cell Cycle, 2010. 9(4): p. 662-9.

16. Biehs, R., et al., *DNA Double-Strand Break Resection Occurs during Non-homologous End Joining in G1 but Is Distinct from Resection during Homologous Recombination.* Mol Cell, 2017. 65(4): p. 671-684 e5.

17. Durante, M., et al., *From DNA damage to chromosome aberrations: joining the break.* Mutat Res, 2013. 756(1-2): p. 5-13.

18. Deriano, L. and D.B. Roth, *Modernizing the nonhomologous end-joining repertoire: alternative and classical NHEJ share the stage.* Annu Rev Genet, 2013. 47: p. 433-55.

19. Iliakis, G., T. Murmann, and A. Soni, *Alternative end-joining repair pathways are the ultimate backup for abrogated classical non-homologous end-joining and homologous recombination repair: Implications for the formation of chromosome translocations.* Mutat Res Genet Toxicol Environ Mutagen, 2015. 793: p. 166-75.

20. Savage, J.R., *Classification and relationships of induced chromosomal structual changes.* J Med Genet, 1976. 13(2): p. 103-22.

21. Maier, P., et al., *Cellular Pathways in Response to Ionizing Radiation and Their Targetability for Tumor Radiosensitization.* Int J Mol Sci, 2016. 17(1).

22. Hall, E.J. and G.A. Freyer, *The molecular biology of radiation carcinogenesis.* Basic Life Sci, 1991. 58: p. 3-19; discussion 19-25.

23. Rothkamm, K. and M. Lobrich, *Misrepair of radiation-induced DNA double-strand breaks and its relevance for tumorigenesis and cancer treatment (review).* Int J Oncol, 2002. 21(2): p. 433-40.

24. Waespe, N., et al., *Cancer predisposition syndromes as a risk factor for early second primary neoplasms after childhood cancer - A national cohort study.* Eur J Cancer, 2021. 145: p. 71-80.

25. Pollard, J.M. and R.A. Gatti, *Clinical radiation sensitivity with DNA repair disorders: an overview.* Int J Radiat Oncol Biol Phys, 2009. 74(5): p. 1323-31.

26. Brodeur, G.M., et al., *Pediatric Cancer Predisposition and Surveillance: An Overview, and a Tribute to Alfred G. Knudson Jr.* Clin Cancer Res, 2017. 23(11): p. e1-e5.

27. Kuhlen, M., et al., *Family-based germline sequencing in children with cancer.* Oncogene, 2019. 38(9): p. 1367-1380.

28. Dutzmann, C.M., et al., *Cancer in Children With Fanconi Anemia and Ataxia-Telangiectasia-A Nationwide Register-Based Cohort Study in Germany.* J Clin Oncol, 2022. 40(1): p. 32-39.

29. Ferlay, J., et al., *Estimating the global cancer incidence and mortality in 2018: GLOBOCAN sources and methods.* Int J Cancer, 2019. 144(8): p. 1941-1953.

30. Delaney, G., et al., *The role of radiotherapy in cancer treatment: estimating optimal utilization from a review of evidence-based clinical guidelines.* Cancer, 2005. 104(6): p. 1129-37.

31. Micke, O., et al., *Low-Dose Radiation Therapy for Benign Painful Skeletal Disorders: The Typical Treatment for the Elderly Patient?* Int J Radiat Oncol Biol Phys, 2017. 98(4): p. 958-963.

32. Steel, G.G., T.J. McMillan, and J.H. Peacock, *The 5Rs of radiobiology.* Int J Radiat Biol, 1989. 56(6): p. 1045-8.

33. Van der Kogel, A. and M. Joiner, *Basic Clinical Radiobiology.* Taylor & Francis. ISBN 978-1-4441-7963-7, 2018.

34. Bucci, M.K., A. Bevan, and M. Roach, 3rd, *Advances in radiation therapy: conventional to 3D, to IMRT, to 4D, and beyond.* CA Cancer J Clin, 2005. 55(2): p. 117-34.

35. Koka, K., et al., *Technological Advancements in External Beam Radiation Therapy (EBRT): An Indispensable Tool for Cancer Treatment.* Cancer Manag Res, 2022. 14: p. 1421-1429.

36. Ruben, J.D., et al., *A comparison of out-of-field dose and its constituent components for intensity-modulated radiation therapy versus conformal radiation therapy: implications for carcinogenesis.* Int J Radiat Oncol Biol Phys, 2011. 81(5): p. 1458-64.

37. Wang, B. and X.G. Xu, *Measurements of non-target organ doses using MOSFET dosemeters for selected IMRT and 3D CRT radiation treatment procedures.* Radiat Prot Dosimetry, 2008. 128(3): p. 336-42.

38. Kase, K.R., et al., *Measurements of dose from secondary radiation outside a treatment field.* Int J Radiat Oncol Biol Phys, 1983. 9(8): p. 1177-83.

39. Durante, M. and J. Flanz, *Charged particle beams to cure cancer: Strengths and challenges.* Semin Oncol, 2019. 46(3): p. 219-225.

40. Jermann, M., *Particle therapy statistics in 2014.* Int. J. Part. Ther. 2, 50–54 2015. 2: p. 50-54.

41. Subedi, P., et al., *Ionizing Radiation Protein Biomarkers in Normal Tissue and Their Correlation to Radiosensitivity: A Systematic Review.* J Pers Med, 2021. 11(2).

42. Holmberg, O., et al., *Current issues and actions in radiation protection of patients.* Eur J Radiol, 2010. 76(1): p. 15-9.

43. Wang, K. and J.E. Tepper, *Radiation therapy-associated toxicity: Etiology, management, and prevention.* CA Cancer J Clin, 2021. 71(5): p. 437-454.

44. Grant, E.J., et al., *Solid Cancer Incidence among the Life Span Study of Atomic Bomb Survivors: 1958-2009.* Radiat Res, 2017. 187(5): p. 513-537.

45. Preston, D.L., et al., *Cancer incidence in atomic bomb survivors. Part III. Leukemia, lymphoma and multiple myeloma, 1950-1987.* Radiat Res, 1994. 137(2 Suppl): p. S68-97.

46. Shapiro, C.L., *Cancer Survivorship.* N Engl J Med, 2018. 379(25): p. 2438-2450.

47. Newhauser, W.D. and M. Durante, *Assessing the risk of second malignancies after modern radiotherapy.* Nat Rev Cancer, 2011. 11(6): p. 438-48.

48. Kumar, S., *Second malignant neoplasms following radiotherapy.* Int J Environ Res Public Health, 2012. 9(12): p. 4744-59.

49. Zahnreich, S. and H. Schmidberger, *Childhood Cancer: Occurrence, Treatment and Risk of Second Primary Malignancies.* Cancers (Basel), 2021. 13(11).

50. Dracham, C.B., A. Shankar, and R. Madan, *Radiation induced secondary malignancies: a review article.* Radiat Oncol J, 2018. 36(2): p. 85-94.

51. Ng, A.K., et al., *Secondary malignancies across the age spectrum.* Semin Radiat Oncol, 2010. 20(1): p. 67-78.

52. Berrington de Gonzalez, A., et al., *Proportion of second cancers attributable to radiotherapy treatment in adults: a cohort study in the US SEER cancer registries.* Lancet Oncol, 2011. 12(4): p. 353-60.

53. Curtis, R.E., et al., *New Malignancies Among Cancer Survivors: SEER Cancer Registries, 1973-2000.* National Cancer Institute, NIH Publ., 2006. No. 05-5302.

54. Yock, T.I. and P.A. Caruso, *Risk of second cancers after photon and proton radiotherapy: a review of the data.* Health Phys, 2012. 103(5): p. 577-85.

55. Taylor, C., et al., *Estimating the Risks of Breast Cancer Radiotherapy: Evidence From Modern Radiation Doses to the Lungs and Heart and From Previous Randomized Trials.* J Clin Oncol, 2017. 35(15): p. 1641-1649.

56. Wall, B.F., et al., *Radiation Risks from Medical X-ray Examinations as a Function of the Age and Sex of the Patient.* Health Protection Agency, Centre for Radiation, Chemical and Environmental Hazards, 2011(HPA-CRCE-028).

57. von Koppenfels, R. and G. Thiede, *Mehrfachmalignome.* Strahlenther, 1973. 146: p. 619-32.

58. Warren, S. and O. Gates, *Multiple primary malignant tumors, a survey of the literature and statistical study.* Am J Cancer, 1932(16): p. 1358–1414.

59. Dörr, W. and T. Herrmann, *Second primary tumors after radiotherapy for malignancies. Treatment-related parameters.* Strahlenther Onkol, 2002. 178(7): p. 357-62.

60. Dörr, W. and T. Herrmann, *Cancer induction by radiotherapy: dose dependence and spatial relationship to irradiated volume.* J Radiol Prot, 2002. 22(3a): p. A117-21.

61. Brenner, D.J., et al., *Second malignancies in prostate carcinoma patients after radiotherapy compared with surgery.* Cancer, 2000. 88(2): p. 398-406.

62. Travis, L.B., et al., *Second malignant neoplasms and cardiovascular disease following radiotherapy.* Health Phys, 2014. 106(2): p. 229-46.

63. Barnett, G.C., et al., *Normal tissue reactions to radiotherapy: towards tailoring treatment dose by genotype.* Nat Rev Cancer, 2009. 9(2): p. 134-42.

64. Dörr, W., *Spätfolgen nach Radiotherapie.* Der Onkologe, 2018. 24: p. 797-801.

65. Brenner, D.J., et al., *Prostate radiotherapy is associated with second cancers in many organs, not just the colorectum.* Gastroenterology, 2005. 129(2): p. 773-4; author reply 774-5.

66. Baxter, N.N., et al., *Increased risk of rectal cancer after prostate radiation: a population-based study.* Gastroenterology, 2005. 128(4): p. 819-24.

67. Abo-Madyan, Y., et al., *Second cancer risk after 3D-CRT, IMRT and VMAT for breast cancer.* Radiother Oncol, 2014. 110(3): p. 471-6.

68. Hall, E.J. and C.S. Wuu, *Radiation-induced second cancers: the impact of 3D-CRT and IMRT.* Int J Radiat Oncol Biol Phys, 2003. 56(1): p. 83-8.

69. Jahreiß, M.C., et al., *Impact of Advanced Radiotherapy on Second Primary Cancer Risk in Prostate Cancer Survivors: A Nationwide Cohort Study.* Front Oncol, 2021. 11: p. 771956.

70. Xiang, M., D.T. Chang, and E.L. Pollom, *Second cancer risk after primary cancer treatment with three-dimensional conformal, intensity-modulated, or proton beam radiation therapy.* Cancer, 2020. 126(15): p. 3560-3568.

71. Journy, N.M., et al., *Second Primary Cancers After Intensity-Modulated vs 3-Dimensional Conformal Radiation Therapy for Prostate Cancer.* JAMA Oncol, 2016. 2(10): p. 1368-1370.

72. Habash, M., et al., *Clinical and Functional Assays of Radiosensitivity and Radiation-Induced Second Cancer.* Cancers (Basel), 2017. 9(11).

73. Andreassen, C.N., et al., *Radiogenomics - current status, challenges and future directions.* Cancer Lett, 2016. 382(1): p. 127-136.

74. Schneider, U., et al., *Estimation of radiation-induced cancer from three-dimensional dose distributions: Concept of organ equivalent dose.* Int J Radiat Oncol Biol Phys, 2005. 61(5): p. 1510-5.

75. Zwahlen, D.R., et al., *Effect of intensity-modulated pelvic radiotherapy on second cancer risk in the postoperative treatment of endometrial and cervical cancer.* Int J Radiat Oncol Biol Phys, 2009. 74(2): p. 539-45.

76. Sproull, M. and K. Camphausen, *State-of-the-Art Advances in Radiation Biodosimetry for Mass Casualty Events Involving Radiation Exposure.* Radiat Res, 2016. 186(5): p. 423-435.

77. IAEA, *Cytogenetic analysis for radiation dose assessment: a manual. Technical reports series.* 2001. 405.

78. Lobrich, M., et al., *In vivo formation and repair of DNA double-strand breaks after computed tomography examinations.* Proc Natl Acad Sci U S A, 2005. 102(25): p. 8984-9.

79. Rothkamm, K. and M. Löbrich, *Evidence for a lack of DNA double-strand break repair in human cells exposed to very low x-ray doses.* Proc Natl Acad Sci U S A, 2003. 100(9): p. 5057-62.

80. Rothkamm, K., et al., *DNA damage foci: Meaning and significance.* Environ Mol Mutagen, 2015. 56(6): p. 491-504.

81. Redon, C.E., et al., *γ-H2AX and other histone post-translational modifications in the clinic.* Biochim Biophys Acta, 2012. 1819(7): p. 743-56.

82. Rube, C.E., et al., *DNA repair alterations in children with pediatric malignancies: novel opportunities to identify patients at risk for high-grade toxicities.* Int J Radiat Oncol Biol Phys, 2010. 78(2): p. 359-69.

83. Schuler, N., et al., *DNA-damage foci to detect and characterize DNA repair alterations in children treated for pediatric malignancies.* PLoS One, 2014. 9(3): p. e91319.

84. Lloyd, D.C., R.J. Purrott, and G.W. Dolphin, *Chromosome aberration dosimetry using human lymphocytes in simulated partial body irradiation.* CA Cancer J Clin, 1973. 18(3): p. 421-31.

85. Sasaki, M.S. and H. Miyata, *Biological dosimetry in atomic bomb survivors.* Nature, 1968. 220(5173): p. 1189-93.

86. Redon, C.E., et al., *Q(gamma-H2AX), an analysis method for partial-body radiation exposure using gamma-H2AX in nonhuman primate lymphocytes.* Radiat Meas, 2011. 46(9): p. 877-881.

87. Woo, T.C., et al., *Body radiation exposure in breast cancer radiotherapy: impact of breast IMRT and virtual wedge compensation techniques.* Int J Radiat Oncol Biol Phys, 2006. 65(1): p. 52-8.

88. Ludwig, V., et al., *Comparison of wedge versus segmented techniques in whole breast irradiation: effects on dose exposure outside the treatment volume.* Strahlenther Onkol, 2008. 184(6): p. 307-12.

89. Chang, S.X., et al., *A comparison of different intensity modulation treatment techniques for tangential breast irradiation.* Int J Radiat Oncol Biol Phys, 1999. 45(5): p. 1305-14.

90. Wang, L. and G.X. Ding, *The accuracy of the out-of-field dose calculations using a model based algorithm in a commercial treatment planning system.* Phys Med Biol, 2014. 59(13): p. N113-28.

91. Huang, J.Y., et al., *Accuracy and sources of error of out-of field dose calculations by a commercial treatment planning system for intensity-modulated radiation therapy treatments.* J Appl Clin Med Phys, 2013. 14(2): p. 4139.

92. Howell, R.M., et al., *Accuracy of out-of-field dose calculations by a commercial treatment planning system.* Phys Med Biol, 2010. 55(23): p. 6999-7008.

93. Zwicker, F., et al., *Biological in-vivo measurement of dose distribution in patients' lymphocytes by gamma-H2AX immunofluorescence staining: 3D conformal- vs. step-and-shoot IMRT of the prostate gland.* Radiat Oncol, 2011. 6: p. 62.

94. Zwicker, F., et al., *In vivo measurement of dose distribution in patients' lymphocytes: helical tomotherapy versus step-and-shoot IMRT in prostate cancer.* J Radiat Res, 2015. 56(2): p. 239-47.

95. Muecke, R., et al., *Demographic, clinical and treatment related predictors for event-free probability following low-dose radiotherapy for painful heel spurs - a retrospective multicenter study of 502 patients.* Acta Oncol, 2007. 46(2): p. 239-46.

96. Heyd, R., et al., *Radiation therapy for painful heel spurs: results of a prospective randomized study.* Strahlenther Onkol, 2007. 183(1): p. 3-9.

97. Rowe, C.R., H.T. Sakellarides, and P.E. Freeman, *Fractures of the Os Calcis A Long-Term Follow-up Study of 146 Patients.* JAMA, 1963. 184: p. 3.

98. Johns, H.E., *Introduction to physics of radiobiology.* Thomas, Springfield, 1961. 2nd edn: p. 353-7.

99. Puck, T.T. and P.I. Marcus, *Action of x-rays on mammalian cells.* J Exp Med, 1956. 103(5): p. 653-66.

100. Beucher, A., et al., *ATM and Artemis promote homologous recombination of radiation-induced DNA double-strand breaks in G2.* EMBO J, 2009. 28(21): p. 3413-27.

101. Sak, A., et al., *gamma-H2AX foci formation in peripheral blood lymphocytes of tumor patients after local radiotherapy to different sites of the body: dependence on the dose-distribution, irradiated site and time from start of treatment.* Int J Radiat Biol, 2007. 83(10): p. 639-52.

102. Werbrouck, J., et al., *Early biomarkers related to secondary primary cancer risk in radiotherapy treated prostate cancer patients: IMRT versus IMAT.* Radiother Oncol, 2013. 107(3): p. 377-81.

103. Brand, M., et al., *X-ray induced DNA double-strand breaks in coronary CT angiography: Comparison of sequential, low-pitch helical and high-pitch helical data acquisition.* Eur J Radiol, 2011.

104. Beels, L., et al., *Dose-length product of scanners correlates with DNA damage in patients undergoing contrast CT.* Eur J Radiol, 2011.

105. Kuefner, M.A., et al., *Effect of CT scan protocols on x-ray-induced DNA double-strand breaks in blood lymphocytes of patients undergoing coronary CT angiography.* Eur Radiol, 2010. 20(12): p. 2917-24.

106. May, M.S., et al., *Induction and repair of DNA double-strand breaks in blood lymphocytes of patients undergoing (1)(8)F-FDG PET/CT examinations.* Eur J Nucl Med Mol Imaging, 2012. 39(11): p. 1712-9.

107. Redon, C.E., et al., *The use of gamma-H2AX as a biodosimeter for total-body radiation exposure in non-human primates.* PLoS One, 2010. 5(11): p. e15544.

108. Roch-Lefèvre, S., et al., *Cytogenetic assessment of heterogeneous radiation doses in cancer patients treated with fractionated radiotherapy.* Br J Radiol, 2010. 83(993): p. 759-66.

109. Matsuoka, A., et al., *Chromosomal aberrations detected by chromosome painting in lymphocytes from cancer patients given high doses of therapeutic X-rays.* J Radiat Res, 1996. 37(4): p. 257-65.

110. Sreedevi, B., et al., *Chromosome aberration analysis in radiotherapy patients and simulated partial body exposures: biological dosimetry for non-uniform exposures.* Radiat Prot Dosimetry, 2001. 94(4): p. 317-22.

111. Matsubara, S., M.S. Sasaki, and T. Adachi, *Dose-response relationship of lymphocyte chromosome aberrations in locally irradiated persons.* J Radiat Res, 1974. 15(4): p. 189-96.

112. Kry, S.F., et al., *The calculated risk of fatal secondary malignancies from intensity-modulated radiation therapy.* Int J Radiat Oncol Biol Phys, 2005. 62(4): p. 1195-203.

113. Grassberger, C., et al., *Differential Association Between Circulating Lymphocyte Populations With Outcome After Radiation Therapy in Subtypes of Liver Cancer.* Int J Radiat Oncol Biol Phys, 2018. 101(5): p. 1222-1225.

114. Karantanos, T., et al., *The absolute lymphocyte count can predict the overall survival of patients with non-small cell lung cancer on nivolumab: a clinical study.* Clin Transl Oncol, 2019. 21(2): p. 206-212.

115. Diehl, A., et al., *Relationships between lymphocyte counts and treatment-related toxicities and clinical responses in patients with solid tumors treated with PD-1 checkpoint inhibitors.* Oncotarget, 2017. 8(69): p. 114268-114280.

116. Suzuki, R., et al., *Prognostic Significance of Total Lymphocyte Count, Neutrophil-to-lymphocyte Ratio, and Platelet-to-lymphocyte Ratio in Limited-stage Small-cell Lung Cancer.* Clin Lung Cancer, 2019. 20(2): p. 117-123.

117. Cho, Y., et al., *Impact of Treatment-Related Lymphopenia on Immunotherapy for Advanced Non-Small Cell Lung Cancer.* Int J Radiat Oncol Biol Phys, 2019. 105(5): p. 1065-1073.

118. Kleinberg, L., et al., *Radiotherapy, Lymphopenia, and Host Immune Capacity in Glioblastoma: A Potentially Actionable Toxicity Associated With Reduced Efficacy of Radiotherapy.* Neurosurgery, 2019. 85(4): p. 441-453.

119. Koukourakis, M.I. and A. Giatromanolaki, *Lymphopenia and intratumoral lymphocytic balance in the era of cancer immuno-radiotherapy.* Crit Rev Oncol Hematol, 2021. 159: p. 103226.

120. Frey, B., et al., *Modulation of inflammation by low and high doses of ionizing radiation: Implications for benign and malign diseases.* Cancer Lett, 2015. 368(2): p. 230-7.

121. Kriz, J., et al., *Updated strategies in the treatment of benign diseases-a patterns of care study of the german cooperative group on benign diseases.* Adv Radiat Oncol, 2018. 3(3): p. 240-244.

122. Surenkok, S., et al., *Heel spur radiotherapy and radiation carcinogenesis risk estimation.* Radiat Med, 2006. 24(8): p. 573-6.

123. Ott, O.J., et al., *DEGRO guidelines for the radiotherapy of non-malignant disorders. Part II: Painful degenerative skeletal disorders.* Strahlenther Onkol, 2015. 191(1): p. 1-6.

124. Leer, J.W., P. van Houtte, and H. Seegenschmiedt, *Radiotherapy of non-malignant disorders: where do we stand?* Radiother Oncol, 2007. 83(2): p. 175-7.

125. Jansen, J.T., et al., *Estimation of the carcinogenic risk of radiotherapy of benign diseases from shoulder to heel.* Radiother Oncol, 2005. 76(3): p. 270-7.

126. Damber, L., et al., *A cohort study with regard to the risk of haematological malignancies in patients treated with x-rays for benign lesions in the locomotor system. I. Epidemiological analyses.* Acta Oncol, 1995. 34(6): p. 713-9.

127. Rothkamm, K., et al., *Leukocyte DNA damage after multi-detector row CT: a quantitative biomarker of low-level radiation exposure.* Radiology, 2007. 242(1): p. 244-51.

128. Jones, D.T.W., et al., *Molecular characteristics and therapeutic vulnerabilities across paediatric solid tumours.* Nat Rev Cancer, 2019. 19(8): p. 420-438.

129. Gröbner, S.N., et al., *The landscape of genomic alterations across childhood cancers.* Nature, 2018. 555(7696): p. 321-327.

130. Zhang, J., K.E. Nichols, and J.R. Downing, *Germline Mutations in Predisposition Genes in Pediatric Cancer.* N Engl J Med, 2016. 374(14): p. 1391.

131. Mody, R.J., et al., *Integrative Clinical Sequencing in the Management of Refractory or Relapsed Cancer in Youth.* Jama, 2015. 314(9): p. 913-25.

132. Chistiakov, D.A., N.V. Voronova, and P.A. Chistiakov, *Genetic variations in DNA repair genes, radiosensitivity to cancer and susceptibility to acute tissue reactions in radiotherapy-treated cancer patients.* Acta Oncol, 2008. 47(5): p. 809-24.

133. Kuhne, M., et al., *A double-strand break repair defect in ATM-deficient cells contributes to radiosensitivity.* Cancer Res, 2004. 64(2): p. 500-8.

134. Palumbo, E., et al., *Individual Radiosensitivity in Oncological Patients: Linking Adverse Normal Tissue Reactions and Genetic Features.* Front Oncol, 2019. 9: p. 987.

135. Cazier, J.B. and I. Tomlinson, *General lessons from large-scale studies to identify human cancer predisposition genes.* J Pathol, 2010. 220(2): p. 255-62.

136. Vodicka, P., et al., *Interactions of DNA repair gene variants modulate chromosomal aberrations in healthy subjects.* Carcinogenesis, 2015. 36(11): p. 1299-306.

137. Bonassi, S., et al., *Chromosomal aberrations in lymphocytes predict human cancer independently of exposure to carcinogens. European Study Group on Cytogenetic Biomarkers and Health.* Cancer Res, 2000. 60(6): p. 1619-25.

138. Bonassi, S., et al., *Chromosomal aberration frequency in lymphocytes predicts the risk of cancer: results from a pooled cohort study of 22 358 subjects in 11 countries.* Carcinogenesis, 2008. 29(6): p. 1178-83.

139. Baeyens, A., et al., *Chromosomal radiosensitivity in breast cancer patients with a known or putative genetic predisposition.* Br J Cancer, 2002. 87(12): p. 1379-85.

140. Baria, K., et al., *Chromosomal radiosensitivity in young cancer patients: possible evidence of genetic predisposition.* Int J Radiat Biol, 2002. 78(5): p. 341-6.

141. Bondy, M.L., et al., *Mutagen sensitivity and risk of gliomas: a case-control analysis.* Cancer Res, 1996. 56(7): p. 1484-6.

142. Bondy, M.L., et al., *Gamma-radiation sensitivity and risk of glioma.* J Natl Cancer Inst, 2001. 93(20): p. 1553-7.

143. Curwen, G.B., et al., *G(2) chromosomal radiosensitivity in Danish survivors of childhood and adolescent cancer and their offspring.* Br J Cancer, 2005. 93(9): p. 1038-45.

144. Knight, R.D., et al., *X-ray-induced chromatid damage in relation to DNA repair and cancer incidence in family members.* Int J Cancer, 1993. 54(4): p. 589-93.

145. Papworth, R., et al., *Sensitivity to radiation-induced chromosome damage may be a marker of genetic predisposition in young head and neck cancer patients.* Br J Cancer, 2001. 84(6): p. 776-82.

146. Parshad, R., K.K. Sanford, and G.M. Jones, *Chromatid damage after G2 phase x-irradiation of cells from cancer-prone individuals implicates deficiency in DNA repair.* Proc Natl Acad Sci U S A, 1983. 80(18): p. 5612-6.

147. Patel, R.K., et al., *DNA repair proficiency in breast cancer patients and their first-degree relatives.* Int J Cancer, 1997. 73(1): p. 20-4.

148. Riches, A.C., et al., *Chromosomal radiosensitivity in G2-phase lymphocytes identifies breast cancer patients with distinctive tumour characteristics.* Br J Cancer, 2001. 85(8): p. 1157-61.

149. Scott, D., et al., *Radiation-induced micronucleus induction in lymphocytes identifies a high frequency of radiosensitive cases among breast cancer patients: a test for predisposition?* Br J Cancer, 1998. 77(4): p. 614-20.

150. Scott, D., et al., *Increased chromosomal radiosensitivity in breast cancer patients: a comparison of two assays.* Int J Radiat Biol, 1999. 75(1): p. 1-10.

151. Scott, D., et al., *Genetic predisposition in breast cancer.* Lancet, 1994. 344(8934): p. 1444.

152. Terzoudi, G.I., et al., *Increased G2 chromosomal radiosensitivity in cancer patients: the role of cdk1/cyclin-B activity level in the mechanisms involved.* Int J Radiat Biol, 2000. 76(5): p. 607-15.

153. Bakshi, S.R., et al., *Chromosomal aberrations in young cancer patients.* Cancer Genet Cytogenet, 1999. 115(2): p. 114-7.

154. Frias, S., et al., *Nonclonal Chromosome Aberrations and Genome Chaos in Somatic and Germ Cells from Patients and Survivors of Hodgkin Lymphoma.* Genes (Basel), 2019. 10(1).

155. Chin, T.F., et al., *Nonclonal Chromosomal Aberrations in Childhood Leukemia Survivors.* Fetal Pediatr Pathol, 2018. 37(4): p. 243-253.

156. Haddy, N., et al., *Repair of ionizing radiation-induced DNA damage and risk of second cancer in childhood cancer survivors.* Carcinogenesis, 2014. 35(8): p. 1745-9.

157. Alter, B.P., *Radiosensitivity in Fanconi's anemia patients.* Radiother Oncol, 2002. 62(3): p. 345-7.

158. Bremer, M., et al., *Fanconi's anemia and clinical radiosensitivity - Report on two adult patients with locally advanced solid tumors treated by radiotherapy.* Strahlentherapie Und Onkologie, 2003. 179(11): p. 748-+.

159. Burnet, N.G. and J.H. Peacock, *Normal cellular radiosensitivity in an adult Fanconi anaemia patient with marked clinical radiosensitivity.* Radiother Oncol, 2002. 62(3): p. 350-1; author reply 351-2.

160. Marcou, Y., et al., *Normal cellular radiosensitivity in an adult Fanconi anaemia patient with marked clinical radiosensitivity.* Radiother Oncol, 2001. 60(1): p. 75-9.

161. Gluckman, E., *Radiosensitivity in Fanconi anemia: application to the conditioning for bone marrow transplantation.* Radiother Oncol, 1990. 18 Suppl 1: p. 88-93.

162. Birkeland, A.C., et al., *Postoperative clinical radiosensitivity in patients with fanconi anemia and head and neck squamous cell carcinoma.* Arch Otolaryngol Head Neck Surg, 2011. 137(9): p. 930-4.

163. Ceccaldi, R., et al., *The Fanconi anaemia pathway: new players and new functions.* Nat Rev Mol Cell Biol, 2016. 17(6): p. 337-49.

164. Higurashi, M. and P.E. Conen, *In vitro chromosomal radiosensitivity in Fanconi's anemia.* Blood, 1971. 38(3): p. 336-42.

165. Sasaki, M.S. and A. Tonomura, *A high susceptibility of Fanconi's anemia to chromosome breakage by DNA cross-linking agents.* Cancer Res, 1973. 33(8): p. 1829-36.

166. Heddle, J.A., et al., *Sensitivity to five mutagens in Fanconi's anemia as measured by the micronucleus method.* Cancer Res, 1978. 38(9): p. 2983-8.

167. Bigelow, S.B., J.M. Rary, and M.A. Bender, *G2 chromosomal radiosensitivity in Fanconi's anemia.* Mutat Res, 1979. 63(1): p. 189-99.

168. Fornace, A.J., Jr., J.B. Little, and R.R. Weichselbaum, *DNA repair in a Fanconi's anemia fibroblast cell strain.* Biochim Biophys Acta, 1979. 561(1): p. 99-109.

169. Duckworth-Rysiecki, G. and A.M. Taylor, *Effects of ionizing radiation on cells from Fanconi's anemia patients.* Cancer Res, 1985. 45(1): p. 416-20.

170. Parshad, R., K.K. Sanford, and G.M. Jones, *Chromosomal radiosensitivity during the G2 cell-cycle period of skin fibroblasts from individuals with familial cancer.* Proc Natl Acad Sci U S A, 1985. 82(16): p. 5400-3.

171. Darroudi, F., et al., *G2 radiosensitivity of cells derived from cancer-prone individuals.* Mutat Res, 1995. 328(1): p. 83-90.

172. Gibbons, B., et al., *Retinoblastoma in association with the chromosome breakage syndromes Fanconi's anaemia and Bloom's syndrome: clinical and cytogenetic findings.* Clin Genet, 1995. 47(6): p. 311-7.

173. Barquinero, J.F., et al., *Cytogenetic sensitivity of three Fanconi anemia heterozygotes to bleomycin and ionizing radiation.* Cancer Genet Cytogenet, 2001. 124(1): p. 80-3.

174. Digweed, M., et al., *Attenuation of the formation of DNA-repair foci containing RAD51 in Fanconi anaemia.* Carcinogenesis, 2002. 23(7): p. 1121-6.

175. Djuzenova, C., M. Flentje, and P.N. Plowman, *Radiation response in vitro of fibroblasts from a fanconi anemia patient with marked clinical radiosensitivity.* Strahlenther Onkol, 2004. 180(12): p. 789-97.

176. Casado, J.A., et al., *Non-homologous end-joining defect in fanconi anemia hematopoietic cells exposed to ionizing radiation.* Radiat Res, 2005. 164(5): p. 635-41.

177. Mohseni-Meybodi, A., H. Mozdarani, and S. Mozdarani, *DNA damage and repair of leukocytes from Fanconi anaemia patients, carriers and healthy individuals as measured by the alkaline comet assay.* Mutagenesis, 2009. 24(1): p. 67-73.

178. Mohseni-Meybodi, A., H. Mozdarani, and P. Vosough, *Cytogenetic sensitivity of G0 lymphocytes of Fanconi anemia patients and obligate carriers to mitomycin C and ionizing radiation.* Cytogenet Genome Res, 2007. 119(3-4): p. 191-5.

179. Leskovac, A., et al., *Fanconi anemia is characterized by delayed repair kinetics of DNA double-strand breaks.* Tohoku J Exp Med, 2010. 221(1): p. 69-76.

180. Leskovac, A., et al., *Radiation-induced mitotic catastrophe in FANCD2 primary fibroblasts.* Int J Radiat Biol, 2014. 90(5): p. 373-81.

181. Liu, Q., et al., *Disruption of SLX4-MUS81 Function Increases the Relative Biological Effectiveness of Proton Radiation.* Int J Radiat Oncol Biol Phys, 2016. 95(1): p. 78-85.

182. Francies, F.Z., et al., *Diagnosis of Fanconi Anaemia by ionising radiation- or mitomycin C-induced micronuclei.* DNA Repair (Amst), 2018. 61: p. 17-24.

183. Deckbar, D., et al., *Chromosome breakage after G2 checkpoint release.* J Cell Biol, 2007. 176(6): p. 749-55.

184. Bunting, S.F., et al., *53BP1 inhibits homologous recombination in Brca1-deficient cells by blocking resection of DNA breaks.* Cell, 2010. 141(2): p. 243-54.

9 Nachdrucke der Originalpublikationen der kumulativen Habilitationsschrift

9.1 Publikation I

Biodosimetry Based on γ-H2AX Quantification and Cytogenetics after Partial- and Total-Body Irradiation during Fractionated Radiotherapy

RADIATION RESEARCH **183**, 432–446 (2015)
0033-7587/15 $15.00

DOI: 10.1667/RR13911.1

Biodosimetry Based on γ-H2AX Quantification and Cytogenetics after Partial- and Total-Body Irradiation during Fractionated Radiotherapy

Sebastian Zahnreich,[a,1] Anne Ebersberger,[a] Bernd Kaina[b] and Heinz Schmidberger[a]

[a] *Department of Radiation Oncology and Radiotherapy, and* [b] *Department of Toxicology, University Medical Center Johannes Gutenberg University Mainz, 55131 Mainz, Germany*

Zahnreich, S., Ebersberger, A., Kaina, B. and Schmidberger, H. Biodosimetry Based on γ-H2AX Quantification and Cytogenetics after Partial- and Total-Body Irradiation during Fractionated Radiotherapy. *Radiat. Res.* 183, 432–446 (2015).

The aim of this current study was to quantitatively describe radiation-induced DNA damage and its distribution in leukocytes of cancer patients after fractionated partial- or total-body radiotherapy. Specifically, the impact of exposed anatomic region and administered dose was investigated in breast and prostate cancer patients receiving partial-body radiotherapy. DNA double-strand breaks (DSBs) were quantified by γ-H2AX immunostaining. The frequency of unstable chromosomal aberrations in stimulated lymphocytes was also determined and compared with the frequency of DNA DSBs in the same samples. The frequency of radiation-induced DNA damage was converted into dose, using *ex vivo* generated calibration curves, and was then compared with the administered physical dose. This study showed that 0.5 h after partial-body radiotherapy the quantity of radiation-induced γ-H2AX foci increased linearly with the administered equivalent whole-body dose for both tumor entities. Foci frequencies dropped 1 day thereafter but proportionality to the equivalent whole-body dose was maintained. Conversely, the frequency of radiation-induced cytogenetic damage increased from 0.5 h to 1 day after the first partial-body exposure with a linear dependence on the administered equivalent whole-body dose, for prostate cancer patients only. Only γ-H2AX foci assessment immediately after partial-body radiotherapy was a reliable measure of the expected equivalent whole-body dose. Local tumor doses could be approximated with both assays after one day. After total-body radiotherapy satisfactory dose estimates were achieved with both assays up to 8 h after exposure. In conclusion, the quantification of radiation-induced γ-H2AX foci, but not cytogenetic damage in peripheral leukocytes was a sensitive and rapid biodosimeter after acute heterogeneous irradiation of partial body volumes that was able to primarily assess the absorbed equivalent whole-body dose. © 2015 by Radiation Research Society

INTRODUCTION

Exposure to therapeutic or accidental ionizing radiation has the potential to induce serious short- and long-term adverse health effects in humans (*1*, *2*). Therefore, the assessment of radiation dose and exposure scenario by measuring the radiation-induced modification of suitable biological molecules for dosimetry is crucial for estimating: the magnitude of radiation-induced damage to exposed individuals, the expected clinical outcomes, and the potential need to initiate medical countermeasures (*3*). Cytogenetic analysis and in particular the scoring of dicentric chromosomes (dic) in peripheral lymphocytes continues to be the ''gold standard'' of biological dosimetry, but low sensitivity and the long time-consuming analysis required limit the applicability of the assay in the routine clinic and after large-scale radiation accidents (*4*). A far more sensitive and rapid radiation biosensor may be the detection of the phosphorylated histone variant γ-H2AX by immunostaining as a surrogate marker of radiation-induced DNA double-strand breaks (DSB) (*5*). The quantity of γ-H2AX signals per cell has been shown to be proportional to the number of DSBs, and to also increase linearly with radiation dose after *in vitro* and *in vivo* exposure (*6*). Visualization of discrete nuclear foci by fluorescence microscopy 30 min postirradiation is highly sensitive (*7*) with a detection threshold of a few mGy (*8*) and each focus corresponding to a DSB (*9*). A major drawback for retrospective biodosimetry is the fast γ-H2AX signal decline with proceeding DSB repair (*10*).

The γ-H2AX foci assay has been applied in numerous *in vivo* studies to monitor radiation-induced DNA damage after radiodiagnostic or radiotherapeutic procedures in humans [reviewed in (*11*)] or in biodosimetric approaches using animals (*12–14*). However, it has thus far been implemented in only a limited number of studies to attempt to correlate the quantity of DSBs in lymphocytes with the

Editor's note. The online version of this article (DOI: 10.1667/RR13911.1) contains supplementary information that is available to all authorized users.

[1] Address for correspondence: Department of Radiation Oncology and Radiotherapy, University Medical Center Johannes Gutenberg University Mainz, Langenbeckstrasse 1, 55131 Mainz, Germany; e-mail: sebastian.zahnreich@unimedizin-mainz.de.

administered physical dose after external beam radiation therapy (*6, 15, 16*). Immediately after local external beam radiation therapy, the frequency of radiation-induced γ-H2AX foci in lymphocytes has been shown to follow a linear dependence on the equivalent whole-body dose, however, the average number and distribution per cell vary with lymphocyte density and kinetics of blood circulation in the exposed anatomic region (*6*). In addition, attempts at γ-H2AX foci quantitation in lymphocytes of patients treated with comparable planning target volumes (PTV) for the same tumor entity, standardizing the physiological variables, revealed differences between radiation therapy techniques in the dose to lymphocyte distribution in accordance with the expected distribution of dose in the normal tissue as predicted by physical dosimetry (*15*). These studies demonstrate the potential for the application of the γ-H2AX foci assay during radiotherapy as a reliable dosimeter to assess the biologically relevant radiation burden of the patient, however the confounding impact of the physiological and radiation-related parameters on the γ-H2AX foci assay has not yet been fully elucidated, and further *in vivo* validation is necessary.

Elimination of tumor cells is the first priority in radiation therapy, but the improvement of therapeutic efficiency during the past decades and the resultant extended survival of cancer patients increase the risk of radiation-induced delayed effects. This will require better biological monitoring of radiation dose that may allow the reduction of dose to healthy tissue in patients during radiation therapy (*17*). Furthermore, the γ-H2AX foci assay may help to identify radiosensitive individuals who have an increased risk for developing severe normal tissue toxicities in the radiologic routine (*8*).

In addition to its application in a clinical setting, where a well defined physical dose is administered to the patient, biodosimetry is important for estimating exposure after a radiation accident, and providing valuable information about the absorbed biological dose and its distribution in the body. The usefulness of the γ-H2AX assay as a rapid biodosimetric triage tool in emergency situations was recently tested in scrap metal workers who were accidentally exposed to radiation (*18*) and in *ex vivo* simulated scenarios (*19–21*), emphasizing its potential application for the rapid identification of severely exposed individuals after acute exposure.

In the current study we investigated the influence of planning target volume size in different anatomic regions on the quantity and distribution of radiation-induced DNA damage detected as γ-H2AX signal or unstable chromosomal aberrations in leukocytes of cancer patients after partial- or total-body exposure during fractionated radiation therapy. Blood was obtained before and at fixed times postirradiation. *Ex vivo* generated calibration curves were used to convert the quantity of DNA damage after irradiation into physical dose for direct comparison with the administered physical dose according to three-dimensional (3D) treatment planning. To account for individual radiosensitivity, the level of DNA damage of each donor was quantified in *ex vivo* exposed blood prior to irradiation.

MATERIALS AND METHODS

Patients

Our study was comprised of 101 cancer patients who were treated at the Department of Radiotherapy at the University Medical Centre Mainz (Mainz, Germany) and 14 apparently healthy donors (HDs). All participants were recruited from November 2011 to February 2014. All donors signed an informed consent form approved by the local ethics committee. Different groups of patients were included in the study to investigate the influence of irradiated body-volume at different anatomic sites after radiotherapy. Partial-body irradiation (PBI) was administered to 62 breast cancer (BC) patients (60 unilateral and 2 bilateral) and 31 prostate cancer (PC) patients. Total-body irradiation (TBI) was administered to 5 patients with acute myeloid leukemia (AML, 1 relapse), 2 with acute lymphoid leukemia (ALL) and 1 with mantle cell lymphoma (MCL). The median age of the patients was 63 years with a range from 19–80 years. Of the breast cancer patients, 5 received neoadjuvant chemotherapy and 14 received adjuvant chemotherapy composed of different combinations of the following drugs: 5-fluoro-uracyle, epirubicine, cyclophosphamide, docetaxel and paclitaxel. Three breast cancer patients had previously received radiation treatment: two had been treated for breast cancer with external photons or intraoperative electrons 13 years or 7 weeks before the current radiation treatment, respectively; and the third patient had been treated with external photons for a heel spur at an unknown date. All AML patients received induction chemotherapy composed of the following: cytarabine and daunorubicine in combination with thioguanine or midastaurine, followed by consolidation chemotherapy composed of cytarabine with danaurobicine or mitoxantrone. For one AML patient this treatment was followed by an additional salvage therapy with cytarabine and mitoxantrone. One AML case was possibly the result of radioiodine therapy for thyroid cancer 18 years ago. All ALL patients underwent chemotherapy based on the GMALL protocol (*22*), with an induction and re-induction composed of the following drugs: dexamethasone, cyclophosphamide, incristine, daunorubicine, methotrexate, asparaginase, cytosine arabinoside, 6-MP, VP16 and VM26. Furthermore, all included ALL patients received prophylactic cranial irradiation with a cumulative dose of 24 Gy delivered in 5 daily fractions of 2 Gy per week at least 4 months before the current TBI. The MCL patient received chemotherapy with cyclophosphamide, doxorubicine, vincristine, prednisone/dexamethasone, cytarabine and cisplatin according to the CHOP/DHAP-protocol (*23*), followed by peripheral blood stem cell transplantation. Every patient underwent a computed tomography (CT) scan (Brilliance CT-Big Bore, Phillips Healthcare, Andover, MA) about 1 week prior to the start of radiation therapy for 3D treatment planning by the Eclipse™ software (Varian Medical Systems Inc., Palo Alto, CA). All PBI patients were irradiated with 5 daily fractions per week and an average single tumor dose of 2 Gy per fraction applied at an average dose rate of 6 Gy per min. Subsets of prostate and breast cancer patients received additional radiation treatment of lymph nodes. Another subgroup of breast cancer patients were treated by a hypofractionated regime with a single tumor dose of 2.67 Gy per fraction. For detailed information see Supplementary Table S1 (http://dx.doi.org/10.1667/RR13911.1.S1). Prostate cancer patients were treated with intensity-modulated radiotherapy (RapidArc®, Varian Medical Systems). Breast cancer patients were treated with tangential 3D-conformal radiotherapy (3D-CRT). TBI was performed by anterior-posterior 3D-CRT. TBI patients received twice-daily 2 Gy fractions given at a dose rate of 0.5–1 Gy per min each that were separated by a recovery period of at least 6 h. Linear accelerators used in this study were Oncor (Siemens, Munich,

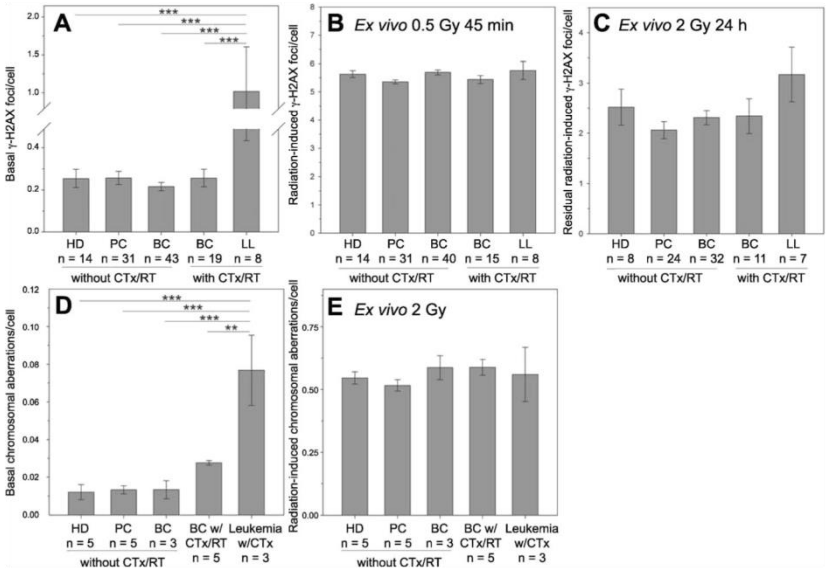

FIG. 1. The average basal and *ex vivo* radiation-induced yield of γ-H2AX foci (panels A, B and C) or unstable chromosomal aberrations (panels D and E) per cell in blood from healthy donors (HD), breast cancer (BC), prostate cancer (PC) and leukemia/lymphoma (LL) patients with or without a previous chemo- (CTx) or radiotherapy (RT). Numbers of analyzed donors (n) are indicated. Error bars represent the standard error of the mean. Pairwise statistical comparison between multiple groups was performed by one-way ANOVA Holm-Sidak method (*$P < 0.05$, **$P < 0.01$, ***$P < 0.001$).

Germany), Clinac® DHX (Varian Medical Systems) and a Unique™ (Varian Medical Systems). All patients were treated with 6 MV photon beams.

Blood Sampling and Leukocyte Isolation

Venous blood was collected in vacuum containers (Li-Heparin Monovette®, Sarstedt, Nümbrecht, Germany). Blood samples from patients treated with PBI were drawn immediately before radiotherapy, 30 min and 24 h after the start of the first fraction of radiation and 30 min after the start of the last fraction of radiation. Blood samples from patients treated with TBI were drawn immediately before and 60 min and 6–8 h after the start of the first radiation treatment. Blood samples taken from HDs or cancer patients before radiation therapy were X irradiated or mock treated (see Ex Vivo Irradiation of Blood section below). Immediately after *ex vivo* irradiation the samples were placed in a water bath at 37°C and transported to the laboratory within 5 min. Blood (1 ml) was diluted with 4 ml X-VIVO™ 15 media (Lonza Group Ltd., Basel, Switzerland) preheated to 37°C and incubated at 37°C, 5% CO_2 in a humidified atmosphere up to 8 h postirradiation until leukocyte separation. All *ex vivo* incubations exceeding 8 h had to be performed with isolated leukocytes to prevent hemolysis. Blood obtained from cancer patients after radiation therapy was immediately placed on ice, transported within 5 min to the laboratory and 1 ml of chilled whole blood was diluted with 4 ml X-VIVO 15 media (Lonza) precooled to 0–4°C. For leukocyte isolation the suspension was transferred to a LeucoSep® centrifuge tube (Greiner Bio-one) containing Histopaque®-1077 (Sigma-Aldrich® LLC, St. Louis, MO) separation media. Leukocytes were separated by density gradient centrifugation and washed in phosphate buffered saline (PBS). All steps were done at 0–4°C to block DNA repair processes and minimize γ-H2AX dephosphorylation. Thereafter cells were fixed and immunostained for γ-H2AX quantification. The average total time at 0–4°C from the start of blood collection until fixation of leukocytes was 30 min.

Ex Vivo Irradiation of Blood

To generate *ex vivo* calibration curves for the calculation of physical doses based on the quantity of DNA damage and to investigate the individual basal yield as well as *ex vivo* induction and repair of DSBs, blood samples that were drawn from HDs or cancer patients prior to radiation therapy were homogeneously exposed to 6 MV X rays from a linear accelerator (Oncor, Siemens) given at a dose rate of 3 Gy/min and ambient temperature or were mock treated, i.e., kept for the same time in the accelerator control room.

Ex vivo calibration curves. *Ex vivo* calibration curves for the quantification of radiation-induced γ-H2AX signal by fluorescence microscopy or flow cytometry were generated according to the method described by Horn *et al.* (*24*). Blood samples from 14 HDs and 6 of the 101 recruited cancer patients were exposed to a range of X-ray doses, and leukocytes were isolated at several time points from 45 min up to 48 h after exposure as described above. For cytogenetic analysis a calibration curve was generated after the exposure of whole blood from 2 HDs to a range of X-ray doses up to 2 Gy and scoring of unstable chromosomal aberrations in first post-exposure mitoses (<1 Gy: 1,000, 1 Gy: 500 and >1 Gy: 250 metaphases per HD).

Ex vivo radiosensitivity. The patient's individual *ex vivo* radiosensitivity was assessed in blood samples that were obtained prior to radiation therapy and irradiated *ex vivo*. The initial number of radiation-induced foci was scored 45 min after 0.5 Gy irradiation. The number of residual radiation-induced foci and frequency of radiation-induced chromosomal aberrations were scored 24 h after 2 Gy irradiation

Fixation, Staining and Scoring of γ-H2AX Foci

Isolated leukocytes were fixed in 3.7% formaldehyde/PBS for 10 min at 4°C and spotted onto slides using Cellspin (Heraeus). Slides

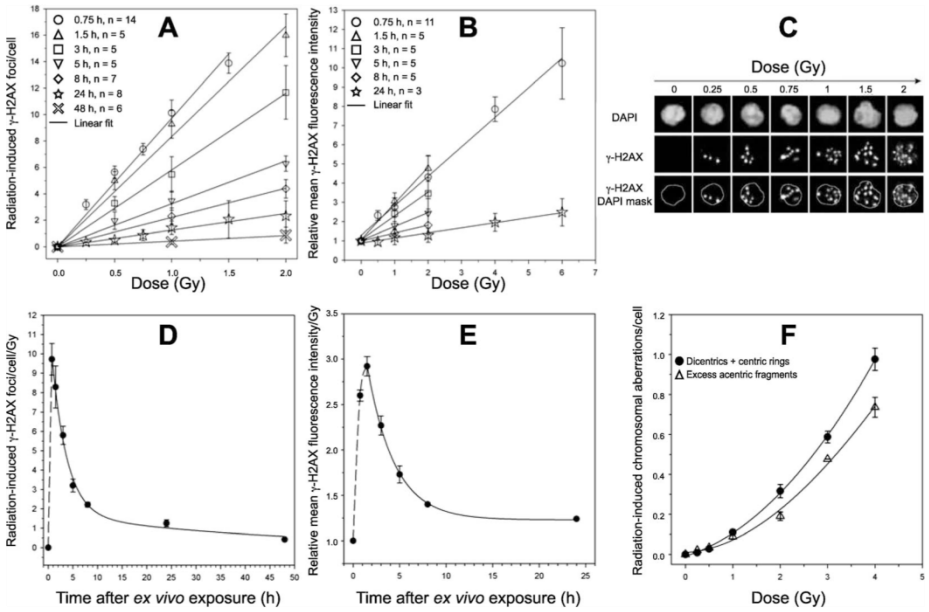

FIG. 2. *Ex vivo* generated calibration curves for radiation-induced γ-H2AX signals and chromosomal aberrations. Dose-dependent linear induction of the average number of radiation-induced γ-H2AX foci per cell (panel A) and the relative mean γ-H2AX fluorescence intensity (RMFI) (panel B) over 48 h and 24 h after X irradiation, respectively. Error bars show the standard deviation between donors (n). Given time points represent the start of leukocyte isolation from whole blood after exposure. Panel C: Representative immunofluorescent images of γ-H2AX foci in DAPI stained leukocyte-nuclei 45 min postirradiation or mock treatment. Dose-normalized and time-dependent induction and loss of the mean number of radiation-induced γ-H2AX foci per cell and Gy (panel D) and the RMFI per Gy (panel E) based on the linear regression coefficients obtained in panels A and B, respectively. Solid lines represent a bi-exponential (panel D) or exponential (panel E) decay fit from the time point of signal loss. Dashed lines were drawn to guide the eye. Error bars represent the standard error of the linear regressions obtained in panels A and B. Panel F: Dose-dependent induction of dicentrics and centric rings or excess acentric fragments per cell fitted by linear-quadratic functions. Error bars show the standard deviation between two donors.

were washed in PBS, fixed a second time in methanol for 10 min at −20°C, washed again in PBS, permeabilized and blocked with 5% (w/v) bovine serum albumin (BSA)/0.5% (v/v) Triton™-X-100/PBS for 30 min at room temperature and incubated with monoclonal γ-H2AX antibody [1:500 in 5% (w/v) BSA/0.1% (v/v) Triton-X-100/PBS, Upstate®, Millipore, Billerica, MA] for at least 1 h at room temperature. Slides were washed several times in PBS and 0.4 *M* NaCL/PBS followed by incubation with AlexaFluor® 488 dye-conjugated goat anti-mouse secondary antibody (1:400 in PBS, Invitrogen™, Carlsbad, CA) for 1 h at room temperature, counter-stained with 0.2 μg/ml 4′,6-diamidino-2-phenylindole (DAPI) for 10 min at room temperature, washed several times in PBS, dried, mounted with Vectashield® (Vector Laboratories, Burlingame, CA), covered with a cover slip and sealed with nail polish. Scanning of slides and image capturing of single nuclei were performed using a Metafer slide scanning platform (MetaSystems, Newton, MA) equipped with an Axio Imager 2 microscope (Carl Zeiss Microscopy GmbH, Jena, Germany), a motorized 8 slide feeder xyz-scanning stage (Märzhäuser Wetzlar GmbH & Co., Wetzlar, Germany) and the Metafer4 version 3.5 MetaCyte software (MetaSystems). Based on DAPI counterstaining and images taken with a 63× objective and an uncooled CCD camera a mask was generated for each nucleus defined by morphological features. Nuclei were scanned for γ-H2AX signals with 20 focal planes at a step distance of 0.4 μm. Image capturing and processing functions were kept constant during the entire study. Z-stack images were combined to maximum projection images and γ-H2AX foci per nucleus were counted manually. After *ex vivo* or *in vivo* exposure an average of 250 or 800 cells were analyzed per data point, respectively. Individual patient data on foci evaluation are provided in Supplementary Table S2 (http://dx.doi.org/10.1667/RR13911.1.S1).

Fixation, Staining and Measurement of γ-H2AX Intensity

For the measurement of γ-H2AX fluorescence intensity by flow cytometry we applied the same protocol as for microscopy with the following modifications. Isolated leukocytes were kept in suspension and fixed in 1% formaldehyde/PBS followed by 70% ethanol for 10 min at 4°C each. γ-H2AX fluorescence intensity was quantified with a FACSCanto™ II cell analyzer (BD Biosciences, San Jose, CA) with constant settings during the study. Using FlowJo software (Tree Star, Inc, Philomath, OR) the leukocyte population of interest was selected based on the forward versus side scatter plot. The relative mean fluorescence intensity (RMFI), normalized to mock-treated cells, was calculated by analyzing at least 9,000 cells per sample. Measurement of RMFI by flow cytometry was performed only after uniform *ex vivo* or *in vivo* exposure because of a considerably reduced sensitivity compared to microscopic foci scoring.

Preparation of Chromosome Slides and Analysis

Chromosome preparations were made according to standard techniques (*25*). Briefly, 1 ml of blood was diluted in 9 ml of

LymphoChrome karyotyping media (BioWhittaker, Inc. Walkersville, MA) and incubated at 37°C, 5% CO_2 in a humidified atmosphere for 48 h in continuous presence of 3 μl/ ml colcemid (Sigma-Aldrich) to accumulate only first division metaphases, which were then harvested, processed and Giemsa stained. Dicentric chromosomes, centric rings (CR) and acentric fragments were scored only in complete metaphases containing 46 centromeres based on the classification criteria of Savage (*26*). In the case of centric rings or dicentric chromosomes, one acentric fragment was assigned to each exchange. Polycentric chromosomes with n centromeres were counted as n – 1 dicentric chromosomes. For the measurement of chromosomal aberrations after *ex vivo* exposure to 2 Gy, 100 metaphases were scored. In blood samples obtained before or 30 min and 24 h after the first fraction of PBI 500 metaphases were scored each. After the last fraction of PBI, on average 470 metaphases were counted. After the first fraction of TBI, on average 340 metaphases were analyzed per time point. Individual patient data on cytogenetic analyses are provided in Supplementary Table S1 (http://dx.doi.org/10.1667/RR13911.1.S1).

Physical Dose and Distribution

Each patient's individual physical equivalent whole-body dose (PEWBD) as the average dose per voxel over the whole body after PBI was calculated according to the method described by Sak *et al.* (*6*). Briefly, the mean dose deposited in the CT scanned body volume per fraction of radiation was weighted with the whole-body proportion of the CT scanned body volume. Information on the CT scanned body volume and the mean dose deposited therein was obtained from the treatment planning software. The whole-body volume was calculated by dividing the patient's weight by body density considering height, age, gender and the percentage of body fat according to the methods describer by Deurenberg *et al.* and Sier (*27, 28*). The distribution of the physical dose within the whole-body structure was calculated based on the cumulative (PBI) or differential (TBI) dose-volume histogram data obtained from the treatment planning software for the CT scanned body volume. To calculate the cumulative dispersion of dose in the whole-body volume after PBI, the cumulative distribution of dose in the CT scanned body volume was normalized to the patient's total-body volume according to the method described by Zwicker *et al.* (*15*). No such normalization had to be performed for TBI since the CT scanned body volume is equal to the total-body structure.

Biological Dose and Dispersion Analysis

The biological (equivalent) whole-body dose was calculated based on the mean frequency of radiation-induced foci, dic + CR per cell or the RMFI using the functions of the respective *ex vivo* calibration curves. Partial-body dose (PBD) estimation based on radiation-induced γ-H2AX foci and chromosomal aberrations was done according to the Qexcess γ-H2AX (*29*) or Qdr (*30*) method regarding the frequencies of radiation-induced γ-H2AX foci or dicentric chromosomes and centric rings (dic + CR) only in radiation damaged cells with at least one radiation-induced γ-H2AX focus or chromosomal aberration, respectively. To test for an overdispersion of γ-H2AX foci or dic + CR among cells from a Poisson distribution with a 95% confidence interval indicating a heterogeneous exposure the Papworth *u* test was applied (*31*). To create integral histograms of the distribution of the biological dose in leukocytes based on the frequency of radiation-induced γ-H2AX foci, the biological dose per leukocyte with at least one radiation-induced γ-H2AX focus was calculated using the *ex vivo* calibration data.

Data and Statistical Analysis

All data were scored by one observer. For each data point a single sample per donor was analyzed due to the limited amount of blood available. The individual background of γ-H2AX signal or chromosomal aberrations was subtracted from the respective yield after *ex vivo* or *in vivo* irradiation. For *ex vivo* exposed samples mock-treated controls were available from the respective donor for any analyzed time point. For postirradiated samples the individual basal yield was scored only prior to the first fraction of radiation. Average values taken from the regression coefficient of a linear fit are given with the standard error. Summarized patient data for one sampling time point is provided as the mean and standard deviation unless stated otherwise. Statistics were done using SigmaPlot™ 11® (Systat® Software Inc., San Jose, CA). The relationship between two variables was analyzed using the Pearson test. For comparison of the means of two or more groups the Student's *t* test or the one-way analysis of variance (ANOVA) with pairwise comparison (Holm-Sidak method) was used, respectively. To test for the heterogeneity of the slopes of linear regressions the analysis of covariance (ANCOVA) was applied. All levels of significance were set at $P < 0.05$.

RESULTS

Basal Yield and Radiosensitivity of Leukocytes Irradiated Ex Vivo

Quantitation of γ-H2AX foci. As shown in Fig. 1A, the analysis of basal foci revealed significantly elevated frequencies in patients with hematologic malignancies compared to HDs and all other cancer types. This discrepancy was attributed to two extremely high outliers among patients with AML carrying on average 2.1 and 4.8 basal foci per leukocyte. Since these patients showed strong leukopenia the elevated level of basal DNA damage could not be confirmed by cytogenetic analysis. The frequencies of radiation-induced foci per cell scored 45 min or 24 h after *ex vivo* exposure to 0.5 or 2 Gy and were comparable between HDs and patients with any type of cancer (Fig. 1B and C).

Quantitation of chromosomal aberrations. Cytogenetic analysis was performed only on a subset of patients that were also analyzed after radiation therapy. The average basal rate of unstable chromosomal aberrations per cell was comparable between HDs and cancer patients without previous chemotherapy or radiation therapy, but was elevated after an earlier radiation exposure (1 breast cancer patient, 13 years before the current radiation therapy) or chemotherapy and increased with the intensity of chemotherapy, leading to a severely escalated background in AML patients as shown in Fig. 1D. After an *ex vivo* exposure to 2 Gy the yield of radiation-induced chromosomal damage was comparable between HDs and patients with any type of cancer (Fig. 1E).

Ex Vivo Calibration Curves

To convert the quantity of radiation-induced DNA damage into physical dose, calibration-curves were generated after uniform *ex vivo* irradiation of blood. The average number of radiation-induced foci per cell and the RMFI followed a linear dose-effect relationship in measurements up to 48 h and 24 h after *ex vivo* exposure, respectively (Fig. 2A–C). Maximum numbers of radiation-induced γ-H2AX foci per cell were observed after 30–45

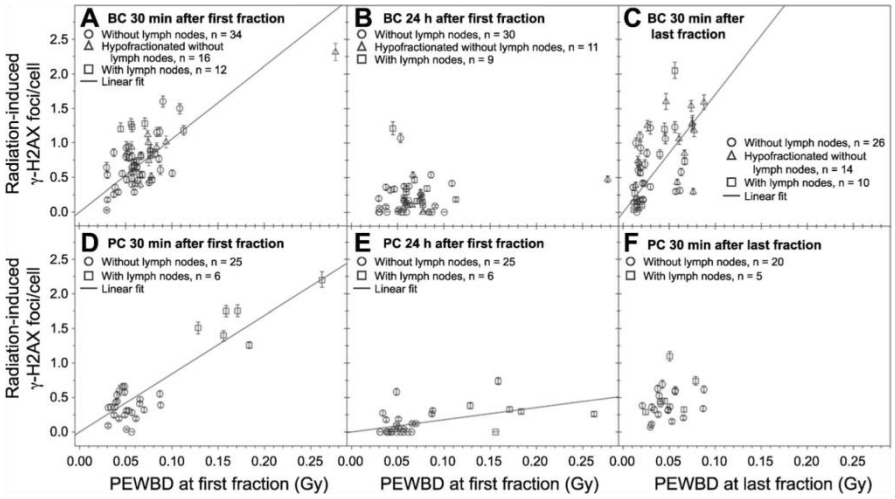

FIG. 3. Relationship between the mean number of radiation-induced γ-H2AX foci per cell and the administered physical equivalent whole-body dose (PEWBD) 30 min (panels A and D) and 24 h (panels B and E) after the first fraction of radiation (RT) or 30 min (panels C and F) after the last fraction of radiation in blood samples from breast cancer (BC) patients (panels A, B and C) and prostate cancer (PC) patients (panels D, E and F). Individual PEWBD at the last fraction of radiation differs from the first fraction because of sequential boost treatments. Linear regressions are only shown for significant correlations ($P < 0.05$). Error bars represent the 95% confidence interval of the Poisson mean. Numbers of analyzed patients (n) per time point are provided.

min and the RMFI measured by flow cytometry reached the highest level after 1.5 h. Maximum γ-H2AX signals were followed by a rapid biphasic loss. Based on the linear regression coefficients of each dose-effect relationship providing the mean number of radiation-induced foci per cell and Gy or of the RMFI per Gy, the dose-normalized kinetics of γ-H2AX signal induction and loss shown in Fig. 2D and E were established. The γ-H2AX signal loss was fitted by a bi-exponential decay with the function $Y = 8.2 \pm 1 \times \exp(-0.33 \pm 0.071 \times X) + 1.7 \pm 1 \times \exp(-0.023 \pm 0.022 \times X)$ for the mean number of radiation-induced foci per cell and Gy; and by an exponential decay with the function $Y = 1.23 \pm 0.02 + 1.7 \pm 0.03 \times \exp(-0.34 \pm 0.014 \times X)$ for the RMFI per Gy. The increment of RMFI per Gy up to 1.5 h postirradiation was fitted by a linear regression with the function $Y = 1.5 \pm 0.5 \times X + 1$. Y represents the mean number of radiation-induced foci per cell or the RMFI, and X represents the time in hours either after exposure for the linear increase of RMFI or after the beginning of signal loss for both decay functions. To calculate partial-body doses according to the Qexcess γ-H2AX method, a standard curve was established in the same manner ignoring cells free of radiation-induced foci. The function of this dose-normalized bi-exponential decay curve (not shown) was $Y = 7.9 \pm 0.33 \times \exp(-0.33 \pm 0.064 \times X) + 2.1 \pm 0.7 \times \exp(-0.0024 \pm 0.0096 \times X)$. Figure 2F shows the dose-effect relationship for radiation-induced unstable chromosomal aberrations in *ex vivo* irradiated blood obtained from 2 HDs. The average frequency of radiation-induced dic + CR per cell was fitted by the linear quadratic function $Y = 0.037 \pm 0.006 \times X + 0.048 \pm 0.003 \times X^2$ according to the IAEA's 2001 technical report series (*25*). The function for the dose-effect curve for radiation-induced excess acentric fragments, necessary for the Qdr method, was $Y = 0.056 \pm 0.006 \times X + 0.031 \pm 0.003 \times X^2$. Y represents the mean number of chromosomal aberrations per cell and X represents the dose.

DNA Damage after In Vivo Radiation Exposure

Quantitation of γ-H2AX. The analysis of radiation-induced foci in leukocytes sampled 30 min after the start of the first fraction of heterogeneous radiation revealed a linear correlation between the mean number per cell and the PEWBD for breast cancer patients (Fig. 3A; $r = 0.7$, $P < 0.001$) and prostate cancer patients (Fig. 3D; $r = 0.9$, $P < 0.001$). The linear increment was significantly steeper for breast cancer compared to prostate cancer patients ($P < 0.001$) with respective regression coefficients of 10.6 ± 2.6 and 8.4 ± 0.7 radiation-induced foci per cell and Gy PEWBD. The average number of radiation-induced foci per cell decreased significantly ($P < 0.001$) in blood obtained from patients of both tumor entities one day after the first radiotherapy session (Fig. 3B and E). However only in the prostate cancer patients was a correlation between the mean number of residual radiation-induced foci per cell and the PEWBD ($r = 0.5$, $P < 0.01$) found resulting in 1.8 ± 0.6 radiation-induced foci per cell and Gy PEWBD. Examples of typical immunofluorescent images of leukocytes before and after the first PBI are shown in Fig. 4. Exceptional treatment modalities such as

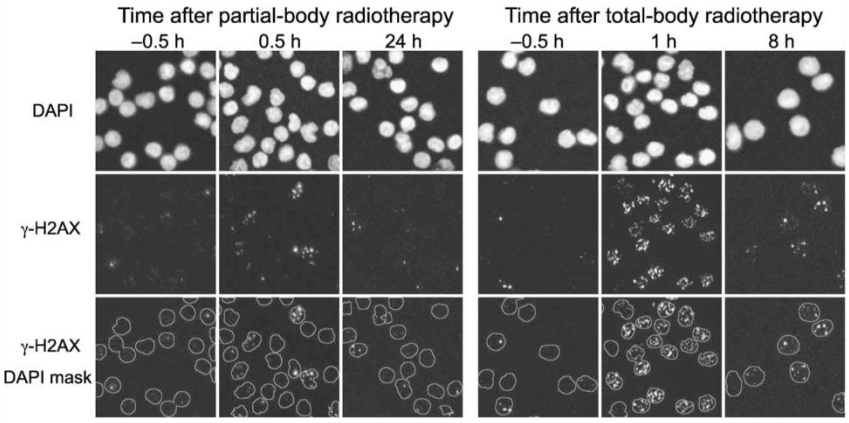

FIG. 4. Representative immunfluorescent images of γ-H2AX in DAPI stained leukocyte-nuclei before and after partial- or total-body radiotherapy.

irradiation of lymph nodes or hypofractionation had no impact on the average dose-normalized rates of radiation-induced foci per cell 30 min and 24 h after the first fraction of radiation for both tumor entities. A final blood sample was also drawn 30 min after the start of the last fraction of heterogeneous radiation. Approaching the end of their radiotherapy sessions, 32 of 50 analyzed breast cancer patients and 7 of 25 analyzed prostate cancer patients received on average 8 fractions of a sequential boost as a dose escalation to the tumor bed. Since no blood samples were drawn prior to the last radiotherapy session, the individual basal foci rate that was assessed before the first fraction of radiation was subtracted from the number of foci scored after the end of radiation therapy, which was then compared to the patient's number of radiation-induced foci after the first fraction of radiation. Minimizing the treatment volume by boost irradiation led, on average, to a significant ($P < 0.001$) 3.4-fold reduction of the PEWBD compared to the first fraction of radiation while the radiation-induced foci rate was significantly ($P < 0.001$) 1.8-fold lower. When no sequential boost was applied, the average yield of radiation-induced foci after the end of the treatment period was 1.3-fold elevated compared to the radiation-induced foci rate scored 30 min after the first fraction of radiation. As shown in Fig. 3C and F, a correlation between the mean numbers of radiation-induced foci per cell and the PEWBD after the end of radiotherapy was found only for breast cancer patients ($r = 0.5$, $P < 0.001$). The linear regression coefficient was significantly higher than 30 min after the first fraction of radiation ($P < 0.001$) and resulted in 17.1 ± 1.7 radiation-induced foci per cell and Gy PEWBD.

Sixty minutes after the start of the first TBI, radiation-induced foci were detected in 93 ± 9% of the analyzed leukocytes extracted from the blood of 8 patients. Radiation-induced foci (16 ± 2) per cell were scored by microscopy and the average RMFI measured by flow cytometry was 6.0 ± 1.4-fold elevated. After recovery for 6–8 h radiation-induced foci were present in 72 ± 16% of leukocytes isolated from 7 patients. Radiation-induced foci (4.5 ± 1.0 per cell) were scored by microscopy and the RMFI was 2.0 ± 0.3-fold increased. Representative immunofluorescent images before and after TBI are shown in Fig. 4.

Quantitation of chromosomal aberrations. The yield of chromosomal aberrations was analyzed for 8 breast cancer and 5 prostate cancer patients after the first fraction of radiation. In blood samples drawn after 30 min the frequency of dic + CR per cell was elevated for 6 breast cancer patients and all analyzed prostate cancer patients compared to the individual basal yield but without any dependence on the PEWBD (Fig. 5A and D). Twenty-four hours thereafter the number of radiation-induced dic + CR per cell further increased in samples from 7 and 4 of the same breast cancer and prostate cancer patients, respectively (Fig. 5B and E), most pronounced and up to threefold in prostate cancer patients with lymph node treatment. Only for prostate cancer patients did the frequencies of radiation-induced dic + CR per cell increase linearly with the PEWBD ($r = 1$, $P < 0.05$) with a regression coefficient of 0.14 ± 0.02 radiation-induced dic + CR per cell and Gy PEWBD. The yield of chromosomal aberrations was analyzed 30 min after the last fraction of radiation for 7 and 4 of the same breast cancer and prostate cancer patients, respectively. An accumulation of cytogenetic damage was found with a linear dependency of the frequency of dic + CR per cell on the cumulative PEWBD for breast cancer patients (Fig. 5C, $r = 0.8$, $P < 0.05$) and prostate cancer patients (Fig. 5F; $r = 1$, $P < 0.01$). The linear regression coefficients as the average yields of radiation-induced dic + CR per cell and Gy cumulative PEWBD of 0.066 ± 0.003 for prostate cancer patients and 0.061 ± 0.003 for breast cancer patients were comparable.

After TBI, the frequencies of radiation-induced dic + CR per cell were highly elevated in blood from 3 AML patients

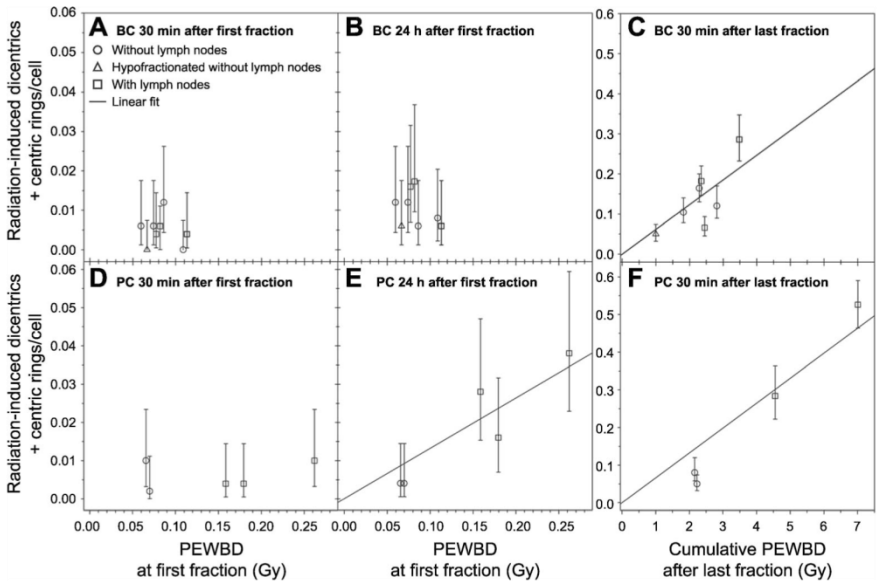

FIG. 5. Relationship between the mean number of radiation-induced dicentrics plus centric rings (dic + CR) per cell and the administered PEWBD 30 min (panels A and D) and 24 h (panels B and E) after the first fraction of radiation (RT) and between the mean number of radiation-induced dic + CR per cell and the cumulative PEWBD (PEWBD per fraction × total number of fractions) (panels C and F) 30 min after the last fraction of radiation in blood samples from breast cancer (BC) patients (panels A, B and C) and prostate cancer (PC) patients (panels D, E and F). Note the tenfold heightened scaling of the Y axis after the last fraction of radiation (panels C and F). Linear regressions are only shown for significant correlations ($P < 0.05$). Error bars represent the 95% confidence interval of the Poisson mean.

to a similar extent in samples taken either 60 min or 6–8 h after radiation therapy was started, with a respective average number of 0.36 ± 0.05 or 0.41 ± 0.04 per cell.

Equivalent Whole-Body Dose Estimates after Irradiation

Dose estimations are shown only after the well-defined conditions of the first radiotherapy session. For dose assessments after PBI based on radiation-induced chromosomal aberrations only the data on the overall higher yield obtained 24 h after the first radiotherapy session was considered. Individual patient data for all dose assessments are provided in Supplementary Tables S1 and S2 (http://dx.doi.org/10.1667/RR13911.1.S1). The results of the equivalent whole-body dose estimates after PBI from all patient samples with detectable radiation-induced γ-H2AX signals or dic + CR are depicted and compared to the average physical value shown in Fig. 6A. The expected PEWBDs were successfully assessed based on the mean numbers of radiation-induced foci per cell scored immediately after PBI in contrast to strong overestimations 24 h thereafter according to radiation-induced residual foci or dic + CR. As shown in Fig. 6B, all whole-body dose approximations after TBI were comparable and agreed with the administered physical dose of 2 Gy except for the measurement of the RMFI 6–8 h postirradiation. Figure 6C and D shows the consistent distributions of the biological dose to leukocytes 1 h after TBI based on radiation-induced foci and of the physical dose within the total-body volume. Six to eight hours after TBI a much broader distribution of biological doses was observed. This is attributed to the inherent reduction of assay sensitivity and resolution of the dose with increasing time after exposure.

Partial-Body Dose Estimates after Irradiation

Partial-body doses were estimated according to the Qexcess γ-H2AX or Qdr method and are shown in comparison to the average physical value shown in Fig. 7A. Partial-body dose assessments based on Qexcess γ-H2AX 30 min after the first radiotherapy session led to a generally strong underestimation of the average local tumor dose of 2 Gy. The average partial-body dose approximation for breast cancer patients was significantly lower (1.4-fold, $P < 0.001$) compared to prostate cancer patients. However, 24 h later the partial-body dose estimation based on residual radiation-induced foci was in better accordance with the expected physical values. The corresponding cumulative distributions of biological dose to circulating leukocytes are shown in Fig. 7B and C in comparison to the cumulative distribution of physical dose within the total-body volume shown in Fig. 7D. The approximation of the average partial-body dose by Qdr agreed with the average local tumor doses, albeit with large inter-individual variations.

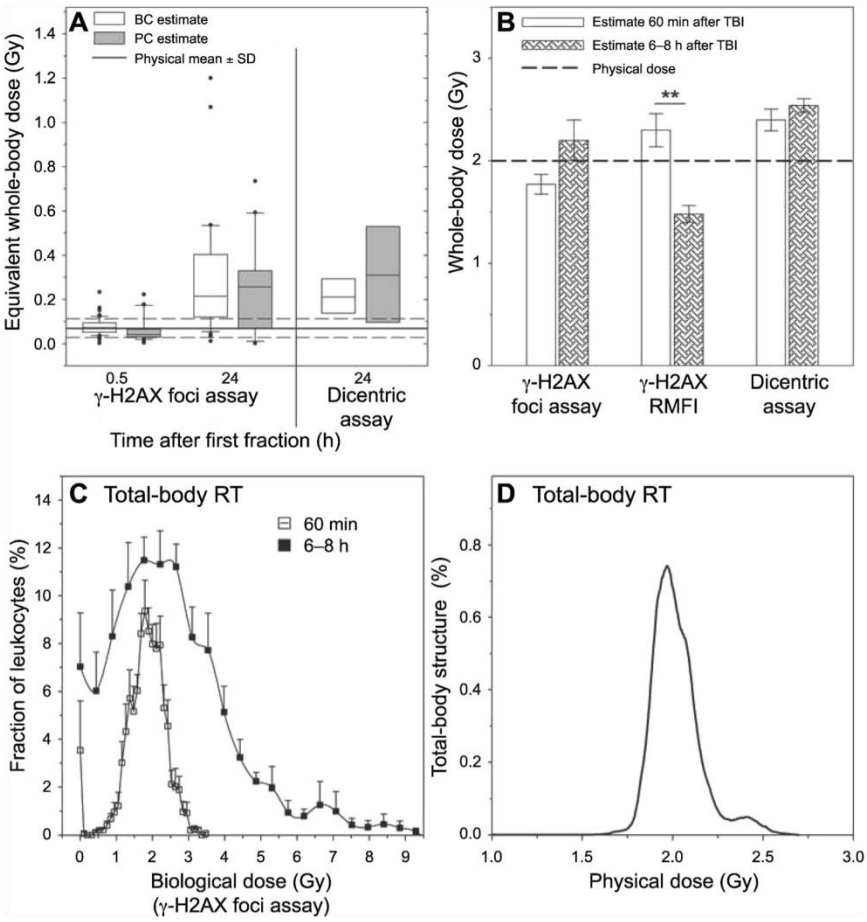

FIG. 6. Whole-body dose estimates based on γ-H2AX quantification or cytogenetic analyses in comparison to the expected average physical value. Only patients with radiation-induced DNA damage above the basal yield prior to radiotherapy (RT) were included. Panel A: Box plot of equivalent whole-body dose estimates for breast cancer (BC) and prostate cancer (PC) patients based on γ-H2AX foci scored 30 min (breast cancer: n = 62, prostate cancer: n = 30) and 24 h (breast cancer: n = 37, prostate cancer: n = 21) after the first fraction of radiation or dicentrics plus centric rings (dic + CR) scored 24 h after the first fraction of radiation (breast cancer: n = 8, prostate cancer: n = 5). Panel B: Mean whole-body dose estimates and their standard error based on the mean number of γ-H2AX foci per cell (n = 8 and n = 7), the relative mean γ-H2AX fluorescence intensity (RMFI; n = 6) or the mean number of dic + CR per cell (n = 3 and n = 3) 60 min and 6–8 h after the first total-body irradiation (TBI). Histograms of the distribution of biological dose to leukocytes (γ-H2AX foci assay) after the first fraction of total-body irradiation (panel C) and of the physical dose within the total-body volume (panel D). The data are presented as mean values of all analyzed patients with the standard error of the mean. Statistical comparison in panel B was performed by *t* test (*$P < 0.05$, **$P < 0.01$, ***$P < 0.001$).

Dispersion Analysis

The distribution of γ-H2AX foci and chromosomal aberrations among cells after uniform exposure to sparsely ionizing radiation is well described by a Poisson distribution because of the random induction of DSBs (*19, 21, 25*). Heterogeneous radiation exposures are characterized by an overdispersion of DNA damage frequency among cells and can therefore be identified by a deviation from the Poisson assumption using the Papworth *u* test (*31*). Dispersion analysis after radiation therapy was performed only on the patient data obtained at time points that were considered as relevant for dose calculations in the previous sections. For comparison the Papworth *u* test was applied to data on foci up to 24 h after homogeneous radiation exposure to 2 Gy. Results on the dispersion analysis of foci are shown in Fig. 8. The frequency of basal foci was inherently overdispersed. Immediately after uniform *ex vivo* exposure the average rate of foci among cells followed a Poisson distribution. With ongoing DNA repair and foci loss over time post exposure, the first overdispersions occurred 5 h after uniform *ex vivo* irradiation, growing over time up to the pre-exposure level. Thirty minutes after the first PBI the average frequency of

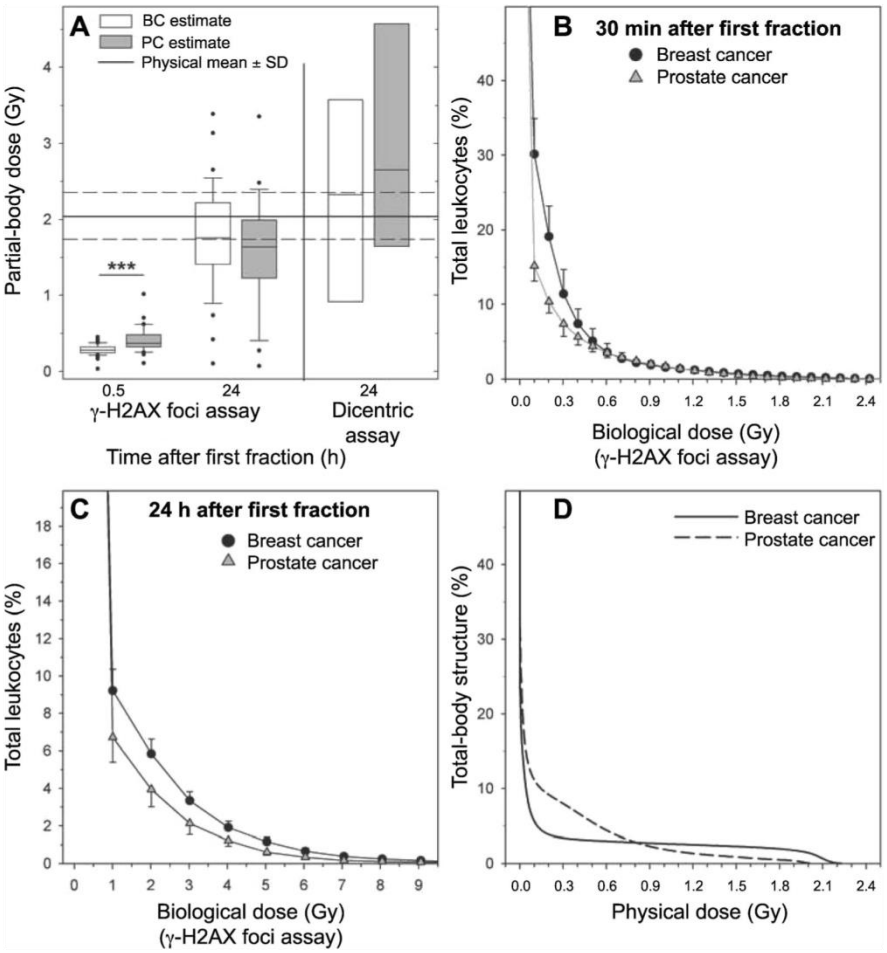

FIG. 7. Partial-body dose estimates based on γ-H2AX foci quantification or cytogenetic analyses in comparison to the expected average physical value. Only patients with radiation-induced DNA damage above the basal yield prior to radiotherapy (RT) were included. Panel A: Box plot of partial-body dose estimates for breast cancer (BC) and prostate cancer (PC) patients based on γ-H2AX foci scored 30 min (breast cancer: n = 62, prostate cancer: n = 30) and 24 h (breast cancer: n = 37, prostate cancer: n = 21) after the first fraction of radiation or unstable aberrations scored 24 h after the first fraction of radiation (breast cancer: n = 8, prostate cancer: n = 5). Integral histograms show the cumulative distribution of biological dose to leukocytes (γ-H2AX foci assay) 30 min (panel B) and 24 h (panel C) after the first fraction of radiation and of the physical dose (panel D) within the total-body volume for patients with breast or prostate cancer. Each data point summarizes the relative mean fraction of leukocytes or of the total-body volume of all analyzed patients with at least the shown absolute dose. Error bars represent the standard error of the mean. Statistical comparison in panel A was performed by *t* test (*$P < 0.05$, **$P < 0.01$, ***$P < 0.001$).

foci among cells was extremely overdispersed and heterogeneous exposures could still be identified at 24 h postirradiation by elevated u values compared to homogeneous *ex vivo* exposure. At both time points of investigation after TBI, the average rate of foci was overdispersed and higher than expected from the uniform *ex vivo* exposure, but still clearly distinguishable from PBI. The frequencies of dic + CR among cells followed a Poisson distribution after homogeneous *ex vivo* or *in vivo* exposure for any analyzed sample. Twenty-four hours after the first PBI the distributions of dic + CR violated the Poisson expectation in only 6 of 13 analyzed patient samples. Detailed information on the individual dispersion of foci and chromosomal aberrations in cancer patients is provided in Supplementary Tables S1 and S2 (http://dx.doi.org/10.1667/RR13911.1.S1).

DISCUSSION

To the best of our knowledge, we report for the first time a quantitative description of the DNA damage induced in leukocytes during fractionated radiotherapy of cancer

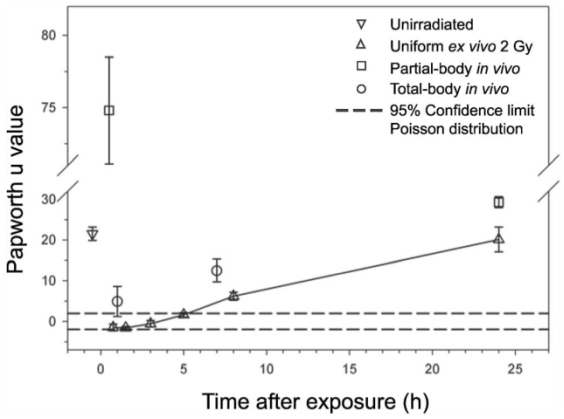

FIG. 8. Dispersion analysis of radiation-induced foci among unirradiated leukocytes (n = 194), after uniform *ex vivo* exposure to 2 Gy (n = 61) and after partial (0.5 h, n = 96; 24 h, n = 85) or total-body (1 h, n = 8; 6–8 h, n = 7) radiotherapy. Results are given as the average values from the Papworth *u* test. Error bars represent the standard error of the mean. 95% confidence intervals for under-dispersion (<–1.96) or overdispersion (>+1.96) of a Poisson distribution are indicated.

patients using parallel quantification of radiation-induced γ-H2AX signals and chromosomal aberrations. In this study, we showed that compared to well-established cytogenetic analyses, the immediate detection of radiation-induced DSBs in peripheral leukocytes as γ-H2AX foci has a leading advantage in terms of both sensitivity and time consumption, and is a more reliable biosensor for monitoring individual patient radiation burden, primarily the equivalent whole-body dose.

As a first step, we compared the basal yield and *ex vivo* radiosensitivity of donors and established calibration curves to relate the quantity of radiation-induced DNA damage to physical dose. In general, the baseline of γ-H2AX foci in human leukocytes, the maximum γ-H2AX signals and kinetics of the dose-dependent linear increment as well as loss after *ex vivo* X irradiation agreed with previously published data (*6, 8, 20*), as did the results of the basal and radiation-induced rates of chromosomal aberration (*32*). A clear clastogenic effect of a previous chemotherapy or radiotherapy on the hematopoietic system has been shown by an elevated background of chromosomal aberrations (Fig. 1D), whereas basal foci counts were unaffected thereof, although even long-term effects of cytostatics on basal foci levels up to several days after administration cannot be ruled out (*33*). Exceptional observations on basal foci counts in leukocytes of two patients with AML might be explained by intrinsic genomic instability as recently described for primary AML myeloblasts (*34*). The observed inter-individual variation in basal foci yield and the impact of medical pretreatments on chromosomal aberrations show the necessity to consider individual background for any exposure, particularly in clinical settings. Background subtraction would not be applied to the *ex vivo* calibration curves if they had to be used for dose estimations after accidental radiation exposure with an unknown basal level of the exposed individual. The average radiosensitivity measured as the yield of radiation-induced chromosomal aberrations or initial or residual foci after *ex vivo* exposure did not show discrepancies between HDs and any tumor entity and was unaffected by previous chemotherapy or radiotherapy. This ensures the general comparability of the *ex vivo* calibration data obtained mostly from HDs and the results of cancer patients, but inter-individual variations of radiosensitivity might still affect the measurements taken after radiation therapy. In our study no donor showed exceptional *ex vivo* radiation response.

The quantitation of DSBs as γ-H2AX foci in peripheral leukocytes immediately after a single acute heterogeneous radiation exposure to a small radiation field on the body is a far more sensitive biosensor and solid indicator of the absorbed equivalent whole-body dose than the analysis of unstable aberrations. In contrast to chromosomal aberrations, the average number of radiation-induced foci per leukocyte correlated linearly with the equivalent whole-body dose for both tumor entities, as previously reported for a variety of radiologic procedures (*11*). The steepness of the linear increment diverged significantly between breast cancer and prostate cancer patients (Fig. 3A and C). Sak *et al.* (*6*) clearly demonstrated that the slope of a linear-dose-response curve for the mean number of γ-H2AX foci in leukocytes underlies site effects when tumors in different anatomic locations are treated with radiation due to variable regional blood volumes and kinetics of lymphocyte circulation. However, the average number of radiation-induced foci per cell was a very reliable measure of the expected equivalent whole-body dose for both tumor types when referred to the *ex vivo* generated calibration curve (Fig. 6A). Contrary to the successful assessment of the patients' equivalent whole-body dose immediately after PBI the average local tumor dose of 2 Gy was strongly underestimated with significant differences between breast cancer and prostate cancer patients (Fig. 7A). The distribution of dose to leukocytes measured by the γ-H2AX foci assay basically reflects the dose distribution within the total-body volume as predicted by 3D treatment planning (Fig. 7B and D) rather than the local tumor dose within the PTV due to the high sensitivity of the assays, as previously demonstrated by Zwicker *et al.* (*15*). Thus, venipuncture that was performed immediately after PBI collected mainly leukocytes, which absorbed on average just 15–20% of the local dose during rapid circulation through the aorta, arteries or veins in the periphery of the irradiated volume. For prostate cancer patients, less leukocytes were irradiated, as can be inferred from the fraction of cells that received at least a biological dose of 0.1 Gy in the cumulative dose to leukocyte histogram (Fig. 7B). However, the shape of the cumulative dose distribution in leukocytes of prostate cancer patients was comparable to that of breast cancer patients. This is in contrast to the

cumulative distribution of the physical dose within the total-body volume taken from the treatment planning software that predicts a higher proportion of the total-body volume and thus suggests a higher fraction of leukocytes irradiated with low doses for prostate cancer patients compared to breast cancer patients (Fig. 7D). The fraction of irradiated peripheral leukocytes depends on multiple factors such as the exposure time (beam-on time), the total time a patient spends on the treatment table from the beginning of the application of the first until the end of the last field as a factor for the redistribution of peripheral circulating leukocytes (table time), the exposed anatomic region with differences in total and regional blood volumes and flow rates therein, but also the dose distribution profiles inherent to the applied radiotherapy technique. The average total time for recirculation of a peripheral leukocyte estimated on the basis of the average total blood volume and cardiac output is approximately 0.7 min (*35*). As for only the parameter time, prostate cancer patients had on average a longer beam-on time (2.5 min) than breast cancer patients (0.9 min), while the average table time was longer for breast cancer patients (4.2 min) than for prostate cancer patients (2.5 min). Therefore, a higher proportion of irradiated leukocytes would be expected for prostate cancer patients than for breast cancer patients, however, it is difficult to draw a realistic conclusion on the fraction of irradiated leukocytes due to the possibility of repeated irradiation of circulating leukocytes during longer beam-on and table times. Actually, the opposite observation of a higher number of leukocytes exposed to lower doses in breast cancer patients might be attributed to the presence of large blood vessels (heart, aorta) and thus a greater blood volume and higher flow rates in the chest than in the pelvis. Although precise local dose assessments failed, heterogeneous radiation exposures could be identified as PBI by extreme overdispersion of radiation-induced foci among cells using the Papworth *u* test (Fig. 8), confirming results that were obtained after heterogeneous radiation exposure of animals as described by Lamkowski *et al.* (*13*).

The frequencies of radiation-induced foci dropped 24 h after the first fraction of radiation with the quantity of residual radiation-induced foci still being proportional to the initial PEWBD (Fig. 3E). So far, a dose-proportional long-term persistence of residual foci up to several days *in vivo* has been shown only after homogeneous exposure of animals (*14*). Based on the frequencies of residual radiation-induced foci heterogeneous exposures were indicated by dispersion analysis (Fig. 8) and the administered average partial-body dose was well approximated (Fig. 7A), since after 24 h of proceeding DSB repair exclusively, cells are detected that were exposed to high initial doses. Obviously these leukocytes absorbed the full local dose due to exposure in a static state while residing in fixed lymphatic tissues or during microcirculation with very low velocity in capillaries within the PTV, instead of a dynamic state like fast circulating peripheral leukocytes in large blood vessels, and could be obtained only through delayed venipuncture due to the slow kinetics of complete lymphocyte recirculation. These results show that even delayed scoring of residual radiation-induced foci after acute PBI might serve as an indicator of the heterogeneous exposure scenario and could still provide a useful approximation of the absorbed local dose.

While the average frequencies of radiation-induced foci per cell decreased one day after the first PBI the rates of chromosomal aberrations increased, most pronounced for prostate cancer patients with radiation treatment of lymph nodes (Fig. 5). Therefore, the most likely reason for the lagged increment of chromosomal aberrations in peripheral blood is the irradiation of lymph nodes in a subset of patients. The average time that is required for a full recirculation of lymphocytes is approximated to be at least 12 h (*25*). Consistent with the observation after the first fraction of radiation in our study, the increment of chromosomal aberrations in prostate cancer patients was shown to be PTV dependent even when lymph nodes were included in the radiation treatment (*36*). By contrast, breast cancer patients show wide inter-individual variations and PTV-independent yields of chromosomal aberrations (*37*) since lymph nodes are treated with separate PTVs and partially dissected before radiation therapy. However, after the last fraction of radiation we also showed a linear dependency for breast cancer patients between the chromosomal aberration yield and the cumulative PEWBD (Fig. 5C). The exposure of lymphatic tissues with high lymphocyte density during radiation therapy is expected to produce a dose-independent escalation of chromosomal aberrations and thus might have led to the overestimation of the expected PEWBDs (Fig. 6A), as previously reported by Roch-Lefèvre *et al.* (*38*). As can be inferred from our data on breast cancer patients we could not observe a clear escalation of chromosomal aberrations when lymph nodes were involved in the radiation therapy, rather a wide general inter-individual variability among all patients. The reason for the large uncertainty and general overestimation of the administered PEWBD after a single fraction of radiation by the dicentric assay may be the significantly reduced sensitivity of the dicentric assay compared to the γ-H2AX foci assay. At very low numbers of dicentrics, as in our work, slight variations would have a significant impact on the maximum likelihood estimate of the equivalent whole-body dose (*39*). However, lower number of analyzed patients (about 10×) than for the γ-H2AX foci assay should also be considered as an influential factor here. Compared to the assessment of the equivalent whole-body dose after local radiotherapy of small body volumes the analysis of dic + CR is a more precise measure of the local dose (*38*) due to the high detection threshold of the assays in terms of the local dose (>1 Gy) and exposed body fraction (>10–20%) (*4*). The average partial-body dose that was approximated from our data by the Qdr method agreed with the expected physical value for both tumor types, albeit with large

uncertainties (Fig. 7A) ascribed to the low yields of dic + CR after a single dose of 2 Gy delivered to a very minor fraction of the lymphoid tissue. Likewise on this account PBI could be identified in only about half of the analyzed heterogeneously exposed patients.

Analysis of the final yield of DNA damage after the final PBI revealed an accumulation over the course of radiation therapy. As expected from the data described in the literature (*40*), an accumulation of chromosomal aberrations was found but to a lesser extent than extrapolated from the cumulative PEWBD, which does not take into account the lowering effects of the dose gradient caused by total dose fractionation (*41*), lymphopenia (*42*) and repopulation (*43*) on the cytogenetic damage in lymphocytes after fractionated exposure. The quantitation of radiation-induced foci after the last fraction of radiation indicated a general trend in a persistence of radiation-induced foci from previous sessions. The reason for individually higher radiation-induced foci rates after the last fraction of radiation compared to the first fraction of radiation remains elusive, since there was no causal relationship with the individual radiation therapy parameters such as the cumulative PEWBD or the number of consecutively administered fractions before the sample was drawn. Our results contradict the findings of Sak *et al.* (*6*), who observed no escalation of basal foci yields in leukocytes taken late during the radiotherapy course prior to receiving a fraction of the dose and even described a trend towards shallower slopes of *in vivo* dose-effect curves because of a reduced γ-H2AX focus formation, discussed with the activation of an adaptive response. In contrast, Mariotti *et al.* (*44*) quantified a maximum time of 12 h for a full recovery of γ-H2AX focus induction after several split-doses in normal human fibroblasts. In our work the *in vivo* dose-effect curve for radiation-induced foci after the last radiotherapy session for breast cancer patients was 1.6-fold steeper than after the first session when referred to the same basal yield prior to the start of radiotherapy (Fig. 3A and C). This observation supports the hypotheses of an unaltered induction of γ-H2AX foci by exposure to radiation and a persistence of residual radiation-induced foci during daily fractionated radiotherapy.

After TBI the dose estimations performed by all biological methods up to 8 h after exposure adequately matched the expected physical whole-body dose of 2 Gy (Fig. 6B) shown in cytogenetic analysis in cancer patients (*45*) or γ-H2AX foci quantification in animals (*12, 14*) subjected to uniform irradiation *in vivo*. RMFI measurement of γ-H2AX signal by flow cytometry was successfully performed immediately after irradiation to overcome the problem of visual underscoring of overlapping foci by microscopy in leukocytes exposed to doses higher than 1.5 Gy, but turned out to be less precise for the lagged measurement because of a reduced sensitivity compared to foci enumeration [(*24*); Fig. 2A and B]. The dispersion analysis on the frequencies of dic + CR after TBI allowed an unambiguous identification of homogeneous exposures. Although the average frequency of radiation-induced foci was already overdispersed immediately after TBI, uniform exposures could still be discriminated from PBI (Fig. 8).

In summary our data substantiates γ-H2AX foci quantification in peripheral leukocytes as a potential biodosimeter that provides reliable estimates of clinically relevant equivalent whole-body doses after a recent single acute PBI or even up to several hours after acute TBI based on *ex vivo* generated calibration data. The confounding influence of physiological and radiation-related parameters on the radiation-induced γ-H2AX foci yield and distribution in leukocytes has to be considered and further clinical validation is necessary. Therefore, the continuative impact of varying radiation treatment parameters and techniques on the γ-H2AX foci assay in leukocytes is currently being studied in our laboratory. As for emergency countermeasure trials after radiation accidents involving even more complex scenarios of exposure, the γ-H2AX foci assay may be useful as a complementary biodosimeter for the rapid identification and selection of severely exposed individuals to initiate first clinical interventions and perform dosimetry by cytogenetic analyses.

SUPPLEMENTARY INFORMATION

Table S1. Detailed information on the individual patient raw data and analysis of chromosomal aberrations.

Table S2. Detailed information on individual patient raw data and analysis of γ-H2AX foci in leukocytes.

ACKNOWLEDGMENTS

We thank Drs. F. Crasselt, M. Dimitrov, A. Franke-Serras, T. Kretzer, A. Mayer, C. Reinke-Kretzer, C. Schwanbeck and M. Stockinger, and M. Rapp for mentoring patients and U. Disque-Kaiser for excellent technical assistance, all of whom are on the medical and technical staff at the University Medical Center of the Johannes Gutenberg University Mainz, Germany. This study was supported by research grant 02NUK016A from the German Federal Ministry of Education and Research.

Received: September 15, 2014; accepted: December 19, 2014; published online: April 6, 2015

REFERENCES

1. Jackson WL Jr., Gallagher C, Myhand RC, Waselenko JK. Medical management of patients with multiple organ dysfunction arising from acute radiation syndrome. BJR 2005; Suppl 27:161–8.
2. Aziz NM. Cancer survivorship research: state of knowledge, challenges and opportunities. Acta Oncol 2007; 46:417–32.
3. Benderitter M, Gourmelon P, Bey E, Chapel A, Clairand I, Prat M, et al. New emerging concepts in the medical management of local radiation injury. Health Phys 2010; 98:851–7.
4. Leonard A, Rueff J, Gerber GB, Leonard ED. Usefulness and limits of biological dosimetry based on cytogenetic methods. Radiat Prot Dosimetry 2005; 115:448–54.
5. Rogakou EP, Pilch DR, Orr AH, Ivanova VS, Bonner WM. DNA double-stranded breaks induce histone H2AX phosphorylation on serine 139. J Biol Chem 1998; 273:5858–68.

6. Sak A, Grehl S, Erichsen P, Engelhard M, Grannass A, Levegrun S, et al. Gamma-H2AX foci formation in peripheral blood lymphocytes of tumor patients after local radiotherapy to different sites of the body: dependence on the dose-distribution, irradiated site and time from start of treatment. Int J Radiat Biol 2007; 83:639–52.
7. Lobrich M, Shibata A, Beucher A, Fisher A, Ensminger M, Goodarzi AA, et al. GammaH2AX foci analysis for monitoring DNA double-strand break repair: strengths, limitations and optimization. Cell Cycle 2010; 9:662–9.
8. Lobrich M, Rief N, Kuhne M, Heckmann M, Fleckenstein J, Rube C, et al. In vivo formation and repair of DNA double-strand breaks after computed tomography examinations. Proc Natl Acad Sci U S A 2005; 102:8984–9.
9. Sedelnikova OA, Rogakou EP, Panyutin IG, Bonner WM. Quantitative detection of (125)IdU-induced DNA double-strand breaks with gamma-H2AX antibody. Radiat Res 2002; 158:486–92.
10. Cucinotta FA, Pluth JM, Anderson JA, Harper JV, O'Neill P. Biochemical kinetics model of DSB repair and induction of gamma-H2AX foci by non-homologous end joining. Radiat Res 2008; 169:214–22.
11. Redon CE, Weyemi U, Parekh PR, Huang D, Burrell AS, Bonner WM. Gamma-H2AX and other histone post-translational modifications in the clinic. Biochim Biophys Acta 2012; 1819:743–56.
12. Moroni M, Maeda D, Whitnall MH, Bonner WM, Redon CE. Evaluation of the gamma-H2AX assay for radiation biodosimetry in a swine model. Int J Mol Sci 2013; 14:14119–35.
13. Lamkowski A, Forcheron F, Agay D, Ahmed EA, Drouet M, Meineke V, et al. DNA damage focus analysis in blood samples of minipigs reveals acute partial body irradiation. PLoS One 2014; 9:e87458.
14. Redon CE, Nakamura AJ, Gouliaeva K, Rahman A, Blakely WF, Bonner WM. The use of gamma-H2AX as a biodosimeter for total-body radiation exposure in non-human primates. PLoS One 2010; 5:e15544.
15. Zwicker F, Swartman B, Sterzing F, Major G, Weber KJ, Huber PE, et al. Biological in-vivo measurement of dose distribution in patients' lymphocytes by gamma-H2AX immunofluorescence staining: 3D conformal- vs. step-and-shoot IMRT of the prostate gland. Radiat Oncol 2011; 6:62.
16. Werbrouck J, Ost P, Fonteyne V, De Meerleer G, De Neve W, Bogaert E, et al. Early biomarkers related to secondary primary cancer risk in radiotherapy treated prostate cancer patients: IMRT versus IMAT. Radiother Oncol 2013; 107:377–81.
17. Delaney G, Jacob S, Featherstone C, Barton M. The role of radiotherapy in cancer treatment: estimating optimal utilization from a review of evidence-based clinical guidelines. Cancer 2005; 104:1129–37.
18. Gupta ML, Srivastava NN, Dutta S, Shukla SK, Dutta A, Verma S, et al. Blood biomarkers in metal scrap workers accidentally exposed to ionizing radiation: a case study. Hum Exp Toxicol 2013; 32:1311–22.
19. Rothkamm K, Barnard S, Ainsbury EA, Al-Hafidh J, Barquinero JF, Lindholm C, et al. Manual versus automated gamma-H2AX foci analysis across five European laboratories: Can this assay be used for rapid biodosimetry in a large scale radiation accident? Mutat Res 2013; 756:170–3.
20. Rothkamm K, Horn S, Scherthan H, Rossler U, De Amicis A, Barnard S, et al. Laboratory Intercomparison on the gamma-H2AX Foci Assay. Radiat Res 2013; 180:149–55.
21. Ainsbury EA, Al-Hafidh J, Bajinskis A, Barnard S, Barquinero JF, Beinke C, et al. Inter- and intra-laboratory comparison of a multibiodosimetric approach to triage in a simulated, large scale radiation emergency. Int J Radiat Biol 2014; 90:193–202.
22. Gokbuget N, Hoelzer D, Arnold R, Bohme A, Bartram CR, Freund M, et al. Treatment of adult ALL according to protocols of the German Multicenter Study Group for Adult ALL (GMALL). Hematol Oncol Clin North Am 2000; 14:1307–25, ix.
23. Lefrere F, Delmer A, Suzan F, Levy V, Belanger C, Djabarri M, et al. Sequential chemotherapy by CHOP and DHAP regimens followed by high-dose therapy with stem cell transplantation induces a high rate of complete response and improves event-free survival in mantle cell lymphoma: a prospective study. Leukemia 2002; 16:587–93.
24. Horn S, Barnard S, Rothkamm K. Gamma-H2AX-based dose estimation for whole and partial body radiation exposure. PLoS One 2011; 6:e25113.
25. Cytogenetic analysis for radiation dose assessment: a manual. IAEA Technical Reports Series No. 405. Vienna, Austria: International Atomic Energy Agency; 2001.
26. Savage JR. Classification and relationships of induced chromosomal structural changes. J Med Genet 1976; 13:103–22.
27. Deurenberg P, Yap M, van Staveren WA. Body mass index and percent body fat: a meta analysis among different ethnic groups. Int J Obes Relat Metab Disord 1998; 22:1164–71.
28. Siri WE. The gross composition of the body. Adv Biol Med Phys 1956; 4:239–80.
29. Redon CE, Nakamura AJ, Gouliaeva K, Rahman A, Blakely WF, Bonner WM. Q(gamma-H2AX), an analysis method for partial-body radiation exposure using gamma-H2AX in nonhuman primate lymphocytes. Radiat Meas 2011; 46:877–81.
30. Sasaki MS, Miyata H. Biological dosimetry in atomic bomb survivors. Nature 1968; 220:1189–93.
31. Papworth DG. Curve fitting by maximum likelihood. Radiat Bot 1975; 15:127–40.
32. Wilkins RC, Romm H, Kao TC, Awa AA, Yoshida MA, Livingston GK, et al. Interlaboratory comparison of the dicentric chromosome assay for radiation biodosimetry in mass casualty events. Radiat Res 2008; 169:551–60.
33. Sak A, Grehl S, Engelhard M, Wierlemann A, Kaelberlah HP, Erichsen P, et al. Long-term in vivo effects of cisplatin on gamma-H2AX foci signaling in peripheral lymphocytes of tumor patients after irradiation. Clin Cancer Res 2009; 15:2927–34.
34. Jacoby MA, De Jesus Pizarro RE, Shao J, Koboldt DC, Fulton RS, Zhou G, et al. The DNA double-strand break response is abnormal in myeloblasts from patients with therapy-related acute myeloid leukemia. Leukemia 2014; 28:1242–51.
35. Williams LR. Reference values for total blood volume and cardiac output in humans. Report ORNL/TM-12814. Oak Ridge, TN: Oak Ridge National Laboratory; 1994.
36. Hartel C, Nikoghosyan A, Durante M, Sommer S, Nasonova E, Fournier C, et al. Chromosomal aberrations in peripheral blood lymphocytes of prostate cancer patients treated with IMRT and carbon ions. Radiother Oncol 2010; 95:73–8.
37. d'Alesio V, Pacelli R, Durante M, Canale Cama G, Cella L, Gialanella G, et al. Lymph nodes in the irradiated field influence the yield of radiation-induced chromosomal aberrations in lymphocytes from breast cancer patients. Int J Radiat Oncol Biol Phys 2003; 57:732–8.
38. Roch-Lefevre S, Pouzoulet F, Giraudet AL, Voisin P, Vaurijoux A, Gruel G, et al. Cytogenetic assessment of heterogeneous radiation doses in cancer patients treated with fractionated radiotherapy. Br J Radiol 2010; 83:759–66.
39. Edwards AA. The use of chromosomal aberrations in human lymphocytes for biological dosimetry. Radiat Res 1997; 148:S39–44.
40. Durante M, Yamada S, Ando K, Furusawa Y, Kawata T, Majima H, et al. Measurements of the equivalent whole-body dose during radiation therapy by cytogenetic methods. Phys Med Biol 1999; 44:1289–98.

41. Ekstrand KE, Dixon RL, Plunkett S, Raben M. The calculation of the dose to lymphocytes in external beam radiation therapy. Radiat Res 1981; 85:399–407.

42. Chee CA, Ilbery PL, Rickinson AB. Depression of lymphocyte replicating ability in radiotherapy patients. Br J Radiol 1974; 47:37–43.

43. Jones TD, Morris MD, Young RW. A mathematical model for radiation-induced myelopoiesis. Radiat Res 1991; 128:258–66.

44. Mariotti LG, Pirovano G, Savage KI, Ghita M, Ottolenghi A, Prise KM, et al. Use of the gamma-H2AX assay to investigate dna repair dynamics following multiple radiation exposures. PLoS One 2013; 8:e79541.

45. Dossou J, Lartigau E, M'Kacher R, Legal JD, Bridier A, Guichard M, et al. Biological dosimetry after total body irradiation (TBI) for hematologic malignancy patients. Int J Radiat Oncol Biol Phys 2000; 46:123–9.

9.2 Publikation II

Quantification of Radiation Biomarkers in Leukocytes of Breast Cancer Patients Treated with Different Modalities of 3D-CRT or IMRT

RADIATION RESEARCH **186**, 508–519 (2016)
0033-7587/16 $15.00

DOI: 10.1667/RR14475.1

Quantification of Radiation Biomarkers in Leukocytes of Breast Cancer Patients Treated with Different Modalities of 3D-CRT or IMRT

Sebastian Zahnreich,[a,1] Anne Ebersberger,[a] Heiko Karle,[a] Bernd Kaina[b] and Heinz Schmidberger[a]

Departments of [a] Radiation Oncology and Radiation Therapy and [b] Toxicology, University Medical Center Johannes Gutenberg University Mainz, 55131 Mainz, Germany

Zahnreich, S., Ebersberger, A., Karle, H., Kaina, B. and Schmidberger, H., Quantification of Radiation Biomarkers in Leukocytes of Breast Cancer Patients Treated with Different Modalities of 3D-CRT or IMRT. *Radiat. Res.* 186, 508–519 (2016).

The goal of this study was to determine whether the quantification of radiation biomarkers in peripheral leukocytes of 111 breast cancer patients after adjuvant treatment with different modalities of three-dimensional conformal radiation therapy (3D-CRT) or intensity-modulated radiation therapy (IMRT) revealed any difference in the patients' radiation burden by out-of-field doses and an associated risk of second malignancies. Whole-breast radiation therapy was performed by 3D-CRT using either a hard wedge (n = 32) or a virtual wedge (n = 49) at dose rates of 3 and 6 Gy per min each. Patients receiving additional radiotherapy to lymph nodes were treated by 3D-CRT (n = 21) or IMRT (n = 9). DNA damage was measured as γ-H2AX foci (n = 111) and as unstable chromosomal aberrations (n = 15) in leukocytes drawn 30 min and 24 h after the first radiation fraction, respectively. The individual basal yield and radiation sensitivity *ex vivo* were assessed in leukocytes obtained before the first treatment. After radiation therapy, the average rate of γ-H2AX foci and chromosomal aberrations per leukocyte were dependent on multiple parameters of irradiation: the treatment volume, the administered equivalent whole-body dose, the number of monitor units and the beam-on time. Different modalities of radiation therapy caused significant variations in the levels of both radiation biomarkers irrespective of the treatment volume and administered dose, and in particular, a twofold higher rate after IMRT compared to 3D-CRT. Any deviation in biomarker response between radiation therapy techniques was directed by a linear dependence on the absolute beam-on time. However, the dispersion of γ-H2AX foci in peripheral leukocytes after radiation therapy correlated very well with the relative distribution of dose in the whole-body volume for each radiation therapy technique. In conclusion, the induction of radiation biomarkers in leukocytes of breast cancer patients by different radiotherapy modalities is dominated by general variables of irradiation. There was no significant difference in peripheral dose exposure observed in the investigated radiation therapy techniques. Radiotherapy techniques with prolonged absolute beam-on time increase the fraction of exposed leukocytes with pronounced risks for hematologic toxicities or immunosuppressive side effects.

INTRODUCTION

Radiation therapy is a mainstay for treatment of approximately half of all newly diagnosed cancer patients (*1*). Current external-beam radiotherapy techniques deliver highly focused and conformal beams to a well-defined planning target volume (PTV) and spare nearby critical structures from high radiation doses. However, radiotherapy is inevitably associated with unwanted exposure of normal tissue far from the PTV. So-called out-of-field doses are generated predominantly by leakage from the medical linear accelerator (linac) treatment head and scatter from collimation devices and, to a lesser extent, by scatter from within the patient's body and backscatter from the linac bunker (*2*). Compared to the high dosage of the primary beam, where most attention is given to deterministic effects, out-of-field doses are low but distributed over large proportions of the body and have been associated with various radiation-related late adverse effects, such as cardiac toxicity and second malignancies as the most detrimental stochastic outcome (*3–5*). Since earlier diagnosis and more sophisticated radiotherapy techniques have progressively prolonged survival and improved cure rates of cancer patients over the past decades, the risk of late adverse effects, including second malignancies, is now a clinical concern not only for pediatric patients, but for adult patients as well (*6, 7*).

The most prevalent tumor entity in females is breast cancer (*8*), which is commonly treated with adjuvant radiotherapy (*9*). In radiation therapy for breast cancer, the development of second malignancies in the normal tissue is

Editor's note. The online version of this article (DOI: 10.1667/RR14475.1) contains supplementary information that is available to all authorized users.

[1] Address for correspondence: Department of Radiation Oncology and Radiation Therapy, University Medical Center Johannes Gutenberg University Mainz, Langenbeckstrasse 1, 55131 Mainz, Germany, e-mail: sebastian.zahnreich@unimedizin-mainz.de.

a relevant concern (*10*), highlighting the need for normal tissue sparing during treatment. Breast cancer treatment is mainly performed with tangential three-dimensional conformal radiation therapy (3D-CRT). Here, opposing beams are shaped by beam compensators, such as hard wedges or virtual and enhanced dynamic wedges, to achieve the desired distribution of dose. Compared to a virtual or dynamic wedge, beam shaping by a hard wedge requires a higher number of monitor units (MU) to achieve the desired dose at the isocenter. Monitor units are a direct measure of the delivered dose according to the beam output of the linac and correlates with beam-on time (BOT) when otherwise similar irradiation parameters are applied. Therefore, longer BOT during radiotherapy with a hard wedge ultimately increases the patient's out-of-field doses since more scattered and leaked radiation is generated compared to a virtual or dynamic wedge (*11–13*).

In addition to 3D-CRT, multibeam intensity-modulated radiation therapy (IMRT) has been recently used more frequently for adjuvant breast cancer treatment when irradiation of the chest wall and regional lymph nodes is indicated (*14*, *15*). Breast cancer treatment with IMRT improves local tumor control and reduces acute toxicity by a more complex and favorable dose distribution (*16*) with a marked reduction of high doses to organs at risk: the lung, heart and contralateral breast (*17*). When compared to 3D-CRT, a drawback of IMRT is a conformal distribution of dose in the PTV with intensity-modulated fields. A larger proportion of the normal tissue is exposed to a ''low-dose-bath'', since more fields must be applied from different angles of incidence. Furthermore, a 3–5 times higher number of MU must be administered and the consequent longer BOT increases the amount of scattered and leaked radiation (*18, 19*). Both factors expand the volume of low-dose-exposed normal tissue and the relative risk of radiation-related second malignancies therein, which is assumed to be doubled for IMRT compared to 3D-CRT (*18, 20, 21*). However, to our knowledge, there have been no published clinical studies on the relative risk of second malignancies after IMRT compared to 3D-CRT, due to the limited period of clinical applications of IMRT. These will require a retrospective analysis in the future. Supplementary Fig. S1 (http://dx.doi.org/10.1667/RR14475.1.S1) provides a comparison of the distribution of dose in dose color wash according to the computed tomography-based treatment planning for 3D-CRT and IMRT of two representative breast cancer patients from the current study.

Most approaches to estimate the out-of-field doses during radiotherapy are based on instant physical dosimetry, analytical calculations and Monte Carlo simulations. Calculations of second cancer risk after radiotherapy are based on the concept of organ-equivalent dose implemented in linear, linear-exponential and plateau dose-response models (*22, 23*), however, these are subject to large uncertainties.

In this study, we used a biodosimetric approach to compare the exposure to out-of-field doses and an associated risk of radiation-related second malignancies for breast cancer patients during adjuvant treatment with different modalities of 3D-CRT or with IMRT. Radiation-induced DNA damage was assessed in leukocytes of 81 patients after 3D-CRT using either a hard wedge or a virtual wedge at dose rates of 3 and 6 Gy per min each. Furthermore, 30 patients indicated for lymph node irradiation who were treated either with 3D-CRT or with IMRT were investigated. DNA damage in leukocytes was quantified as γ-H2AX foci, a surrogate marker of DNA double-strand breaks (*24*), and as chromosomal aberrations arising from erroneous double-strand break repair 30 min and 24 h after the first fraction of radiation, respectively. The individual basal yield and radiation sensitivity *ex vivo* were assessed in leukocytes obtained before the first treatment. Both radiation biomarkers are regarded as estimators of the absorbed equivalent whole-body dose during partial-body irradiation (*25–27*) and represent early indicators of health risks after genotoxic events, closely related to adverse long-term effects, including cancer (*28–34*). Of note, data from 57 patients treated with 3D-CRT are in part derived from our recently published data set (*27*).

MATERIALS AND METHODS

Patients

Female breast cancer patients (n = 111) who were treated at the Department of Radiation Oncology and Radiation Therapy at the University Medical Centre Mainz (Germany) were consecutively enrolled in this study and signed an informed consent form approved by the local Ethics Committee. The PTV included the breast (n = 101) or the chest wall (n = 10). A subset of patients received additional radiation therapy to the lymph nodes (n = 30). Fifty-five patients were treated for left-sided and 56 for right-sided breast cancer. For 13 patients who were treated for left-sided breast cancer, deep inspiration breath-hold techniques (*35*) were applied. There were 43 patients who received neoadjuvant (n = 13) and adjuvant (n = 30) chemotherapy. Four patients had previously received radiotherapy. Every patient underwent a computed tomography scan (Brilliance CT-Big Bore, Phillips Healthcare, Andover, MA) approximately one week prior to radiotherapy for 3D treatment planning (Eclipse™ ver. 10.0; Varian Medical Systems Inc., Palo Alto, CA). Patients received five daily radiation fractions per week and an average tumor dose of 1.8–2 Gy per fraction. A subgroup of patients was treated with a hypofractionated regime with a tumor dose of 2.67 Gy per fraction according to the UK Standardization of Breast Radiotherapy (START) Trial B (*36*). All patients were treated with a 6 MV photon beam. Three different linacs were used in this study: 9 patients were treated with an ONCOR™/MD2 (Siemens, Munich, Germany); 15 patients with a Clinac® DHX (Varian Medical Systems Inc.) and 87 patients with a UNIQUE™ (Varian Medical Systems Inc.). Patients who did not receive additional radiation to the lymph nodes were treated by 3D-CRT either with a 15° or 30° hard wedge or with a virtual wedge and the field-in-field technique at a dose rate of 300 or 600 MU per min, equivalent to 3 and 6 Gy per min, each. Patients receiving additional radiation to the lymph nodes were treated by 3D-CRT or by multibeam step-and-shoot IMRT. Table 1 shows summarized information on patient numbers for each radiotherapy technique and their respective irradiation parameters. Patients were recruited on a

daily basis without any interference to their planned treatment, resulting in an unequal distribution among the radiotherapy techniques.

Blood Sampling and Processing

Venous blood was collected immediately before as well as 30 min and 24 h after the first radiotherapy fraction. To assess the basal yield and radiation sensitivity *ex vivo*, blood taken before irradiations was sham- or 0.5 and 2 Gy X-ray irradiated to score foci in leukocytes, which were isolated from whole blood 45 min after exposure, and unstable aberrations in first post-exposure mitoses, respectively. To determine the amount of radiation-induced DNA damage in leukocytes, foci and chromosomal aberrations were scored 30 min and 24 h after the first radiation fraction, respectively. The respective time points of analysis after the first radiotherapy session were chosen to obtain maximum yields for each radiation biomarker assay as evaluated in our previously published study (*27*). The basal rate of DNA damage was subtracted from the yield after any irradiation *ex vivo* or *in vivo*. A detailed description of blood collection, irradiation *ex vivo* and leukocyte isolation from whole blood is provided in our previously published study (*27*).

Gamma-H2AX Foci Quantification

Fixation of leukocytes, γ-H2AX immunostaining, microscopy, image capturing and scoring of foci were performed as previously described (*27*). After irradiation *ex vivo* or *in vivo*, an average of 250 or 800 cells were counted manually for each data point, respectively.

Cytogenetic Analysis

Chromosome preparation and scoring of dicentric chromosomes, centric rings and acentric fragments in Giemsa-stained first division metaphases was performed as described previously (*27*). After 2 Gy irradiation *ex vivo*, 100 metaphases were scored. Before and after the first radiation fraction, 500 metaphases were scored each.

Equivalent Whole-Body Dose

The individual equivalent whole-body dose (EWBD) as the average dose per voxel over the whole-body volume after partial-body irradiation was calculated as described previously (*27*). Briefly, the mean dose deposited in the CT-scanned body volume per fraction was weighted with the whole-body proportion of the CT-scanned body volume, both obtained from the treatment planning software. The whole-body volume was calculated by dividing weight by body density, considering height, age, gender and body fat percentage (*37, 38*). The distribution of the physical dose within the whole-body structure was calculated based on the data of the cumulative dose-volume histogram for the CT-scanned body volume that was normalized to the whole-body volume according to Zwicker *et al.* (*39*).

Data and Statistical Analysis

For each patient, a single sample was analyzed per data point and error bars were calculated based on Poisson statistics as indicated. Summarized patient data is presented as the mean and standard deviation (SD). The relationship between two variables was analyzed using Pearson's test and is provided as the correlation coefficient (r). For comparison of the means of two or more groups the Student's *t* test or one-way analysis of variance (ANOVA) with pairwise comparison (Holm-Sidak method) was used, respectively. Statistics on the distribution of foci in leukocytes or physical dose in the whole-body volume were performed by comparing each of the respective data points for the different radiotherapy modalities. All levels of significance were set at $P < 0.05$.

RESULTS

Gamma-H2AX Foci and Chromosomal Aberrations before Radiation Therapy and after Irradiation Ex Vivo

The basal rate of chromosomal aberrations in leukocytes prior to the first radiation fraction was significantly higher in patients who had a previous chemotherapy or radiotherapy, showing 0.026 ± 0.002 ($n = 11$) aberrations per cell compared to patients without any previous chemo- or radiotherapy carrying 0.014 ± 0.003 ($n = 4$) aberrations per cell ($P < 0.01$). The average yield of foci per leukocyte was similar among these groups of patients with respective numbers of 0.25 ± 0.03 ($n = 45$) and 0.23 ± 0.02 ($n = 66$). After irradiation *ex vivo*, both the average number of radiation-induced chromosomal aberrations per leukocyte after 2 Gy irradiation and of radiation-induced foci per leukocyte 45 min after 0.5 Gy irradiation was comparable among patients with or without previous chemotherapy or radiotherapy with respective average numbers of 0.59 ± 0.02 ($n = 11$) or 0.53 ± 0.06 ($n = 4$) and 5.98 ± 0.11 ($n = 41$) or 5.97 ± 0.08 ($n = 62$). Therefore, an impact of a clastogenic medical pretreatment before the current radiotherapy on the rate of the actual radiation-induced DNA damage in leukocytes was considered to be highly unlikely, in agreement with our previously published results (*27*).

Gamma-H2AX Foci and Chromosomal Aberrations after Radiation Therapy

As the initial step for determining the yield of foci and dicentrics plus centric rings in patients' leukocytes after the first radiation fraction, we examined any relationship with the radiation-related variables PTV, EWBD, BOT and MU, as shown in Figs. 1A–D and 2A–D, respectively. Information on the irradiation parameters of each patient group is summarized in Table 1. Given the broad heterogeneity of treatment parameters for the different irradiation techniques, Table 2 provides a detailed correlation analysis of the rate of radiation-induced foci or dicentrics plus centric rings per leukocyte and the radiotherapy parameters for each patient population.

For patients who were treated with one of the five different modalities of 3D-CRT we found significant relationships between the frequency of radiation-induced foci and the EWBD or PTV in four or three of the patient groups, respectively (Table 2). The summary of patient data for 3D-CRT revealed a strong correlation of the average number of radiation-induced foci with the EWBD, and medium-to-moderate correlations with the PTV, BOT and number of MU (Fig. 1A–D and Table 2). Compared to 3D-CRT, the number of radiation-induced foci per leukocyte was higher in IMRT-treated patients, with similar PTV (Fig. 1A) and EWBD (Fig. 1B). As shown in Fig. 1C and D, prolonged BOT and more MU during IMRT increased the frequency of radiation-induced foci and improved correlations compared to 3D-CRT (Table 2).

TABLE 1
Respective Numbers of 111 Breast Cancer Patients Analyzed by each Biomarker Assay and the Corresponding Technical Parameters of the Applied Modalities of Radiation Therapy

Biodosimetric assay	Gamma-H2AX foci			
Radiation therapy technique	3D-CRT[a]			
	Virtual wedge "field-in-field"		Hard wedge	
Patient subset	Without lymph nodes			
Dose rate (monitor units/min)	300	600	300	600
Number of analyzed patients	15	34	13	19
Tumor dose (Gy)	2.2 ± 0.4	2.2 ± 0.4	2.3 ± 0.4	2.4 ± 0.4
Number of fields	4.7 ± 1.5	4.5 ± 1.1	3.4 ± 0.9	3.2 ± 1.1
Beam-on time (min)	1.06 ± 0.19	0.56 ± 0.12	1.59 ± 0.48	0.86 ± 0.18
Monitor units (AU)	267 ± 46	266 ± 48	417 ± 83	410 ± 87
Planning target volume (cm^3)	1206 ± 611	1024 ± 404	967 ± 455	1136 ± 703
Equivalent whole-body dose (Gy)	0.060 ± 0.022	0.061 ± 0.017	0.079 ± 0.028	0.071 ± 0.024

Notes. Data are provided as the mean ± SD and have been partially derived for: [a]45, [b]12 and [c]8 patients from a previously published data set (*27*). 3D-CRT = three-dimensional conformal radiation therapy; IMRT = intensity-modulated radiation therapy; dic + CR: dicentrics plus centric rings.

As shown in Fig. 2A and B, radiation-induced cytogenetic damage, measured as dicentrics plus centric rings in leukocytes of 15 patients after 3D-CRT or IMRT, did not correlate with the PTV or EWBD (Table 2). As for radiation-induced foci, longer BOT and more MU during IMRT compared to 3D-CRT increased the rate of radiation-induced dicentrics plus centric rings, resulting in strong correlations (Fig. 2C and D, respectively; Table 2). As shown in Fig. 3, in 15 patient samples analyzed by both assays, the frequency of radiation-induced foci and dicentrics plus centric rings per leukocyte correlated with a fitted linear function of $Y = 0.61 \pm 0.30 + 45.6 \pm 17.8 \times X$ ($r = 0.60$, $P < 0.01$).

Detection of Out-of-Field Doses by Gamma-H2AX Foci and Chromosomal Aberrations

We investigated whether any deviation in out-of-field doses among different radiotherapy techniques could be

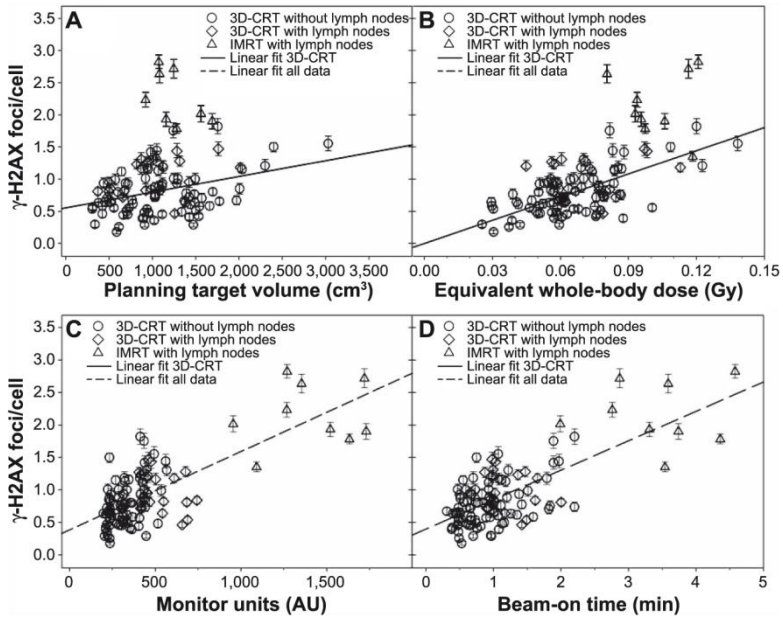

FIG. 1. Relationships of the mean number of radiation-induced γ-H2AX foci per cell and the irradiated volume (panel A), equivalent whole-body dose (panel B), number of monitor units (panel C) and beam-on time (panel D). Error bars represent the 95% confidence interval of the Poisson mean. The relationship shown in panel B has been published previously for 57 patients after 3D-CRT (*27*). Selected linear fits are shown for significant correlations ($P < 0.05$). For detailed correlation data see Table 2.

TABLE 1
Extended.

Gamma-H2AX foci		Chromosomal aberrations (dic + CR)		
3D-CRT[b]	IMRT	3D-CRT[c]		IMRT
		Virtual wedge "field-in-field"		
With lymph nodes		Without lymph nodes	With lymph nodes	
600	600	600	600	600
21	9	5	5	5
1.8 ± 0	1.8 ± 0.1	2.0 ± 0.4	1.8 ± 0	1.8 ± 0
7.0 ± 2.2	10 ± 3.0	4.4 ± 2.3	6.8 ± 1.4	11 ± 3.0
1.17 ± 0.33	3.42 ± 0.80	0.68 ± 0.23	0.99 ± 0.54	3.3 ± 0.90
522 ± 109	1394 ± 276	250 ± 48	448 ± 186	1388 ± 309
951 ± 434	1227 ± 252	1513 ± 610	1136 ± 567	1306 ± 321
0.070 ± 0.017	0.103 ± 0.014	0.079 ± 0.019	0.079 ± 0.024	0.094 ± 0.009

elucidated in leukocytes using the radiation biomarker approach. EWBD calculations in the current study and other comparable published studies (*25, 27, 40*) are based on data from commercial treatment planning systems. Since their algorithms are primarily designed for precise calculations of the high dosage in the PTV, out-of-field doses are substantially underestimated (*41–43*). To this end, the average yield of radiation-induced DNA damage per leukocyte was normalized to the predicted EWBD for each patient.

As shown in Fig. 4A–D, the EWBD-normalized data on radiation-induced foci and dicentrics plus centric rings in leukocytes of all patient populations correlated well with the BOT as well as the total number of administered MU, particularly for radiation-induced foci. The respective functions of the linear regressions for EWBD-weighted, radiation-induced foci were: $Y = 8.83 \pm 0.48 + 3.72 \pm 0.28 \times X$ ($r = 1$, $P < 0.001$) and $Y = 9.57 \pm 0.88 + 0.0086 \pm 0.0013 \times X$ ($r = 1$, $P < 0.01$). Based on these correlations, the average rate of EWBD-normalized, radiation-induced foci and dicentrics plus centric rings per leukocyte was doubled after IMRT compared to all 3D-CRT modalities. Significance was only reached for data on foci ($P < 0.01$). However, despite the general linear dependency

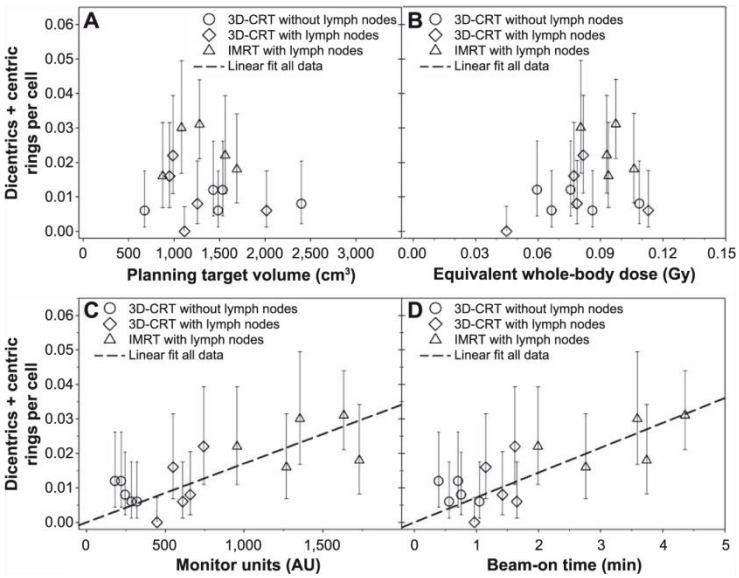

FIG. 2. Relationships of the mean number of radiation-induced dicentrics plus centric rings per cell and the irradiated volume (panel A), equivalent whole-body dose (panel B), number of monitor units (panel C) and beam-on time (panel D). Error bars represent the 95% confidence interval of the Poisson mean. The relationship shown in panel B has been published previously for 8 patients after 3D-CRT (*27*). Selected linear fits are shown for significant correlations ($P < 0.05$). For detailed correlation data see Table 2.

TABLE 2
Pearson Product-Moment Correlation Coefficients (r), *P* Values and Slopes ± Standard Deviations of Linear Regressions for the Relationships between the Average Frequency of Radiation Therapy-Induced γ-H2AX Foci and Dicentrics plus Centric Rings per Leukocyte for each Modality of Radiation Therapy and the Treatment Parameters: Equivalent Whole-Body Dose (EWBD), Planning Target Volume (PTV), Beam-On Time (BOT) and Monitor Units (MU)

		Gamma-H2AX foci[a]	
Radiation therapy technique	Pearson	EWBD (Gy)	PTV (cm^3)
3D-CRT			
Virtual wedge without lymph nodes			
300 MU/min	r value	0.78	0.59
γ-H2AX foci: n = 15	*P* value	<0.001	<0.05
	Slope ± SD	10.70 ± 2.40	$3*10^{-4} \pm 1*10^{-4}$
600 MU/min	r value	0.45	0.25
γ-H2AX foci: n = 34	*P* value	<0.01	n.s.
	Slope ± SD	6.16 ± 2.18	-
Hard wedge without lymph nodes			
300 MU/min	r value	0.76	0.45
γ-H2AX foci: n = 13	*P* value	<0.01	n.s.
	Slope ± SD	10.60 ± 2.73	-
600 MU/min	r value	0.62	0.55
γ-H2AX foci: n = 19	*P* value	<0.01	<0.05
	Slope ± SD	8.91 ± 2.78	$3*10^{-4} \pm 1*10^{-4}$
All patients without lymph nodes	r value	0.68	0.38
γ-H2AX foci: n = 81	*P* value	<0.00001	<0.001
dic + CR: n = 5	Slope ± SD	10.50 ± 1.28	$3*10^{-4} \pm 7*10^{-5}$
With lymph nodes	r value	0.27	0.52
γ-H2AX foci: n=21	*P* value	n.s.	<0.05
dic + CR: n = 5	Slope ± SD	-	$4*10^{-4} \pm 1*10^{-4}$
All 3D-CRT patients	r value	0.62	0.36
γ-H2AX foci: n=102	*P* value	<0.00001	<0.001
dic + CR: n = 5	Slope ± SD	10.0 ± 1.30	$2*10^{-4} \pm 6*10^{-5}$
IMRT			
With lymph nodes	r value	0.01	–0.21
γ-H2AX foci: n = 9	*P* value	n.s.	n.s.
dic + CR: n = 5	Slope ± SD	-	-
3D-CRT and IMRT			
With lymph nodes	r value	0.65	0.42
γ-H2AX foci: n = 30	*P* value	<0.001	<0.05
dic + CR: n = 10	Slope ± SD	19.60 ± 4.37	$7*10^{-4} \pm 3*10^{-4}$
Σ all patients	r value	0.66	0.29
γ-H2AX foci: n = 111	*P* value	<0.00001	<0.01
dic + CR: n = 15	Slope ± SD	14.8 ± 1.61	$3*10^{-4} \pm 9*10^{-5}$

Notes. Data are provided as the mean ± standard deviation and have been partially derived for: [a]57 and [b]8 patients from a previously published data set (*27*). Slopes of linear regressions are provided for significant correlations ($P < 0.05$). 3D-CRT = three-dimensional conformal radiation therapy; IMRT = intensity-modulated radiation therapy.

of EWBD-normalized, radiation-induced foci per leukocyte on the administered MU for all patient groups, halving the dose rate during 3D-CRT without lymph node irradiation increased the average level of EWBD-normalized foci 1.3-fold ($P < 0.05$) for a hard wedge and 1.2-fold ($P > 0.05$) for a virtual wedge (Fig. 4C) when a comparable number of total MU was administered.

Physical Dose Distribution in Whole-Body Volume and of Gamma-H2AX Foci in Leukocytes after Radiation Therapy

Previously published studies have suggested that the dispersion of radiation-induced foci in leukocytes correlates with the calculated physical dose distribution in the whole-body volume and can be applied as a comparative measure in whole-body dosimetry (*39, 44*). Therefore, we compared the dispersion of radiation-induced foci in peripheral leukocytes with the physical dose distribution predicted by cumulative dose–volume histograms of the treatment planning software for each radiotherapy technique.

Differences in the dispersion of foci in leukocytes among the 3D-CRT modalities without irradiation of lymph nodes matched the respective distinctions in physical dose distribution in the whole-body volume as shown comparatively in Fig. 5A and B, respectively. The fraction of leukocytes with less than six foci and the proportion of the whole-body volume that received ≤0.2 Gy varied significantly among the four 3D-CRT modalities ($P < 0.05$), notably between a hard wedge at 300 MU per min and a virtual wedge at 600 MU per min. An even more pronounced difference among the distributions of radiation-induced foci in leukocytes or the physical dose in the

TABLE 2
Extended.

Gamma-H2AX foci[a]		Chromosomal aberrations (dicentrics plus centric rings)[b]			
BOT(min)	MU (AU)	EWBD (Gy)	PTV (cm^3)	BOT(min)	MU (AU)
–0.06	0.15				
n.s.	n.s.				
-	-				
0.18	0.23				
n.s.	n.s.				
-	-				
0.11	0.26				
n.s.	n.s.				
-	-				
0.19	0.30				
n.s.	n.s.				
-	-				
0.45	0.47	–0.15	–0.04	0.52	–0.16
<0.0001	<0.00001	n.s.	n.s.	n.s.	n.s.
0.35 ± 0.08	$1.7*10^{-3} \pm 4*10^{-4}$	-	-	-	-
–0.14	–0.28	0.27	–0.44	0.44	0.72
n.s.	n.s.	n.s.	n.s.	n.s.	n.s.
-		-	-	-	-
0.40	0.38	0.12	–0.31	0.57	0.57
<0.0001	<0.0001	n.s.	n.s.	n.s.	n.s.
0.32 ± 0.07	$1.0*10^{-3} \pm 3*10^{-4}$	-	-	-	-
0.06	0.16	–0.50	–0.10	053	0.15
n.s.	n.s.	n.s.	n.s.	n.s.	n.s.
-	-	-	-	-	-
0.75	0.77	0.35	–0.20	0.74	0.70
<0.00001	<0.00001	n.s.	n.s.	<0.05	<0.05
0.43 ± 0.07	$1.2*10^{-3} \pm 2*10^{-4}$	-	-	$6.2*10^{-3} \pm 2*10^{-3}$	$1.5*10^{-5} \pm 5.4*10^{-6}$
0.72	0.74	0.31	–0.25	0.82	0.79
<0.00001	<0.00001	n.s.	n.s.	<0.001	<0.001
0.45 ± 0.04	$1.2*10^{-3} \pm 1*10^{-4}$	-	-	$6.7*10^{-3} \pm 1.3*10^{-3}$	$1.5*10^{-5} \pm 3.4*10^{-6}$

whole-body volume, again with matching patterns, was found between IMRT and 3D-CRT as shown in Fig. 5C and D, respectively. Compared to 3D-CRT, IMRT resulted in a significantly higher fraction of leukocytes with less than 10 radiation-induced foci and a whole-body volume exposed to <0.7 Gy ($P < 0.05$).

DISCUSSION

Physical dosimetry and modeling data demonstrate deviating distributions of low out-of-field doses in normal tissue for different techniques of external photon-beam radiotherapy. This has been associated with different relative risks for second malignancies as a fatal late consequence of radiotherapy (*18, 20, 21, 23, 45*). In this study, we compared the genotoxic radiation load of 111 breast cancer patients after adjuvant treatment with different modalities of 3D-CRT or IMRT by quantification of γ-H2AX foci and chromosomal aberrations in leukocytes, generally considered as intermediate end points and risk indicators of carcinogenesis (*31, 34*).

As indicated in previously published data, the average rate of radiation-induced γ-H2AX foci and chromosomal aberrations in leukocytes depends on the size of the PTV and the administered EWBD after radiotherapy in patients who are treated for the same tumor entity (*25–27*), even when different techniques of external photon-beam radiotherapy are applied (*39, 40*). The data presented in this work show significant deviations from these correlations after adjuvant treatment of breast cancer with different radiotherapy techniques, in particular, an approximately twofold-higher yield of DNA damage after IMRT compared to 3D-CRT. Any PTV- and dose-independent variation of radiation biomarkers in leukocytes among radiotherapy techniques was governed by the absolute BOT and could

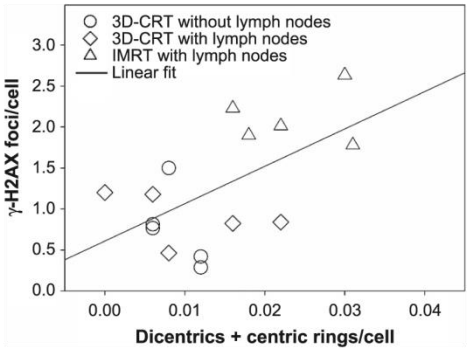

FIG. 3. Relationship of radiation-induced γ-H2AX foci per cell and dicentrics plus centric rings per cell scored in peripheral blood leukocytes of 15 breast cancer patients 30 min and 24 h after the first radiotherapy fraction, respectively.

not be attributed to an intrinsic radiation burden of the respective radiotherapy techniques.

The main focus of this study was to demonstrate a contribution of differing out-of-field doses of various radiotherapy techniques to the integral radiation burden of breast cancer patients. Published phantom studies of tangential breast radiation therapy showed 2.4 to 3.3-fold-higher extra target doses with the use of physical wedge-compared to virtual wedge-segmented techniques due to the higher number of MU to compensate absorption within the physical wedge (*11–13*). For IMRT treatment plans, Ruben *et al*. (*18*) reported an 80% greater out-of-field integral dose by 3.7 times more MU compared to 3D-CRT plans with similar numbers and field sizes. Of note, the resultant differences relative to the absolute prescribed doses are very low. We have therefore concentrated on the γ-H2AX foci assay as an radiation biomarker *in vivo* with a high sensitivity down to a few mGy (*46*). As for the calculation of the out-of-field doses, radiation treatment planning systems in general demonstrate poor accuracy and underestimate the actual peripheral doses with increasing distance from the field edge. For conventional radiotherapy (*43*) and IMRT (*41, 42*), an underestimation of out-of-field doses has been shown to a similar extend of 40 and 50% for different radiation treatment planning systems compared to measurements using thermoluminescent detectors on anthropomorphic phantoms. To reveal any effect of the out-of-field doses of different radiotherapy techniques on the level of radiation biomarkers in leukocytes in the current study, the generated data was normalized to the treatment planning data-based EWBD. The resultant normalized data followed a striking linear increment with the absolute BOT (Fig. 4A).

To rule out *a priori* an effect of the exposure time on the yield of radiation-induced DNA damage in the dynamic system of circulating peripheral leukocytes, we compared dose rates of 300 and 600 MU per min for 3D-CRT with a hard wedge and a virtual wedge each. Since leaked and scattered dose is proportional to the total dose delivered by the primary beam, the integral out-of-field dose should not be affected by variations in dose rate and should be comparable for patients treated by 3D-CRT with equal EWBD and the same beam-modifying device. As for the dynamic test system of circulating peripheral leukocytes, for irradiation *in vivo* of patients with a similar EWBD, a high

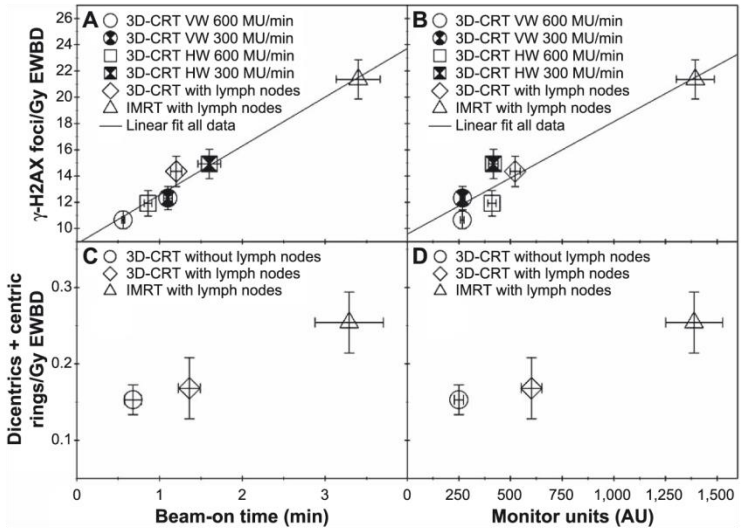

FIG. 4. Relationship of the equivalent whole-body dose (EWBD)-normalized mean number of radiation-induced γ-H2AX foci (panels A and C) or dicentrics plus centric rings (panels B and D) per leukocyte and the beam-on time (panels A and B) or the monitor units [MU (panels C and D)] in patients grouped according to the applied radiation therapy technique (see Table 1). Error bars represent the standard error of the mean. Linear fits are shown for significant correlations ($P < 0.05$). VW = virtual wedge; HW = hard wedge.

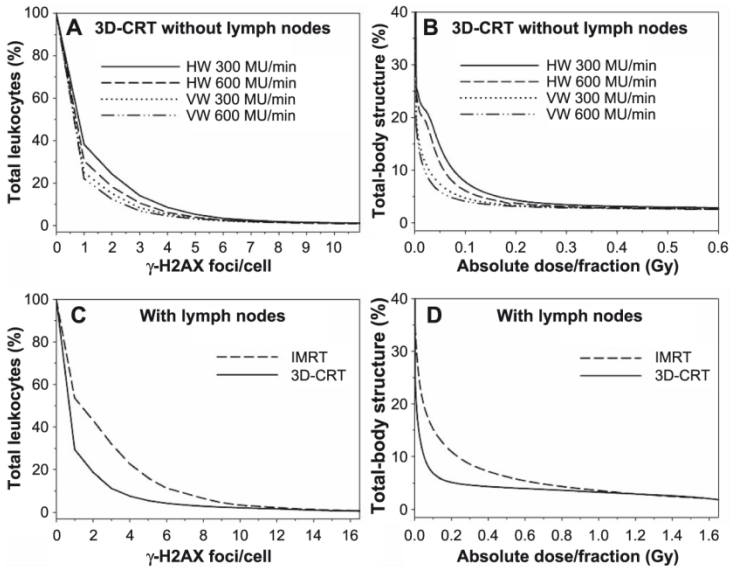

FIG. 5. Integral histograms of the dispersion of radiation-induced γ-H2AX foci in leukocytes (panels A and C) and of the physical dose to the whole-body volume according to the treatment planning software (panels B and D) for all patients grouped according to the applied radiotherapy technique (see Table 1). Each data point represents either the mean cumulative fraction of leukocytes with at least the corresponding number of radiation-induced γ-H2AX foci (panels A and C) or the total-body volume, which absorbed at least the corresponding dose (panels B and D). VW = virtual wedge; HW = hard wedge; MU = monitor units.

dose rate is expected to cause a low frequency of irradiated cells with high frequencies of DNA damage and *vice versa* (*47*), whereby the average rate per cell is comparable. First, in agreement with this assumption, the dispersion of radiation-induced foci in leukocytes showed that a longer BOT, due to the application of more MU or a halved dose rate, increased the fraction of leukocytes exposed to low proportions of the isodose (Fig. 5). The divergent distributions of radiation-induced foci in leukocytes correlated very well with the relative dose distributions in the whole-body volume based on dose-volume histograms of the radiation treatment planning software. However, doubling the absolute BOT by a halved dose rate during 3D-CRT with otherwise similar irradiation parameters unexpectedly increased the average frequency of EWBD-normalized foci in leukocytes significantly, even though the same total number of MU was applied (Fig. 4A and B). Although this BOT-dependent increase in blood dose could not be related to a higher whole-body dose, lymphoid tissue damage itself represents an important side effect of radiotherapy (*48, 49*). Since the fraction of aberrant lymphocytes has been shown to correlate with the reduction of the whole-blood cell count during radiotherapy (*50*), the observed effect of absolute BOT on the amount of radiation-induced DNA damage in leukocytes is of clinical concern. For example, this may play an important role in concomitant treatment of cancer patients undergoing radiotherapy and immunotherapy, which relies on T-cell activation to induce or improve antitumor immunity (*51*).

An effect of the dose rate itself on the number of radiation-induced γ-H2AX foci assessed 30 min after exposure is not expected for acute exposure with a high-dose output of 3 or 6 Gy per min. In the region of low-dose rates of 30 mGy, 10 mGy and 0.1 mGy per min, Beels *et al.* (*52*) observed no difference in the yield of γ-H2AX foci in leukocytes 15–30 min after static X-ray irradiation *ex vivo* of blood samples.

Syme *et al.* (*53*) showed that 2 Gy irradiation of normal human fibroblasts in a blocked 6 MV photon-beam configuration, comparable to the penumbral radiation of the primary beam, induced a 20% higher γ-H2AX signal than open-beam radiation given at the same dose rate. This finding has been conducted to a higher relative biological effectiveness by different electron fluence spectra of scattered radiation corresponding to an increase in the linear energy transfer, also successfully applied to chromosomal aberration data by Kirkby *et al.* (*54*). However, in the current study, it is very unlikely that a reduction of the dose rate of the primary beam during 3D-CRT altered the quality of the scattered radiation by decreasing its linear energy transfer, which might have caused the observed higher yield of γ-H2AX foci for 3D-CRT at 3 Gy per min compared to 6 Gy per min.

Recently, Zwicker *et al.* (*44*) reported on a twofold-higher average yield of γ-H2AX foci in leukocytes of prostate cancer patients after step-and-shoot IMRT compared to helical tomotherapy, which has been performed with similar irradiation parameters, except at a fourfold-higher dose rate.

The higher yield of foci after step-and-shoot IMRT was addressed, with effects of divergent relative peripheral doses due to the different structural designs of the two linacs used in the respective radiotherapy techniques. In another published study by Zwicker *et al.* (*39*), in contrast to our findings, they reported no observed difference between the average rate of γ-H2AX foci scored in leukocytes of prostate cancer patients after IMRT or 3D-CRT performed at the same linac for comparable PTV, despite a fivefold extended BOT and twice the number of treatment fields for IMRT. Physiological variables of the irradiated anatomical region and an approximately 10-times-greater PTV for breast cancer treatment appear to be causative for this difference between the two tumor entities. The use of three different linacs in the current work does not represent a crucial variable since, for each radiotherapy modality, on average 80% of patients were treated with the same machine, the Varian UNIQUE. We did not observe an effect of anatomical variables for breast cancer radiotherapy itself, with respect to the irradiated blood volume, by a more pronounced exposure of larger blood vessels such as the heart or aorta. There was no difference in normalized foci data among left- and right-sided breast cancer patient groups, those receiving whole-breast or post-mastectomy chest wall radiotherapy, or those using breath-hold techniques (data not shown). In addition, the hypofractionated 3D-CRT regime, with a higher single tumor dose, did not have a significant effect on the yield of DNA damage in leukocytes compared to conventional fractionation (data not shown). This observation is of interest with regard to the application of 3D-CRT for accelerated partial-breast irradiation with a prescribed dose of 3.85 Gy × 10 fractions delivered twice daily for a total dose of 38.5 Gy within one week (*55*). In addition, IMRT is considered for accelerated partial-breast irradiation with the previously discussed advantages during whole-breast IMRT compared to 3D-CRT (*56*). Our data do not allow for us to provide general recommendations regarding the investigated irradiation techniques in routine clinical applications, except for the above-mentioned reference to a combination of radiotherapy and immune modulating therapy. The optimal choice in radiotherapy technique is still based on the individual risk/benefit ratio of each breast cancer patient based on the risks of late cardiac and pulmonary complications, deterministic effects in the healthy tissue and stochastic long-term effects. Today, more sophisticated irradiation techniques, such as tangential IMRT and IMRT with full modulation of multiple beams or modulated arcs, are applied more often for adjuvant breast cancer radiotherapy (*20*). The advantage of better dose homogeneity needs to be balanced against higher costs. Likely, tangential IMRT will increase the dose burden to peripheral lymphocytes, as indicated by our investigation. However, this observation is not sufficiently robust to influence therapeutic decisions at this time. It might be worth consideration when different radiotherapy techniques allow a similar homogeneous dose distribution towards the application of the technique with a shorter BOT.

In summary, any PTV- and dose-independent variation of the average level of radiation biomarkers in leukocytes of breast cancer patients among various radiotherapy techniques was directed by the absolute BOT and could not be related to an effect of different peripheral doses on the patient's integral dose. Prolonged absolute BOT during radiotherapy significantly increased the proportion of exposed leukocytes and should be considered in clinical practice as a relevant side effect of hematologic toxicity. However, compared to the average yield of DNA damage in leukocytes, dispersion analysis might be a more suitable measure in comparative dosimetry during radiologic exposures with regard to the exposure of whole-body volume and the hematologic system.

SUPPLEMENTARY INFORMATION

Figure S1. Computed tomography-based treatment planning in color wash for 3D-CRT and IMRT of two representative breast cancer patients treated for the whole breast as well as the ipsilateral supraclavicular and parasternal lymph nodes.

ACKNOWLEDGMENTS

We thank the medical staff at the Department of Radiation Oncology and Radiation Therapy at the University Medical Centre Mainz, Germany, for mentoring of patients and blood sampling as well as U. Disque-Kaiser for excellent technical assistance. This study was supported by the German Federal Ministry of Education and Research (grant no. 02NUK016A).

Received: March 29, 2016; accepted: August 8, 2016; published online: October 27, 2016

REFERENCES

1. Delaney G, Jacob S, Featherstone C, Barton M. The role of radiotherapy in cancer treatment: estimating optimal utilization from a review of evidence-based clinical guidelines. Cancer 2005; 104:1129–37.
2. Kase KR, Svensson GK, Wolbarst AB, Marks MA. Measurements of dose from secondary radiation outside a treatment field. Int J Radiat Oncol Biol Phys 1983; 9:1177–83.
3. Travis LB, Ng AK, Allan JM, Pui CH, Kennedy AR, Xu XG, et al. Second malignant neoplasms and cardiovascular disease following radiotherapy. Health Phys 2014; 106:229–46.
4. Dörr W, Herrmann T. Second tumors after oncologic treatment. Strahlenther Onkol 2008; 184:67–72.
5. Diallo I, Haddy N, Adjadj E, Samand A, Quiniou E, Chavaudra J, et al. Frequency distribution of second solid cancer locations in relation to the irradiated volume among 115 patients treated for childhood cancer. Int J Radiat Oncol Biol Phys 2009; 74:876–83.
6. Newhauser WD, Durante M. Assessing the risk of second malignancies after modern radiotherapy. Nat Rev Cancer 2011; 11:438–48.
7. Tubiana M. Can we reduce the incidence of second primary malignancies occurring after radiotherapy? A critical review. Radiother Oncol 2009; 91:4–15; discussion 1–3.
8. Parkin DM, Bray F, Ferlay J, Pisani P. Global cancer statistics, 2002. CA Cancer J Clin 2005; 55:74–108.

9. Habermann EB, Abbott A, Parsons HM, Virnig BA, Al-Refaie WB, Tuttle TM. Are mastectomy rates really increasing in the United States? J Clin Oncol 2010; 28:3437–41.
10. Grantzau T, Overgaard J. Risk of second non-breast cancer after radiotherapy for breast cancer: a systematic review and meta-analysis of 762,468 patients. Radiother Oncol 2015; 114:56–65.
11. Woo TC, Pignol JP, Rakovitch E, Vu T, Hicks D, O'Brien P, et al. Body radiation exposure in breast cancer radiotherapy: impact of breast IMRT and virtual wedge compensation techniques. Int J Radiat Oncol Biol Phys 2006; 65:52–8.
12. Ludwig V, Schwab F, Guckenberger M, Krieger T, Flentje M. Comparison of wedge versus segmented techniques in whole breast irradiation: effects on dose exposure outside the treatment volume. Strahlenther Onkol 2008; 184:307–12.
13. Chang SX, Deschesne KM, Cullip TJ, Parker SA, Earnhart J. A comparison of different intensity modulation treatment techniques for tangential breast irradiation. Int J Radiat Oncol Biol Phys 1999; 45:1305–14.
14. Ma J, Li J, Xie J, Chen J, Zhu C, Cai G, et al. Post mastectomy linac IMRT irradiation of chest wall and regional nodes: dosimetry data and acute toxicities. Radiat Oncol 2013; 8:81.
15. Krueger EA, Fraass BA, McShan DL, Marsh R, Pierce LJ. Potential gains for irradiation of chest wall and regional nodes with intensity modulated radiotherapy. Int J Radiat Oncol Biol Phys 2003; 56:1023–37.
16. Kestin LL, Sharpe MB, Frazier RC, Vicini FA, Yan D, Matter RC, et al. Intensity modulation to improve dose uniformity with tangential breast radiotherapy: initial clinical experience. Int J Radiat Oncol Biol Phys 2000; 48:1559–68.
17. Rudat V, Alaradi AA, Mohamed A, Ai-Yahya K, Altuwaijri S. Tangential beam IMRT versus tangential beam 3D-CRT of the chest wall in postmastectomy breast cancer patients: a dosimetric comparison. Radiat Oncol 2011; 6:26.
18. Ruben JD, Lancaster CM, Jones P, Smith RL. A comparison of out-of-field dose and its constituent components for intensity-modulated radiation therapy versus conformal radiation therapy: implications for carcinogenesis. Int J Radiat Oncol Biol Phys 2011; 81:1458–64.
19. Wang B, Xu XG. Measurements of non-target organ doses using MOSFET dosemeters for selected IMRT and 3D CRT radiation treatment procedures. Radiat Prot Dosimetry 2008; 128:336–42.
20. Abo-Madyan Y, Aziz MH, Aly MM, Schneider F, Sperk E, Clausen S, et al. Second cancer risk after 3D-CRT, IMRT and VMAT for breast cancer. Radiother Oncol 2014; 110:471–6.
21. Hall EJ, Wuu CS. Radiation-induced second cancers: the impact of 3D-CRT and IMRT. Int J Radiat Oncol Biol Phys 2003; 56:83–8.
22. Schneider U, Zwahlen D, Ross D, Kaser-Hotz B. Estimation of radiation-induced cancer from three-dimensional dose distributions: Concept of organ equivalent dose. Int J Radiat Oncol Biol Phys 2005; 61:1510–5.
23. Zwahlen DR, Ruben JD, Jones P, Gagliardi F, Millar JL, Schneider U. Effect of intensity-modulated pelvic radiotherapy on second cancer risk in the postoperative treatment of endometrial and cervical cancer. Int J Radiat Oncol Biol Phys 2009; 74:539–45.
24. Rogakou EP, Pilch DR, Orr AH, Ivanova VS, Bonner WM. DNA double-stranded breaks induce histone H2AX phosphorylation on serine 139. J Biol Chem 1998; 273:5858–68.
25. Sak A, Grehl S, Erichsen P, Engelhard M, Grannass A, Levegrun S, et al. gamma-H2AX foci formation in peripheral blood lymphocytes of tumor patients after local radiotherapy to different sites of the body: dependence on the dose-distribution, irradiated site and time from start of treatment. Int J Radiat Biol 2007; 83:639–52.
26. Durante M, Yamada S, Ando K, Furusawa Y, Kawata T, Majima H, et al. Measurements of the equivalent whole-body dose during radiation therapy by cytogenetic methods. Phys Med Biol 1999; 44:1289–98.
27. Zahnreich S, Ebersberger A, Kaina B, Schmidberger H. Biodosimetry based on gamma-H2AX quantification and cytogenetics after partial- and total-body irradiation during fractionated radiotherapy. Radiat Res 2015; 183:432–46.
28. Hagmar L, Stromberg U, Bonassi S, Hansteen IL, Knudsen LE, Lindholm C, et al. Impact of types of lymphocyte chromosomal aberrations on human cancer risk: results from Nordic and Italian cohorts. Cancer Res 2004; 64:2258–63.
29. Sedelnikova OA, Horikawa I, Redon C, Nakamura A, Zimonjic DB, Popescu NC, et al. Delayed kinetics of DNA double-strand break processing in normal and pathological aging. Aging Cell 2008; 7:89–100.
30. Hagmar L, Bonassi S, Stromberg U, Brogger A, Knudsen LE, Norppa H, et al. Chromosomal aberrations in lymphocytes predict human cancer: a report from the European Study Group on Cytogenetic Biomarkers and Health (ESCH). Cancer Res 1998; 58:4117–21.
31. Bonassi S, Hagmar L, Stromberg U, Montagud AH, Tinnerberg H, Forni A, et al. Chromosomal aberrations in lymphocytes predict human cancer independently of exposure to carcinogens. European Study Group on Cytogenetic Biomarkers and Health. Cancer Res 2000; 60:1619–25.
32. Chua ML, Somaiah N, A'Hern R, Davies S, Gothard L, Yarnold J, et al. Residual DNA and chromosomal damage in ex vivo irradiated blood lymphocytes correlated with late normal tissue response to breast radiotherapy. Radiother Oncol 2011; 99:362–6.
33. Kodama K, Mabuchi K, Shigematsu I. A long-term cohort study of the atomic-bomb survivors. J Epidemio 1996; 6:S95–105.
34. Burns FJ, Tang MS, Wu F, Schmid E. Linking gamma-H2AX foci and cancer in rat skin exposed to heavy ions and electron radiation. Health Phys 2015; 109:157–70.
35. Latty D, Stuart KE, Wang W, Ahern V. Review of deep inspiration breath-hold techniques for the treatment of breast cancer. J Med Radiat Sci 2015; 62:74–81.
36. Group ST, Bentzen SM, Agrawal RK, Aird EG, Barrett JM, Barrett-Lee PJ, et al. The UK Standardisation of Breast Radiotherapy (START) Trial B of radiotherapy hypofractionation for treatment of early breast cancer: a randomised trial. Lancet 2008; 371:1098–107.
37. Deurenberg P, Yap M, van Staveren WA. Body mass index and percent body fat: a meta analysis among different ethnic groups. Int J Obes Relat Metab Disord 1998; 22:1164–71.
38. Siri WE. The gross composition of the body. Adv Biol Med Phys 1956; 4:239–80.
39. Zwicker F, Swartman B, Sterzing F, Major G, Weber KJ, Huber PE, et al. Biological in-vivo measurement of dose distribution in patients' lymphocytes by gamma-H2AX immunofluorescence staining: 3D conformal- vs. step-and-shoot IMRT of the prostate gland. Radiat Oncol 2011; 6:62.
40. Werbrouck J, Ost P, Fonteyne V, De Meerleer G, De Neve W, Bogaert E, et al. Early biomarkers related to secondary primary cancer risk in radiotherapy treated prostate cancer patients: IMRT versus IMAT. Radiother Oncol 2013; 107:377–81.
41. Wang L, Ding GX. The accuracy of the out-of-field dose calculations using a model based algorithm in a commercial treatment planning system. Phys Med Biol 2014; 59:N113–28.
42. Huang JY, Followill DS, Wang XA, Kry SF. Accuracy and sources of error of out-of field dose calculations by a commercial treatment planning system for intensity-modulated radiation therapy treatments. J Appl Clin Med Phys 2013; 14:4139.
43. Howell RM, Scarboro SB, Kry SF, Yaldo DZ. Accuracy of out-of-field dose calculations by a commercial treatment planning system. Phys Med Biol 2010; 55:6999–7008.
44. Zwicker F, Swartman B, Roeder F, Sterzing F, Hauswald H, Thieke C, et al. In vivo measurement of dose distribution in patients' lymphocytes: helical tomotherapy versus step-and-shoot IMRT in prostate cancer. J Radiat Res 2015; 56:239–47.

45. Kry SF, Salehpour M, Followill DS, Stovall M, Kuban DA, White RA, et al. The calculated risk of fatal secondary malignancies from intensity-modulated radiation therapy. Int J Radiat Oncol Biol Phys 2005; 62:1195–203.

46. Lobrich M, Rief N, Kuhne M, Heckmann M, Fleckenstein J, Rube C, et al. In vivo formation and repair of DNA double-strand breaks after computed tomography examinations. Proc Natl Acad Sci U S A 2005; 102:8984–9.

47. Roch-Lefevre S, Pouzoulet F, Giraudet AL, Voisin P, Vaurijoux A, Gruel G, et al. Cytogenetic assessment of heterogeneous radiation doses in cancer patients treated with fractionated radiotherapy. Br J Radiol 2010; 83:759–66.

48. Wild AT, Ye X, Ellsworth SG, Smith JA, Narang AK, Garg T, et al. The association between chemoradiation-related lymphopenia and clinical outcomes in patients with locally advanced pancreatic adenocarcinoma. Am J Clin Oncol 2015; 38:259–65.

49. Cho O, Oh YT, Chun M, Noh OK, Lee HW. Radiation-related lymphopenia as a new prognostic factor in limited-stage small cell lung cancer. Tumour Biol 2016; 37:971–8.

50. Durante M, Yamada S, Ando K, Furusawa Y, Kawata T, Majima H, et al. X-rays vs. carbon-ion tumor therapy: cytogenetic damage in lymphocytes. Int J Radiat Oncol Biol Phys 2000; 47:793–8.

51. Wattenberg MM, Fahim A, Ahmed MM, Hodge JW. Unlocking the combination: potentiation of radiation-induced antitumor responses with immunotherapy. Radiat Res 2014; 182:126–38.

52. Beels L, Bacher K, De Wolf D, Werbrouck J, Thierens H. gamma-H2AX foci as a biomarker for patient X-ray exposure in pediatric cardiac catheterization: are we underestimating radiation risks? Circulation 2009; 120:1903–9.

53. Syme A, Kirkby C, Mirzayans R, MacKenzie M, Field C, Fallone BG. Relative biological damage and electron fluence in and out of a 6 MV photon field. Phys Med Biol 2009; 54:6623–33.

54. Kirkby C, Field C, MacKenzie M, Syme A, Fallone BG. A Monte Carlo study of the variation of electron fluence in water from a 6 MV photon beam outside of the field. Phys Med Biol 2007; 52:3563–78.

55. Vicini F, Winter K, Straube W, Wong J, Pass H, Rabinovitch R, et al. A phase I/II trial to evaluate three-dimensional conformal radiation therapy confined to the region of the lumpectomy cavity for Stage I/II breast carcinoma: initial report of feasibility and reproducibility of Radiation Therapy Oncology Group (RTOG) Study 0319. Int J Radiat Oncol Biol Phys 2005; 63:1531–7.

56. Moorthy S, Elhateer HS, Majumdar S, Mohammed S, Patnaik R, Narayanamurty. Dosimetric comparison of three dimensional conformal radiation therapy versus intensity modulated radiation therapy in accelerated partial breast irradiation. Indian J Cancer 2016; 53:147–51.

9.3 Publikation III

Radiation-induced DNA double-strand breaks in peripheral leukocytes and therapeutic response of heel spur patients treated by orthovoltage X-rays or a linear accelerator

Strahlenther Onkol (2020) 196:1116–1127
https://doi.org/10.1007/s00066-020-01662-4

ORIGINAL ARTICLE

Radiation-induced DNA double-strand breaks in peripheral leukocytes and therapeutic response of heel spur patients treated by orthovoltage X-rays or a linear accelerator

Sebastian Zahnreich[1] · Hans-Peter Rösler[1] · Carina Schwanbeck[1] · Heiko Karle[1] · Heinz Schmidberger[1]

Received: 11 April 2020 / Accepted: 22 June 2020 / Published online: 10 July 2020

Abstract

Purpose Biodosimetric assessment and comparison of radiation-induced deoxyribonucleic acid (DNA) double-strand breaks (DSBs) by γH2AX immunostaining in peripheral leukocytes of patients with painful heel spur after radiation therapy (RT) with orthovoltage X-rays or a 6-MV linear accelerator (linac). The treatment response for each RT technique was monitored as a secondary endpoint.

Patients and methods 22 patients were treated either with 140-kV orthovoltage X-rays ($n = 11$) or a 6-MV linac ($n = 11$) with two weekly fractions of 0.5 Gy for 3 weeks. In both scenarios, the dose was prescribed to the International Commission on Radiation Units and Measurements (ICRU) dose reference point. Blood samples were obtained before and 30 min after the first RT session. γH2AX foci were quantified by immunofluorescence microscopy to assess the yield of DSBs at the basal level and after radiation exposure ex vivo or in vivo. The treatment response was assessed before and 3 months after RT using a five-level functional calcaneodynia score.

Results RT for painful heel spurs induced a very mild but significant increase of γH2AX foci in patients' leukocytes. No difference between the RT techniques was observed. High and comparable therapeutic responses were documented for both treatment modalities. This trial was terminated preliminarily after an interim analysis (22 patients randomized).

Conclusion Low-dose RT for painful heel spurs with orthovoltage X-rays or a 6-MV linac is an effective treatment option associated with a very low and comparable radiation burden to the patient, as confirmed by biodosimetric measurements.

Keywords Radiotherapy · Benign disease · Heel spur · Biodosimetry · γH2AX

Introduction

The successful treatment of benign inflammatory and degenerative conditions like calcaneodynia (painful heel spur) and painful shoulder or elbow syndrome with low-dose radiation therapy (RT) has a longstanding history in Germany and accounts for more than a third of all RT patients treated annually [1]. Local administration of photon doses below 1 Gy has been shown to attenuate inflammatory responses as the causative factor for these painful diseases [2]. Clinical studies documented comparable positive results for treatment schedules with single fractions of 0.5 Gy or 1 Gy applied twice a week for 3 or 6 weeks [3–5]. Accordingly, the iso-effective single dose of 0.5 Gy over a course of 3 weeks is used for radiation protection purposes to reduce the radiation burden to the patient and the risk of potential radiation-induced (RI) stochastic late effects such as radiation carcinogenesis [6]. The risk of adverse late effects induced by low-dose RT for benign diseases is generally considered to be negligible and the benefit for the patient outweighs [7–9]. Anthropomorphic phantom-based studies by Jansen et al. [10] using an effective dose concept for a cumulative dose of 6 Gy administered in six fractions of 1 Gy predict rough estimations for the risk of RI fatal tumors of 20–40 per 1000 patients for heterotopic ossification, 1.5 per 1000 patients for gonarthrosis, 0.5 per 1000 patients for heel spurs, and 1 per 1000 female patients for hidradenitis suppurativa. Other predominant factors that influence the risk of radiation carcinogenesis besides the target dose are the field size, photon energies, the exposed anatomic region/organs, sex, and age at exposure. In general, such risk estimates are fraught with large uncertainties in the order of a factor of 2 and are expected to be much less for low-dose RT of benign diseases, since this treatment is predom-

✉ Sebastian Zahnreich
zahnreic@uni-mainz.de

[1] Department of Radiation Oncology and Radiotherapy, University Medical Center, Mainz, Germany

inantly performed in elderly patients with a strongly and up to nine-fold reduced excess lifetime risk for RI solid tumors when compared to young adults [10–12].

Calcaneodynia is observed in 10–15% of the population and is associated with severe heel pain causing restrictions and reduced quality in everyday life [13, 14]. In Germany, approximately 10,000 heel spur patients per annum are treated by low-dose RT in about 340 active facilities offering RT for benign diseases [15]. Treatments are usually conducted with a medical linear accelerator (linac) and megavoltage (MV) photons or orthovoltage devices delivering X-rays in the range of 100–400 keV, with a prevalence for linacs [15]. Compared to an orthovoltage device, RT with a linac achieves a more homogeneous dose distribution in the target volume, which has been discussed to have improved therapeutic effectiveness [16]. However, the penetration depth of MV photons from a linac exceeds the cross-section of the patient and causes reflections in the RT bunker that contribute to an inevitable dose burden to the patient's normal tissue outside the target volume. So-called out-of-field doses are also generated by scattering and leakage from the linac treatment head, collimation devices, and, to a lesser extent, by scattering from within the patient's body [17]. Such low-dose exposures far from the primary beam have been associated with various radiation-related late adverse effects [18, 19]. Orthovoltage RT with low-energy photons has an inferior dose distribution but allows for protection of the patient's healthy tissue by lead shielding which cannot be applied for high-energy photon units due to the generation of scatter radiation within the shielding equipment. However, for linac RT, treatment planning including field collimation can be conducted to protect the patients' healthy tissue outside the target volume.

Besides conventional physical measurements to determine the patient's radiation exposure, the detection of biological indicators of RI deoxyribonucleic acid (DNA) damage in peripheral leukocytes has been frequently applied for biodosimetric purposes in patients undergoing various radiologic procedures or RT [20–29]. By far the most sensitive and rapid measure is the immediate quantification of RI DNA double-strand breaks (DSB) using the phosphorylated histone variant H2AX (γH2AX) or tumor protein 53 binding protein 1 (53BP1), representing well-established surrogate markers of DSBs [30]. Immunostaining and fluorescence microscopic quantification of so-called γH2AX or 53BP1 foci at the level of single cells is proportional to the number of RI DSBs and therefore increases linearly with radiation dose after ex vivo and in vivo exposure with a detection threshold of a few mGy [22, 26, 27].

However, it is hitherto unknown whether the largely random application of linac or orthovoltage RT for the treatment of painful heel spur is associated with a varying unwanted but inevitable radiation exposure of the patients' normal healthy tissue to out-of-field doses and differing therapeutic effectiveness. Therefore, we conducted this prospective randomized trial as a biodosimetric approach to assess the radiation burden of heel spur patients treated either with orthovoltage X-rays or a linac by quantitation of the DSB marker γH2AX in peripheral leukocytes. RT was given twice per week with a single dose of 0.5 Gy and six total fractions. Venous blood samples were drawn immediately before and 30 min after the first fraction of RT and were processed for fluorescence microscopic scoring of γH2AX foci in leukocytes. As a secondary endpoint the analgesic effectiveness was monitored based on a five-level function calcaneodynia score (CS) before and 3 months after RT.

Patients and methods

Patients and radiation therapy

Patients suffering from painful heel spur were enrolled based on the following inclusion criteria: radiologic evidence of spur formation, anamnesis of a painful heel and functional impairment, painful symptoms for a least 3 months, age ≥40 years, overall condition allowing for repeated venous blood sampling, and a signed an informed consent form approved by the local ethics committee. The following exclusion criteria were applied: known gene defects associated with compromised DNA repair (e.g., ataxia–telangiectasia, Werner syndrome, or Bloom syndrome), age <40 years, previous RT or trauma in the treated anatomical region, any exposure to ionizing radiation less than 5 days before the start of RT, any additional inflammatory or rheumatic disease, pregnancy, breastfeeding, intellectual disability or psychiatric disorder, legal care in health matters, and lack of a signed informed consent form approved by the local ethics committee. The characteristics of the participants are summarized in Table 1. Based on these criteria, 22 patients (36%) of a total number of 61 entered the study between August 2016 and August 2019, and were randomized into two groups: 11 patients (50%) were treated with orthovoltage X-rays (140 kV, D3150 X-Ray Therapy System, Gulmay Ltd., Byfleet, UK) and 11 patients (50%) were treated with a linac (6 MV, Clinac DHX, Unique™ or Truebeam® Varian Medical Systems, Palo Alto, CA, USA) at the Department of Radiation Oncology and Radiation Therapy at the University Medical Centre Mainz, Germany. All patients received two weekly fractions of 0.5 Gy applied as two lateral opposing fields up to a total dose of 3 Gy. The calcaneus and the plantar aponeurosis were included in the target volume. The average field size for both RT techniques was $8 \times 10\,cm^2$. For orthovoltage

Table 1 Patient characteristics and previous treatments

Criteria	All patients *n* (%)	Orthovoltage *n* (%)	Linac *n* (%)
Patients	22	11 (50%)	11 (50%)
Sex			
Females	14 (64%)	6 (55%)	8 (73%)
Males	8 (36%)	5 (45%)	3 (27%)
Age (years)			
Median (range)	54 (40–77)	57 (40-77)	53 (42–69)
Site			
Left	11 (50%)	7 (64%)	4 (36%)
Right	11 (50%)	4 (36%)	7 (64%)
Duration of symptoms (months)			
Median (range)	9 (2–36)	8 (2–36)	9 (3–36)
≤6 months	7 (35%)	4 (40%)	3 (30%)
>6 months	13 (65%)	6 (60%)	7 (70%)
Previous treatments			
Insoles	1 (5%)	0 (0%)	1 (9%)
NSAID	5 (23%)	3 (27%)	0 (0%)
ESWT/ultrasound	7 (32%)	6 (55%)	1 (9%)
Corticoid infiltration	3 (14%)	10 (91%)	2 (18%)
Heel pad	17 (77%)	10 (91%)	7 (64%)
TENS	1 (5%)	1 (9%)	0 (0%)
Ice bag	3 (14%)	1 (9%)	2 (18%)

Linac linear accelerator, *ESWT* extracorporeal shock wave therapy, *NSAID* nonsteroidal anti-inflammatory drugs, *TENS* transcutaneous electrical nerve stimulation

RT the field size was defined by a mechanical applicator with a diameter of 15 cm to collimate the beam and set the source-to-skin distance (SSD) and was further adjusted using lead rubber shielding. For linac RT the treatment field was defined by the aperture with no collimation, since no computed tomography-based treatment planning was performed. Representative treatment planning images for both RT techniques are shown in Fig. 1. The dose rate for orthovoltage RT was 3.64 Gy per minute and approximately 3 Gy per minute for linac RT, resulting in comparable average beam-on times of 0.17 and 0.19 min, respectively. The average SSD for orthovoltage and linac RT was 25 cm and 97 cm, respectively. The study was approved by the Ethics Committee of the Medical Association of Rhineland-Palatinate, number 837.216.15 (9984) on 07/30/2015, and by the expert committee of the DEGRO (German Society for Radiation Oncology). Patients were assigned to one of the RT techniques by block randomization with an equal probability for both arms. According to the results of our previous biodosimetric studies based on γH2AX foci quantification in peripheral leukocytes after fractionated RT of prostate and breast cancer patients [26, 27], 60 patients are required to detect a difference of 25% with a power of 80% and an error probability of 5%. To detect a difference of 10% in the CS scores with a power of 80% and an error probability of 5%, we estimated a total number of 120 participants. This trial was terminated preliminarily after an interim analysis (22 patients randomized).

Treatment response

The treatment response was documented based on standardized questionnaires using a five-level functional CS score according to [3, 31] before and 3 months after the first course of RT. Data were available for 20 patients pre-RT and 19 patients post RT.

Blood sampling and ex vivo irradiation

Venous blood collection, irradiation of whole blood, and isolation of leukocytes were performed as described previously [26, 27]. Venous blood was drawn immediately before and 30 min after the first fraction of RT. Blood samples

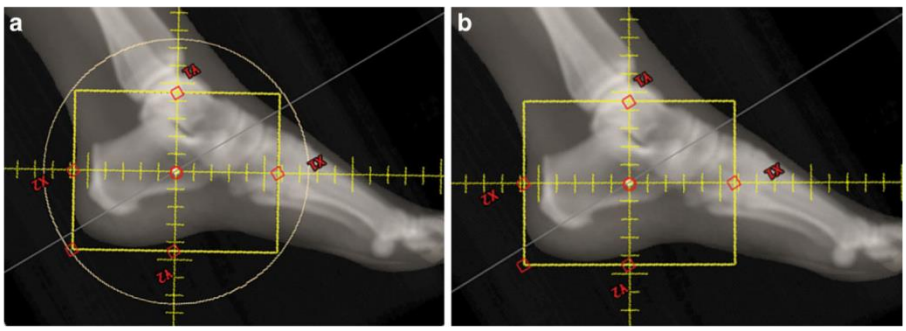

Fig. 1 Exemplary representation of radiation therapy (RT) for plantar fasciitis treated either by **a** orthovoltage X-rays performed with a round mechanical applicator with a diameter of 15 cm or **b** linac RT. The treatment field was shaped for orthovoltage therapy using lead rubber shielding and for linac RT using the aperture only with no collimation. Simulated radiographs are shown since no computed tomography-based treatment planning was performed

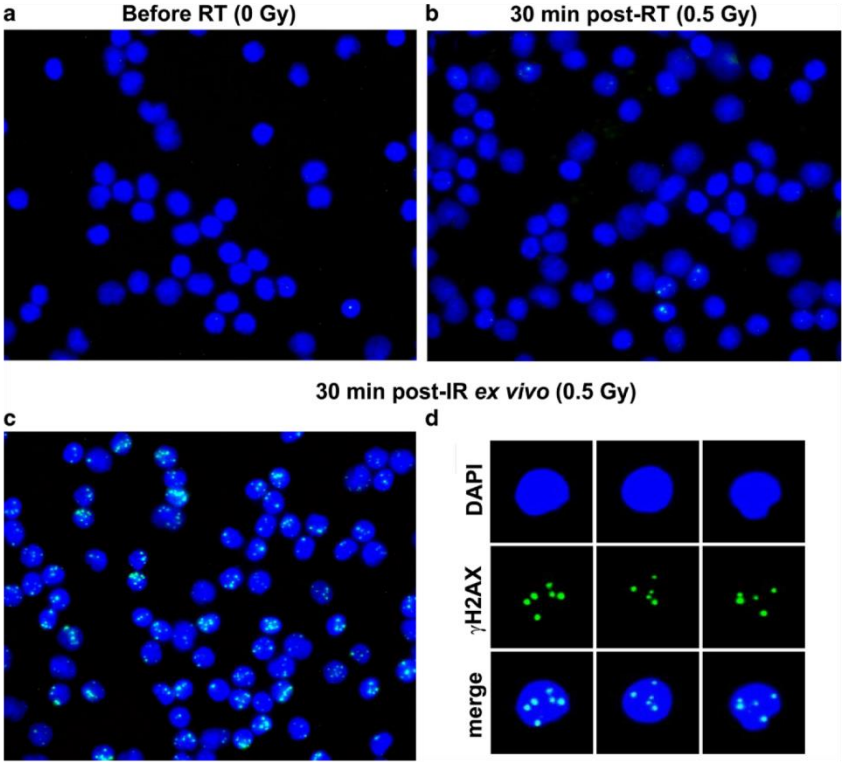

Fig. 2 Immunofluorescence staining for γH2AX (*green*) in DAPI-stained (*blue*) nuclei of peripheral leukocytes 30 min after **a** sham irradiation, **b** the first fraction of radiation therapy (RT) or **c**, **d** homogeneous ionizing radiation (IR) exposure ex vivo. **d** Nuclei extracted from **c** as used for manual counting of γH2AX foci at the level of single cells

taken before RT were sham irradiated or exposed to a test dose of 0.5 Gy X-rays and analyzed 30 min after irradiation to assess the individual yield of basal or RI DSBs by γH2AX foci quantitation, respectively. Ex vivo irradiation of whole blood was performed with a D3150 X-Ray Therapy System (Gulmay Ltd., Byfleet, UK) at 140 kV and a dose rate of 3.6 Gy per min at room temperature. Sham-irradiated cells were kept under the same conditions in the radiation device control room.

γH2AX foci quantification

Fixation of leukocytes, γH2AX immunostaining, fluorescence microscopy, image capturing, and scoring of foci was performed as described previously [26, 27]. After irradiation ex vivo or in vivo, at least 100 or 1000 cells were analyzed manually for each datapoint, respectively. Representative immunofluorescent images for γH2AX foci quantitation are shown in Fig. 2.

Equivalent whole-body dose estimation

To approximate an equivalent whole-body dose (EWBD) for each patient according to [32], calculations were performed based on the formula:

$$\text{Integral dose} = (1.44 \times D_0 \times d_{1/2} \times A \times [1 - \exp(-0.6938 d/d_{1/2})] \times (1 + 2.88 d_{1/2}/f))/1000$$

where D_0 represents the administered dose (Gy), A the field area (cm^2), d the patient diameter (cm), $d_{1/2}$ the half-value thickness (140 kV = 5 cm and 6 MV = 15 cm), and f the SSD (cm). The formula was applied to each treatment field to obtain an integrated dose that was divided by the patient's weight to obtain the EWBD.

Data and statistical analysis

For quantification of γH2AX foci in leukocytes a single sample was available and analyzed per datapoint for each patient. Due to the limited amount of blood, no biological or technical replicates could be performed. All data were scored by one observer. To obtain the numbers of RI foci only, the individual basal yield of γH2AX foci was sub-

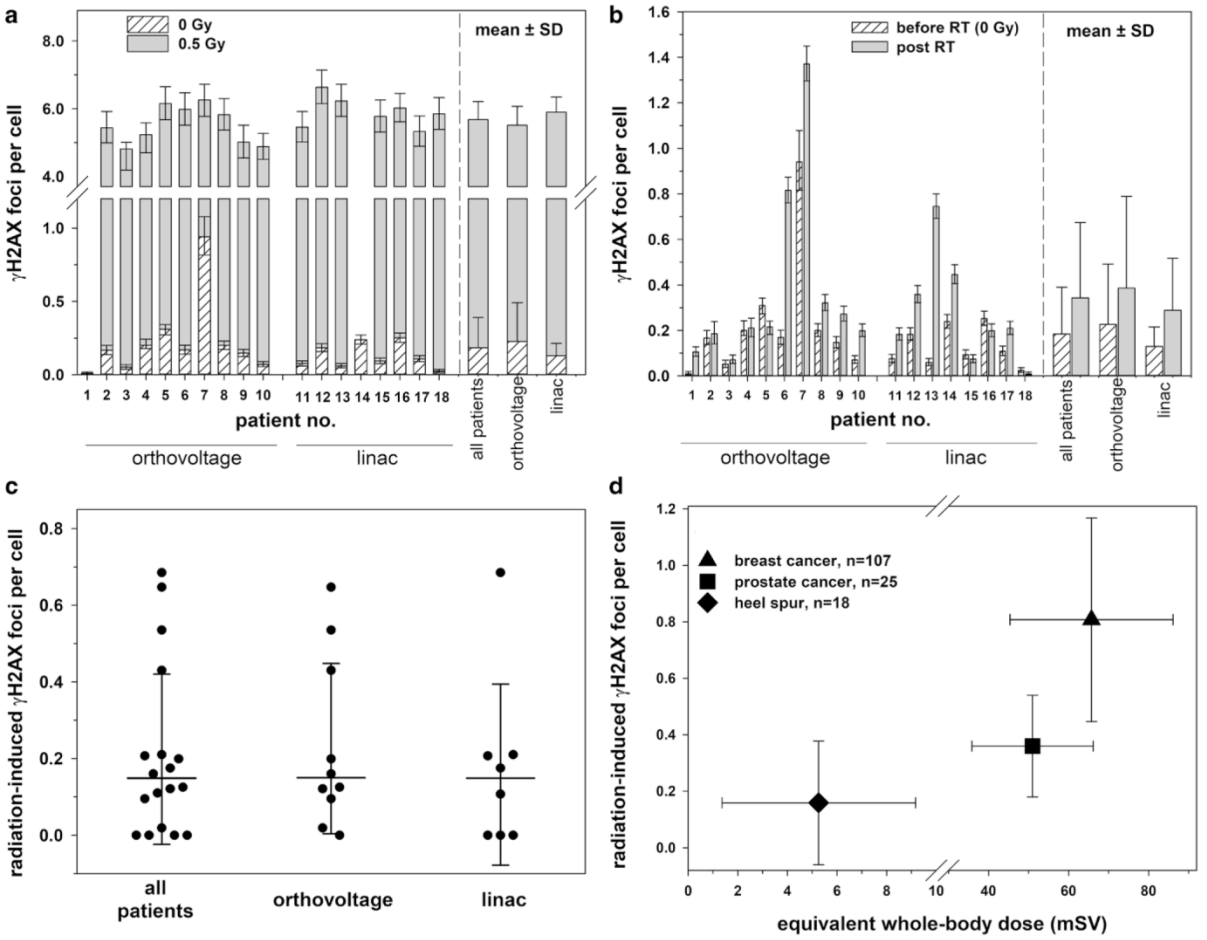

Fig. 3 Scoring of γH2AX foci in patients' leukocytes. Average numbers of γH2AX foci per leukocyte in sham-irradiated cells before radiotherapy (RT) and **a** 30 min after ex vivo exposure to 0.5-Gy X-rays or **b** 30 min after RT for each patient as well as the respective mean ± standard deviation (SD) of all patients ($n = 18$) and patients treated by orthovoltage ($n = 10$) or linac ($n = 8$) RT. Ex vivo irradiated samples of donors 1 and 14 were not available. Error bars for individual patients represent the 95% confidence interval of the Poisson mean. **c** Average numbers of radiation-induced γH2AX foci per leukocyte 30 min after the first fraction of RT in all patients and patients treated by orthovoltage RT or linac RT only. *Dots* show the individual values of each patient. *Solid lines* represent the mean and *error bars* the SD. **d** Comparison of the average yield of radiation-induced γH2AX foci per leukocyte in all heel spur patients of the present study and in tumor patients as obtained in our previous studies [26, 27] in dependence of the administered equivalent whole-body dose. *Error bars* represent the SD

tracted from the yield after ex vivo or in vivo irradiation. Summarized patient data are provided as the mean and standard deviation unless stated otherwise. Data handling, plotting, and statistics were performed using SigmaPlot™11® (Systatt Software Inc., San Jose, CA, USA). The relationship between two variables was analyzed using the Pearson correlation. For comparison of two groups the Student's *t*-test or the Mann–Whitney rank sum test was used. The comparison between two categorical variables was performed using the Fishers' exact test. All levels of significance were set at $p < 0.05$.

Results

γH2AX foci before radiation therapy and after irradiation ex vivo

To examine the individual basal level of DSBs and the ex vivo radiation response in patients' leukocytes, blood samples obtained before RT were sham irradiated or exposed to 0.5 Gy X-rays and analyzed 30 min post radiation. The results are shown in Fig. 3a and detailed information on γH2AX foci quantitation are provided in Table 2. The average rate of basal γH2AX foci in leukocytes scored in 18 patients was 0.184 ± 0.206 per cell. The en-

Table 2 γH2AX foci per cell before RT, 30 min after ex vivo exposure to 0.5 Gy or 30 min after the first fraction of RT

RT	EWBD (mSV)	γH2AX foci per cell		
		Before RT 0 Gy	Ex vivo 0.5 Gy	Post RT
Orthovoltage	2.52	0.011	n.a.	0.106
	2.36	0.167	5.44	0.186
	2.79	0.051	4.81	0.072
	3.49	0.200	5.23	0.211
	2.44	0.310	6.15	0.215
	2.55	0.169	5.98	0.816
	3.24	0.940	7.32	1.371
	3.15	0.200	5.82	0.321
	2.34	0.147	5.02	0.272
	2.39	0.071	4.88	0.199
Mean ± SD	2.73 ± 0.42	0.227 ± 0.265	5.63 ± 0.80	0.377 ± 0.406
Linac	9.99	0.076	5.46	0.183
	13.48	0.183	6.81	0.358
	9.97	0.060	6.23	0.745
	14.67	0.239	n.a.	0.446
	10.96	0.093	5.77	0.074
	13.30	0.252	6.02	0.199
	9.50	0.109	5.33	0.210
	12.63	0.025	5.84	0.010
Mean ± SD	11.81 ± 1.95	0.130 ± 0.085	5.92 ± 0.499	0.278 ± 0.235
All patients Mean ± SD	5.26 ± 3.90	0.184 ± 0.206	5.76 ± 0.680	0.333 ± 0.335

RT radiation therapy, *EWBD* equivalent whole-body dose, *SD* standard deviation, *Linac* linear accelerator

dogenous level of γH2AX foci in leukocytes before RT did not correlate with the patients' age (r = 0.346, $p = 0.160$), gender (r = –0.159, $p = 0.528$), or CS sum score prior to RT (r = –0.063, $p = 0.817$). 30 min after exposure to 0.5-Gy X-rays ex vivo we observed a comparable induction of γH2AX foci per leukocyte for all patients. On average, 5.76 ± 0.68 γH2AX foci per cell were scored in 16 analyzable patient samples corresponding to an excess of 5.57 ± 0.56 RI foci per cell. Thus, despite large variations in the individual background number of γH2AX foci in patients' leukocytes, a more uniform and comparable response after homogeneous ex vivo exposure to ionizing radiation was observed. There was no significant difference in the average yield of basal ($p = 0.625$) or ex vivo RI ($p = 0.223$) γH2AX foci per leukocyte between the two RT groups.

γH2AX foci after radiation therapy

After the first session of RT the frequency of γH2AX foci per leukocyte exceeded the background rate in 78% (14/18) of all patients. Increments were detected in 90% (9/10) of patients after orthovoltage RT and 63% (5/8) of patients after linac RT, with no significant difference between the treatment arms ($p = 0.725$). Fig. 3b, c show the level of γH2AX foci before and after the different in vivo exposure scenarios and detailed information is provided in Table 2. After RT the rate of γH2AX foci per leukocyte increased significantly from the average basal number of 0.184 ± 0.206 to 0.333 ± 0.335 ($p = 0.045$) for all patients, corresponding to an excess of 0.149 ± 0.222 RI foci per cell. No significant increment of γH2AX foci after RT was observed within the orthovoltage ($p = 0.089$) or linac ($p = 0.091$) arm only. In patients treated with orthovoltage X-rays or a linac, the average rate of RI γH2AX foci post RT reached a comparable level of 0.150 ± 0.222 or 0.149 ± 0.236, respectively ($p = 0.51$). However, the average EWBD of linac RT (11.81 ± 1.95 mSV) was significantly higher than for orthovoltage RT (2.73 ± 0.42 mSV; $p < 0.0001$, Table 2). Accordingly, we observed no correlation between the calculated EWBD and the yield of RI γH2AX foci per cell post RT (r = –0.074, $p = 0.769$).

To evaluate the patient's radiation burden during RT of heel spurs, Fig. 3d shows the mean frequencies of RI γH2AX foci 30 min after RT from this work related to data from our previous biodosimetric studies 30 min after RT of breast or prostate cancer patients with an average single dose of 2 Gy [26, 27]. Compared to the mean number of RI γH2AX foci in leukocytes after heel spur RT with a single dose of 0.5 Gy (0.159 ± 0.227, $n = 18$), the rate of γH2AX foci was 2.4- or 5.5-fold higher after the first fraction of

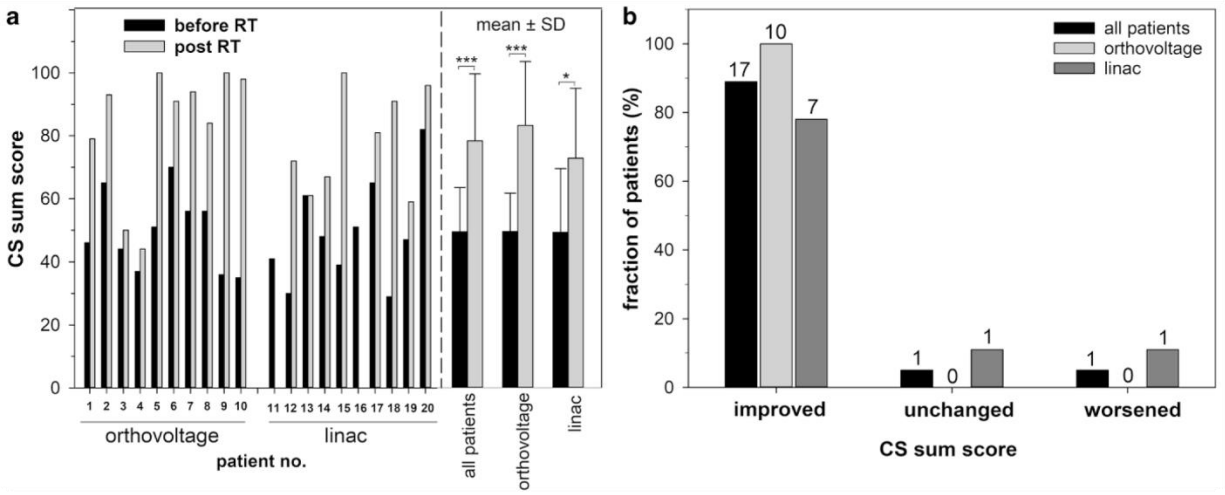

Fig. 4 Variation of the summed calcaneodynia score (CS) before and at 3 months after radiotherapy (RT) for **a** each patient and compiled for all patients or orthovoltage RT or linac RT only. **b** Summarized data on changes in the sum score 3 months after RT. Numbers of patients are indicated. The CS score of patient no. 16 at a 3-month follow-up was not available. Statistical comparisons between two groups were performed by the student's t-test. *SD* standard deviation, $*p<0.05$, $**p<0.01$, $***p<0.001$

prostate (0.360 ± 0.0180, $n=25$) or breast (0.807 ± 0.360, $n=107$) cancer RT, respectively.

Treatment response

For each patient the CS single score criteria and the sum score were assessed before and 3 months after RT and are shown in Fig. 4a. The average CS sum score for all patients before RT was 49.5 ± 14.1 and was comparable for patients treated with an orthovoltage device (49.6 ± 12.2) or a linac (49.3 ± 16.4; $p=0.963$). At 3 months follow-up we observed a significant 1.6-fold increase of the CS sum score up to 78.4 ± 14.1 for all patients ($p<0.001$) and to 83.3 ± 20.3 ($p=0.017$) or 72.9 ± 22.2 ($p=0.017$) in the orthovoltage or linac arms, respectively. There was no significant difference in the sum score post RT between patients treated by orthovoltage or linac RT ($p=0.301$). 89% (17/19) of patients in both arms had an improved sum score and unchanged or worsened conditions were reported by only 5.5% (1/19) of the patients each (Fig. 4b). After orthovoltage RT all patients had an elevated sum score, whereas after linac RT the sum score increased in 78% (7/9) of patients only and was unchanged or worsened in 11% (1/9) of the patients each. Statistical comparison of the proportions of patients with an improved sum score showed no significant difference between the two RT groups ($p=0.211$).

Fig. 5 shows the distribution of patients classified in the performance categories excellent (CS sum score 90–100), good (CS sum score 70–85), moderate (CS sum score 45–65), or poor (CS sum score 0–40). Before RT, none of the patients were classified as excellent and only 10% (2/19) as good (Fig. 5a). The majority of patients, 53% (10/19) and 37% (7/19), were in the categories moderate and poor, respectively. Before RT the patients were distributed similarly among the four categories between both RT techniques (Fig. 5b, c). At 3 months follow-up, 47% (9/19) of all patients were ranked as excellent, 21% (4/19) as good or moderate each, and the remaining 11% (2/19) as poor (Fig. 5a). After orthovoltage RT, 56% (5/9) of the patients were in the category excellent, 22% (2/9) in good, and 11% (1/9) in moderate or poor each (Fig. 5b). After linac RT, 40% (7/10) of patients were in the category excellent, 20% (2/10) in good, 30% (3/10) in moderate, and 10% (1/10) in poor (Fig. 5c). No correlation was found between an improved sum score and patient's age ($r=0.439$, $p=0.0601$), duration of painful symptoms ($r=0.228$, $p=0.347$), or gender ($r=0.259$, $p=0.285$). Information on patient characteristics is provided in Table 1.

Discussion

In the present study we measured RI DSBs by γH2AX foci quantification in peripheral leukocytes of painful heel spur patients treated with a 140 kV orthovoltage device or a 6-MV linac to assess the patients' radiation burden for radiation protection purposes. Immediately after the first fraction of RT we detected an overall slight but significant increase of γH2AX foci with no difference between orthovoltage and linac RT. The application of either RT technique led to significant and comparable pain relief at 3 months follow-up. Based on this outcome as well as low participation and inclusion rates, the trial was terminated preliminarily after an interim analysis (22 patients randomized).

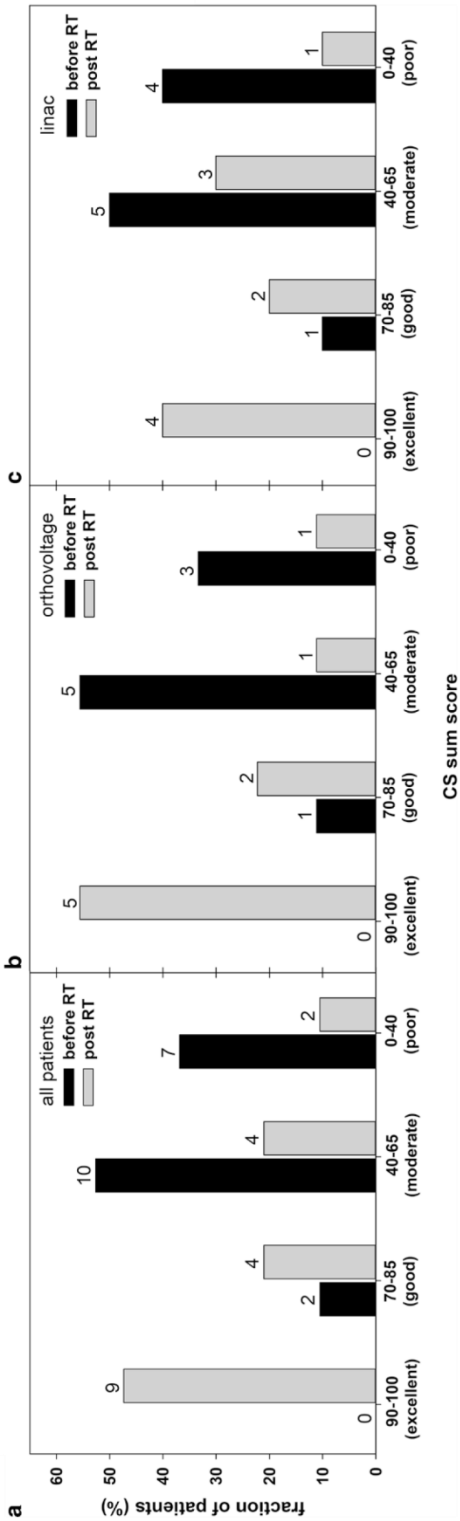

Fig. 5 Performance status according to categories of the summarized calcaneodynia score (CS) before and 3 months after radiotherapy (RT) for **a** all patients or patients treated by **b** orthovoltage RT or **c** linac RT. Numbers of patients are indicated

DSBs are potently induced by ionizing radiation and represent the most deleterious DNA lesion causing cell death, chromosomal rearrangements, and malignant transformation [33]. The by far most prominent biomarker of RI DSBs is the phosphorylated histone variant γH2AX, which has been applied in numerous studies to evaluate the in vivo radiation exposure of patients after low-dose radiologic examinations like computed tomography (CT) (e.g., [20, 22, 23, 34]) and mammography [21, 25], or after high-dose RT of tumor patients [24, 26–29]. The present study is the first, at least to our knowledge, to apply this method with a biodosimetric intention in patients treated by low-dose RT for benign inflammatory and degenerative diseases with pain relief as the second clinical endpoint. RT of this medical condition is very well received and frequently used in German-speaking regions but is barely applied in other, particularly Anglo-American, countries [1]. Such geographical differences are due to fear of RI late adverse effects, which, however, are estimated to be very low or negligible for this type of local low-dose RT [7, 8]. Various studies on the RT of heel spurs showed equal effectiveness for single doses of 1 Gy or 0.5 Gy administered twice a week for 3 or 6 weeks [3–5, 16]. Accordingly, the lower dose of 0.5 Gy represents the standard option to decrease the potential risk for radiation-related late adverse effects [6]. Depending on the institutional equipment, benign diseases are treated either with a linac and MV photons or with an orthovoltage device operating in the low-energy kV range. This instrumentation-specific difference might be associated with varying therapeutic effectiveness [16] but also with divergent exposures to undesirable out-of-field doses [17]. Also, from a health economic perspective, orthovoltage RT is associated with lower costs compared to linac RT. Based on this rationale, we investigated both endpoints in this prospective randomized trial after low-dose RT of calcaneodynia patients with a linac or orthovoltage unit for a treatment schedule of 0.5 Gy given twice a week over a course of 3 weeks. According to our scoring criteria adapted from Rowe et al. [31] and Heyd et al. [3], we observed high response rates and pain reduction in up to 89% of patients at 3 months follow-up in line with improvement rates of previous studies ranging between 65–100% [16]. About 50% of patients reported on an excellent and pain-free performance status after the first RT series. We did not observe any difference in the therapeutic response between the two RT techniques, but the small number of participants does not allow meaningful statistical comparisons. Previously, Muecke et al. [16] performed a retrospective study on the long-term treatment success of low-dose RT for painful heel spurs in 502 patients treated either with 6–10-MV photons twice per week or with 175 kV X-rays three times per week at four different facilities in Germany. Patients received 10 fractions of 0.5 Gy or 5–6 fractions of 1 Gy for 6–10-MV photons or six fractions of 1 Gy for orthovoltage X-rays. In their study, multivariate analysis revealed a significantly worse prognosis for orthovoltage RT than for MV photons, with no impact of radiation dose. This finding has been related to a more homogeneous and favorable dose distribution achieved with MV units. No other study has yet confirmed this observation. Although a better distribution of dose is achieved in the target volume for linac RT, it may increase the radiation burden of the patient through higher peripheral doses outside the primary beam caused by radiation scattering, leakage, and reflections [17]. Besides physical dosimetry, biodosimetric attempts have been made to compare the inherent radiation exposure of different RT techniques [27–29] or CT protocols [35] based on the quantification of RI γH2AX foci in peripheral leukocytes. Thresholds for this highly sensitive assay to monitor the induction of RI DSBs in vitro and in vivo have been set at 1 mGy and 3 mGy, respectively [22, 36]. So far, only few comparable studies on foci quantification of DSB repair proteins in systemic lymphocytes after a planned medical IR exposure in vivo are available for the low EWBDs of the present work, which were able to demonstrate dose-dependent increments or even differences between radiation techniques. Kuefner et al. [35] reported on significantly reduced levels ofγH2AX foci in peripheral leukocytes 30 min after multidetector coronary CT angiography performed with a dose-reducing sequential protocol compared to a conventional helical protocol in line with physical dose estimates. For an approximated median effective dose ranging from 2.1 to 23.8 mSv, the authors described a linear dose response for the induction of excess γH2AX foci in vivo from 0.04 to 0.71 foci per leukocyte with a median of 0.33 in line with similar studies [22]. In another study these authors investigated the impact of digital mammography executed with doses even lower than for CT examinations [25]. Again, a very slight but significant increment of γH2AX foci was found in systemic leukocytes of 20 patients. The average EWBD in our study was estimated to be in the range of just 2.34–14.67 mSV and was significantly higher for linac than for orthovoltage RT. Based on our calculations, this variation of the EWBD between the radiation techniques was determined by differences in the SSD and half-value thickness. For otherwise identical parameterization, a higher SSD for linac RT caused an average 1.9-fold reduction of the integral dose compared to orthovoltage RT and, conversely, the higher half-value thickness for linac RT resulted in a six-fold increment of the integral dose than for orthovoltage RT. The impact of these two parameters resulted in a general significant 4.4-fold increase of the integral dose for linac RT compared to orthovoltage RT. This value also applied for calculated EWBD, since there were no significant differences in the distribution of the patients' bodyweight between the two radiation modali-

ties. We observed a general slight but significant increase of γH2AX foci per cell after RT for all patients but no difference between the RT techniques nor a correlation with the EWBD. 30 min after RT the numbers of excess γH2AX foci per cell were in a low range of 0 to 0.685, with a median of 0.104.

In our previous studies on the quantification of γH2AX foci in peripheral leukocytes of breast and prostate cancer patients after RT, we have shown linear dose–response relationships and good approximations of the administered whole-body dose based on ex vivo calibration data [26, 27]. However, cancer patients were exposed to significantly higher EWBDs compared to patients with benign diseases of the present study (Fig. 3d). According to our reference data on linear dose–response relationships of γH2AX foci in leukocytes at various times post exposure [26], the average frequency of 0.149 RI foci per cell after RT of all patients in the present work equates to a mean absorbed X-ray dose of 15.1 mGy, which exceeds our calculated average EWBD of 6.77 mSv. But assuming that the number of foci of DSB repair proteins in peripheral leukocytes after RT is a quantitative measure of the patient's dose burden and correlates with the risk of adverse side and late effects of medical radiation exposure, it is expectedly and significantly far lower in heel spur patients than for tumor patients. However, as we reported in our previous work [26, 27], the induction of DSBs in peripheral leukocytes during RT depends on various radiation and physiological parameters, which strongly limits such direct comparisons. Although the yield of γH2AX foci in peripheral leukocytes during RT of cancer patients is primarily governed by general RT parameters such as the planning target volume or the administered EWBD, we described volume- and dose-independent variations of radiation biomarkers in leukocytes among different RT techniques for breast cancer treatment which were heavily dominated by the absolute beam-on time [27]. Therefore, the radiation parameters between the two RT techniques of the present study, such as the field size or the dose rate, were adjusted as well as possible to achieve comparable exposure scenarios and beam-on times, to detect the impact of diverse out-of-field doses only. Besides, a strong dependency of foci induction in systemic leukocytes on physical variables such as the regional blood volume and kinetics of leukocyte circulation in the exposed anatomic region has to be considered for any comparative tactic [22, 24]. These confounding factors also greatly deteriorate the accuracy of radiation biomarkers for dose estimates after RT, in particular in the range of very low doses.

Taken together, using a biodosimetric approach to monitor the radiation burden of heel spur patients after the first fraction of RT with a single dose of 0.5 Gy administered with a 140-kV orthovoltage device or a 6-MV linac, we observed a marginal but significant overall increase in the DSB surrogate marker γH2AX in peripheral leukocytes, with no difference between the RT techniques. Both treatment modalities were associated with very modest radiation exposures and showed high and comparable analgesic effectiveness. Our data confirm the use of low-dose RT as an attractive treatment option for benign diseases.

Acknowledgements We thank U. Disque-Kaiser for excellent technical assistance, all patients who have participated in this study, and the medical staff at the Department of Radiation Oncology and Radiation Therapy at the University Medical Centre Mainz, Germany, for mentoring of patients and blood sampling.

Funding This research was supported by the German Federal Ministry of Education and Research, grant 02NUK016A and 02NUK042A.

Author Contribution H. Schmidberger, H.-P. Rösler, and S. Zahnreich conceived and designed the study. H. Karle was responsible for the medical physics part of this study. H.-P. Rösler and C. Schwanbeck acquired patient and clinical data on CS scores. S. Zahnreich performed experiments, γH2AX foci quantitation, and all data analysis. S. Zahnreich and H. Schmidberger wrote the paper.

Funding Open Access funding provided by Projekt DEAL.

Conflict of interest S. Zahnreich, H.-P. Rösler, C. Schwanbeck, H. Karle, and H. Schmidberger declare that they have no competing interests.

References

1. Leer JW, van Houtte P, Davelaar J (1998) Indications and treatment schedules for irradiation of benign diseases: a survey. Radiother Oncol 48(3):249–257. https://doi.org/10.1016/s0167-8140(98)00051-6
2. Frey B, Hehlgans S, Rodel F, Gaipl US (2015) Modulation of inflammation by low and high doses of ionizing radiation: implications for benign and malign diseases. Cancer Lett. https://doi.org/10.1016/j.canlet.2015.04.010
3. Heyd R, Tselis N, Ackermann H, Roddiger SJ, Zamboglou N (2007) Radiation therapy for painful heel spurs: results of a prospective randomized study. Strahlenther Onkol 183(1):3–9. https://doi.org/10.1007/s00066-007-1589-1
4. Ott OJ, Jeremias C, Gaipl US, Frey B, Schmidt M, Fietkau R (2014) Radiotherapy for benign calcaneodynia: long-term results of the Erlangen dose optimization (EDO) trial. Strahlenther Onkol 190(7):671–675. https://doi.org/10.1007/s00066-014-0618-0
5. Niewald M, Holtmann H, Prokein B, Hautmann MG, Rosler HP, Graeber S, Dzierma Y, Ruebe C, Fleckenstein J (2015) Randomized

multicenter follow-up trial on the effect of radiotherapy on painful heel spur (plantar fasciitis) comparing two fractionation schedules with uniform total dose: first results after three months' follow-up. Radiat Oncol 10:174. https://doi.org/10.1186/s13014-015-0471-z
6. Ott OJ, Niewald M, Weitmann HD, Jacob I, Adamietz IA, Schaefer U, Keilholz L, Heyd R, Muecke R (2015) DEGRO guidelines for the radiotherapy of non-malignant disorders. Part II: painful degenerative skeletal disorders. Strahlenther Onkol 191(1):1–6. https://doi.org/10.1007/s00066-014-0757-3
7. Surenkok S, Dirican B, Beyzadeoglu M, Oysul K (2006) Heel spur radiotherapy and radiation carcinogenesis risk estimation. Radiat Med 24(8):573–576. https://doi.org/10.1007/s11604-006-0075-5
8. Leer JW, van Houtte P, Seegenschmiedt H (2007) Radiotherapy of non-malignant disorders: where do we stand? Radiother Oncol 83(2):175–177. https://doi.org/10.1016/j.radonc.2007.04.008
9. Damber L, Larsson LG, Johansson L, Norin T (1995) A cohort study with regard to the risk of haematological malignancies in patients treated with x-rays for benign lesions in the locomotor system. I. Epidemiological analyses. Acta Oncol 34(6):713–719. https://doi.org/10.3109/02841869509127177
10. Jansen JT, Broerse JJ, Zoetelief J, Klein C, Seegenschmiedt HM (2005) Estimation of the carcinogenic risk of radiotherapy of benign diseases from shoulder to heel. Radiother Oncol 76(3):270–277. https://doi.org/10.1016/j.radonc.2005.06.034
11. Pierce DA, Shimizu Y, Preston DL, Vaeth M, Mabuchi K (1996) Studies of the mortality of atomic bomb survivors. Report 12, Part I. Cancer: 1950–1990. Radiat Res 146(1):1–27
12. UNSCEAR (2000) Sources and effects of ionizing radiation. UNSCEAR 2000 report volume I: sources. United Nations Publications, New York
13. Cole C, Seto C, Gazewood J (2005) Plantar fasciitis: evidence-based review of diagnosis and therapy. Am Fam Physician 72(11):2237–2242
14. Riepert T, Drechsler T, Urban R, Schild H, Mattern R (1995) The incidence, age dependence and sex distribution of the calcaneal spur. An analysis of its x-ray morphology in 1027 patients of the central European population. Rofo 162(6):502–505. https://doi.org/10.1055/s-2007-1015925
15. Kriz J, Seegenschmiedt HM, Bartels A, Micke O, Muecke R, Schaefer U, Haverkamp U, Eich HT (2018) Updated strategies in the treatment of benign diseases—a patterns of care study of the german cooperative group on benign diseases. Adv Radiat Oncol 3(3):240–244. https://doi.org/10.1016/j.adro.2018.02.008
16. Muecke R, Micke O, Reichl B, Heyder R, Prott FJ, Seegenschmiedt MH, Glatzel M, Schneider O, Schafer U, Kundt G (2007) Demographic, clinical and treatment related predictors for event-free probability following low-dose radiotherapy for painful heel spurs—a retrospective multicenter study of 502 patients. Acta Oncol 46(2):239–246. https://doi.org/10.1080/02841860600731935
17. Kase KR, Svensson GK, Wolbarst AB, Marks MA (1983) Measurements of dose from secondary radiation outside a treatment field. Int J Radiat Oncol Biol Phys 9(8):1177–1183. https://doi.org/10.1016/0360-3016(83)90177-3
18. Dorr W, Herrmann T (2008) Second tumors after oncologic treatment. Strahlenther Onkol 184(2):67–72. https://doi.org/10.1007/s00066-008-1807-5
19. Diallo I, Haddy N, Adjadj E, Samand A, Quiniou E, Chavaudra J, Alziar I, Perret N, Guerin S, Lefkopoulos D, de Vathaire F (2009) Frequency distribution of second solid cancer locations in relation to the irradiated volume among 115 patients treated for childhood cancer. Int J Radiat Oncol Biol Phys 74(3):876–883. https://doi.org/10.1016/j.ijrobp.2009.01.040
20. Beels L, Bacher K, Smeets P, Verstraete K, Vral A, Thierens H (2012) Dose-length product of scanners correlates with DNA damage in patients undergoing contrast CT. Eur J Radiol 81(7):1495–1499. https://doi.org/10.1016/j.ejrad.2011.04.063
21. Depuydt J, Baert A, Vandersickel V, Thierens H, Vral A (2013) Relative biological effectiveness of mammography X-rays at the level of DNA and chromosomes in lymphocytes. Int J Radiat Biol 89(7):532–538. https://doi.org/10.3109/09553002.2013.782447
22. Lobrich M, Rief N, Kuhne M, Heckmann M, Fleckenstein J, Rube C, Uder M (2005) In vivo formation and repair of DNA double-strand breaks after computed tomography examinations. Proc Natl Acad Sci U S A 102(25):8984–8989. https://doi.org/10.1073/pnas.0501895102
23. Rothkamm K, Balroop S, Shekhdar J, Fernie P, Goh V (2007) Leukocyte DNA damage after multi-detector row CT: a quantitative biomarker of low-level radiation exposure. Radiology 242(1):244–251. https://doi.org/10.1148/radiol.2421060171
24. Sak A, Grehl S, Erichsen P, Engelhard M, Grannass A, Levegrun S, Pottgen C, Groneberg M, Stuschke M (2007) gamma-H2AX foci formation in peripheral blood lymphocytes of tumor patients after local radiotherapy to different sites of the body: dependence on the dose-distribution, irradiated site and time from start of treatment. Int J Radiat Biol 83(10):639–652. https://doi.org/10.1080/09553000701596118
25. Schwab SA, Brand M, Schlude IK, Wuest W, Meier-Meitinger M, Distel L, Schulz-Wendtland R, Uder M, Kuefner MA (2013) X-ray induced formation of gamma-H2AX foci after full-field digital mammography and digital breast-tomosynthesis. PLoS One 8(7):e70660. https://doi.org/10.1371/journal.pone.0070660
26. Zahnreich S, Ebersberger A, Kaina B, Schmidberger H (2015) Biodosimetry based on gamma-H2AX quantification and cytogenetics after partial- and total-body irradiation during fractionated radiotherapy. Radiat Res 183(4):432–446. https://doi.org/10.1667/RR13911.1
27. Zahnreich S, Ebersberger A, Karle H, Kaina B, Schmidberger H (2016) Quantification of radiation biomarkers in leukocytes of breast cancer patients treated with different modalities of 3D-CRT or IMRT. Radiat Res 186(5):508–519. https://doi.org/10.1667/RR14475.1
28. Zwicker F, Swartman B, Roeder F, Sterzing F, Hauswald H, Thieke C, Weber KJ, Huber PE, Schubert K, Debus J, Herfarth K (2014) In vivo measurement of dose distribution in patients' lymphocytes: helical tomotherapy versus step-and-shoot IMRT in prostate cancer. J Radiat Res. https://doi.org/10.1093/jrr/rru096
29. Zwicker F, Swartman B, Sterzing F, Major G, Weber KJ, Huber PE, Thieke C, Debus J, Herfarth K (2011) Biological in-vivo measurement of dose distribution in patients' lymphocytes by gamma-H2AX immunofluorescence staining: 3D conformal- vs. step-and-shoot IMRT of the prostate gland. Radiat Oncol 6:62. https://doi.org/10.1186/1748-717X-6-62
30. Wang H, Adhikari S, Butler BE, Pandita TK, Mitra S, Hegde ML (2014) A perspective on chromosomal double strand break markers in mammalian cells. Jacobs J Radiat Oncol 1(1):3
31. Rowe CR, Sakellarides HT, Freeman PE (1963) Fractures of the os calcis a long-term follow-up study of 146 patients. JAMA 184:3
32. Johns HE (1961) Introduction to physics of radiobiology, 2nd edn. Thomas, Springfield, pp 353–357
33. Agarwal S, Tafel AA, Kanaar R (2006) DNA double-strand break repair and chromosome translocations. DNA Repair 5(9–10):1075–1081. https://doi.org/10.1016/j.dnarep.2006.05.029
34. Brand M, Sommer M, Achenbach S, Anders K, Lell M, Lobrich M, Uder M, Kuefner MA (2012) X-ray induced DNA double-strand breaks in coronary CT angiography: comparison of sequential, low-pitch helical and high-pitch helical data acquisition. Eur J Radiol 81(3):e357–362. https://doi.org/10.1016/j.ejrad.2011.11.027
35. Kuefner MA, Grudzenski S, Hamann J, Achenbach S, Lell M, Anders K, Schwab SA, Haberle L, Lobrich M, Uder M (2010) Effect of CT scan protocols on x-ray-induced DNA double-strand breaks in blood lymphocytes of patients undergoing coronary CT

angiography. Eur Radiol 20(12):2917–2924. https://doi.org/10.1007/s00330-010-1873-9
36. Kuefner MA, Grudzenski S, Schwab SA, Wiederseiner M, Heckmann M, Bautz W, Lobrich M, Uder M (2009) DNA double-strand breaks and their repair in blood lymphocytes of patients undergoing angiographic procedures. Invest Radiol 44(8):440–446. https://doi.org/10.1097/RLI.0b013e3181a654a5

9.4 Publikation IV

Spontaneous and Radiation-Induced Chromosome Aberrations in Primary Fibroblasts of Patients With Pediatric First and Second Neoplasms

frontiers in Oncology

ORIGINAL RESEARCH
published: 07 August 2020
doi: 10.3389/fonc.2020.01338

Spontaneous and Radiation-Induced Chromosome Aberrations in Primary Fibroblasts of Patients With Pediatric First and Second Neoplasms

Sebastian Zahnreich[1], Alicia Poplawski[2], Carola Hartel[3], Lukas Stefan Eckhard[4], Danuta Galetzka[1], Thomas Hankeln[5], Markus Löbrich[6], Manuela Marron[7], Johanna Mirsch[6], Sylvia Ritter[3], Peter Scholz-Kreisel[2], Claudia Spix[8] and Heinz Schmidberger[1]*

[1] Department of Radiation Oncology and Radiation Therapy, University Medical Centre of the Johannes Gutenberg University Mainz, Mainz, Germany, [2] Institute of Medical Biostatistics, Epidemiology and Informatics, University Medical Centre of the Johannes Gutenberg University Mainz, Mainz, Germany, [3] Department of Biophysics, GSI Helmholtzzentrum für Schwerionenforschung GmbH, Darmstadt, Germany, [4] Department of Orthopedic Surgery, University Medical Centre of the Johannes Gutenberg University Mainz, Mainz, Germany, [5] Institute of Organismic and Molecular Evolution, Molecular Genetics and Genome Analysis, Johannes Gutenberg University Mainz, Mainz, Germany, [6] Radiation Biology and DNA Repair, Technical University of Darmstadt, Darmstadt, Germany, [7] Department of Epidemiological Methods and Etiologic Research, Leibniz Institute for Prevention Research and Epidemiology – BIPS, Bremen, Germany, [8] German Childhood Cancer Registry, Institute of Medical Biostatistics, Epidemiology and Informatics, University Medical Centre of the Johannes Gutenberg University Mainz, Mainz, Germany

OPEN ACCESS

Edited by:
Turid Hellevik, University Hospital of North Norway, Norway

Reviewed by:
Aidan D. Meade, Technological University Dublin, Ireland
Adayabalam Sambasivan Balajee, Oak Ridge Institute for Science and Education (ORISE), United States

***Correspondence:**
Sebastian Zahnreich
zahnreic@uni-mainz.de

Specialty section:
This article was submitted to Radiation Oncology, a section of the journal Frontiers in Oncology

Received: *19 November 2019*
Accepted: *26 June 2020*
Published: *07 August 2020*

Citation:
Zahnreich S, Poplawski A, Hartel C, Eckhard LS, Galetzka D, Hankeln T, Löbrich M, Marron M, Mirsch J, Ritter S, Scholz-Kreisel P, Spix C and Schmidberger H (2020) Spontaneous and Radiation-Induced Chromosome Aberrations in Primary Fibroblasts of Patients With Pediatric First and Second Neoplasms. Front. Oncol. 10:1338. doi: 10.3389/fonc.2020.01338

The purpose of the present study was to investigate whether former childhood cancer patients who developed a subsequent secondary primary neoplasm (SPN) are characterized by elevated spontaneous chromosomal instability or cellular and chromosomal radiation sensitivity as surrogate markers of compromised DNA repair compared to childhood cancer patients with a first primary neoplasm (FPN) only or tumor-free controls. Primary skin fibroblasts were obtained in a nested case-control study including 23 patients with a pediatric FPN, 22 matched patients with a pediatric FPN and an SPN, and 22 matched tumor-free donors. Clonogenic cell survival and cytogenetic aberrations in Giemsa-stained first metaphases were assessed after X-irradiation in G1 or on prematurely condensed chromosomes of cells irradiated and analyzed in G2. Fluorescence *in situ* hybridization was applied to investigate spontaneous transmissible aberrations in selected donors. No significant difference in clonogenic survival or the average yield of spontaneous or radiation-induced aberrations was found between the study populations. However, two donors with an SPN showed striking spontaneous chromosomal instability occurring as high rates of numerical and structural aberrations or non-clonal and clonal translocations. No correlation was found between radiation sensitivity and a susceptibility to a pediatric FPN or a treatment-associated SPN. Together, the results of this unique case-control study show genomic stability and normal radiation sensitivity in normal somatic cells of donors with an early and high intrinsic or therapy-associated tumor risk. These findings provide valuable information for future studies on the etiology of sporadic childhood cancer and therapy-related SPN as well as for the establishment of predictive biomarkers based on altered DNA repair processes.

Keywords: childhood cancer, second primary malignancies, ionizing radiation, chromosome aberrations, radiation sensitivity, spontaneous chromosomal instability

INTRODUCTION

Over the past decades, the number of cancer survivors increased constantly due to earlier diagnosis as well as optimized and new oncologic therapies with increased effectiveness in local and systemic tumor control (1). However, the benefit of prolonged survival of cancer patients is compromised by an elevated risk for therapy-related adverse late-effects, with second primary neoplasms (SPN) representing the heaviest burden for the patients (2). This is of particular concern for the treatment of highly cancer-prone individuals with pediatric malignancies who are at the utmost risk for SPN because of high innate susceptibility, the clastogenic impact of anti-tumor treatments and prolonged survival after effectual cancer therapy with an average 5-year survival rate of about 80% (3). In childhood cancer patients, the successful control of a first primary neoplasm (FPN) by chemotherapy (CT) or radiation therapy (RT) increases the relative risk to develop a therapy-related SPN up to about 6-fold compared to the healthy population, corresponding to an incidence of more than 20% at 30 years after the diagnosis of the FPN (4–6). RT in particular, which is applied to treat more than 50% of all cancer patients during their clinical management, represents a high and established risk factor for therapy-related SPN (7). However, despite such correlations there is still a large variation in the individual susceptibility to treatment-induced SPN which has been attributed to genetic variation.

Pediatric cancers reflect a very heterogeneous group of disorders of mostly unidentified etiology. Only 5–10% of early-onset malignancies can be ascribed to known inherited or *de novo* familial mutations in high-penetrance predisposing genes (8). It is commonly assumed that genetic alterations in DNA repair and damage response pathways increase the inherent cancer risk and the vulnerability to adverse side-effects of oncologic therapies (9–11). However, the causalities for the vast majority of sporadic childhood cancers or an inherent susceptibility to iatrogenic SPN remain to be unraveled.

A clinical approach to identify individuals with an elevated cancer-proneness or hypersensitivity toward genotoxic anti-tumor therapies are functional bioassays which monitor the efficiency and accuracy of DNA repair in somatic cells after exposure to cytostatic drugs or ionizing radiation (IR). For this purpose, test systems have been developed to measure the efficiency and fidelity of DNA repair in lymphocytes or fibroblasts after *in vitro* IR exposure based on the quantification of chromosome aberrations or DNA double-strand break (DSB) repair foci [γH2AX or tumor protein 53 binding protein 1 (53BP1)] (12).

Common cytogenetic assays that are used to test for intrinsic chromosomal IR sensitivity investigate the rate of IR-induced chromosome aberrations in first metaphases after G0/1 exposure (G1 assay) or the frequency of chromatid aberrations in metaphases after irradiation of exponentially growing cells in G2 (G2 assay). The G2 assay allows for a prompter analysis of IR-induced cytogenetic damage since cells progress from G2 to mitosis within a few hours after irradiation. A variation of the G2 assay, which overcomes the problems of the IR-induced G2/M arrest and low mitotic indices, is drug-induced premature chromosome condensation in G2 (G2-PCC) (13). In most studies, a predisposition to RT-related severe normal tissue toxicities or cancer proneness correlated with a compromised repair of IR-induced DSBs and elevated rates of cytogenetic aberrations (14–31). Also, the level of spontaneous chromosome aberrations in normal somatic cells is considered a strong indicator of tumor incidence (32, 33). However, to identify patients who are at high risk for a pediatric FPN or a therapy-related SPN based on such surrogate biomarkers of compromised DNA repair and genome instability is still a major and unsolved clinical challenge.

To this end, we examined spontaneous chromosome aberrations as well as cellular and chromosomal IR sensitivity in primary skin fibroblasts obtained from a carefully matched case-control study nested in a cohort of childhood cancer survivors who were successfully treated for a sporadic FPN and either developed an SPN or not. Our findings will provide relevant clinical information whether sporadic and IR-induced chromosome aberrations and thus a limited DNA repair capacity in normal somatic cells can be used as a measure of risk assessment and stratification for the development of pediatric FPN or subsequent SPN.

MATERIALS AND METHODS

Patients

FPN and SPN patients were registered at the German Childhood Cancer Registry at the University Medical Centre in Mainz, Germany (34) and were matched according to the entity of the FPN, the age at diagnosis of the FPN, the year of diagnosis of the FPN, the age at biopsy and sex. Participants with any entity of FPN or SPN were included. An overview of the patient characteristics is provided in **Table 1**. SPN donors had to survive for at least 1 year after the diagnosis of the SPN. Skin biopsies to obtain primary fibroblasts were collected from 23 patients suffering from a variety of pediatric FPN and no SPN, 22 patients with the same type of FPN, and an SPN after the successful treatment of the FPN and from 22 donors with no neoplasm (NN) after written informed consent. For each of the matched doublets of an FPN and an SPN case, a NN donor was matched according to sex and the age at biopsy within a 5-year age range. Biopsies of NN donors were sampled at the Department of Accident Surgery and Orthopedics at the University Medical Centre in Mainz, Germany during a planned surgery within the KiKme study (Marron et al., in review)[1]. Following this

Abbreviations: SPN, second primary neoplasm; FPN, first primary neoplasm; NN, no neoplasm; CT, chemotherapy; RT, radiation therapy; DSB, DNA double-strand break; 53BP1, tumor protein 53 binding protein 1; IR, ionizing radiation; G2-PCC, G2 premature chromosome condensation; FISH, fluorescence *in situ* hybridization; mFISH, 24-multicolor fluorescence *in situ* hybridization; t, translocation; ins, insertion; dic, dicentric chromosome; T, truncated; SF2, surviving fraction at 2 Gy; pATM, phosphorylated ataxia telangiectasia mutated.

[1]Marron M, Brackmann L, Grandt C, Zahnreich S, Galetzka D, Schmitt I, et al. An innovative nested case-control study to identify genetic predispositions of childhood and second primary cancers related to ionizing radiation - the KiKme study. (in review).

procedure, we obtained 18 matched triplets with a matched NN, FPN, and SPN donor each, two quadruplets with an additional FPN donor each, a quadruplet with an additional NN donor, and a single SPN donor (also indicated in **Tables 2–4** presenting the raw data of our analyses). The study was approved by the Ethics Committee of the Medical Association of Rhineland-Palatinate [No. 837.440.03 (4102) and No. 837.262.12(8363-F)].

Cell Culture and Irradiation

To obtain primary human skin fibroblasts from cancer patients, biopsies were taken on the inside of the cubital region and for NN donors at the site of the planned surgery. Biopsies were dissected and kept in rich cell culture medium (Amniogrow, CytoGen GmbH, Wetzlar, Germany) in a humidified incubator at 37°C and 5% CO_2 to allow for outgrowth and expansion of primary fibroblasts. After the first passage, cells were cultured in Dulbecco's Minimal Essential Medium (Sigma-Aldrich, St. Louis, USA) containing 1% non-essential amino acids (Biochrom, Berlin, Germany), 15% fetal bovine serum (Biochrom, Berlin, Germany), and 1% penicillin/streptomycin (Biochrom, Berlin, Germany). Passaging was done using 0.05% trypsin with 0.1% ethylene-diamine-tetra-acetate (Biochrom, Berlin, Germany). After further expansion, cells were cryopreserved in liquid nitrogen. Only cells with <20 population doublings were used for experiments.

To irradiate fibroblasts selectively in G1 for clonogenic survival and the cytogenetic G1 assay, cells were synchronized by contact inhibition. To obtain confluent cultures, fibroblasts were seeded at a density of 9,000 cells/cm^2 in cell culture dishes with a diameter of 10 cm (Greiner Bio-One GmbH, Frickenhausen, Germany) and were allowed to grow at least for 14 days with a medium change every 4 days. Synchronization in G1 was confirmed by flow cytometric cell cycle analysis revealing that more than 90% of the population was in G1 when the cells were exposed to X-rays. To irradiate and analyze cells selectively in G2 (G2 assay), 9,000 cells/cm^2 were seeded in cell culture dishes with a diameter of 10 cm (Greiner Bio-One GmbH, Frickenhausen, Germany). Two days later exponentially growing cells were exposed to X-rays.

Irradiation was performed with a D3150 X-Ray Therapy System (Gulmay Ltd., Surrey, UK) at 140 kV and a dose rate of 3.6 Gy/min at room temperature. Control cells were sham-irradiated, i.e., kept at the same conditions in the radiation device control room.

Clonogenic Survival

To determine the clonogenic survival of G1 fibroblasts, confluent cultures were irradiated. Cells were harvested 24 h after irradiation and seeded in culture dishes with a diameter of 10 cm (Greiner Bio-One GmbH, Frickenhausen, Germany). 13, 26, 52, and 65 cells/cm^2 were plated after exposure to 0, 2, 4, and 6 Gy X-rays, respectively, with three technical replicates per IR dose. After incubation for 14 days to allow for the formation of colonies, cells were fixed, stained, and scored according to the protocol of Puck and Marcus (36), and survival curves were established considering the plating efficiencies of sham-irradiated controls. The average numbers of surviving cells per technical

TABLE 1 | Overview of patient characteristics.

	First primary neoplasms, *n* (%)	Second primary neoplasms, *n* (%)
Total	45	22
Female	19 (42%)	10 (46%)
Male	26 (58%)	12 (54%)
Age (years) at diagnosis, *median (range)*	5.0 (0–14)	15.5 (5–30)
<2	5 (11%)	
2–5	19 (42%)	
5–10	7 (16%)	2 (9%)
10–15	14 (31%)	7 (32%)
15–20		9 (41%)
20–25		2 (9%)
25–30		2 (9%)
Calendar year at diagnosis, *median (range)*	1985 (1980–1998)	1997 (1985–2003)
1980–1985	19 (42%)	
1985–1990	13 (29%)	2 (9%)
1990–1995	7 (16%)	6 (27%)
1995–2000	6 (13%)	8 (36%)
2000–2005		6 (27%)
Latency (years) between FPN and SPN, *median (range)*		8 (1–21)
1–5		2 (9%)
5–10		12 (55%)
10–15		2 (9%)
15–20		4 (18%)
20–25		2 (9%)
Age (years) at skin biopsy, *median (range)*	25 (21–36)[a]	26 (20–40)
20–25	8 (35%)[a]	8 (36%)
25–30	13 (57%)[a]	12 (55%)
30–35	1 (4%)[a]	1 (5%)
35–40	1 (4%)[a]	1 (5%)
Tumor entity according to ICC-3 code		
Leukemia (I)		
Lymphoid leukemias (Ia)	21 (47%)	1 (5%)
Acute myeloid leukemias (Ib)	2 (4%)	
Myelodysplastic syndrome and other myeloproliferative diseases (Id)	1 (2%)	1 (5%)
Lymphoma (II)		
Hodgkin lymphomas (IIa)	8 (18%)	1 (5%)
Non-Hodgkin lymphomas (except Burkitt lymphoma) (IIb)		5 (23%)
Burkitt lymphoma (IIc)	2 (4%)	
CNS and miscellaneous intracranial and intraspinal neoplasms (III)		
Ependymomas and choroid plexus tumor (IIIa)		1 (5%)
Astrocytomas (IIIb)		1 (5%)
Medulloblastoma (IIIc, 1.)	2 (4%)	
Other specified intracranial and intraspinal neoplasms (IIIe, 5.)		2 (9%)

(Continued)

TABLE 1 | Continued

	First primary neoplasms, *n* (%)	Second primary neoplasms, *n* (%)
Neuroblastoma and other peripheral nervous cell tumors (IV)		
Neuroblastoma and ganglioneuroblastoma (IVa)	2 (4%)	
Retinoblastoma (V)	2 (4%)	
Renal tumors (VI)		
Nephroblastoma and other non-epithelial renal tumors (VIa)	2 (4%)	
Soft tissue and other extraosseous sarcomas (IX)		
Rhabdomyosarcomas (IXa)	3 (7%)	
Other specified soft tissue sarcomas (IXd)		1 (5%)
Other malignant epithelial neoplasms and malignant melanomas (XI)		
Thyroid carcinomas (XIb)		6 (27%)
Carcinomas of salivary glands (XIf, 1.)		3 (14%)
Oncologic therapies		
CT– RT–	1 (2%)	8 (36%)
CT+ RT–	12 (27%)	5 (23%)
CT– RT+	1 (2%)	5 (23%)
CT+ RT+	31 (69%)	4 (18%)

First primary neoplasms comprise all cancer patients if not stated otherwise. Tumor entities were classified according to (35).
[a]Cancer patients with a first primary neoplasm and no subsequent second primary neoplasm only.
CT, chemotherapy; RT, radiation therapy including radioiodine-therapy for papillary thyroid cancer.

replicate counted as colonies with at least 50 cells after exposure to 0, 2, 4, and 6 Gy X-rays from all available samples were 59.3 ± 39.3, 65.6 ± 39.9, 58.0 ± 39.9, and 25.6 ± 20.7 (mean ± standard deviation), respectively.

Cytogenetic Assays

G1 Assay

Confluent fibroblasts were harvested 24 h after exposure to 3 Gy X-rays and seeded at a density of 9,000 cells/cm^2 in 75 cm^2 cell culture flasks (Greiner Bio-One GmbH, Frickenhausen, Germany). After 24 h, 0.02 µg/ml Colcemid (Roche, Basel, Switzerland) was added to collect only first metaphases after IR exposure as confirmed by BrdU labeling and fluorescence plus Giemsa staining performed according to Perry and Wolff (37). This approach was further validated by measuring the cell cycle progression after delayed plating by flow cytometry (**Supplementary Figure S1**). Forty-eight hours after delayed plating cells were trypsinized, chromosome spreads were prepared, and Giemsa-stained as described previously (38). This technique allows the detection of unstable chromosome aberrations which are categorized as being not transmissible to daughter cells comprising dicentric chromosomes, centric rings, and excess acentric fragments as well as chromatid breaks and exchanges (radials). For

TABLE 2 | Clonogenic survival after X-ray exposure of fibroblasts in G1.

Donor	Surviving fraction		
	2 Gy	4 Gy	6 Gy
NN1	0.621 ± 0.070	0.188 ± 0.032	0.065 ± 0.019
FPN1	0.583 ± 0.144	0.160 ± 0.032	0.044 ± 0.025
SPN1	0.589 ± 0.092	0.220 ± 0.028	0.046 ± 0.010
NN2	0.333 ± 0.110	0.201 ± 0.079	-
FPN2	0.490 ± 0.031	0.260 ± 0.031	0.051 ± 0.022
SPN2	0.473 ± 0.179	0.188 ± 0.060	0.033 ± 0.003
NN3	0.456 ± 0.046	0.358 ± 0.102	0.070 ± 0.038
FPN3	0.917 ± 0.011	0.446 ± 0.018	0.095 ± 0.008
SPN3	0.483 ± 0.059	0.312 ± 0.024	0.119 ± 0.001
NN4	0.581 ± 0.031	0.266 ± 0.016	0.080 ± 0.014
FPN4	0.559 ± 0.049	0.202 ± 0.036	0.072 ± 0.010
SPN4	0.512 ± 0.026	0.222 ± 0.021	0.059 ± 0.012
SPN5	0.375 ± 0.225	0.363 ± 0.115	0.090 ± 0.079
NN6	0.541 ± 0.016	0.247 ± 0.013	0.116 ± 0.006
FPN6	0.365 ± 0.113	0.223 ± 0.027	0.119 ± 0.031
SPN6	0.588 ± 0.017	0.307 ± 0.010	0.134 ± 0.010
NN7	0.489 ± 0.059	0.292 ± 0.009	0.137 ± 0.007
FPN7	0.523 ± 0.072	0.222 ± 0.024	0.100 ± 0.005
SPN7	0.493 ± 0.036	0.186 ± 0.020	0.092 ± 0.007
NN8	0.500 ± 0.164	0.329 ± 0.035	0.116 ± 0.018
FPN8	0.452 ± 0.128	0.149 ± 0.036	0.055 ± 0.027
FPN8a	0.448 ± 0.047	0.168 ± 0.022	0.038 ± 0.004
SPN8	0.722 ± 0.106	0.278 ± 0.042	0.010 ± 0.006
NN9	0.677 ± 0.162	0.399 ± 0.048	0.193 ± 0.034
FPN9	0.393 ± 0.110	0.157 ± 0.016	-
SPN9	0.344 ± 0.116	0.172 ± 0.033	0.059 ± 0.020
NN10	0.478 ± 0.049	0.168 ± 0.061	0.112 ± 0.019
FPN10	0.524 ± 0.078	0.263 ± 0.042	0.097 ± 0.010
SPN10	0.425 ± 0.064	0.331 ± 0.037	0.128 ± 0.030
NN11	0.357 ± 0.076	0.140 ± 0.017	0.056 ± 0.017
FPN11	0.604 ± 0.088	0.212 ± 0.066	0.115 ± 0.008
SPN11	0.548 ± 0.129	0.274 ± 0.035	0.097 ± 0.014
NN12	0.374 ± 0.011	0.179 ± 0.020	0.041 ± 0.009
FPN12	0.779 ± 0.104	0.209 ± 0.036	0.073 ± 0.054
FPN12a	0.385 ± 0.037	0.134 ± 0.006	0.044 ± 0.011
SPN12	0.407 ± 0.028	0.197 ± 0.024	0.041 ± 0.009
NN13	0.684 ± 0.052	0.234 ± 0.028	0.074 ± 0.004
FPN13	0.653 ± 0.128	0.215 ± 0.019	0.086 ± 0.010
SPN13	0.239 ± 0.042	0.120 ± 0.008	0.023 ± 0.040
NN14	0.613 ± 0.032	0.265 ± 0.033	0.090 ± 0.005
FPN14	0.489 ± 0.032	0.212 ± 0.029	0.106 ± 0.026
SPN14	0.407 ± 0.070	0.222 ± 0.031	0.061 ± 0.024
NN15	0.178 ± 0.031	0.081 ± 0.013	0.012 ± 0.011
FPN15	0.920 ± 0.466	0.349 ± 0.025	0.076 ± 0.036
SPN15	0.568 ± 0.070	0.197 ± 0.056	0.081 ± 0.043
NN16	0.887 ± 0.054	0.365 ± 0.042	0.136 ± 0.027
FPN16	0.386 ± 0.164	0.175 ± 0.092	0.022 ± 0.007
SPN16	0.587 ± 0.035	0.266 ± 0.035	0.064 ± 0.010
NN17	0.500 ± 0.107	0.362 ± 0.101	0.109 ± 0.025

(Continued)

TABLE 2 | Continued

Donor	Surviving fraction		
	2 Gy	4 Gy	6 Gy
FPN17	0.507 ± 0.013	0.212 ± 0.023	0.067 ± 0.009
SPN17	0.682 ± 0.074	0.324 ± 0.059	0.106 ± 0.013
NN18	0.658 ± 0.111	0.097 ± 0.023	0.017 ± 0.013
FPN18	0.647 ± 0.280	0.390 ± 0.046	0.018 ± 0.018
SPN18	0.631 ± 0.043	0.284 ± 0.022	0.093 ± 0.008
NN19	0.551 ± 0.033	0.299 ± 0.026	0.135 ± 0.012
FPN19	0.628 ± 0.064	0.286 ± 0.040	0.036 ± 0.006
SPN19	0.737 ± 0.178	0.204 ± 0.057	0.044 ± 0.020
NN20	0.804 ± 0.197	0.331 ± 0.076	0.127 ± 0.016
FPN20	0.743 ± 0.086	0.323 ± 0.058	0.136 ± 0.016
SPN20	0.950 ± 0.108	0.339 ± 0.015	0.074 ± 0.007
NN21	0.521 ± 0.007	0.293 ± 0.011	0.063 ± 0.010
FPN21	0.628 ± 0.096	0.236 ± 0.090	0.096 ± 0.036
SPN21	0.670 ± 0.075	0.292 ± 0.009	0.130 ± 0.025
NN22	0.417 ± 0.036	0.234 ± 0.095	0.055 ± 0.023
NN22a	n.a.	n.a.	n.a.
FPN22	0.683 ± 0.136	0.233 ± 0.026	0.059 ± 0.013
SPN22	0.551 ± 0.092	0.203 ± 0.011	0.056 ± 0.015

Data are presented as the mean fraction of surviving cells and the standard deviation of three technical replicates from one experiment for each donor.
NN, no neoplasm; FPN, first primary neoplasm; SPN, second primary neoplasm.

each sample 100 complete diploid metaphases were analyzed according to the criteria defined by Savage (39). The fraction of tetraploid cells was calculated as the ratio of metaphases with 92 chromosomes divided by the total number of all analyzed diploid and tetraploid metaphases. To assess the proportion of tetraploid cells on average 506 metaphases were scored for each sample.

G2 Assay

For the analysis of chromatid aberrations in cells exposed to 1 Gy X-rays in G2, 2.25 h after irradiation 50 nM calyculin A (LC Laboratories, Woburn, US) was added for 45 min to the cultures to induce G2-PCC. Detached cells were collected and chromosome preparation and Giemsa staining were performed as described previously (38). Chromatid aberrations were scored as breaks, gaps, and exchanges (radials) in G2-PCCs with at least 46 chromosome pieces. Gaps, which are usually considered to be achromatic lesions rather than true chromatid discontinuities, were included due to the obscure structure of chromosomes after G2-PCC. Chromatid exchanges were rare and scored as one aberration. Isochromatid breaks were scored as 2 chromatid breaks. Generally, 100 G2-PCCs were analyzed for each control sample and 50 G2-PCCs were analyzed for each irradiated sample.

Cytogenetic Data

The yield of spontaneous aberrations in sham-irradiated cells was subtracted from that in irradiated samples. If the desired number of metaphases or G2-PCCs was not achieved due to poor proliferation even in repeated experiments, all available metaphases or G2-PCCs were used for the analysis. The exact numbers of analyzed cells are provided in **Tables 3**, **4**.

Three- and Twenty-Four-Color Fluorescence *in situ* Hybridization

To detect transmissible aberrations in metaphase spreads obtained in the G1 assay, e.g., translocations or insertions which are not detected by the monochromic Giemsa method, fluorescence *in situ* hybridization (FISH) was performed for selected donors. Three-color FISH with a commercial cocktail of whole chromosome probes 1, 2, and 4 was conducted following the manufacturer's protocol (Metasystems, Altlussheim, Germany). Images of metaphases were obtained using an Axioimager1 microscope and the AxioVision software (Carl Zeiss AG, Oberkochen, Germany). Structural aberrations were scored only when painted chromosomes were involved. Analysis by 24-multicolor FISH (mFISH) which is capable of providing more detailed cytogenetic information (40) was performed as described previously (41). Slides were hybridized with a 24XCyte mFISH kit according to the manufacturer's protocol (Metasystems, Altlussheim, Germany). Captured images of metaphases were obtained with a Zeiss Axio-Imager Z2 microscope (Zeiss, Jena, Germany) and processed and analyzed with the Isis software (In Situ Imaging Systems, Metasystems, Germany). Structural aberrations were classified according to the mPAINT system (42). In brief, basic aberration forms such as translocations (t), insertions (ins), or dicentric chromosomes (dic) are described. Chromosome fragments containing a centromere are indicated by an apostrophe. An uppercase "T" indicates a truncated centric element which has become visibly shortened. For example, a reciprocal translocation between chromosomes 1 and 2 is designated "t (1′-2) (2′-1)." Identical chromosome aberrations were termed clonal if they were present in at least two metaphases of one sample. For each sample 100 diploid metaphases were analyzed.

Data and Statistical Analysis

The clonogenic survival after IR exposure was analyzed using a linear mixed model with the fixed variables dose, dose^2, group (NN, FPN, or SPN) and intercept including the patient as a random effect. The model was fitted using the lmer function in lme4 R package (43). Aberrations scored in the G1 and G2 assay were analyzed separately using the R package glmmTMB (44). Mixed models were fitted to estimate the effect of dose, group (NN, FPN, or SPN), a previous RT or CT, gender, and tumor entity on the number of aberrations. The negative binomial model with the patient as a random variable fitted best. Adding the matching group as an additional random variable did not improve the model. Age, sex, and tumor entity showed no significant impact on aberrations and were therefore excluded from the final model. The relationship between two variables was analyzed using Pearson's test and is provided as the correlation coefficient (r). All levels of significance were set at $p<0.05$. Average rates of chromosome aberrations or the fraction of surviving cells of pooled donors of the different study populations are provided as the mean ± standard deviation.

TABLE 3 | Spontaneous and radiation-induced chromosome aberrations per cell in first post-exposure metaphases collected 48 h after irradiation of fibroblasts in G1 with 3 Gy X-rays (G1 assay).

Donor	0 Gy									3 Gy							
	Cells	Aberrant cells (%)	Aberrations	dic	*r*	ace	ctb	cte	4N (%)	Cells	Aberrant cells (%)	Aberrations	dic	*r*	ace	ctb	cte
NN1	100	17.0	0.26	0.01	–	0.10	0.15	–	3.6	100	61.0	0.77	0.36	0.03	0.35	0.01	0.02
FPN1	100	7.0	0.08	0.02	–	0.05	0.01	–	1.5	100	54.0	0.59	0.36	0.02	0.21	–	–
SPN1	100	15.0	0.21	0.07	–	0.10	0.03	0.01	0.8	71	60.6	0.59	0.18	0.03	0.37	0.01	–
NN2	100	4.0	0.04	–	0.02	–	0.02	–	0.6	100	49.0	0.70	0.39	–	0.28	0.03	–
FPN2	100	8.0	0.10	–	–	0.06	0.04	–	1.2	100	52.0	0.66	0.36	0.02	0.28	–	–
SPN2	100	4.0	0.05	0.01	–	0.03	0.01	–	1.2	100	48.0	0.66	0.34	0.02	0.29	–	0.01
NN3	100	9.0	0.12	–	–	0.04	0.08	–	1.2	100	47.0	0.54	0.31	0.01	0.22	–	–
FPN3	100	1.0	0.01	–	–	0.01	–	–	0.4	100	44.0	0.60	0.32	0.01	0.27	–	–
SPN3	100	7.0	0.09	–	–	0.07	0.02	–	2.0	100	49.0	0.55	0.35	0.02	0.17	0.01	–
NN4	100	1.0	0.01	–	–	–	0.01	–	2.3	57	63.2	0.74	0.23	0.04	0.47	–	–
FPN4	100	3.0	0.03	–	–	0.01	0.02	–	2.1	100	56.0	0.87	0.40	–	0.44	0.03	–
SPN4	100	10.0	0.10	0.01	0.01	0.04	0.04	–	1.0	100	57.0	0.73	0.38	–	0.35	–	–
SPN5	100	2.0	0.02	–	–	0.01	0.01	–	1.3	100	57.0	0.66	0.38	0.01	0.27	–	–
NN6	100	3.0	0.04	–	–	0.03	0.01	–	0.2	100	58.0	0.76	0.26	0.04	0.42	0.04	–
FPN6	n.a				–					n.a.							
SPN6	100	13.0	0.18	–	–	0.16	0.02	–	0.7	100	50.0	0.58	0.27	0.01	0.30	–	–
NN7	100	2.0	0.02	–	–	0.01	0.01	–	1.0	100	65.0	0.79	0.38	0.03	0.38	–	–
FPN7	100	2.0	0.02	–	–	0.02	–	–	1.5	100	49.0	0.65	0.35	0.02	0.26	0.02	–
SPN7	58	12.1	0.14	0.02	0.02	0.07	0.03	–	1.6	76	60.5	0.80	0.35	–	0.44	0.01	–
NN8	100	6.0	0.06	–	–	0.06	–	–	0.8	100	40.0	0.47	0.26	–	0.21	–	–
FPN8	100	7.0	0.07	0.04	–	0.03	–	–	1.8	100	57.0	0.77	0.40	–	0.31	0.06	–
FPN8a	100	–	–	–	–	–	–	–	1.5	100	61.0	0.94	0.34	0.01	0.57	0.01	–
SPN8	100	1.0	0.01	–	–	0.01	–	–	2.3	100	52.0	0.64	0.35	0.02	0.27	–	–
NN9	100	14.0	0.16	0.01	–	0.07	0.08	–	0.4	100	46.0	0.48	0.25	0.02	0.21	–	–
FPN9	100	17.0	0.18	0.04	–	0.14	–	–	1.7	100	56.0	0.48	0.29	0.02	0.17	–	–
SPN9	100	2.0	0.02	–	–	0.02	–	–	4.0	47	48.9	0.58	0.28	0.02	0.28	–	–
NN10	100	3.0	0.03	–	–	0.01	0.02	–	2.8	100	50.0	0.64	0.30	0.01	0.31	0.02	–
FPN10	100	9.0	0.09	–	–	0.06	0.03	–	2.0	n.a							
SPN10	100	1.0	0.02	–	–	0.02	–	–	1.1	n.a							
NN11	100	18.0	0.23	0.03	–	0.07	0.13	–	2.2	100	56.0	0.76	0.39	0.03	0.34	–	–
FPN11	78	7.7	0.09	–	–	0.09	–	–	–	100	56.0	0.61	0.26	0.06	0.28	0.01	–
SPN11	100	6.0	0.07	–	–	0.05	0.02	–	1.0	100	57.0	0.68	0.46	0.01	0.21	–	–
NN12	100	2.0	0.02	–	–	0.02	–	–	1.3	88	51.1	0.61	0.28	0.02	0.26	0.03	–
FPN12	100	3.0	0.03	0.01	–	0.02	–	–	0.2	100	59.0	0.80	0.36	–	0.43	0.01	–
FPN12a	100	12.0	0.14	–	–	0.03	0.09	0.02	2.5	29	65.5	0.90	0.45	–	0.45	–	–
SPN12	100	18.0	0.25	–	–	0.13	0.12	–	1.8	100	54.0	0.56	0.35	0.03	0.18	–	–
NN13	100	8.0	0.09	0.01	–	0.06	0.02	–	1.8	100	48.0	0.59	0.28	0.01	0.30	–	–
FPN13	100	9.0	0.01	–	–	0.07	0.03	–	1.7	100	49.0	0.53	0.29	–	0.24	–	–
SPN13	88	19.3	0.22	0.02	–	0.07	0.13	–	3.3	100	70.0	0.87	0.30	0.01	0.56	–	–
NN14	100	5.0	0.06	0.02	–	0.03	0.01	–	0.3	100	59.0	0.74	0.35	0.01	0.33	0.05	–
FPN14	100	15.0	0.17	0.08	–	0.05	0.04	–	0.2	94	62.8	0.71	0.41	–	0.30	–	–
SPN14	100	5.0	0.06	0.02	–	0.03	0.01	–	1.0	100	56.0	0.72	0.34	0.01	0.32	0.05	–
NN15	100	6.0	0.06	0.01	–	0.02	0.03	–	0.2	n.a							
FPN15	74	10.8	0.12	0.01	–	0.10	0.01	–	0.2	n.a							
SPN15	100	17.0	0.21	0.03	–	0.14	0.04	–	0.2	66	29.0	0.41	0.24	0.02	0.14	–	–
NN16	100	6.0	0.06	0.02	–	0.04	–	–	1.4	100	55.0	0.80	0.45	–	0.35	–	–
FPN16	100	13.0	0.15	0.05	–	0.09	0.01	–	7.4	100	58.0	0.79	0.45	0.03	0.27	0.04	–

(Continued)

TABLE 3 | Continued

Donor	0 Gy									3 Gy							
	Cells	Aberrant cells (%)	Aberrations	dic	*r*	ace	ctb	cte	4N (%)	Cells	Aberrant cells (%)	Aberrations	dic	*r*	ace	ctb	cte
SPN16	100	3.0	0.03	–	–	0.03	–	–	1.6	96	51.0	0.77	0.35	–	0.42	–	–
NN17	100	6.0	0.06	–	–	0.06	–	–	2.0	100	50.0	0.58	0.33	–	0.25	–	–
FPN17	100	16.0	0.22	–	–	0.17	0.05	–	1.2	100	47.0	0.45	0.25	–	0.20	–	–
SPN17	100	10.0	0.11	0.02	–	0.08	0.01	–	1.0	59	50.9	0.64	0.29	0.03	0.29	0.02	–
NN18	100	9.0	0.09	–	–	0.06	0.03	–	1.2	100	38.0	0.49	0.29	–	0.20	–	–
FPN18	100	1.0	0.01	–	–	0.01	–	–	8.8	100	48.0	0.63	0.31	0.02	0.30	–	–
SPN18	100	5.0	0.09	0.01	–	0.08	–	–	1.2	45	46.7	0.53	0.28	0.07	0.16	0.02	–
NN19	100	3.0	0.03	0.01	–	0.01	0.01	–	0.8	100	51.0	0.70	0.40	0.01	0.29	–	–
FPN19	100	7.0	0.07	–	–	0.07	–	–	0.6	100	59.0	0.87	0.45	0.01	0.41	–	–
SPN19	100	1.0	0.01	0.01	–	–	–	–	0.5	100	52.0	0.69	0.39	–	0.30	–	–
NN20	100	11.0	0.11	–	–	0.08	0.03	–	0.6	100	40.0	0.43	0.23	0.01	0.19	–	–
FPN20	100	12.0	0.12	–	–	0.09	0.03	–	0.8	100	45.0	0.52	0.31	0.03	0.18	–	–
SPN20	100	3.0	0.05	0.01	–	0.03	0.01	–	1.8	87	50.6	0.72	0.40	–	0.32	–	–
NN21	100	9.0	0.10	0.04	–	0.05	0.10	–	5.4	100	54.0	0.65	0.36	–	0.29	–	–
FPN21	100	7.0	0.07	0.03	–	0.04	–	–	4.0	100	57.0	0.61	0.26	0.01	0.34	–	–
SPN21	100	21.0	0.30	0.01	–	0.11	0.16	0.02	5.1	100	44.0	0.43	0.29	0.01	0.13	–	–
NN22	100	16.0	0.18	0.04	–	0.06	0.07	0.01	2.0	100	53.0	0.63	0.35	0.03	0.25	–	–
NN22a	100	5.0	0.07	–	–	0.07	–	–	0.8	100	54.0	0.63	0.28	0.03	0.31	0.01	–
FPN22	100	5.0	0.06	0.01	–	0.05	–	–	1.2	n.a.							
SPN22	100	3.0	0.03	–	–	0.03	–	–	2.2	100	37.0	0.40	0.24	0.04	0.12	–	–

For some donors the cytogenetic analysis was not available (n.a.) due to an insufficient mitotic index.
NN, no neoplasm; FPN, first primary neoplasm; SPN, second primary neoplasm; dic, dicentric chromosome; r, centric ring chromosome; ace, excess acentric fragment; ctb, chromatid break; cte, chromatid exchange (radial); 4N, fraction of tetraploid mitoses.

RESULTS

Patient Characteristics

An overview of the summarized characteristics of cancer patients is provided in **Table 1**. Total numbers of 23 cases with FPN only and 22 cases with the same FPN and a subsequent SPN as well as 22 NN donors were enclosed in the study. Hematopoietic and lymphoid cancers represented the majority of FPN (76%) and only a minor fraction of SPN (36%). Information on oncologic therapies is provided to the best of our knowledge based on the documentation of treating physicians voluntarily and on patient-based self-reports during a medical interview. All FPNs except for two retinoblastomas were treated by CT. However, since no matching of oncologic therapies has been performed between the corresponding FPN and SPN cases, differences in the application of RT were noted as follows: Four SPN and two FPN cases received radiochemotherapy compared to their respective FPN and SPN counterparts treated with CT only. In at least two other cases RT was administered to different or unknown anatomic regions. One FPN donor was treated by surgery only for unilateral retinoblastoma whereas the matched SPN case received RT only for bilateral retinoblastoma. One FPN and six SPN patients received a bone marrow or stem cell transplant during therapy without preconditioning by total body RT. For all patients, RT was administered locally to the site of a solid tumor, as cranial or craniospinal irradiation for leukemia, mainly at the thoracic and neck region for lymphoma or as radioiodine-therapy for papillary thyroid cancer. According to the common RT plans for the enclosed tumor entities, the treatment fields of partial-body RT did not involve the site of skin biopsy near the cubital region. Due to the retrospective nature of the study with an inevitable long follow-up, skin biopsies were collected from young adults on average 20 years after the diagnosis of the pediatric FPN and on average 10 years after the diagnosis of the adolescent SPN.

Clonogenic Survival

The cellular IR sensitivity of primary fibroblasts was measured as clonogenic survival after X-ray exposure of cells in G1. The summarized results for FPN, SPN, and NN donors are presented in **Figure 1** and raw data for each donor is provided in **Table 2**. The average plating efficiencies of NN, FPN, and SPN donors were similar with fractions of 6.4 ± 3.9%, 4.7 ± 3.4%, and 6.8 ± 3.9% of cells forming colonies, respectively. After irradiation, no significant difference in the fraction of surviving cells was found between NN and FPN or SPN donors. Mean surviving fractions at 2 Gy (SF2) of NN, FPN, and SPN donors were 0.54 ± 0.16, 0.58 ± 0.16, and 0.53 ± 0.16, respectively.

Chromosome Aberrations

G1 Assay

For the G1 assay, a total of 65 donors were analyzed for the rate of spontaneous chromosome aberrations, yielding a mean of 0.091 ± 0.073 aberrations per cell. Concerning the

TABLE 4 | Spontaneous and radiation-induced chromatid aberrations per G2-PCC 3 h after irradiation of exponentially growing fibroblasts with 1 Gy X-rays (G2 assay).

Donor	0 Gy					1 Gy				
	Cells	Aberrant cells (%)	Aberrations	ctb/gaps	cte	Cells	Aberrant cells (%)	Aberrations	ctb/gaps	cte
NN1	100	45.0	1.09	1.09	–	50	96.0	6.03	6.03	–
FPN1	100	44.0	0.98	0.98	–	50	100	5.74	5.74	–
SPN1	100	44.0	1.10	1.10	–	50	100	5.64	5.64	–
NN2	100	20.0	0.33	0.33	–	50	100	6.85	6.79	0.06
FPN2	96	20.8	0.62	0.62	–	49	100	6.92	6.92	–
SPN2	100	28.0	0.46	0.46	–	54	100	6.50	6.50	–
NN3	100	27.0	0.50	0.50	–	50	92.0	5.96	5.92	0.04
FPN3	100	31.0	0.59	0.59	–	50	96.0	4.25	4.25	–
SPN3	100	40.0	0.65	0.65	–	50	100	6.05	6.05	–
NN4	100	30.0	0.65	0.64	0.01	50	98.0	6.70	6.64	0.03
FPN4	100	50.0	1.26	1.26	–	50	100	4.32	4.28	0.02
SPN4	100	38.0	0.56	–	–	50	100	6.50	6.34	0.08
SPN5	100	14.0	0.17	0.17	–	38	100	5.47	5.44	0.03
NN6	100	44.0	0.98	0.98	–	50	100	6.18	6.14	0.04
FPN6	n.a.					n.a.				
SPN6	100	48.0	1.60	1.58	0.02	50	96.0	5.92	5.92	–
NN7	100	22.0	0.40	0.40	–	50	98.0	5.36	5.36	–
FPN7	83	33.7	0.69	0.69	–	46	100	5.16	5.16	–
SPN7	82	29.3	0.62	0.62	–	33	100	5.83	5.77	0.06
NN8	100	31.0	0.46	0.44	0.02	50	100	5.28	5.28	-
FPN8	100	31.0	0.61	0.58	0.03	50	100	7.83	7.68	0.15
FPN8a	100	26.0	0.33	0.32	0.01	50	100	6.50	6.50	-
SPN8	100	34.0	0.65	0.65	–	50	100	6.93	6.81	0.06
NN9	100	32.0	0.58	0.58	–	n.a.				
FPN9	100	18.0	0.43	0.43	–	23	100	5.57	5.57	–
SPN9	100	10.0	0.13	0.13	–	50	100	5.23	5.19	0.04
NN10	100	21.0	0.42	0.42	–	50	98.0	5.28	5.24	0.04
FPN10	100	40.0	0.78	0.78	–	50	100	5.70	5.68	0.02
SPN10	52	9.0	0.35	0.35	–	n.a.				
NN11	84	28.6	0.73	0.73	–	50	100	6.75	6.69	0.06
FPN11	74	48.7	0.96	0.96	–	49	98.0	5.60	5.60	–
SPN11	100	39.0	0.94	0.94	–	50	100	5.02	5.02	–
NN12	100	16.0	0.31	0.31	–	50	100	4.83	4.83	–
FPN12	100	36.0	0.62	0.62	–	50	100	5.18	5.18	–
FPN12a	100	47.0	0.85	0.78	0.07	50	100	5.69	5.64	0.05
SPN12	100	46.0	1.20	1.16	0.03	38	100	5.55	5.55	-
NN13	100	51.0	1.06	1.04	0.02	50	98.0	4.78	4.74	0.04
FPN13	100	41.0	1.05	1.02	0.03	50	100	6.06	6.06	–
SPN13	100	20.0	0.30	0.30	–	50	100	5.84	5.72	0.12
NN14	100	38.0	0.54	0.53	0.01	50	100	6.44	6.37	0.07
FPN14	100	31.0	0.77	0.74	0.03	50	100	5.73	5.68	0.05
SPN14	100	30.0	0.68	0.68	–	32	100	5.45	5.38	0.06
NN15	100	31.0	0.74	0.69	0.05	50	100	6.11	6.11	–
FPN15	100	8.0	0.11	–	–	50	100	5.35	5.35	–
SPN15	98	24.5	0.39	0.39	–	48	100	5.57	5.47	0.10
NN16	100	46.0	1.22	1.22	–	49	98.0	7.64	7.62	0.02
FPN16	n.a.				–	n.a.				
SPN16	100	53.0	1.18	1.18	–	50	98.0	5.32	5.32	–
NN17	100	19.0	0.49	0.48	0.01	50	100	5.67	5.60	0.07

(Continued)

TABLE 4 | Continued

Donor	0 Gy					1 Gy				
	Cells	Aberrant cells (%)	Aberrations	ctb/gaps	cte	Cells	Aberrant cells (%)	Aberrations	ctb/gaps	cte
FPN17	100	42.0	1.37	1.31	0.06	50	100	8.59	8.47	0.12
SPN17	100	52.0	1.23	1.14	0.09	50	100	9.39	9.22	0.17
NN18	87	13.8	0.17	0.17	–	50	98.0	6.15	6.05	0.10
FPN18	100	40.0	1.13	1.01	0.03	50	100	6.32	6.25	0.07
SPN18	100	41.0	0.65	0.65	–	50	100	5.37	5.35	0.02
NN19	100	27.0	0.43	0.43	–	50	100	5.47	5.43	0.04
FPN19	100	27.0	0.39	0.39	–	50	100	4.83	4.77	0.06
SPN19	67	25.4	0.37	0.37	–	49	100	4.99	4.95	0.04
NN20	100	18.0	0.39	0.39	–	50	100	4.51	4.49	0.02
FPN20	100	36.0	1.04	0.96	0.08	50	100	6.58	6.48	0.10
SPN20	100	24.0	0.55	0.53	0.02	50	98.0	6.03	5.95	0.08
NN21	100	54.0	2.16	2.02	0.07	50	100	4.89	4.86	0.03
FPN21	100	41.0	0.82	0.79	0.03	37	100	6.48	6.32	0.16
SPN21	100	28.0	0.66	0.64	0.02	50	100	4.90	4.82	0.08
NN22	100	36.0	0.76	0.75	0.01	50	100	5.93	5.93	–
NN22a	100	22.0	0.48	0.48	–	50	98.0	5.47	5.47	–
FPN22	100	42.0	0.91	0.87	0.04	50	100	5.89	5.85	0.04
SPN22	73	34.3	0.55	0.55	–	56	100	6.29	6.29	–

For some donors the cytogenetic analysis was not available (n.a.) due to poor proliferation and an insufficient G2-index.
NN, no neoplasm; FPN, first primary neoplasm; SPN, second primary neoplasm; ctb, chromatid break; cte, chromatid exchange (radial).

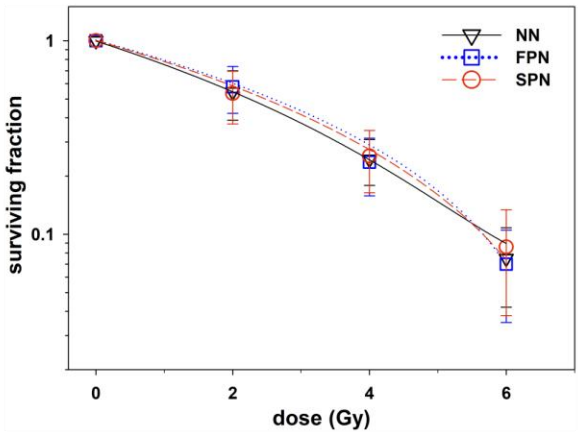

FIGURE 1 | Clonogenic survival of primary skin fibroblasts from donors with no neoplasm (NN, $n = 22$), only a first primary neoplasm (FPN, $n = 23$) or an FPN and a subsequent second primary neoplasm (SPN, $n = 21$) after exposure to X-rays. Error bars represent the standard deviation. All lines were fitted by a linear-quadratic function.

different study populations, the highest, although insignificantly elevated average rate of 0.103 ± 0.083 aberrations per cell was found in SPN donors compared to 0.083 ± 0.064 in FPN donors and 0.086 ± 0.068 in NN donors as shown in **Figure 2A**. For the different types of aberrations, the only divergence was a very mild increase of chromatid exchanges in SPN donors. Detailed information on the rate of chromosome aberrations scored in the G1 assay is provided in **Table 3**.

Remarkably, metaphase analysis of sham-irradiated cells revealed a striking chromosomal instability in two SPN donors. One SPN donor, who suffered from lymphoma as the FPN and SPN, showed exceptionally high numbers of numerical and unstable structural aberrations in 4 out of 100 analyzed metaphases. Representative pictures of such highly aberrant metaphases of this donor are shown in **Figure 2C**. Otherwise stable ploidy levels were observed for all other donors. The mean proportion of tetraploid cells in sham-irradiated samples of all donors was 1.68 ± 1.60% (range 0–8.8%) with no significant differences between the study populations ($p = 0.703$). Detailed information on tetraploidy is provided in **Table 3**. For a second SPN donor, Giemsa-analysis already indicated the presence of two clonal translocations as shown in **Figure 3**. Since this patient suffered from a pediatric rhabdomyosarcoma as the FPN which has been associated with the translocations (2;13)(q35;q14) or (1;13)(p36;q14) in tumor specimen (45), we screened all four donors of the respective quadruplet with two FPN cases for the involvement of chromosomes 1, 2, and 4 in cytogenetic alterations by three-color FISH. The NN donor and the two FPN donors showed no or a very low frequency of aberrations involving chromosome 1 in ≤3% of metaphases, whereas it was involved in aberrations in 84% of the metaphases of the SPN donor. Chromosomes 2 and 4 were not involved in aberrations in any donor analyzed. Subsequent mFISH analysis of the SPN donor revealed the following translocations: t (15′-1) (1′T) clonal in 53% of metaphases, t (1′-5) (5′T) clonal in 28% of metaphases,

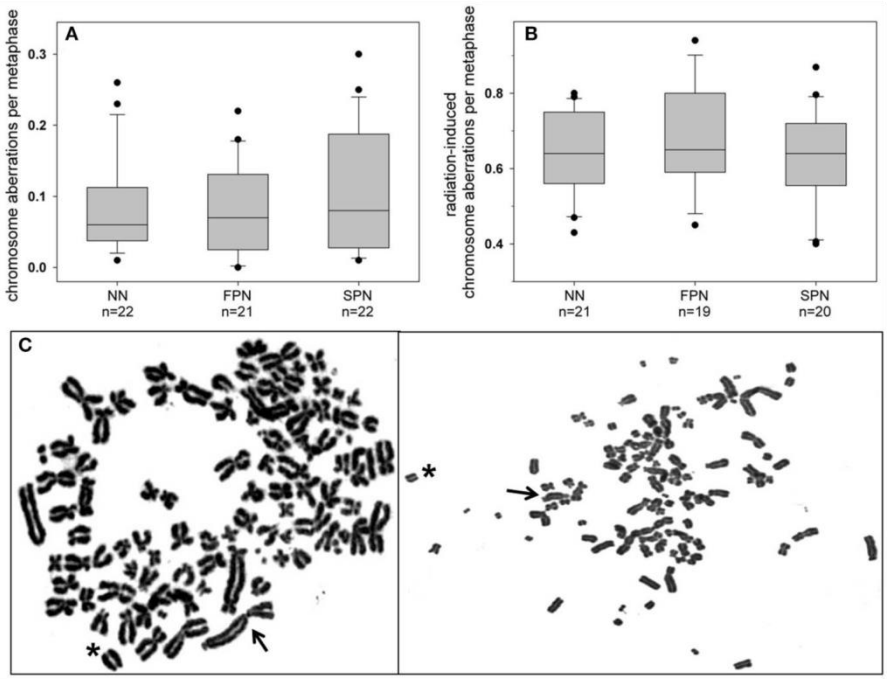

FIGURE 2 | Box and whisker plots of **(A)** spontaneous and **(B)** radiation-induced chromosome aberrations in primary skin fibroblasts from donors with no neoplasm (NN), only a first primary neoplasm (FPN), or an FPN and a subsequent second primary neoplasm (SPN). Aberrations were scored in metaphases of the first cell cycle after exposure in G1 to 3 Gy X-rays. Boxes include 50% of the data. The inner line represents the median value, whiskers represent the minimum and maximum values, and circles mark outliers. **(C)** Two representative Giemsa-stained complete metaphases from an SPN donor showing an abnormally high rate of spontaneous numerical and structural aberrations. Differences in the morphology of chromosomes between metaphases result from the different degrees of condensation. Structural aberrations are exemplarily indicated (arrow: dicentric chromosome, asterisk: acentric fragment).

t (15′-21) (21′-15) clonal in 5% of metaphases, t (15‘-6) (6‘-15), t (11‘-8) (8‘T) clonal in 2% of metaphases as well as non-clonal translocations t (15′-1) (1′T) t (2′-12) (12′-2), and t (16′-17) (17′-16) in one metaphase each. In total 90% aberrant metaphases were detected by mFISH. The aberrations were found in different cell cultures and passages of cells from this donor which were performed for the extensive cytogenetic analyses. Representative pictures of aberrant metaphases and karyotypes of this SPN donor after Giemsa-staining, three-color FISH, and mFISH are shown in **Figure 3** and **Supplementary Figure S2**.

After irradiation of fibroblasts with 3 Gy X-rays in G1 the mean yield of IR-induced chromosome aberrations in first post-exposure mitoses of a total of 61 donors was 0.650 ± 0.129 per cell. Shown in **Figure 2B**, the different sub-groups of donors had comparable average rates of IR-induced aberrations per cell of 0.642 ± 0.114 in NN donors, 0.683 ± 0.148 in FPN donors and 0.628 ± 0.124 in SPN donors. For a qualitative examination of the accuracy of DSB repair the average rates of RI interchromosomal exchanges scored as dicentric chromosomes were compared between the different donor groups. RI dicentrics occurred at similar frequencies per cell of 0.321 ± 0.062 in NN donors, 0.348 ± 0.065 in FPN donors, and 0.324 ± 0.065 in SPN donors.

G2 Assay

The analysis of chromatid aberrations in G2-PCCs from a total number of 64 donors showed a mean yield of spontaneous aberrations of 0.706 ± 0.377 per cell, primarily attributed to the occurrence of chromatid breaks and gaps. The rates for the different sub-groups of donors were comparable with 0.615 ± 0.274 aberrations per cell in NN donors, 0.767 ± 0.321 in FPN donors, and 0.742 ± 0.495 in SPN donors (**Figure 4A**). Three hours after exposure to 1 Gy X-rays the average yield of IR-induced chromatid aberrations in 63 donors was 5.88 ± 0.921 per G2-PCC. The different study populations showed similar mean rates of IR-induced chromatid aberrations per G2-PCC amounting to 5.83 ± 0.791 in NN donors, 5.90 ± 1.08 in FPN donors, and 5.91 ± 0.982 in SPN donors (**Figure 4B**). Detailed information on the rate of chromatid aberrations scored in G2-PCCs is provided in **Table 4**.

Correlations Between Assays and Patient Characteristics

Concerning a relationship between the results of the G1 and the G2 assay, only the level of spontaneous aberrations correlated weakly ($r = 0.41$, $p < 0.001$). No correlation was observed between the SF2 obtained in the clonogenic survival assay and

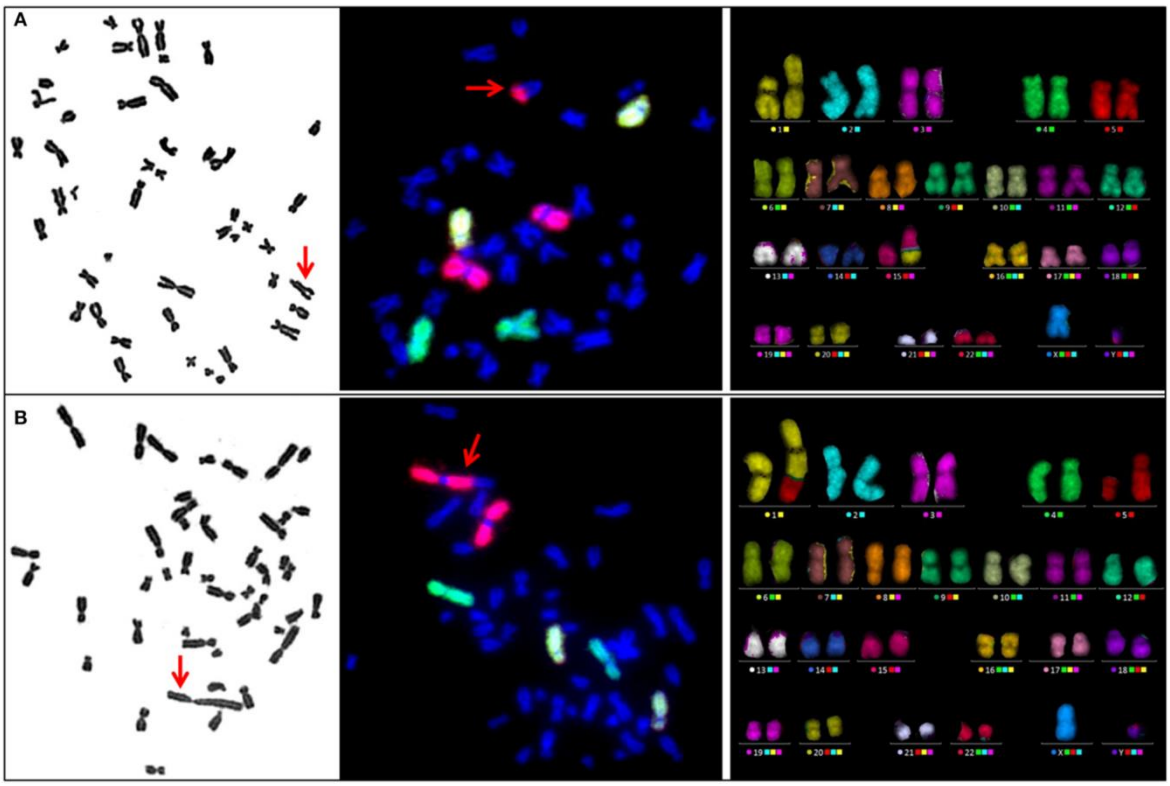

FIGURE 3 | Representative metaphases of an SPN donor carrying the spontaneous clonal translocations **(A)** t (15′-1) (1′T) and **(B)** t (1′-5) (5′T) after Giemsa staining (left panel), three-color FISH (central panel, red: chr. 1, green: chr. 2, yellow: chr. 4) and mFISH (right panel). Translocations are indicated by red arrows in metaphase spreads after Giemsa staining and three-color FISH.

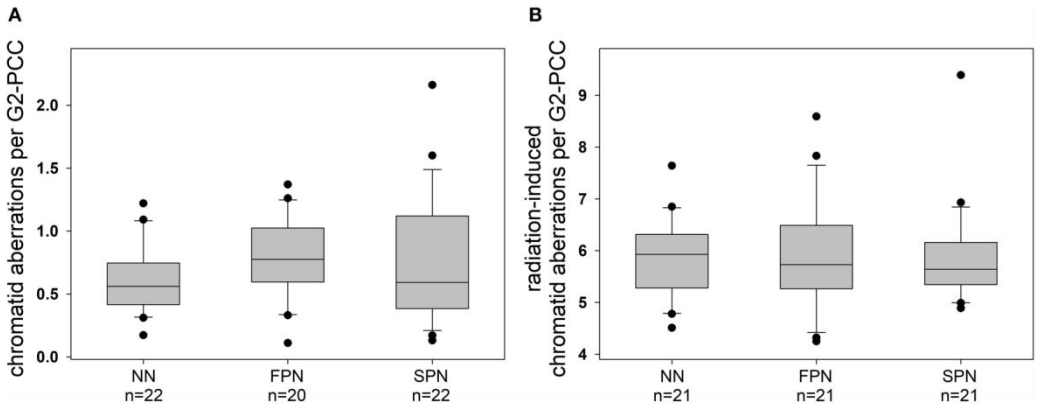

FIGURE 4 | Box and whisker plots of **(A)** spontaneous and **(B)** radiation-induced chromatid aberrations in primary skin fibroblasts from donors with no neoplasm (NN), only a first primary neoplasm (FPN), or an FPN and a subsequent second primary neoplasm (SPN). Aberrations were scored in prematurely condensed chromosomes of G2 cells (G2-PCCs) 3 h after the exposure of exponentially growing cells to 1 Gy X-rays. Boxes include 50% of the data. The inner line represents the median value, whiskers represent the minimum and maximum values, and circles mark outliers.

the results of any cytogenetic evaluation. Statistical analysis did not reveal a significant impact of a previous RT, CT, gender, or tumor entity (solid vs. hematopoietic or lymphoid) as well as FPN or SPN on the average level of spontaneous or IR-induced chromosome aberrations in both assays. Only *in vitro* exposure to IR increased the probability for the formation of a chromosome aberration per cell significantly by 8.1- and 10.4-fold for the G1 and G2 assay, respectively. Details on statistical evaluations are provided in **Supplementary Tables S1**, **S2**.

DISCUSSION

With increasing success in tumor control due to the constant progress of diagnostics and therapeutic strategies in oncology, treatment-related adverse late-effects inevitably gain high clinical relevance. Iatrogenic high-grade toxicities and second primary malignancies are a major threat and cause of long-term morbidity for the continuously increasing number of cancer survivors, in particular for childhood cancer patients (1, 2, 6). The present study examined if a relation between the susceptibility to pediatric FPNs or therapy-related SPNs and impaired genome maintenance exists. Therefore, measurements of sporadic chromosomal instability and cellular or chromosomal IR sensitivity in normal somatic cells were performed in matched SPN, FPN, and NN donors. We observed no significant difference for clonogenic cell survival after IR or the average yield of spontaneous and IR-induced chromosome aberrations between the study populations. Striking spontaneous chromosomal abnormities were found in two donors with SPN only. The results obtained in this study population indicate that the etiology of sporadic childhood cancer or the risk for SPN might underlie limited DNA repair capacities and provide useful information for future studies including the need for other biomarkers.

Since intrinsic proneness to cancer has been closely related to alterations in the DNA damage response a variety of studies have been conducted to identify high-risk patients by using biomarkers of DNA damage and repair. Over the past two decades evidence accumulated that chromosomal IR sensitivity of lymphocytes assessed by the conventional analysis of metaphases after irradiation of cells in G2 may serve as an indicator for proneness to an FPN. Such correlations of an increased innate chromosomal IR sensitivity and cancer susceptibility have been discussed regarding the presence of unknown, low-penetrance predisposing genes, in particular for patients with early-onset malignancies (27, 46). Many studies used classification criteria based on the average yield or arbitrary thresholds for the dispersion of IR-induced chromosome aberrations in G2 lymphocytes obtained at diagnosis to stratify for normal and sensitive IR responders and showed higher fractions of IR sensitive patients with sporadic and familial histories of breast cancer (14–21, 24, 47), with brain tumors (22, 23), head and neck squamous cell carcinomas (26), colorectal cancer (24), or suffering from different tumor entities (25). Moreover, these results point toward higher fractions of IR sensitive individuals among young adults with early-onset cancers (14, 26). For pediatric FPNs, Baria et al. (27) and Curwen et al. (28) confirmed an increased chromosomal IR sensitivity of G2 lymphocytes from childhood cancer patients. Using bioassays to quantify DSBs visualized as foci of γH2AX, 53BP1, or pATM (phosphorylated ataxia telangiectasia mutated), Rube et al. (30) and Schuler et al. (31) reported a compromised repair of IR-induced DSBs in G0 lymphocytes of childhood cancer patients suffering from different tumor entities, most pronounced in patients developing life-threatening or even lethal normal-tissue toxicities. Their findings also emphasize the strong selection criterion and potential bias of our study by examining only long-term survivors of pediatric FPNs compared to the vast majority of studies conducted on lymphocytes drawn at the time of tumor diagnosis. Hitherto, a sole nested case-control study performed by Haddy et al. (29) investigated differences in the repair of IR-induced DSBs between childhood cancer patients with an FPN and patients with a subsequent SPN. Applying γH2AX fluorescence intensity measurements by flow cytometry as a surrogate marker for DSBs in patient-derived lymphoblastoid cell lines established on average 24 years after the diagnosis of the FPN, an association between higher rates of basal as well as IR-induced DSBs and the risk of SPN in childhood cancer survivors was demonstrated. However, no tumor-free controls were included in the study.

To the best of our knowledge, the nested case-control study presented here is the first comparing the intrinsic genome integrity as well as the cellular and cytogenetic response to IR in primary fibroblasts obtained from patients with an FPN who developed an SPN or not and matched tumor-free controls. The above-cited studies have been performed with primary peripheral blood lymphocytes or lymphoblastoid cell lines which might affect the comparability with the results obtained in fibroblasts in the present study. Even though systemic lymphocytes are by far more easily accessible by minimal invasive venepuncture, we have chosen to conduct our investigations on primary skin fibroblasts since the use of lymphocytes is fraught with some major drawbacks: (1) they are unsuitable for long-term conservation and propagation unless immortalization with the Epstein-Barr virus transformation is performed which has profound impacts on cell cycle regulation via the expression of viral oncogenes, (2) they are largely exposed to genotoxic anticancer drugs including irradiation of bone marrow during radiotherapy, (3) they are prone to hematopoietic mosaicisms, and (4) they are unsuitable after a bone marrow or stem cell transplantation. The latter applies in particular to the present study since seven former childhood cancer patients received a bone marrow or stem cell transplant during their course of cancer therapy. As known from various studies of donors with chromosomal instability syndromes like Fanconi anemia, Bloom or Nijmegen breakage syndrome, sporadic as well as clastogen-induced chromosome aberrations in lymphocytes can be very well recapitulated in different cell types of the same donor such as skin fibroblasts (48, 49) or buccal epithelial cells (50). In this field, the use of skin fibroblasts is even preferred for diagnostic purposes since the occurrence of hematopoietic mosaicisms can obscure germline mutations and generate false-negative results (48, 49). Furthermore, a study by Lobrich et al. (51) demonstrated that the intrinsic defect in DSB

repair of a patient showing radiation hypersensitivity during radiotherapy could be detected qualitatively and quantitatively to a comparable extent in his lymphocytes and fibroblasts by γH2AX foci quantification after IR exposure. We are aware that the quantity and quality of IR-induced chromosome aberrations are dependent on various factors including nuclear geometry and architecture (52, 53) which differs between adherent and flat fibroblasts or spherical lymphocytes in suspension. However, this study did not aim to draw a direct quantitative comparison on the yield of IR-induced aberrations between previous studies using lymphocytes and our fibroblast data but to compare sporadic and IR-induced aberrations in the same cell type between the different donor groups. Using primary skin fibroblasts as a model of the normal somatic tissue we did not observe any difference in the average rate of spontaneous chromosome aberrations or clonogenic survival and aberrations after IR exposure between the study populations. Thus, our results show a comparable efficiency of genome maintenance between former pediatric patients with a high proneness to cancer *per se* or an SPN and tumor-free donors. Only a slight trend toward elevated spontaneous aberrations in SPN donors was observed with two SPN-cases displaying exceptional chromosomal instability. SPN donors showed a larger degree of variation in the clonogenic survival as well as for the level of spontaneous unstable aberrations in both assays when compared to FPN cases and tumor-free donors. Improving statistics by a larger cohort size or by increasing the number of evaluated cells through automated scoring of cytogenetic damage might corroborate these results in the future. Studies based on large epidemiological cohorts already showed an association between high levels of spontaneous unstable chromosome aberrations in peripheral blood lymphocytes of healthy individuals and cancer risk independent of previous exposures to carcinogens (32, 33, 54). Also, cytogenetic evaluations in somatic cells of pediatric cancer patients suggest that constitutional or treatment-related karyotype instability might promote the development of an SPN (54–56).

In this present study, the occurrence of aneuploid (near tetraploid) metaphases with a very high burden of structural aberrations in fibroblasts of an SPN donor who suffered from two independent lymphomas reflects a tumor-like karyotype and is a very clear indicator of exceptional chromosomal instability. Tetraploidization and a mild accumulation of aberrant metaphases can be a feature of *in vitro* aged primary fibroblasts approaching replicative senescence but are usually not found in recently established cultures at low passages as used here (57). Apart from the case described above, ploidy levels were normal with comparable fractions of tetraploid cells for all participants. Another SPN donor with a rhabdomyosarcoma as the FPN and a subsequent lymphoma as the SPN displayed high rates of clonal and non-clonal translocations in 90% of metaphases detected by high-resolution mFISH. Non-clonal translocations as well as their clonal expansion have been documented in skin fibroblasts from patients with hematopoietic malignancies after high-dose CT plus total-body RT before bone marrow transplantation (58). However, such aberrations can also occur as an artifact during the *in-vitro* cultivation of fibroblasts from normal donors (41). Here, RT was administered as partial-body irradiation and skin biopsies were taken outside the treatment field according to common RT plans of the enclosed tumor entities. Therefore, the observed translocations were generated most probably spontaneous *in vivo* or *in vitro*. Although the translocations detected in the SPN donor showed frequent participation of chromosomes 1 and 15, the involvement of at least 9 different chromosomes in multiple translocations shows a genome-wide chromosomal instability in his normal somatic cells. Sporadic structural and numerical chromosomal instability are hallmarks and drivers of carcinogenesis and have been attributed to dysfunctions in the mitotic checkpoint, DNA repair, and replication (59). However, for example, DNA damage generated by replicative stress differs substantially in signal transduction and repair pathways compared to DSBs caused by IR, the inductor of DNA-damage used in our study (60). Thus, approaches using a predictive functional assay with a singular end-point as a surrogate marker for cancer sensitivity bear a high risk of missing the actual affected gene-products and pathways which define innate cancer proneness (12).

In conclusion, our results do not support previous findings of overall elevated spontaneous or IR-induced chromosome aberrations in normal somatic cells of individuals with early and high cancer incidence. Striking cytogenetic abnormalities, suggesting an elevated tumor risk, were detected in two SPN donors, only. High-resolution cytogenetic analysis by FISH for all donors which allows much more sensitive detection of cytogenetic damage including transmissible aberrations that are missed by conventional solid-staining may sustain such findings in the future. Besides, testing the study population of this work for their proficiency to deal with replication stress-associated DNA damage induced by physical obstacles to the replication machinery is a future task to mimic and investigate the vulnerability to such pathophysiological processes related to cancer risk.

A drawback of this study is no intended matching of oncologic therapies between the corresponding FPN and SPN cases, in particular for RT, as it represents the highest risk factor for SPNs. Information on clinical management and medical histories of cancer patients has been provided only by the treating physicians voluntarily as well as on patient-based self-reports during a medical interview and is therefore very sparse and not standardized. Currently the cohort of the KiKme study is largely extended in a epidemiological nested case-control study design to obtain primary skin fibroblasts from 101 SPN and 340 FPN cases as well as from 150 tumor-free donors (Marron et al., in review)[1]. Detailed questionnaires will provide information on lifestyle, socio-economical and anthropometric factors as well as on health, family history of diseases, and medical radiation history including phantom based dosimetry to obtain distinct organ doses. Detailed analysis of genetic predispositions and other molecular-biological factors is already underway. Next-generation sequencing approaches and functional assays on DNA repair in a high-throughput design will be performed to unravel risk factors and potential predictive biomarkers for childhood cancers and treatment-related second malignancies for the most benefit of future cancer patients.

DATA AVAILABILITY STATEMENT

All datasets generated for this study are included in the article/**Supplementary Material**.

ETHICS STATEMENT

The studies involving human participants were reviewed and approved by Ethics Committee of the Medical Association of Rhineland-Palatinate [No. 837.440.03 (4102) and No. 837.262.12(8363-F)]. The patients/participants provided their written informed consent to participate in this study.

AUTHOR CONTRIBUTIONS

SZ, HS, MM, CS, DG, and ML: conception and design. SZ and HS: development of methodology. SZ, CH, DG, and LE: acquisition of biopsies and data. SZ, AP, CH, SR, and JM: analysis and interpretation of data (e.g., statistical analysis, biostatistics, and computational analysis). SZ: initial draft of the manuscript. SZ, AP, CH, TH, MM, JM, SR, PS-K, CS, and HS: writing, review, and/or revision of the manuscript. All authors contributed to the article and approved the submitted version.

FUNDING

This study was supported by the German Federal Ministry of Education and Research, Grants 02NUK016A, 02NUK042A, 02NUK042B, 02NUK042C, and 02NUK042D.

ACKNOWLEDGMENTS

We thank U. Disque-Kaiser for excellent technical assistance and cancer patients as well as healthy donors who have participated in this study.

SUPPLEMENTARY MATERIAL

The Supplementary Material for this article can be found online at: https://www.frontiersin.org/articles/10.3389/fonc.2020.01338/full#supplementary-material

REFERENCES

1. Shapiro CL. Cancer survivorship. *N Engl J Med.* (2018) 379:2438–50. doi: 10.1056/NEJMra1712502
2. Tubiana M. Can we reduce the incidence of second primary malignancies occurring after radiotherapy? A critical review. *Radiother Oncol.* (2009) 91:4–15. doi: 10.1016/j.radonc.2008.12.016
3. *Surveillance, Epidemiology, and End Results (SEER), Statistics Review 1975-2015.* Bethesda, MD: National Cancer Institute (2016). Available online at: http://seer.cancer.gov/csr/1975_2002/ (accessed September 18, 2019).
4. Jenkinson HC, Hawkins MM, Stiller CA, Winter DL, Marsden HB, Stevens MC. Long-term population-based risks of second malignant neoplasms after childhood cancer in Britain. *Br J Cancer.* (2004) 91:1905–10. doi: 10.1038/sj.bjc.6602226
5. MacArthur AC, Spinelli JJ, Rogers PC, Goddard KJ, Phillips N, McBride ML. Risk of a second malignant neoplasm among 5-year survivors of cancer in childhood and adolescence in British Columbia, Canada. *Pediatr Blood Cancer.* (2007) 48:453–9. doi: 10.1002/pbc.20921
6. Cardous-Ubbink MC, Heinen RC, Bakker PJ, van den Berg H, Oldenburger F, Caron HN, et al. Risk of second malignancies in long-term survivors of childhood cancer. *Eur J Cancer.* (2007) 43:351–62. doi: 10.1016/j.ejca.2006.10.004
7. Braunstein S, Nakamura JL. Radiotherapy-induced malignancies: review of clinical features, pathobiology, and evolving approaches for mitigating risk. *Front Oncol.* (2013) 3:73. doi: 10.3389/fonc.2013.00073
8. Grobner SN, Worst BC, Weischenfeldt J, Buchhalter I, Kleinheinz K, Rudneva VA, et al. The landscape of genomic alterations across childhood cancers. *Nature.* (2018) 555:321–7. doi: 10.1038/nature25480
9. Chistiakov DA, Voronova NV, Chistiakov PA. Genetic variations in DNA repair genes, radiosensitivity to cancer and susceptibility to acute tissue reactions in radiotherapy-treated cancer patients. *Acta Oncol.* (2008) 47:809–24. doi: 10.1080/02841860801885969
10. Kuhne M, Riballo E, Rief N, Rothkamm K, Jeggo PA, Lobrich M. A double-strand break repair defect in ATM-deficient cells contributes to radiosensitivity. *Cancer Res.* (2004) 64:500–8. doi: 10.1158/0008-5472.CAN-03-2384
11. Palumbo E, Piotto C, Calura E, Fasanaro E, Groff E, Busato F, et al. Individual radiosensitivity in oncological patients: linking adverse normal tissue reactions and genetic features. *Front Oncol.* (2019) 9:987. doi: 10.3389/fonc.2019.00987
12. Habash M, Bohorquez LC, Kyriakou E, Kron T, Martin OA, Blyth BJ. Clinical and functional assays of radiosensitivity and radiation-induced second cancer. *Cancers.* (2017) 9:147. doi: 10.3390/cancers9110147
13. Gotoh E, Durante M. Chromosome condensation outside of mitosis: mechanisms and new tools. *J Cell Physiol.* (2006) 209:297–304. doi: 10.1002/jcp.20720
14. Baeyens A, Thierens H, Claes K, Poppe B, Messiaen L, De Ridder L, et al. Chromosomal radiosensitivity in breast cancer patients with a known or putative genetic predisposition. *Br J Cancer.* (2002) 87:1379–85. doi: 10.1038/sj.bjc.6600628
15. Scott D, Barber JB, Levine EL, Burrill W, Roberts SA. Radiation-induced micronucleus induction in lymphocytes identifies a high frequency of radiosensitive cases among breast cancer patients: a test for predisposition? *Br J Cancer.* (1998) 77:614–20. doi: 10.1038/bjc.1998.98
16. Scott D, Barber JB, Spreadborough AR, Burrill W, Roberts SA. Increased chromosomal radiosensitivity in breast cancer patients: a comparison of two assays. *Int J Radiat Biol.* (1999) 75:1–10. doi: 10.1080/095530099140744
17. Scott D, Spreadborough A, Levine E, Roberts SA. Genetic predisposition in breast cancer. *Lancet.* (1994) 344:1444. doi: 10.1016/S0140-6736(94)90615-7
18. Knight RD, Parshad R, Price FM, Tarone RE, Sanford KK. X-ray-induced chromatid damage in relation to DNA repair and cancer incidence in family members. *Int J Cancer.* (1993) 54:589–93. doi: 10.1002/ijc.2910540412
19. Parshad R, Price FM, Bohr VA, Cowans KH, Zujewski JA, Sanford KK. Deficient DNA repair capacity, a predisposing factor in breast cancer. *Br J Cancer.* (1996) 74:1–5. doi: 10.1038/bjc.1996.307
20. Patel RK, Trivedi AH, Arora DC, Bhatavdekar JM, Patel DD. DNA repair proficiency in breast cancer patients and their first-degree relatives. *Int J Cancer.* (1997) 73:20–4. doi: 10.1002/(SICI)1097-0215(19970926)73:1<20::AID-IJC4>3.0.CO;2-3
21. Riches AC, Bryant PE, Steel CM, Gleig A, Robertson AJ, Preece PE, et al. Chromosomal radiosensitivity in G2-phase lymphocytes identifies breast cancer patients with distinctive tumour characteristics. *Br J Cancer.* (2001) 85:1157–61. doi: 10.1054/bjoc.2001.2086
22. Bondy ML, Kyritsis AP, Gu J, de Andrade M, Cunningham J, Levin VA, et al. Mutagen sensitivity and risk of gliomas: a case-control analysis. *Cancer Res.* (1996) 56:1484–6.

23. Bondy ML, Wang LE, El-Zein R, de Andrade M, Selvan MS, Bruner JM, et al. Gamma-radiation sensitivity and risk of glioma. *J Natl Cancer Inst.* (2001) 93:1553–7. doi: 10.1093/jnci/93.20.1553
24. Baria K, Warren C, Roberts SA, West CM, Scott D. Chromosomal radiosensitivity as a marker of predisposition to common cancers? *Br J Cancer.* (2001) 84:892–6. doi: 10.1054/bjoc.2000.1701
25. Terzoudi GI, Jung T, Hain J, Vrouvas J, Margaritis K, Donta-Bakoyianni C, et al. Increased G2 chromosomal radiosensitivity in cancer patients: the role of cdk1/cyclin-B activity level in the mechanisms involved. *Int J Radiat Biol.* (2000) 76:607–15. doi: 10.1080/095530000138268
26. Papworth R, Slevin N, Roberts SA, Scott D. Sensitivity to radiation-induced chromosome damage may be a marker of genetic predisposition in young head and neck cancer patients. *Br J Cancer.* (2001) 84:776–82. doi: 10.1054/bjoc.2000.1692
27. Baria K, Warren C, Eden OB, Roberts SA, West CM, Scott D. Chromosomal radiosensitivity in young cancer patients: possible evidence of genetic predisposition. *Int J Radiat Biol.* (2002) 78:341–6. doi: 10.1080/09553000110117359
28. Curwen GB, Winther JF, Tawn EJ, Smart V, Whitehouse CA, Rees GS, et al. G(2) chromosomal radiosensitivity in Danish survivors of childhood and adolescent cancer and their offspring. *Br J Cancer.* (2005) 93:1038–45. doi: 10.1038/sj.bjc.6602807
29. Haddy N, Tartier L, Koscielny S, Adjadj E, Rubino C, Brugieres L, et al. Repair of ionizing radiation-induced DNA damage and risk of second cancer in childhood cancer survivors. *Carcinogenesis.* (2014) 35:1745–9. doi: 10.1093/carcin/bgu077
30. Rube CE, Fricke A, Schneider R, Simon K, Kuhne M, Fleckenstein J, et al. DNA repair alterations in children with pediatric malignancies: novel opportunities to identify patients at risk for high-grade toxicities. *Int J Radiat Oncol Biol Phys.* (2010) 78:359–69. doi: 10.1016/j.ijrobp.2009.08.052
31. Schuler N, Palm J, Kaiser M, Betten D, Furtwangler R, Rube C, et al. DNA-damage foci to detect and characterize DNA repair alterations in children treated for pediatric malignancies. *PLoS ONE.* (2014) 9:e91319. doi: 10.1371/journal.pone.0091319
32. Bonassi S, Hagmar L, Stromberg U, Montagud AH, Tinnerberg H, Forni A, et al. Chromosomal aberrations in lymphocytes predict human cancer independently of exposure to carcinogens. European study group on cytogenetic biomarkers and health. *Cancer Res.* (2000) 60:1619–25. Available online at: https://cancerres.aacrjournals.org/content/60/6/1619
33. Bonassi S, Norppa H, Ceppi M, Stromberg U, Vermeulen R, Znaor A, et al. Chromosomal aberration frequency in lymphocytes predicts the risk of cancer: results from a pooled cohort study of 22 358 subjects in 11 countries. *Carcinogenesis.* (2008) 29:1178–83. doi: 10.1093/carcin/bgn075
34. Scholz-Kreisel P, Kaatsch P, Spix C, Schmidberger H, Marron M, Grabow D, et al. Second malignancies following childhood cancer treatment in Germany from 1980 to 2014. *Dtsch Arztebl Int.* (2018) 115:385–92. doi: 10.3238/arztebl.2018.0385
35. Steliarova-Foucher E, Stiller C, Lacour B, Kaatsch P. International classification of childhood cancer, third edition. *Cancer.* (2005) 103:1457–67. doi: 10.1002/cncr.20910
36. Puck TT, Marcus PI. Action of x-rays on mammalian cells. *J Exp Med.* (1956) 103:653–66. doi: 10.1084/jem.103.5.653
37. Perry P, Wolff S. New giemsa method for the differential staining of sister chromatids. *Nature.* (1974) 251:156–8. doi: 10.1038/251156a0
38. Zahnreich S, Ebersberger A, Kaina B, Schmidberger H. Biodosimetry based on gamma-H2AX quantification and cytogenetics after partial- and total-body irradiation during fractionated radiotherapy. *Radiat Res.* (2015) 183:432–46. doi: 10.1667/RR13911.1
39. Savage JR. Classification and relationships of induced chromosomal structural changes. *J Med Genet.* (1976) 13:103–22. doi: 10.1136/jmg.13.2.103
40. Loucas BD, Shuryak I, Cornforth MN. Three-color chromosome painting as seen through the eyes of mFISH: another look at radiation-induced exchanges and their conversion to whole-genome equivalency. *Front Oncol.* (2016) 6:52. doi: 10.3389/fonc.2016.00052
41. Zahnreich S, Krunic D, Melnikova L, Szejka A, Drossel B, Sabatier L, et al. Duplicated chromosomal fragments stabilize shortened telomeres in normal human IMR-90 cells before transition to senescence. *J Cell Physiol.* (2012) 227:1932–40. doi: 10.1002/jcp.22921
42. Cornforth MN. Analyzing radiation-induced complex chromosome rearrangements by combinatorial painting. *Radiat Res.* (2001) 155:643–59. doi: 10.1667/0033-7587.2001.155[0643:ARICCR]2.0.CO;2
43. Douglas B, Martin M, Bolker B, Walker S. Fitting linear mixed-effects models using lme4. *J Stat Softw.* (2015) 67:1–48. doi: 10.18637/jss.v067.i01
44. Brooks E, Kristensen K, van Benthem KJ, Magnusson A, Berg CW, Nielsen A, et al. glmmTMB balances speed and flexibility among packages for zero-inflated generalized linear mixed modeling. *R J.* (2017) 9:378–400. doi: 10.32614/RJ-2017-066
45. Shrestha A, Ritz B, Ognjanovic S, Lombardi CA, Wilhelm M, Heck JE. Early life factors and risk of childhood rhabdomyosarcoma. *Front Public Health.* (2013) 1:17. doi: 10.3389/fpubh.2013.00017
46. Scott D. Chromosomal radiosensitivity and low penetrance predisposition to cancer. *Cytogen Genome Res.* (2004) 104:365–70. doi: 10.1159/000077517
47. Howe OL, Daly PA, Seymour C, Ormiston W, Nolan C, Mothersill C. Elevated G2 chromosomal radiosensitivity in Irish breast cancer patients: a comparison with other studies. *Int J Radiat Biol.* (2005) 81:373–8. doi: 10.1080/09553000500147642
48. Alter BP, Joenje H, Oostra AB, Pals G. Fanconi anemia: adult head and neck cancer and hematopoietic mosaicism. *Arch Otolaryngol Head Neck Surg.* (2005) 131:635–9. doi: 10.1001/archotol.131.7.635
49. Pinto FO, Leblanc T, Chamousset D, Le Roux G, Brethon B, Cassinat B, et al. Diagnosis of Fanconi anemia in patients with bone marrow failure. *Haematologica.* (2009) 94:487–95. doi: 10.3324/haematol.13592
50. Ramirez MJ, Minguillon J, Loveless S, Lake K, Carrasco E, Stjepanovic N, et al. Chromosome fragility in the buccal epithelium in patients with Fanconi anemia. *Cancer Lett.* (2020) 472:1–7. doi: 10.1016/j.canlet.2019.12.008
51. Lobrich M, Rief N, Kuhne M, Heckmann M, Fleckenstein J, Rube C, et al. In vivo formation and repair of DNA double-strand breaks after computed tomography examinations. *Proc Natl Acad Sci USA.* (2005) 102:8984–9. doi: 10.1073/pnas.0501895102
52. Durante M, Pignalosa D, Jansen JA, Walboomers XF, Ritter S. Influence of nuclear geometry on the formation of genetic rearrangements in human cells. *Radiat Res.* (2010) 174:20–6. doi: 10.1667/RR2063.1
53. Foster HA, Estrada-Girona G, Themis M, Garimberti E, Hill MA, Bridger JM, et al. Relative proximity of chromosome territories influences chromosome exchange partners in radiation-induced chromosome rearrangements in primary human bronchial epithelial cells. *Mutat Res.* (2013) 756:66–77. doi: 10.1016/j.mrgentox.2013.06.003
54. Bakshi SR, Patel RK, Roy SK, Alladi PA, Trivedi AH, Bhatavdekar JM, et al. Chromosomal aberrations in young cancer patients. *Cancer Genet Cytogen.* (1999) 115:114–7. doi: 10.1016/S0165-4608(99)00068-0
55. Frias S, Ramos S, Salas C, Molina B, Sanchez S, Rivera-Luna R. Nonclonal chromosome aberrations and genome chaos in somatic and germ cells from patients and survivors of Hodgkin lymphoma. *Genes.* (2019) 10:37. doi: 10.3390/genes10010037
56. Chin TF, Ibrahim K, Thirunavakarasu T, Azanan MS, Oh L, Lum SH, et al. Nonclonal chromosomal aberrations in childhood leukemia survivors. *Fetal Pediatr Pathol.* (2018) 37:243–53. doi: 10.1080/15513815.2018.1492054
57. Zahnreich S, Melnikova L, Winter M, Nasonova E, Durante M, Ritter S, et al. Radiation-induced premature senescence is associated with specific cytogenetic changes. *Mutat Res.* (2010) 701:60–6. doi: 10.1016/j.mrgentox.2010.03.010
58. Massenkeil G, Zschieschang P, Thiel G, Hemmati PG, Budach V, Dorken B, et al. Frequent induction of chromosomal aberrations in *in vivo* skin fibroblasts after allogeneic stem cell transplantation: hints to chromosomal instability after irradiation. *Radiat Oncol.* (2015) 10:266. doi: 10.1186/s13014-015-0576-4
59. Burrell RA, McClelland SE, Endesfelder D, Groth P, Weller MC, Shaikh N, et al. Replication stress links structural and numerical cancer chromosomal instability. *Nature.* (2013) 494:492–6. doi: 10.1038/nature11935

60. Nikitaki Z, Hellweg CE, Georgakilas AG, Ravanat JL. Stress-induced DNA damage biomarkers: applications and limitations. *Front Chem.* (2015) 3:35. doi: 10.3389/fchem.2015.00035

Conflict of Interest: The authors declare that the research was conducted in the absence of any commercial or financial relationships that could be construed as a potential conflict of interest.

9.5 Publikation V

Compromised repair of radiation-induced DNA double-strand breaks in Fanconi anemia fibroblasts in G2

DNA Repair 96 (2020) 102992

Contents lists available at ScienceDirect

DNA Repair

journal homepage: www.elsevier.com/locate/dnarepair

Compromised repair of radiation-induced DNA double-strand breaks in Fanconi anemia fibroblasts in G2

Sebastian Zahnreich [a,*], Britta Weber [a], Gundula Rösch [a], Detlev Schindler [b], Heinz Schmidberger [a]

[a] Department of Radiation Oncology and Radiation Therapy, University Medical Centre of the Johannes Gutenberg, University Mainz, Germany
[b] Institute of Human Genetics, Julius-Maximilians-University, Würzburg, Germany

ARTICLE INFO

Keywords:
Fanconi anemia
Primary fibroblasts
Ionizing radiation
DNA double-strand breaks
γH2AX
53BP1
Chromosome aberrations

ABSTRACT

Fanconi anemia (FA) is a rare chromosomal instability syndrome with various clinical features and high cancer incidence. Despite being a DNA repair disorder syndrome and a frequently observed clinical hypersensitivity of FA patients towards ionizing radiation, the experimental evidence regarding the efficiency of radiation-induced DNA double-strand break (DSB) repair in FA is very controversial. Here, we performed a thorough analysis of the repair of radiation-induced DSBs in G1 and G2 in FA fibroblasts of complementation groups A, C, D1 (BRCA2), D2, E, F, G and P (SLX4) in comparison to normal human lung and skin fibroblasts. γH2AX, 53BP1, or RPA foci quantification after X-irradiation was combined with cell cycle markers. Cytogenetic analyses were performed on first metaphases after irradiation in G1 and by premature chromosome condensation after exposure in G2. Furthermore, the role of canonical-NHEJ and alternative-NHEJ for the fidelity of the repair of radiation-induced DSBs was examined. In FA fibroblasts, DSB repair was normal in G1 but compromised and more error-prone in the slow repair component of G2 as suggested by higher yields of radiation-induced γH2AX and 53BP1 foci as well as chromatid exchanges. However, RPA foci quantification in G2 indicated proficiency for homology-directed repair of DSBs in FA except for FA D1 (BRCA2). In lung fibroblasts, DSB repair in G1 was conducted with normal kinetics but elevated chromosome exchanges compared to skin fibroblasts. The overall repair of radiation-induced DSBs and the formation of chromosome exchanges in normal and FA fibroblasts in G1 and G2 were governed by canonical-NHEJ with no contribution of alternative-NHEJ. Together, we show impaired repair of radiation-induced DSBs in various FA complementation groups in the slow repair component of G2 that might promote the formation of potentially oncogenic aberrations and clinical radiation hypersensitivity.

1. Introduction

Fanconi anemia (FA) is a rare X-linked or autosomal recessive disease characterized by clinical features such as congenital malformations, progressive bone marrow failure, and escalated proneness to hematologic and solid malignancies [1]. This complex and heterogeneous syndrome of impaired DNA repair and genomic instability is based on mutations in a constantly growing number of hitherto 23 FA complementation groups. FA gene products cooperate in the FA and breast cancer-associated (FA/BRCA) pathway with essential functions in DNA interstrand crosslink (ICL) repair, nucleotide excision repair (NER), translesion synthesis (TLS), and homologous recombination (HR) [2]. The investigation of DNA repair in FA after genotoxic treatments has a longstanding history and revealed the primary function of the FA pathway in the repair of replication-associated DNA damage caused by a blockade of replication forks *via* ICL-induction by endogenous metabolites or cytostatic drugs. Impaired repair of replication-associated DNA damage by a loss of FA pathway function fosters the promiscuous use of error-prone DNA repair mechanisms and the formation of oncogenic chromosome rearrangements, representing a hallmark of FA [3].

Following the recognition of an ICL, the FA M/ Fanconi anemia core complex-associated protein 24 (FAAP24) translocase binds to damaged chromatin and recruits the FA core complex consisting of FA A, B, C, E, F, G, L, and FA associated proteins 10/MHF2 16/MHF1, 20, 24 and 100 (FA complex I). The activated FA core complex functions as a ubiquitin ligase to activate the paralogs FA D2 and I by monoubiquitylation to form the FA ID heterodimer (FA complex II). The FA ID heterodimer is considered as the main regulator of the FA/BRCA pathway *via*

* Corresponding author.
E-mail address: zahnreic@uni-mainz.de (S. Zahnreich).

https://doi.org/10.1016/j.dnarep.2020.102992
Received 15 June 2020; Received in revised form 4 September 2020; Accepted 23 September 2020
Available online 6 October 2020

interaction with downstream factors of HR, NER, and TLS (FA complex III) [4]. During the ICL unhooking event introduced by the ID complex and conducted by SLX4 (FA P), the structure-specific endonuclease ERCC4/XPF (FA Q)-ERCC1 heterodimer and the crossover junction endonuclease MUS81-EME1 [5], a DNA double-strand break (DSB) is generated by nucleolytic incision. To finalize ICL-repair, the DSB is repaired by HR comprising several of the late acting members of the FA/BRCA pathway such as FA D1 (breast cancer 2, BRCA2), FA J (breast cancer 1 (BRCA1)-interacting protein 1, BRIP1), FA N (partner and localizer of BRCA2, PALB2), FA O (RAD51C), FA R (RAD51) or FA S (BRCA1).

In general, DSBs are repaired by two major pathways: by canonical non-homologous end joining (c-NHEJ) which is active throughout the cell cycle and by HR during S phase and in G2. DSBs are repaired with biphasic kinetics in G1 and G2. In both cell cycle phases, c-NHEJ represents the fast component repairing more than 80 % of DSBs within the first hours after induction. This is followed by a slow component where the remaining DSBs in G1 are repaired by a resection-dependent subtype of c-NHEJ and in G2 by HR [6]. c-NHEJ functions without any sequence homologies and relies on the DNA-dependent protein kinase (DNA-PK) holoenzyme formed by the Ku70/80 heterodimer and the catalytic subunit of DNA-PK [7]. Ligating steps are performed by the DNA ligase IV (Lig4), X-ray repair cross-complementing protein 4 (XRCC4), XRCC4-like factor (XLF) and paralog of XRCC4 and XLF (PAXX) [8]. The initiation of HR is dependent on the resection of DSB ends which is orchestrated and executed by BRCA1 (FA S), C-terminal binding protein (CtBP)-interacting protein (CtIP), MRE11, EXO1 and DNA2 followed by loading of replication protein A (RPA) on the 3` single-stranded DNA overhang [9]. RPA is subsequently replaced by RAD51 (FA R) with the help of BRCA2 (FA D1), its cofactor PALB2 (FA N) and the RAD51 paralogs Rad51B, Rad51C (FA O), Rad51D, XRCC2, and XRCC3 to form the Rad51 nucleoprotein filament and to invade HR templates provided by replicated sister chromatids for error-free repair. Molecular regulation between c-NHEJ and homology-directed repair is subjected to the mutual antagonism of tumor suppressor p53-binding protein 1 (53BP1) and BRCA1 (FA S) for DSB end resection, a major determinant of DSB repair pathway choice [10]. Besides c-NHEJ and HR, cells may draw on alternative-NHEJ (alt-NHEJ) operating slowly and with low fidelity, causing large scale sequence alterations and translocations [11]. Alt-NHEJ is dependent on minimal DSB resection by CtIP, MRE11, and EXO1 as well as DNA polymerase theta, poly-(ADP-ribose)-polymerases (PARPs), Ligase1 or 3 and XRCC1 [12,13]. More extensive DSB-resection conducted by Bloom syndrome helicase, EXO1, and DNA2 initiates Rad52-dependent single-strand annealing (SSA) associated with sequence deletions [14].

A wide spectrum of DNA damage and in particular the most detrimental DSBs are potently induced by ionizing radiation (IR) [15]. Although FA is a syndrome of DNA repair disorder and activation of the FA/BRCA pathway after IR exposure has been previously reported [16], studies on the IR sensitivity of FA cells *in vitro* are highly controversial ([17–37] and compiled in Supplementary Table S1 and Supplementary Fig. S1). Given the elevated cancer susceptibility of FA patients, their sensitivity toward IR is of high clinical concern due to the inevitable and frequent application of radiation therapy as a mainstay of cancer treatment. Increased clinical sensitivity of FA patients to radiation therapy is well documented as severe and fatal normal tissue toxicities [38–43]. So far, however, no general correlation could be drawn between the cellular or chromosomal IR sensitivity assessed with functional bioassays and the clinical response to IR for FA patients. Previous studies on the IR response of FA cells *in vitro* were mostly conducted with primary fibroblasts or lymphocytes of various but often undefined FA complementation groups to investigate the repair of IR-induced DSBs using cytogenetic methods [17–20,22–26,28,30] or the detection of DSB repair foci [27,28,32–36], such as the phosphorylated histone variant H2AX (γH2AX) or 53BP1. Very few of these studies explored the repair of IR-induced DSBs in FA in a cell cycle-dependent manner, but their outcomes on the efficiency and fidelity of DSB repair remain contradicting and this clinically relevant issue has not yet been explored and clarified to its full extent.

In the present work, we investigated the repair of IR-induced DSBs in primary skin fibroblasts of FA complementation groups A, C, D1 (BRCA2), D2, E, F, G, and P (SLX4) compared to skin and lung fibroblasts from healthy donors by quantification of DSB repair foci of γH2AX, 53BP1 or RPA in combination with cell cycle markers selectively in G1 and G2. Cytogenetic analyses were performed on first post-exposure mitoses after irradiation in G1 and by premature chromosome condensation of cells exposed in G2 (G2-PCC). Besides, we examined a contribution of c-NHEJ and alt-NHEJ to the repair of IR-induced DSBs and the formation of chromosome rearrangements.

2. Materials and methods

2.1. Cell culture

Primary human skin fibroblasts from FA complementation groups A, C, D1 (BRCA2), D2, E, F, G, and P (SLX4) were established and provided by Professor Detlev Schindler (Institute of Human Genetics, Julius-Maximilians-University, Würzburg, Germany). HDFa skin (Cellsystems, Germany), BJ skin (ATCC, USA), WI38 lung (ECACC, UK), and MRC5 lung (ECACC, UK) fibroblasts were used as controls from healthy donors. 180BR (LIG4) skin fibroblasts (ECACC, UK) served as a control for impaired c-NHEJ by DNA ligase IV deficiency [44]. FA D1 (BRCA2) and 180BR (LIG4) fibroblasts were cultured in rich cell culture medium (Amniogrow, CytoGen GmbH, Germany) due to low proliferation activities. All other cells were cultured in low glucose Dulbecco's minimal essential medium (Sigma Aldrich, USA) containing 1% non-essential amino acids (Biochrom, Germany), 15 % fetal bovine serum (Gibco, Germany) and 1% penicillin/streptomycin (Biochrom, Germany). Cells were kept in a humidified incubator at 37 °C with 5% CO_2 (Heracell Vios 160i, Thermo Fisher Scientific, USA). Passaging of cells was done using 0.05 % trypsin with 0.1 % ethylene diamine tetraacetate (Biochrom, Germany). Irradiation was performed with a D3150 X-Ray Therapy System (Gulmay Ltd, UK) at 140 kV and a dose rate of 3.6 Gy/min at room temperature. Sham-irradiated cells were kept under the same conditions in the radiation device control room.

2.2. Mitomycin C and olaparib treatment

To test fibroblasts for sensitivity towards ICL-induction or a catalytic inhibition and trapping of PARP 1/2, exponentially growing cells were treated with 50 nM mitomycin C (MMC, medac, Germany) for 24 h or with 1 μM olaparib (Selleckchem, USA) for 48 h, respectively. 4 h before chromosome preparation 0.1 μg/mL colcemid (Roche, Switzerland) was added to accumulate metaphases followed by G2-PCC induced by 50 nM calyculin A (LC Laboratories, USA) 30 min before chromosome preparation. Chromosome preparation and Giemsa-staining was conducted as described previously [45]. Chromatid breaks and exchanges (radials) were scored in 25 or 50 metaphases and G2-PCCs in 3 independent experiments after MMC or olaparib treatment, respectively. Chromatid exchanges were scored as one aberration. Isochromatid breaks were scored as 2 chromatid breaks.

2.3. Detection of replication stress-induced FA D2 foci

To test the functionality of the FA core complex and FA D2, the accumulation of FA D2 at replication stress-induced DNA damage was detected by immunofluorescence microscopy. Fibroblasts were seeded on glass coverslips and exponentially growing cells were treated with 1 μg/mL of the DNA-polymerase inhibitor aphidicolin (Enzo Life Sciences GmbH, Germany) for 4 h in the presence of 20 μM EdU (Lumiprobe, Germany) serving as a marker of replication. For FA D2 detection cells were pre-extracted before fixation according to [46] to remove any

non-chromatin bound proteins. Thereafter, cells were fixed in 3.7 % formaldehyde/PBS for 10 min and permeabilized in 5% bovine serum albumin (BSA)/0.5 % Triton-X-100/PBS for 30 min at room temperature. EdU-staining dye (8 μM sulfo-Cy3- or -Cy5-azide (Lumiprobe, Germany)/2 mM Copper (II) sulfate pentahydrate (Sigma Aldrich, USA)/20 mg/mL ascorbic acid (Sigma Aldrich, USA)) was added for 30 min at room temperature. Cells were washed in PBS and incubated with a mouse anti-γH2AX antibody (Merck Millipore, Germany) and a rabbit anti-FA D2 antibody (Thermo Fisher Scientific, Germany) overnight at 4 °C. Cells were washed in PBS and incubated with a goat anti-mouse Alexa Fluor 488® antibody (Thermo Fisher Scientific, Germany) and a goat anti-rabbit-Cy3 or -Cy5 antibody (Abcam, UK) for one hour at room temperature. Cells were washed in PBS and mounted in Vectashield mounting medium with 0.2 μg/mL 4,6-diamino-2-phenylindole (DAPI, Serva Electrophoresis, Germany). Fluorescence microscopic image acquisition was performed with an Axio Imager.A1 microscope (Zeiss, Germany).

2.4. γH2AX, 53BP1, and RPA foci quantification

For immunofluorescence analysis of γH2AX, 53BP1 and RPA foci cells were seeded on glass coverslips. To quantify IR-induced DSBs 24 h after the exposure of G1-synchronized cells by γH2AX/53BP1 foci detection, cells were grown to confluency and treated with 20 μM EdU (Lumiprobe, Germany) from 6 h before IR-exposure on to exclude any proliferating cells from the analysis. To quantify γH2AX, 53BP1, or RPA foci selectively in G1 or G2, exponentially growing cells were treated with a double thymidine block before the radiation experiment to obtain sufficient numbers of G2 cells. Fibroblasts synchronized at the G1/S-border were released from the second thymidine block to proliferate for 6 h to yield a maximum of G2 cells (Supplementary Fig. S2). Before irradiation, 20 μM EdU (Lumiprobe, Germany) and 1 μg/mL aphidicolin (Enzo Life Science, Germany) were added to label replicating cells and to prevent the progression of cells irradiated in S to G2, respectively (Supplementary Fig. S3). Cells destined for RPA immunostaining were treated with 1 μg/mL aphidicolin (Enzo Life Science, Germany) only. Cells in S phase showed strong pan-nuclear RPA staining and were excluded from the analysis. For experiments aimed to investigate the contribution of c-NHEJ and alt-NHEJ to the repair of IR-induced DSBs, the DNA-PK inhibitor (DNA-PKi, NU7441, Tocris, UK) or the PARP inhibitor (PARPi, olaparib, Selleckchem, USA) was added 1 h before irradiation at a final concentration of 5 μM each. At defined times after IR exposure cells were fixed, permeabilized, EdU- and immunostained as described in Section 2.3 with pre-extraction before fixation only for RPA foci detection. For quantification of γH2AX, 53BP1 or RPA foci in G1 or G2, cells were incubated with a rabbit anti-CENP-F-antibody (Abcam, UK) and either a mouse anti-γH2AX antibody (Merck Millipore, Germany), a mouse anti-53BP1 antibody (Chemicon International, USA) or a mouse anti-RPA32/RPA2 antibody (Abcam, UK). For the detection of γH2AX/53BP1 foci in confluent G1 cells, incubation with a combination of the respective antibodies only was performed. Secondary antibodies were used as described in Section 2.3. Image acquisition by fluorescence microscopy was performed with an Axio Imager.A1 microscope (Zeiss, Germany) or a Metafer slide scanning platform (Metasystems, Germany) equipped with an Axio Imager.A2 microscope (Zeiss, Germany), a motorized 8 slide feeder xyz-scanning stage, and the Metafer4 version 3.5 MetaCyte software (MetaSystems, Germany). Based on DAPI counterstaining and images that were taken with a 63 x objective and an uncooled CCD camera a mask was generated for each nucleus defined by morphological features. Nuclei were scanned for foci signals with 10 focal planes at a step distance of 0.4 μm and z-stack images were combined to maximum projection images. Representative immunofluorescence images are shown in Figs. 2, 3, and 4. Cells exposed during S phase were positive for EdU and CENP-F and were excluded from the analysis. Cells irradiated in G2 were negative for EdU and positive for CENP-F. G1 cells were negative for EdU and CENP-F. Based on this classification, G1 and G2 cells were selected manually on fluorescence microscopic images for manual scoring of foci in G1 and G2 nuclei. This methodology enables a differentiated analysis of the cells in G1 or G2 at fixed times post-IR but does not provide such detailed information on repair kinetics and dynamics as achieved by live-cell imaging using time-lapse microscopy. The cell cycle distribution during these experimental conditions was measured exemplarily and is provided as Supplementary Fig. S2. For each data point, γH2AX and 53BP1 foci were scored in at least 30 G1 and 30 G2 cells, RPA foci in at least 30 G2 cells, and γH2AX/53BP1 foci in at least 300 G1 cells in 3 independent experiments each.

2.5. Cytogenetic analyses

2.5.1. G1 assay

Confluent fibroblasts synchronized in G1 were exposed to 3 Gy X-rays, harvested immediately, and seeded at a low density to allow for proliferation. After 24 h, 0.02 μg/mL colcemid (Roche, Switzerland) was added to collect only metaphases of the first cell cycle post-IR. 48 h after exposure the cells were trypsinized and treated for chromosome preparation and Giemsa staining as described previously [45]. The cell cycle distribution during this treatment was measured exemplarily and is provided in Supplementary Fig. S2. To investigate the impact of PARPi on the formation of IR-induced chromosome aberrations in WI38 lung fibroblasts in G1, confluent cells were incubated with 3 μM olaparib (Selleckchem, USA) 2 h before exposure to 3 Gy X-rays. WI38 cells were harvested immediately after IR and seeded at a low density to allow for proliferation in the presence of 3 μM olaparib (Selleckchem, USA). After 24 h, the medium was replaced by a medium without olaparib containing 0.02 μg/mL colcemid (Roche, Switzerland). Chromosome preparation and Giemsa staining were performed 48 h after irradiation as described previously [45]. The cytogenetic G1 assay was not performed for FA D1 (BRCA2) and 180BR (LIG4) cells since G1-synchronization by confluency was not achieved at the high cell counts required for this assay due to low proliferation rates. The following aberrations were scored: chromatid breaks and exchanges (radials) as well as dicentric chromosomes, centric rings, and excess acentric fragments. For each sample of 3 independent experiments, 100 diploid metaphases were analyzed.

2.5.2. G2-PCC

Exponentially growing cells were treated with 1 μg/mL aphidicolin (Enzo Life Science, Germany) to inhibit the transition of cells irradiated in S to G2 (Supplementary Fig. S3) and were exposed to 3 Gy X-rays. 7.5 h after irradiation G2-PCC was induced chemically by adding 50 nM calyculin A (LC Laboratories, US) for 30 min. Detached cells were collected and chromosome preparation and Giemsa staining were performed as described previously [45]. G2-PCCs of sham-irradiated cells had to be sampled 4 h after irradiation because of an exhaustion of G2 cells that had progressed into and past mitosis at 8 h after IR. In irradiated samples, the IR-induced G2/M arrest ensured a sufficient yield of G2-PCCs at 8 h after IR. The cell cycle distribution during this treatment was measured exemplarily and is provided in Supplementary Fig. S2. Inhibitor treatments with a DNA-PKi or PARPi were performed as described in Section 2.4 and G2-PCCs were harvested 4 h after irradiation. For each sample of 3 independent experiments, chromatid breaks and exchanges (radials) were scored in 50 G2-PCCs.

2.6. Data and statistical analysis

The yield of spontaneous foci or cytogenetic aberrations in sham-irradiated cells was subtracted from that in irradiated samples to provide only the number of IR-induced events except for DNA-PKi- or PARPi-treatments to score chromatid aberrations in G2-PCCs or γH2AX foci. The summarized average yield of DNA damage foci or cytogenetic aberrations of healthy donors is provided as the mean ± standard deviation unless stated otherwise. Data handling, plotting, and statistics

were done using SigmaPlot Version 14 (Systat Software, USA). The relationship between two variables was analyzed using the Pearson test. For comparison of the means of two or more groups, the Student's *t*-test or the one-way analysis of variance (ANOVA) was used, respectively. All levels of significance were set at $p < 0.05$.

3. Results

3.1. Validation of FA

To confirm the various FA complementation groups of this study using functional bioassays, exponentially growing fibroblasts were exposed to different replication stressors. Fig. 1A shows the immunostaining of FA D2 and markers of replication (EdU) and DNA damage (γH2AX) after treatment with aphidicolin. Loss of function of the FA core complex and FA D2 itself by a lack of FA D2 accumulation at sites of replication stress-induced DNA damage was confirmed for the FA complementation groups A, C, E, F, G, and D2. The induction of chromatid aberrations by MMC treatment is exemplarily shown in Fig. 1B and caused a significant increase of chromatid aberrations in all FA complementation groups compared to the average yield in healthy donors (0.91 ± 0.18 aberrations/ cell, Fig. 1C). Chromosomes of MMC treated FA D1 (BRCA2) cells were not analyzable due to low numbers of metaphases and G2-PCCs with shattered morphology. After catalytic inhibition and trapping of PARP1/ 2 by olaparib, only FA D1 (BRCA2) cells showed a significant increment of replication-associated chromatid aberrations compared to the average yield of healthy donors (0.69 ± 0.68 aberrations/ cell, Fig. 1D), confirming the paradigmatic susceptibility to synthetic lethal PARP-inhibition in BRCAness.

3.2. Cell cycle-dependent repair of IR-induced DSBs

The repair of IR-induced DSBs was monitored selectively in G1 and G2 by γH2AX, 53BP1, and RPA foci quantification combined with cell cycle markers to account for the impact of the cell cycle phase on DNA repair pathway choice. Besides, cell cycle-specific cytogenetic analyses were conducted to supplement DSB repair foci detections and to examine DSB repair fidelity.

3.2.1. Foci quantification reveals impaired DSB repair in FA in late G2

Representative immunofluorescence microscopic images of the cell cycle-dependent detection of γH2AX foci in G1 and G2 or γH2AX/53BP1 foci in confluent G1 cells are provided in Fig. 2 A and B, respectively. The quantification of γH2AX foci up to 24 h after exposure to 2 Gy X-rays in G1 showed a comparable repair of IR-induced DSBs in all donors except for 180BR (LIG4) cells (Fig. 2C, left panel).

All fibroblasts populations with an asynchronous cell cycle distribution showed similar basal levels of γH2AX foci whereas G1-synchronization by confluence for the analysis of IR-induced foci 24 h after exposure caused a strong increment of basal γH2AX/53BP1 foci in FA D1 (BRCA2) and 180BR (LIG4) cells. In contrast to G1, elevated numbers of IR-induced γH2AX foci were observed in G2 6 h post 2 Gy X-rays in FA fibroblasts reaching significance for FA F and FA D1 (BRCA2) cells compared to the average yield in healthy donors (9.74 ± 0.79 IR-induced γH2AX foci/ G2 cell, Fig. 2C right panel). Also in G2, 180BR (LIG4) cells showed the most severe defect in DSB repair. The basal level of γH2AX foci in G2 was significantly increased in the majority of FA cells 0.5 h and 2 h post IR compared to the average rate in healthy donors (7.45 ± 1.36 and 7.31 ± 2.09 basal γH2AX foci/ G2 cell at 0.5 h and 2 h post-IR, respectively). The elevated level of endogenous and

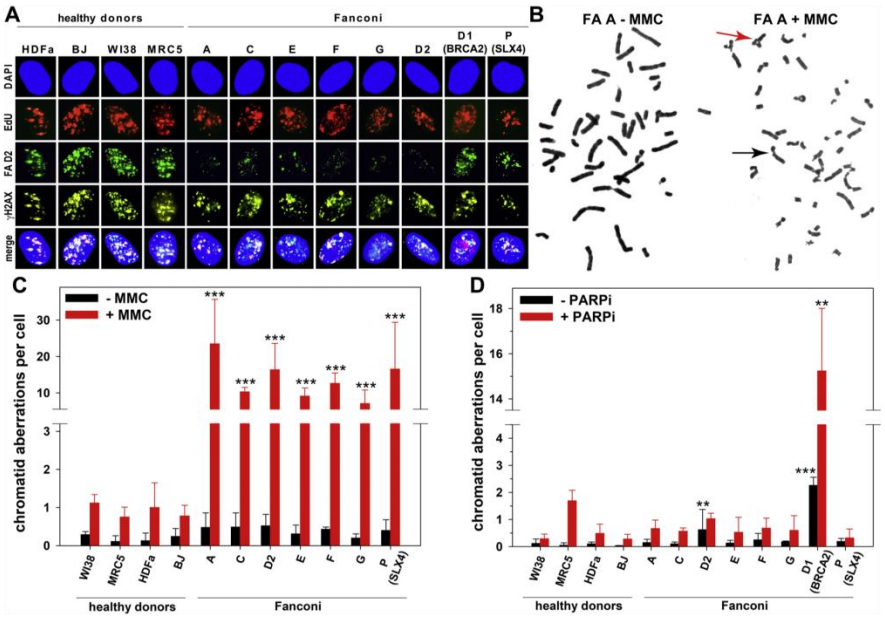

Fig. 1. Characterization of FA complementation groups by functional bioassays. (A) Detection of FA D2 at sites of replication-stress induced DNA damage (γH2AX) after aphidicolin treatment (1 μg/mL) in normal and FA fibroblasts by immunofluorescence microscopy. DNA synthesis in replicating cells was labeled by EdU incorporation. (B) Representative images of prematurely condensed chromosomes in G2 of FA A fibroblasts without (left) and with (right) mitomycin C (MMC, 50 nM, 24 h) treatment. A representative chromatid break (black arrow) and exchange (red arrow) after MMC treatment is indicated. Quantification of chromatid aberrations in metaphases and G2-PCCs after treatment with (C) MMC (50 nM, 24 h), or (D) the PARP-inhibitor (PARPi) olaparib (1 μM, 48 h). Statistics were performed by one-way ANOVA comparison to the mean of all healthy donors (*$p < 0.05$; **$p < 0.01$; ***$p < 0.001$).

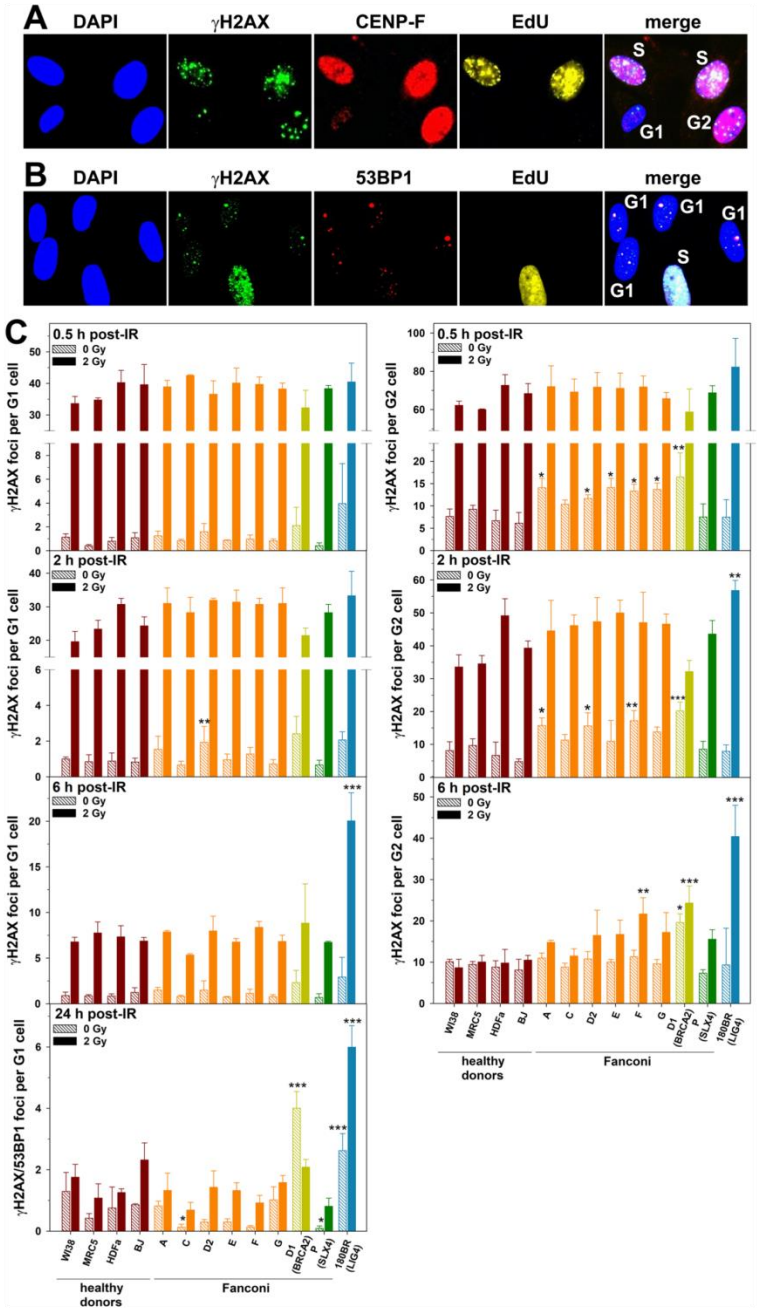

Fig. 2. Cell cycle-specific quantification of γH2AX foci in G1 and G2 or of γH2AX/53BP1 foci in G1. (A) Representative immunofluorescence microscopic images of combined immunostaining of DAPI, γH2AX, CENP-F, and EdU to score foci selectively in G1 and G2. Cells that progressed through S phase during or after irradiation were positive for EdU and CENP-F and were excluded from the analysis. Cells irradiated in G2 were negative for EdU and positive for CENP-F. G1 cells were negative for EdU and CENP-F. (B) Cells immunostained for γH2AX, 53BP1, EdU, and DAPI to score γH2AX/53BP1 foci in EdU-negative G1 cells 24 h after irradiation of confluent monolayers. (C) Basal and radiation-induced γH2AX and γH2AX/53BP1 foci scored at 0.5 h, 2 h, 6 h, or 24 h after 2 Gy X-rays in G1 (left panel) and G2 (right panel). Basal foci in unirradiated samples were subtracted from foci numbers in irradiated samples. The data is shown as the mean and standard deviation of three independent experiments. Statistics were performed by one-way ANOVA comparison to the mean of all healthy donors (*$p < 0.05$; **$p < 0.01$; ***$p < 0.001$).

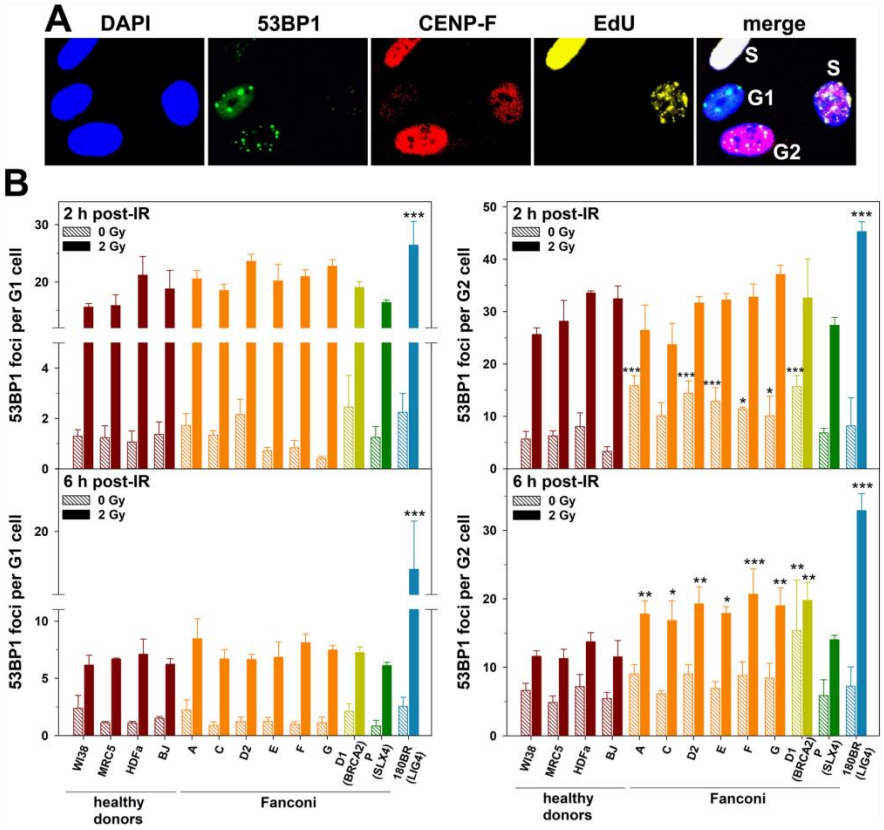

Fig. 3. Cell cycle-specific quantification of 53BP1 foci in G1 and G2. (A) Representative immunofluorescence microscopic images of combined immunostaining of DAPI, 53BP1, CENP-F, and EdU to score foci selectively in G1 and G2. (B) Basal and radiation-induced 53BP1 foci scored at 2 h and 6 h after 2 Gy X-rays in G1 (left panel) and G2 (right panel). Basal foci in unirradiated samples were subtracted from the foci in the irradiated samples. The data is shown as the mean and standard deviation of three independent experiments. Statistics were performed by one-way ANOVA comparison to the mean of all healthy donors (*$p < 0.05$; **$p < 0.01$; ***$p < 0.001$).

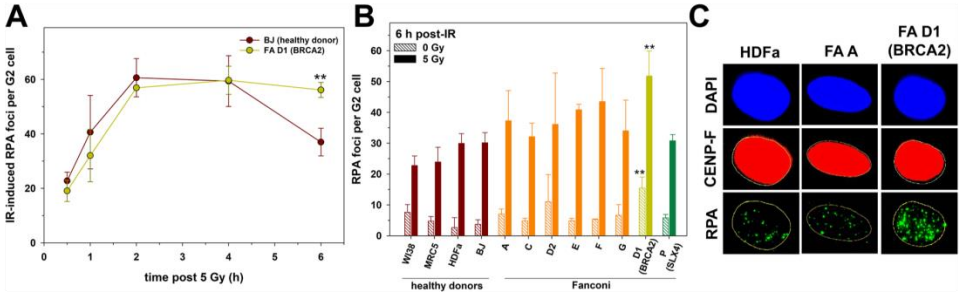

Fig. 4. Quantification of RPA foci in G2. (A) Kinetics of the induction and degradation of RPA foci in fibroblasts from a healthy donor (BJ) and an HR-deficient FA D1 (BRCA2) donor in G2 up to 6 h post 5 Gy X-rays. (B) Basal and radiation-induced RPA foci in G2 fibroblasts of healthy donors and FA patients scored 6 h after 5 Gy. Basal foci in unirradiated samples were subtracted from the foci in the irradiated samples. (C) Representative immunofluorescence microscopic images of RPA foci in CENP-F-positive G2 cells 6 h post 5 Gy X-rays. The data is shown as the mean and standard deviation of three independent experiments. Statistics were performed using the Student's *t*-test in (A) or by one-way ANOVA comparison to the mean of all healthy donors in (B) (*$p < 0.05$; **$p < 0.01$; ***$p < 0.001$).

replication-associated DSBs in FA cells occurring early after the progression from S to G2 decreased to the level of healthy donors at 6 h post-IR (9.12 ± 0.85 basal γH2AX foci/ G2 cell), except for FA D1 (BRCA2) cells.

Taking these results as the first indicator of compromised repair of IR-induced DSBs in the slow repair component of G2 in FA cells, we aimed to consolidate our findings using 53BP1 foci as another marker of IR-induced DSBs and as a determinant of DSB repair pathway choice [10]. Representative immunofluorescence microscopic images of 53BP1 foci in G1 and G2 cells are provided in Fig. 3A. In G1, the quantification of 53BP1 foci at 2 h and 6 h post 2 Gy X-rays confirmed the results of the γH2AX foci detection showing elevated 53BP1 foci only in 180BR (LIG4) cells compared to the average yield in healthy donors (17.87 ± 2.65 and 6.55 ± 0.44 IR-induced γH2AX foci/ G1 cell at 2 h and 6 h post-IR, respectively, Fig. 3B left panel). No differences were found in the basal level of 53BP1 foci in G1. In G2, 6 h post-IR all FA complementation groups except for FA P (SLX4) displayed significantly elevated numbers of IR-induced 53BP1 foci compared to the average yield in healthy donors (12.1 ± 1.13 IR-induced 53BP1 foci/ G2 cell, Fig. 3B right panel). Again, 180BR (LIG4) cells showed the strongest defect in DSB repair. IR-induced γH2AX and 53BP1 foci detected at 6 h post-IR correlated in a strong and highly significant manner ($r = 0.95$, $p < 0.0001$, supplementary Fig. S4). Significantly elevated numbers of basal 53BP1 foci in G2 were observed at 2 h post-IR for almost all FA complementation groups compared to the average rate in healthy donors (5.81 ± 1.95 53BP1 basal foci/ G2 cell, Fig. 3B right panel), which decreased to the level of healthy controls (6.03 ± 1.07 basal 53BP1 foci/ G2 cell) at 6 h post-IR, except for FA D1 (BRCA2) cells. Together, this data demonstrates elevated replication-associated DSBs in early G2 and compromised repair of IR-induced DSBs during the slow repair component in G2 in various FA complementation groups.

Since HR represents the relevant mechanism of DSB-repair in late G2 and because of the close interplay between the FA pathway and HR, we investigated the decay of IR-induced RPA foci 6 h post 5 Gy X-rays as an indicator for proficient homology-directed DSB-repair [47]. RPA coats single-stranded 3′ overhangs at resected DSBs and the removal is essential to stimulate HR, SSA, or alt-NHEJ. At first, we assessed the kinetics of the induction and degradation of RPA foci in G2 fibroblasts from a healthy donor (BJ) and in HR-deficient FA D1 (BRCA2) cells up to 6 h after 5 Gy X-rays (Fig. 4A). After a comparable increase reaching a plateau of maximum RPA foci numbers 2–4 h after IR-exposure, RPA foci in BJ cells decreased at 6 h post-IR but remained at the peak level in FA D1 (BRCA2) cells. The analysis of RPA foci 6 h post 5 Gy X-rays in G2 fibroblasts of all FA and healthy donors showed significantly elevated levels of basal and IR-induced RPA foci in no other FA complementation group than FA D1 (BRCA2) compared to the average rate in healthy donors (4.7 ± 2.1 and 26.7 ± 3.9 basal and IR-induced RPA foci/ G2 cell, respectively, Fig. 4B). Exemplary immunofluorescence microscopic

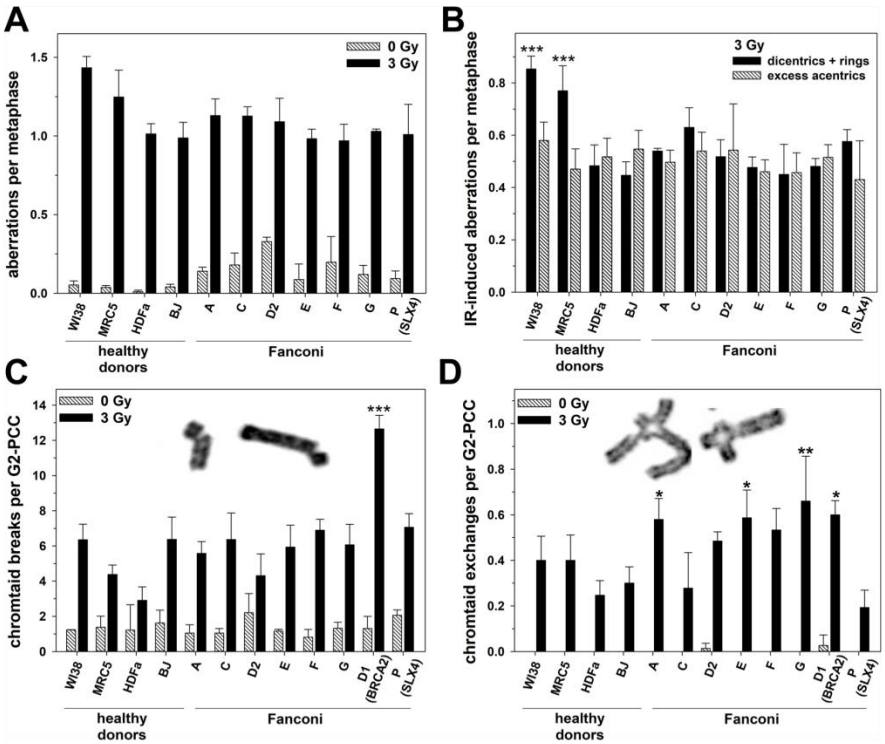

Fig. 5. Cell cycle-specific quantification of cytogenetic damage after exposure to 3 Gy X-rays in G1 or G2. (A) Basal and ionizing radiation (IR)-induced unstable chromosome aberrations and (B) IR-induced dicentric chromosomes plus centric rings or excess acentric fragments in first post-exposure metaphases after G1-irradiation. Basal and IR-induced (C) chromatid breaks and (D) exchanges in G2-PCCs 8 h after G2-irradiation. Representative chromatid breaks and exchanges are shown in (C) and (D), respectively. Aberrations in unirradiated samples were subtracted from the aberration yield in the irradiated samples. The data is shown as the mean and standard deviation of three independent experiments. Statistics in (B) were performed by one-way ANOVA comparison of all donors and in (C) and (D) by one-way ANOVA comparison to the mean of all healthy donors (*$p < 0.05$; **$p < 0.01$; ***$p < 0.001$).

images of IR-induced RPA foci in G2 at 6 h post 5 Gy X-rays are depicted in Fig. 4C.

3.2.2. Cytogenetic analyses

3.2.2.1. G1 assay: Normal chromosomal radiation sensitivity of FA cells but elevated aberrations in lung fibroblasts in G1. The rate of spontaneous and IR-induced chromosome aberrations in first metaphases 48 h after exposure to 3 Gy X-rays in G1 is shown in Fig. 5A. Fibroblasts of FA patients displayed higher rates of spontaneous aberrations compared to healthy donors due to elevated chromatid aberrations. Following IR exposure, similar yields of IR-induced aberrations were found in cells of FA or healthy donors. Lung fibroblasts from healthy donors (WI38 and MRC5) showed the highest numbers of IR-induced aberrations compared to skin fibroblasts from healthy donors (HDFa, BJ) and FA patients due to significantly elevated rates of chromosomal exchanges detected as dicentric chromosomes and centric rings (Fig. 5B). To rule out any impact of differential regulation of the IR-induced cell cycle arrest on the yield of aberrations scored in lung and skin fibroblasts, we performed cumulative EdU labeling and assessed mitotic indices after IR exposure in G1 (Supplementary Fig. S5). No relationship was found between cell cycle progression post-IR and higher rates of IR-induced chromosome aberrations in lung *versus* skin fibroblasts.

3.2.2.2. G2-PCC: FA donors show elevated chromatid-exchanges in G2. To examine the repair of IR-induced DSBs in G2 in the chromosomal context, chromatid aberrations were analyzed in G2-PCCs 8 h after exposure to 3 Gy X-rays. Shown in Fig. 5C, a significantly elevated rate of IR-induced chromatid breaks was observed only in FA D1 (BRCA2) cells compared to the average yield in healthy donors (5.0 ± 1.68 IR-induced breaks/ G2-PCC). To account for the DSB repair fidelity in G2, the yield of chromatid exchanges in G2-PCCs is depicted in Fig. 5D. The rate of chromatid exchanges in G2-PCCs was subject to large variation, however, significant increments were observed in FA fibroblasts of complementation groups A, D1, D2, E, F, and G when compared to the average yield in healthy donors (0.34 ± 0.08 IR-induced chromatid exchanges/ G2-PCC).

3.2.2.3. DSB-repair and translocation formation in normal and FA fibroblasts depend on c-NHEJ with no function of alt-NHEJ. Concerning the pronounced formation of IR-induced chromosome exchanges in lung fibroblasts in G1 (Fig. 5B) and of chromatid exchanges in FA fibroblasts in G2 (Fig. 5D) we examined the contribution of DNA-PK-dependent c-NHEJ and PARP-dependent alt-NHEJ to the overall repair of IR-induced DSBs and the formation of cytogenetic rearrangements in fibroblasts of healthy donors and selected FA complementation groups. Cytogenetic analysis was performed 4 h after exposure to 3 Gy X-rays with concomitant DNA-PKi or PARPi in G2 where all DSB repair mechanisms are available. Only the inhibition of DNA-PK-dependent c-NHEJ had an impact on DSB-repair as detected by a significant increment of chromatid breaks and a steep decline of chromatid exchanges (Fig. 6A and B, respectively). The inhibition of PARP-dependent alt-NHEJ with or without concomitant DNA-PKi did not affect the repair of IR-induced DSBs. Cytogenetic analysis of first metaphases of WI38 lung fibroblasts after exposure to 3 Gy X-rays in G1 showed no effect of PARPi on the total yield of chromosome aberrations or the formation of chromosome exchanges (Fig. 6C). These results were confirmed by γH2AX foci quantification in G1 and G2 6 h after exposure to 2 Gy X-rays under inhibitor treatment (Fig. 6D and E, respectively). Comprehensive statistics on the data depicted in Fig. 6 are provided in Supplementary Table S2.

4. Discussion

FA is a syndrome of DNA repair disorder and chromosomal instability associated with high susceptibility to cancer. The use of IR in radiation therapy as a cornerstone of genotoxic anti-cancer treatment is therefore complicated and limited in FA by serious and fatal normal

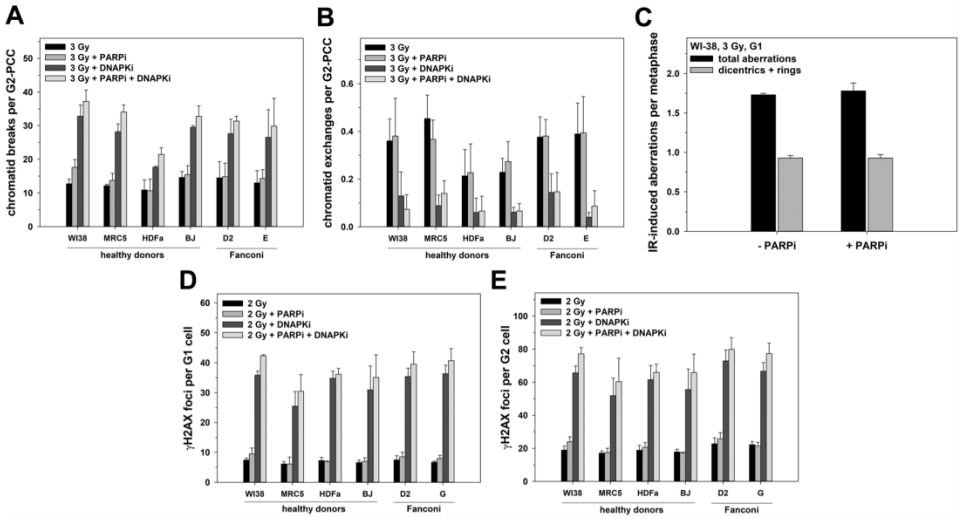

Fig. 6. The contribution of DNA-PK-dependent c-NHEJ and PARP-dependent alt-NHEJ to the repair of ionizing radiation (IR)-induced DNA double-strand breaks. (A) Chromatid breaks and (B) chromatid exchanges in G2-PCCs 4 h post 3 Gy X-rays without or with DNA-PKi and PARPi treatment. (C) IR-induced induced chromosome aberrations in first post-exposure metaphases 48 h after G1-irradiation of WI38 lung fibroblasts with 3 Gy X-rays with or without PARPi treatment. Quantification of γH2AX foci in (E) G1 and (F) G2 6 h post 2 Gy without or with DNA-PKi and PARPi treatment. The data is shown as the mean and standard deviation of three independent experiments. Statistics were performed by one-way ANOVA comparison of the different treatment conditions for each donor and are provided in Supplementary Table S2.

tissue radiotoxicity, but the underlying factors are still largely unknown. In the present study, we investigated the repair of IR-induced DSBs in primary skin fibroblasts of a well-defined set of various FA complementation groups comprising A, C, D1 (BRCA2), D2, E, F, G, and P (SLX4) compared to lung and skin fibroblasts of healthy donors. We quantified IR-induced foci of γH2AX, 53BP1, and RPA as well as cytogenetic aberrations in a cell cycle-dependent manner after X-ray exposure selectively in G1 and G2 to account for the utilization of different DSB repair pathways. FA cells displayed compromised repair of IR-induced DSBs only in the slow repair component of G2. Lung fibroblasts conducted DSB repair with normal kinetics but elevated chromosome exchanges in G1. The efficacy and fidelity of the repair of IR-induced DSBs were only regulated by DNA-PK-dependent c-NHEJ with no involvement of PARP-dependent alt-NHEJ.

The highly sensitive quantification of γH2AX and 53BP1 foci, as well as chromosome aberrations after IR exposure in G1, showed normal repair of IR-induced DSBs in all FA complementation groups investigated in our work. Data from previous studies on the capacity of FA cells to repair IR-induced DNA damage in G0/1 are conflicting ([17–19,21,25,26,29–33,35,37], Supplementary Table S1 and Supplementary Fig. S1). Cell cycle-dependent analyses of cytogenetic aberrations after IR exposure in unstimulated lymphocytes or synchronized fibroblasts in G0/G1 have shown a similar extend of increased (43 %, 3/7 [17,25,37]) or comparable (57 %, 4/7 [18,19,26,30]) rates of IR-induced aberrations between FA patients and healthy donors. However, each of the studies that examined IR-induced DSB repair foci in FA cells in G1 [33–35] or asynchronous populations [27,28,32,34,36] showed compromised DSB repair by elevated foci numbers in FA. In general, and particularly in G1, DSB repair is dominated by c-NHEJ. However, a suppressive effect of the FA/BRCA pathway on c-NHEJ has only been reported during S phase for the processing of replication-associated DNA damage by stimulation of DSB end resection which is primarily attributed to S and G2 to initiate HR, SSA, or alt-NHEJ [10,48]. Recently, Biehs et al. [49] revealed the use of resection-dependent c-NHEJ in late G1 to repair a subset of about 10–20 % of IR-induced DSBs with low fidelity causing deletions and translocations. But so far, a potential activation and c-NHEJ-suppressive function of the FA/BRCA pathway outside of S phase has not yet been demonstrated. Although a potent initiation of the FA pathway has been reported after high doses of IR in human tumor cells and complemented fibroblasts or EBV-transformed lymphoblast lines of FA patients [16], this has been mainly confined to S and G2 [50,51].

Surprisingly, after IR exposure in G1, we observed a 1.6-fold increase in chromosome exchanges in primary normal human lung fibroblasts with otherwise similar γH2AX and 53BP1 foci numbers compared to normal and FA skin fibroblasts. The increased rate of aberrations in lung fibroblasts could not be ascribed to differences in cell cycle regulation or a contribution of alt-NHEJ to the formation of chromosome exchanges, as previously suggested for WI38 lung fibroblasts [52]. More frequent utilization of error-prone pathways of DSB end-joining that may promote the risk of malignant transformation in cells from lung tissues remains to be unraveled but is a clinically relevant issue since human lungs are frequently subjected to DNA damage induced by thoracic radiology and radiation therapy or through inhalation of genotoxic chemicals and the radioactive noble gas radon.

In contrast to G1, FA fibroblasts except for FA P (SLX4) exhibited an impaired repair of IR-induced DSBs during the slow repair component in G2. In FA, the level of IR-induced γH2AX and 53BP1 foci in late G2 was elevated compared to healthy donors but lower than in c-NHEJ-deficient 180BR (LIG4) cells. In particular, 53BP1 foci were increased to a comparable extent in FA fibroblasts of the FA core complex, FA D2, and FA D1 (BRCA2) cells with compromised HR [53]. Impaired DSB repair by elevated IR-induced γH2AX foci has been previously demonstrated in FA A and FA D2 fibroblasts compared to non-FA donors or non-FA patients with bone marrow failure but without a specific assignment to cell cycle phase [32,54]. Liu et al. [36] demonstrated higher yields of γH2AX foci in asynchronous immortalized human fibroblasts derived from a FA P patient with bi-allelic SLX4 mutations after irradiation with photons and even more pronounced after exposure with protons. The latter are charged particles causing slightly more complex and clustered DNA damage compared with photons that require HR for efficient DNA repair and cell survival [55]. This finding was primarily attributed to an aborted interaction of SLX4 with MUS81 leading to a potentiation of IR-induced DNA lesions through replication stress, thus radiosensitization and γH2AX foci accumulation in S and G2. Similar observations were made by Zhu et al. [51] in FA D2 deficient cells after the induction of clustered DNA damage by exposure to charged particles of high mass and energy (Fe-ions). In the present work, however, no replication-associated effects such as those provoked by IR-induced obstacles to the replication machinery could be observed because the progression through S phase was abrogated by aphidicolin. Our results on γH2AX and 53BP1 foci quantification showed a limited DSB repair capacity in the late repair component of G2 in FA and suggest compromised HR. Therefore, we examined the retention of IR-induced RPA foci in G2. RPA at 3′ Overhangs of DSBs is replaced either by Rad51 in a BRCA2/PALB2-dependent manner, by Rad52 or by polymerase theta/unknown protein to initiate HR, SSA, or alt-NHEJ, respectively [8,56]. The retention of RPA foci at IR-induced DSBs is considered an indicator of dysfunctional homology-directed DSB repair, which, however, has been shown in the present study only for FA D1 (BRCA2) fibroblasts. Consistent with this observation but converse to the data on γH2AX and 53BP1 foci, only FA D1 (BRCA2) cells displayed significantly increased numbers of IR-induced chromatid breaks in G2-PCCs. A lack of correlation between the γH2AX or 53BP1 foci data and the rate of chromatid breaks in late G2 except for FA D1 (BRCA2) might be attributed to the higher sensitivity of DSB foci quantification compared to cytogenetic methods. In general, a 1: 3–6 ratio between IR-induced chromatid breaks in G2-PCCs and DSBs or γH2AX foci is assumed [57]. In most FA donors, we rather observed increased rates of chromatid exchanges in late G2. The generation of IR-induced chromatid exchanges in G2 is a rapid process that begins a few minutes after exposure and is completed within about 30 min [58]. Hence, the formation of chromatid exchanges in normal human cells in G2 is generally attributed to the fast and prevailing process of c-NHEJ as confirmed by our experiments using a DNAPKi in G2 (Fig. 6B). However, other repair mechanisms such as gene conversion, SSA, or alt-EJ can process DSBs in G2 depending on the DSB load, whereby c-NHEJ dominates at higher DSB burden as induced in our work [59]. Our finding on elevated chromatid exchanges in G2 in FA is in line with increased 53BP1 foci in late G2 acting as an antagonist of BRCA1 and suppressor of homology-directed repair in favor of end-joining mechanisms that lead to the formation of translocations. Although 53BP1-dependent channeling of DSB repair into c-NHEJ at the expense of homology-directed repair may appear unfavorable at first, it protects against excessive DSB resection that fuels genome instability by SSA and alt-NHEJ. Another potential role for 53BP1 in the formation of chromosome rearrangements and translocations has been recently related to a function in chromatin relaxation to repair IR-induced DSBs in heterochromatic regions and to promote their pairing [60], as well as to increase the mobility and synapsis of distal DSBs [61,62]. Our results on elevated numbers of residual IR-induced 53BP1 foci in G2 show compromised repair of IR-induced DSBs and may indicate a preference for c-NHEJ in FA cells, but their consequence and impact on DSB repair fidelity remains elusive due to the diverse and still emerging functions of 53BP1 [63].

A disturbed balance between the utilization of different DNA repair pathways can stimulate erroneous repair mechanisms and foster the formation of tumorigenic chromosomal rearrangements. Chromosome exchanges such as unstable dicentric and ring chromosomes or transmissible translocations are primarily generated by end-joining repair mechanisms and are accountable for mitotic catastrophes and cell death or malignant transformation. A substantial role in the formation of

chromosomal interchanges has been attributed to alt-NHEJ, especially as a backup-pathway in human cancer and rodent cells with impaired c-NHEJ or HR [64]. Although alt-NHEJ seems to have little or no function in normal human cells [49,65] this cannot be completely ruled out [52]. By using inhibitor approaches we confirmed the dominant role of DNA-PK-dependent c-NHEJ for the repair of stochastically IR-induced DSBs in human primary normal and FA fibroblasts. No contribution could be demonstrated for PARP-dependent alt-NHEJ, even when DNA-PK was abolished by a DNA-PKi which promotes resection-dependent and homology-directed repair [66]. We also did not recapitulate an involvement of PARP-dependent repair of IR-induced DSBs in normal human WI38 lung fibroblasts as suggested previously by Wray et al. [52].

In summary, by examining the repair of IR-induced DSBs in a strict cell cycle-dependent manner in G1 and G2 we demonstrate impaired repair of IR-induced DSBs in fibroblasts of various FA complementation groups in the slow repair component of G2, associated with elevated chromatid exchanges. This bears an oncogenic potential and might contribute to the frequent clinical radiation hypersensitivity of FA patients. On the other, our observations hold opportunities for a radiosensitization of tumors with genetic and epigenetic mutations in FA genes and targeting of the FA pathway for cancer intervention.

Author contributions

Conceived and designed the experiments: SZ, DS and HS. Performed the experiments: SZ, BW and GR. Analyzed the data: SZ. Wrote the paper: SZ. All authors contributed to the article and approved the submitted version.

Acknowledgments

We thank U. Disque-Kaiser for excellent technical assistance.

Funding

The study was supported by the German Federal Ministry of Education and Research (grant no. 02NUK042A) and by intramural research funding of the University Medical Centre Mainz, Germany.

Appendix A. Supplementary data

Supplementary material related to this article can be found, in the online version, at doi:https://doi.org/10.1016/j.dnarep.2020.102992.

References

[1] G. Fanconi, Familial constitutional panmyelocytopathy, Fanconi's anemia (F.A.). I. clinical aspects, Semin Hematol 4 (1967) 233–240.
[2] S. Hashimoto, H. Anai, K. Hanada, Mechanisms of interstrand DNA crosslink repair and human disorders, Genes Environ. 38 (2016) 9.
[3] G.E. Bloom, S. Warner, P.S. Gerald, L.K. Diamond, Chromosome abnormalities in constitutional aplastic anemia, N. Engl. J. Med. 274 (1966) 8–14.
[4] B. Haynes, N. Saadat, B. Myung, M.P. Shekhar, Crosstalk between translesion synthesis, Fanconi anemia network, and homologous recombination repair pathways in interstrand DNA crosslink repair and development of chemoresistance, Mutat. Res. Rev. Mutat. Res. 763 (2015) 258–266.
[5] K.N. Yamamoto, S. Kobayashi, M. Tsuda, H. Kurumizaka, M. Takata, K. Kono, J. Jiricny, S. Takeda, K. Hirota, Involvement of SLX4 in interstrand cross-link repair is regulated by the Fanconi anemia pathway, Proc Natl Acad Sci U S A 108 (2011) 6492–6496.
[6] M. Ensminger, M. Löbrich, One end to rule them all: non-homologous end-joining and homologous recombination at DNA double-strand breaks, Br. J. Radiol. (2020), 20191054.
[7] N. Jette, S.P. Lees-Miller, The DNA-dependent protein kinase: a multifunctional protein kinase with roles in DNA double strand break repair and mitosis, Prog. Biophys. Mol. Biol. 117 (2015) 194–205.
[8] T. Ochi, A.N. Blackford, J. Coates, S. Jhujh, S. Mehmood, N. Tamura, J. Travers, Q. Wu, V.M. Draviam, C.V. Robinson, T.L. Blundell, S.P. Jackson, DNA repair. PAXX, a paralog of XRCC4 and XLF, interacts with Ku to promote DNA double-strand break repair, Science 347 (2015) 185–188.
[9] C. Wyman, R. Kanaar, DNA double-strand break repair: all's well that ends well, Annu. Rev. Genet. 40 (2006) 363–383.
[10] S.F. Bunting, E. Callen, N. Wong, H.T. Chen, F. Polato, A. Gunn, A. Bothmer, N. Feldhahn, O. Fernandez-Capetillo, L. Cao, X. Xu, C.X. Deng, T. Finkel, M. Nussenzweig, J.M. Stark, A. Nussenzweig, 53BP1 inhibits homologous recombination in Brca1-deficient cells by blocking resection of DNA breaks, Cell 141 (2010) 243–254.
[11] L. Deriano, D.B. Roth, Modernizing the nonhomologous end-joining repertoire: alternative and classical NHEJ share the stage, Annu. Rev. Genet. 47 (2013) 433–455.
[12] H. Wang, B. Rosidi, R. Perrault, M. Wang, L. Zhang, F. Windhofer, G. Iliakis, DNA ligase III as a candidate component of backup pathways of nonhomologous end joining, Cancer Res. 65 (2005) 4020–4030.
[13] M. Lee-Theilen, A.J. Matthews, D. Kelly, S. Zheng, J. Chaudhuri, CtIP promotes microhomology-mediated alternative end joining during class-switch recombination, Nat. Struct. Mol. Biol. 18 (2011) 75–79.
[14] R. Bhargava, D.O. Onyango, J.M. Stark, Regulation of single-strand annealing and its role in genome maintenance, Trends Genet. 32 (2016) 566–575.
[15] J.F. Ward, DNA damage produced by ionizing radiation in mammalian cells: identities, mechanisms of formation, and reparability, Prog. Nucleic Acid Res. Mol. Biol. 35 (1988) 95–125.
[16] I. Garcia-Higuera, T. Taniguchi, S. Ganesan, M.S. Meyn, C. Timmers, J. Hejna, M. Grompe, A.D. D'Andrea, Interaction of the fanconi anemia proteins and BRCA1 in a common pathway, Mol. Cell 7 (2001) 249–262.
[17] M. Higurashi, P.E. Conen, In vitro chromosomal radiosensitivity in Fanconi's anemia, Blood 38 (1971) 336–342.
[18] M.S. Sasaki, A. Tonomura, A high susceptibility of Fanconi's anemia to chromosome breakage by DNA cross-linking agents, Cancer Res. 33 (1973) 1829–1836.
[19] J.A. Heddle, C.B. Lue, E.F. Saunders, R.D. Benz, Sensitivity to five mutagens in Fanconi's anemia as measured by the micronucleus method, Cancer Res. 38 (1978) 2983–2988.
[20] S.B. Bigelow, J.M. Rary, M.A. Bender, G2 chromosomal radiosensitivity in Fanconi's anemia, Mutat. Res. 63 (1979) 189–199.
[21] A.J. Fornace Jr., J.B. Little, R.R. Weichselbaum, DNA repair in a Fanconi's anemia fibroblast cell strain, Biochim. Biophys. Acta 561 (1979) 99–109.
[22] G. Duckworth-Rysiecki, A.M. Taylor, Effects of ionizing radiation on cells from Fanconi's anemia patients, Cancer Res. 45 (1985) 416–420.
[23] R. Parshad, K.K. Sanford, G.M. Jones, Chromosomal radiosensitivity during the G2 cell-cycle period of skin fibroblasts from individuals with familial cancer, Proc Natl Acad Sci U S A 82 (1985) 5400–5403.
[24] F. Darroudi, R.C. Vyas, S. Vermeulen, A.T. Natarajan, G2 radiosensitivity of cells derived from cancer-prone individuals, Mutat. Res. 328 (1995) 83–90.
[25] B. Gibbons, D. Scott, J.L. Hungerford, K.L. Cheung, C. Harrison, S. Attard-Montalto, M. Evans, J.M. Birch, J.E. Kingston, Retinoblastoma in association with the chromosome breakage syndromes Fanconi's anaemia and Bloom's syndrome: clinical and cytogenetic findings, Clin. Genet. 47 (1995) 311–317.
[26] J.F. Barquinero, L. Barrios, M. Ribas, J. Egozcue, M.R. Caballin, Cytogenetic sensitivity of three Fanconi anemia heterozygotes to bleomycin and ionizing radiation, Cancer Genet. Cytogenet. 124 (2001) 80–83.
[27] M. Digweed, S. Rothe, I. Demuth, R. Scholz, D. Schindler, M. Stumm, M. Grompe, A. Jordan, K. Sperling, Attenuation of the formation of DNA-repair foci containing RAD51 in Fanconi anaemia, Carcinogenesis 23 (2002) 1121–1126.
[28] C. Djuzenova, M. Flentje, P.N. Plowman, Radiation Response in Vitro of Fibroblasts From a Fanconi Anemia Patient With Marked Clinical Radiosensitivity, Strahlentherapie Und Onkologie : Organ Der Deutschen Rontgengesellschaft ... [et Al], 180, 2004, pp. 789–797.
[29] J.A. Casado, M.I. Nunez, J.C. Segovia, J.M. Ruiz de Almodovar, J.A. Bueren, Non-homologous end-joining defect in fanconi anemia hematopoietic cells exposed to ionizing radiation, Radiat. Res. 164 (2005) 635–641.
[30] A. Mohseni-Meybodi, H. Mozdarani, P. Vosough, Cytogenetic sensitivity of G0 lymphocytes of Fanconi anemia patients and obligate carriers to mitomycin C and ionizing radiation, Cytogenet. Genome Res. 119 (2007) 191–195.
[31] A. Mohseni Meybodi, H. Mozdarani, DNA damage in leukocytes from Fanconi anemia (FA) patients and heterozygotes induced by mitomycin C and ionizing radiation as assessed by the comet and comet-FISH assay, Iran. Biomed. J. 13 (2009) 1–8.
[32] A. Leskovac, D. Vujic, M. Guc-Scekic, S. Petrovic, I. Joksic, P. Slijepcevic, G. Joksic, Fanconi anemia is characterized by delayed repair kinetics of DNA double-strand breaks, Tohoku J. Exp. Med. 221 (2010) 69–76.
[33] C.E. Rube, A. Fricke, R. Schneider, K. Simon, M. Kuhne, J. Fleckenstein, S. Graber, N. Graf, C. Rube, DNA repair alterations in children with pediatric malignancies: novel opportunities to identify patients at risk for high-grade toxicities, Int. J. Radiat. Oncol. Biol. Phys. 78 (2010) 359–369.
[34] A. Leskovac, S. Petrovic, M. Guc-Scekic, D. Vujic, G. Joksic, Radiation-induced mitotic catastrophe in FANCD2 primary fibroblasts, Int. J. Radiat. Biol. 90 (2014) 373–381.
[35] N. Schuler, J. Palm, M. Kaiser, D. Betten, R. Furtwangler, C. Rube, N. Graf, C. E. Rube, DNA-damage foci to detect and characterize DNA repair alterations in children treated for pediatric malignancies, PLoS One 9 (2014), e91319.
[36] Q. Liu, T.S. Underwood, J. Kung, M. Wang, H.M. Lu, H. Paganetti, K.D. Held, T. S. Hong, J.A. Efstathiou, H. Willers, Disruption of SLX4-MUS81 function increases the relative biological effectiveness of proton radiation, Int. J. Radiat. Oncol. Biol. Phys. 95 (2016) 78–85.
[37] F.Z. Francies, R. Wainwright, J. Poole, K. De Leeneer, I. Coene, G. Wieme, H. A. Poirel, B. Brichard, S. Vermeulen, A. Vral, J. Slabbert, K. Claes, A. Baeyens,

Diagnosis of Fanconi Anaemia by ionising radiation- or mitomycin C-induced micronuclei, DNA Repair (Amst) 61 (2018) 17–24.
[38] B.P. Alter, Radiosensitivity in Fanconi's anemia patients, Radiother. Oncol. 62 (2002) 345–347.
[39] M. Bremer, D. Schindler, M. Grob, T. Dork, S. Morlot, J.H. Karstens, Fanconi's anemia and clinical radiosensitivity - Report on two adult patients with locally advanced solid tumors treated by radiotherapy, Strahlenther. Und Onkol. 179 (2003), 748-+.
[40] N.G. Burnet, J.H. Peacock, Normal cellular radiosensitivity in an adult Fanconi anaemia patient with marked clinical radiosensitivity, Radiother. Oncol. 62 (2002) 350–351, author reply 351-352.
[41] Y. Marcou, A.D. Andrea, P.A. Jeggo, P.N. Plowman, Normal cellular radiosensitivity in an adult Fanconi anaemia patient with marked clinical radiosensitivity, Radiother. Oncol. 60 (2001) 75–79.
[42] E. Gluckman, Radiosensitivity in Fanconi anemia: application to the conditioning for bone marrow transplantation, Radiother. Oncol. 18 (Suppl 1) (1990) 88–93.
[43] A.C. Birkeland, A.D. Auerbach, E. Sanborn, B. Parashar, W.I. Kuhel, S. C. Chandrasekharappa, A. Smogorzewska, D.I. Kutler, Postoperative clinical radiosensitivity in patients with fanconi anemia and head and neck squamous cell carcinoma, Arch. Otolaryngol. Head Neck Surg. 137 (2011) 930–934.
[44] C. Badie, G. Iliakis, N. Foray, G. Alsbeih, G.E. Pantellias, R. Okayasu, N. Cheong, N. S. Russell, A.C. Begg, C.F. Arlett, et al., Defective repair of DNA double-strand breaks and chromosome damage in fibroblasts from a radiosensitive leukemia patient, Cancer Res. 55 (1995) 1232–1234.
[45] S. Zahnreich, A. Ebersberger, B. Kaina, H. Schmidberger, Biodosimetry based on gamma-H2AX quantification and cytogenetics after partial- and total-body irradiation during fractionated radiotherapy, Radiat. Res. 183 (2015) 432–446.
[46] P. Chanut, S. Britton, J. Coates, S.P. Jackson, P. Calsou, Coordinated nuclease activities counteract Ku at single-ended DNA double-strand breaks, Nat. Commun. 7 (2016) 12889.
[47] A. Beucher, J. Birraux, L. Tchouandong, O. Barton, A. Shibata, S. Conrad, A. A. Goodarzi, A. Krempler, P.A. Jeggo, M. Lobrich, ATM and Artemis promote homologous recombination of radiation-induced DNA double-strand breaks in G2, EMBO J. 28 (2009) 3413–3427.
[48] A. Adamo, S.J. Collis, C.A. Adelman, N. Silva, Z. Horejsi, J.D. Ward, E. Martinez-Perez, S.J. Boulton, A. La Volpe, Preventing nonhomologous end joining suppresses DNA repair defects of Fanconi anemia, Mol. Cell 39 (2010) 25–35.
[49] R. Biehs, M. Steinlage, O. Barton, S. Juhasz, J. Kunzel, J. Spies, A. Shibata, P. A. Jeggo, M. Lobrich, DNA double-strand break resection occurs during non-homologous end joining in G1 but is distinct from resection during homologous recombination, Mol. Cell 65 (2017), 671-+.
[50] P.C. Bosch, M. Bogliolo, J. Surralles, Activation of the Fanconi anemia/BRCA pathway at low doses of ionization radiation, Mutat. Res. Genet. Toxicol. Environ. Mutagen. 793 (2015) 9–13.
[51] J. Zhu, F. Su, S. Mukherjee, E. Mori, B. Hu, A. Asaithamby, FANCD2 influences replication fork processes and genome stability in response to clustered DSBs, Cell Cycle 14 (2015) 1809–1822.
[52] J. Wray, E.A. Williamson, S.B. Singh, Y. Wu, C.R. Cogle, D.M. Weinstock, Y. Zhang, S.H. Lee, D. Zhou, L. Shao, M. Hauer-Jensen, R. Pathak, V. Klimek, J.A. Nickoloff, R. Hromas, PARP1 is required for chromosomal translocations, Blood 121 (2013) 4359–4365.
[53] S.K. Sharan, M. Morimatsu, U. Albrecht, D.S. Lim, E. Regel, C. Dinh, A. Sands, G. Eichele, P. Hasty, A. Bradley, Embryonic lethality and radiation hypersensitivity mediated by Rad51 in mice lacking Brca2, Nature 386 (1997) 804–810.
[54] I. Joksic, D. Vujic, M. Guc-Scekic, A. Leskovac, S. Petrovic, M. Ojani, J.P. Trujillo, J. Surralles, M. Zivkovic, A. Stankovic, P. Slijepcevic, G. Joksic, Dysfunctional telomeres in primary cells from Fanconi anemia FANCD2 patients, Genome Integr. 3 (2012) 6.
[55] N. Grosse, A.O. Fontana, E.B. Hug, A. Lomax, A. Coray, M. Augsburger, H. Paganetti, A.A. Sartori, M. Pruschy, Deficiency in homologous recombination renders Mammalian cells more sensitive to proton versus photon irradiation, Int. J. Radiat. Oncol. Biol. Phys. 88 (2014) 175–181.
[56] T. Kent, G. Chandramouly, S.M. McDevitt, A.Y. Ozdemir, R.T. Pomerantz, Mechanism of microhomology-mediated end-joining promoted by human DNA polymerase θ, Nat. Struct. Mol. Biol. 22 (2015) 230–237.
[57] D. Deckbar, J. Birraux, A. Krempler, L. Tchouandong, A. Beucher, S. Walker, T. Stiff, P. Jeggo, M. Lobrich, Chromosome breakage after G2 checkpoint release, J. Cell Biol. 176 (2007) 749–755.
[58] E. Gotoh, T. Kawata, M. Durante, Chromatid break rejoining and exchange aberration formation following gamma-ray exposure: analysis in G2 human fibroblasts by chemically induced premature chromosome condensation, Int. J. Radiat. Biol. 75 (1999) 1129–1135.
[59] A. Soni, T. Murmann-Konda, M. Siemann-Loekes, G.E. Pantelias, G. Iliakis, Chromosome breaks generated by low doses of ionizing radiation in G(2)-phase are processed exclusively by gene conversion, DNA Repair (Amst) 89 (2020), 102828.
[60] M. Yamauchi, A. Shibata, K. Suzuki, M. Suzuki, A. Niimi, H. Kondo, M. Miura, M. Hirakawa, K. Tsujita, S. Yamashita, N. Matsuda, Regulation of pairing between broken DNA-containing chromatin regions by Ku80, DNA-PKcs, ATM, and 53BP1, Sci. Rep. 7 (2017) 41812.
[61] S. Difilippantonio, E. Gapud, N. Wong, C.Y. Huang, G. Mahowald, H.T. Chen, M. J. Kruhlak, E. Callen, F. Livak, M.C. Nussenzweig, B.P. Sleckman, A. Nussenzweig, 53BP1 facilitates long-range DNA end-joining during V(D)J recombination, Nature 456 (2008) 529–533.
[62] F. Lottersberger, R.A. Karssemeijer, N. Dimitrova, T. de Lange, 53BP1 and the LINC complex promote microtubule-dependent DSB mobility and DNA repair, Cell 163 (2015) 880–893.
[63] Z. Mirman, T. de Lange, 53BP1: a DSB escort, Genes Dev. 34 (2020) 7–23.
[64] G. Iliakis, T. Murmann, A. Soni, Alternative end-joining repair pathways are the ultimate backup for abrogated classical non-homologous end-joining and homologous recombination repair: implications for the formation of chromosome translocations, Mutat. Res. Genet. Toxicol. Environ. Mutagen. 793 (2015) 166–175.
[65] H. Ghezraoui, M. Piganeau, B. Renouf, J.B. Renaud, A. Sallmyr, B. Ruis, S. Oh, A. E. Tomkinson, E.A. Hendrickson, C. Giovannangeli, M. Jasin, E. Brunet, Chromosomal translocations in human cells are generated by canonical nonhomologous end-joining, Mol. Cell 55 (2014) 829–842.
[66] F. Robert, M. Barbeau, S. Ethier, J. Dostie, J. Pelletier, Pharmacological inhibition of DNA-PK stimulates Cas9-mediated genome editing, Genome Med. 7 (2015) 93.